# Regulation of Stem Cell Metabolism by the Lin28/let-7 Axis

**HARVARD UNIVERSITY**
**Graduate School of Arts and Sciences**

## DISSERTATION ACCEPTANCE CERTIFICATE

The undersigned, appointed by the

Division of Medical Sciences

in the subject of Biological and Biomedical Sciences

have examined a dissertation entitled

*Regulation of Stem Cell Metabolism by the Lin28/let-7 Axis*

presented by Shyh Chang Ng

candidate for the degree of Doctor of Philosophy and hereby certify that it is worthy of acceptance.

*Signature:* _____

*Typed Name:* Dr. Amy Wagers

*Signature:* _____

*Typed Name:* Dr. Yi Zhang

*Signature:* _____

*Typed Name:* Dr. Phillip Zamore

_____

Dr. David Van Vactor, Program Head

*Date:* October 21, 2013

_____

Dr. David Lopes Cardozo, Director of Graduate Studies

# Regulation of Stem Cell Metabolism by the *Lin28/let-7* Axis

A dissertation presented

by

**Shyh Chang Ng**

to

**The Division of Medical Sciences**

in partial fulfillment of the requirements

for the degree of

Doctor of Philosophy

in the subject of

Biological and Biomedical Sciences

Harvard University

Cambridge, Massachusetts

October 2013

Dissertation Adviser: George Q. Daley Shyh Chang Ng

**Regulation of Stem Cell Metabolism by the *Lin28/let-7* Axis**

## Abstract

This thesis is focused on two fundamental aspects of stem cell metabolism: (1) the role of Lin28 in programming stem cell metabolism, and (2) how metabolism in turn fuels and governs pluripotency. Our studies led us to discover that the stem cell factor *Lin28a* promotes organismal overgrowth by enhancing glucose metabolism in mice, corroborating discoveries that *LIN28B* polymorphisms influence human height. Subsequently, we discovered that the *Lin28/let-7* pathway controls glucose metabolism by orchestrating the upregulation of multiple components of the insulin-PI3K-mTORsignaling pathway, particularly in skeletal muscle. Since *let-7* accumulates with aging, our discoveries suggest that antagonism of *let-7* could represent a new strategy for treating insulin resistance and type 2 diabetes. During these studies, we also observed that *Lin28a* enhances tissue regeneration when expression is reactivated in adult tissues. Regeneration capacity has long been known to decline with aging, but why juvenile organisms show enhanced tissue repair has been unexplained. We found that *Lin28a* reactivation improved the regrowth of skin, hair, cartilage, bone and mesenchyme after injuries. *Let-7* repression was necessary but insufficient to explain these phenotypes. In parallel, *Lin28a* bound to and enhanced the translation of mRNAs for several oxidative enzymes, thereby increasing OxPhos. *Lin28a*-mediated tissue repair was negated by OxPhos inhibition, whereas a pharmacologically-induced increase in OxPhos promoted wound repair. Thus, *Lin28a*

enhanced tissue regeneration in adults by reprogramming cellular bioenergetics. My interest in the central principles of stem cell metabolism also led us to map the metabolic pathways associated with pluripotency during somatic cell reprogramming and *Lin28/let-7* perturbation. Surprisingly, we found that Thr-Gly-S-adenosylmethionine (SAM) metabolism consistently showed the best correlation with pluripotency. $^{13}$Carbon isotope metabolomics further revealed that Thr was catabolized to generate Gly and acetyl-CoA, and ultimately SAM - essential for all methylation reactions. Thr is required for SAM and histone H3K4 methylation in mouse ESCs, thus regulating the open euchromatin and pluripotency of ESCs. Our study shed light on a novel amino acid pathway in stem cells, and demonstrated that metabolic conditions can direct cell fate. In summary, my work has helped us to understand how we can reprogram and manipulate metabolic networks to regulate stem cell homeostasis.

## Table of Contents

**Table of Figures**

## List of Tables

**Acknowledgements**

Completing my PhD thesis would have been impossible without the help and support from my mentors, lab-mates, friends and family.

Right from day one, my mentor Prof. George Daley has been teaching me to think big. “Think of a *really* big problem”, he said, “Then *grab* it by the horns and tackle it.” I have strove to make that my approach to science ever since! From my happy days of playing around ideas of what I wanted to work on during rotations, to the exhilarating years of discovering the roles of Lin28 in stem cell metabolism and tissue repair, to the painful months of struggling with harsh reviewers, then finally the sweet crescendo towards publications and graduation – George has always been supportive of my myriad ideas, and guiding me to see them through even when I thought it was impossible. I know this is a rare privilege for a PhD student, uncommon even in Harvard. I want to sincerely thank him for providing me these opportunities and trusting me to shoulder these projects. It was a blast! George is also my role model in his fearless leadership, his superhuman energy, his electric charisma, and his passion for life - be it risottos, wine, skiing, or karaoke. He has been awe-inspiring. It makes me want to live up to his brilliant example.

My co-mentor and dissertation chair, Prof. Lewis Cantley, moulded the other half of my PhD training. Watching him think about science is literally like watching a wizard at work sometimes. His effusive energy for scientific ideas (day or night), his rebelliousness against convention, and his uncanny speed at tearing through the morass of data to see connections between seemingly unrelated observations at the biochemical level, never fail to astonish me. Every lab meeting I try to best Lew at it, and every lab meeting I fail

miserably. But that is what makes lab meeting with him such great fun, something we look forward to every time! It is leadership by example. He has set an incredibly high bar for scientific originality, curiosity, and rigor. A bar that I have sworn I will keep training and trying to cross. Another high bar that Lew has set, is for partying. He works hard, but plays *even* harder with us. Yet despite such sheer intensity, Lew is also one of the nicest people I have ever had the privilege of working with. I want to thank him for taking me under his wings as well, teaching me his values, inspiring me to greater heights than I had ever imagined, and imparting to me an amazing example of the scientific life.

I am incredibly humbled and proud to have both George and Lew as my mentors for life.

I also want to thank all my Daley lab colleagues and Cantley lab colleagues for their great camaraderie and helping me along this journey. Special thanks to my buddies in the Lin28 subgroup, aka the “Honey Badgers”. Especially Hao Zhu, my long-time collaborator, friend, and big brother, and also Michael Kharas, Harith Rajagopalan, Gen Shinoda, John Powers, Kaloyan Tsanov, Sutheera Ratanasirintrawoot ‘Mam’, Alena Yermalovich, Tarja Yvanka de Soysa, Marc Seligson, Samar Shah, Will Einhorn, and Mathew Lensch ‘Willy’. Also huge thanks to my buddies in the Cantley lab, especially Costas Lyssiotis, Jason Locasale, Jihye Yun, Edouard Mullarky, Hye Seok Shim, Yuxiang Zheng, Hai Hu, Hui Liu, Ning Wu, Min Yuan, and John Asara. They have all become my friends for life.

Finally, I want to thank my family. My parents, especially, for letting their only son run so far away from our home in Singapore – for 8 years – to pursue his dreams of becoming a scientist. My father’s faith and my mother’s support have fueled me throughout my

journey. And most importantly, my wife Rachel Wang whom I married while at Harvard. Over the past 6 years, Rachel has become my closest friend, confidante, partner and lover. Together, we've helped each other withstand numerous trials – from little things like suffering experimental failures in our PhD work – to bigger things like surviving the Boston Marathon terrorist attack. And we kept emerging stronger from every trial and tribulation. I want to thank Rachel for understanding my workaholism, encouraging my passions, and fighting alongside me. I would not have done it without her.

## Chapter 1: Lin28, A Primal Regulator of Growth and Metabolism in Stem Cells

### Introduction

A central question in stem cell biology is whether common factors exist to define "stemness" in multiple tissue lineages. Arguably, one such candidate is the RNA-binding protein Lin28, which was first identified in the nematode *C. elegans* through screens for *lineage*-modifying genes that alter developmental timing, or heterochrony (*lin-28*; Ambros and Horvitz 1984). Two other prominent heterochronic genes, *lin-4* and *let-7*, were the first microRNAs to be discovered, and both directly repress *lin-28* to suppress heterochronic reiterations of cell lineages. Heterochronic "reiteration" of nematode progenitor cells, as *C. elegans* geneticists first observed, was strongly reminiscent of mammalian stem cell self-renewal (Chalfie et al. 1981; Ambros and Horvitz 1984).

This connection was reinforced by the discovery that mouse embryonic stem cells (ESCs) express high levels of mammalian Lin28, which decrease upon differentiation (Moss and Tang 2003). Successful reprogramming of human fibroblasts into induced pluripotent stem cells (iPSCs) using Lin28, along with Oct4, Sox2, and Nanog, further corroborated its role in pluripotent stem cells (Yu et al. 2007), but the mechanism of action for Lin28 remained unclear. A subsequent flurry of studies showing that Lin28 directly inhibits *let-7* maturation in ESCs rapidly validated Lin28's function in ESC self-renewal (Viswanathan et al. 2008; Rybak et al. 2008; Heo et al. 2008; Newman et al. 2008). With the discovery that Lin28 is also important in cancer, the germ lineage, and cellular metabolism (Viswanathan et al. 2009; West et al. 2009; Zhu et al. 2011), understanding the role of Lin28 in stem cells during development and disease pathogenesis has emerged as a new field of research. In this Review, we will discuss

the Lin28 pathway and its complex molecular mechanisms, outline its known roles in stem cells, tissue development, and pathogenesis, and examine its ramifications for re-engineering mammalian physiology.

## Lin28/*let-7:* A Conserved Bistable Switch

Current insights into Lin28 rest heavily on precedents in *C. elegans* genetics. *Lin-28* was first discovered through mutagenesis screens for heterochronic genes (Horvitz and Sulston 1980; Sulston and Horvitz 1981; Ambros and Horvitz 1984). Loss-of-function in *lin-28* accelerates differentiation of the hypodermal and vulval progenitor cells (called seam cells and VPCs respectively in nematodes). In contrast, gain-of-function in *lin-28* promotes self-renewal and delays differentiation of the hypodermal and vulval progenitor cells, leading to proliferation of hypodermal progenitors and a cell-cycle delay in vulval progenitors (Moss et al. 1997). *Lin-28* is highly expressed during embryogenesis and during early larval development in the hypodermal, neural and muscle cells, but gradually diminishes and disappears by adulthood.

Two heterochronic microRNAs (miRNAs) repress *lin-28* post-transcriptionally via direct binding sites in its 3' UTR: *lin-4* and *let-7* (Reinhart et al. 2000; Pasquinelli et al. 2000; Roush et al. 2008). Although the canonical *let-7* is only expressed late in larval development to drive the transition to adulthood, three *let-7* homologs (*mir-48, mir-84* and *mir-241*) display overlapping expression with *lin-28*. Indeed, loss-of-function in these *let-7* homologs phenocopied *lin-28* gain-of-function in the hypodermal progenitors, and *lin-28* was epistatic to the three *let-7* homologs (Abbott et al. 2005). Mutation of the *let-7* binding site in the *lin-28* 3' UTR also led to an increase in *lin-28* 3' UTR-lacZ

reporter expression (Morita and Han 2006), suggesting that *let-7* binding contributes to *lin-28* repression, and underlies their opposing roles in regulating differentiation.

The role of *lin-28* in mammalian stem cells was less clear until quite recently. The first glimpse of a connection came from the discovery that the mammalian *lin-28* ortholog is highly expressed in mouse ESCs and human embryonal carcinoma cells (Moss and Tang 2003). The connection was further validated when human Lin28 was used with Oct4, Sox2 and Nanog to reprogram human somatic fibroblasts into pluripotent stem cells (Yu et al. 2007). Around the same time, a post-transcriptional mechanism was proposed to be responsible for the dramatic disparity between high levels of pri-*let-7* transcript and the deficiency of mature *let-7* microRNA in early mouse embryos and ESCs (Thomson et al. 2006; Wulczyn et al. 2007). These two lines of inquiry rapidly converged through a flurry of studies that showed that Lin28 (now routinely termed Lin28a) and its paralog Lin28b directly inhibit the post-transcriptional maturation of *let-7* in ESCs (Viswanathan et al. 2008; Rybak et al. 2008; Heo et al. 2008; Newman et al. 2008). A generally similar mechanism was later verified to be conserved in *C. elegans* (Lehrbach et al. 2009; Van Wynsberghe et al. 2011). Since Lin28a/b inhibit the biogenesis of *let-7* microRNAs, which in turn repress Lin28a/b expression, it became clear that this bistable switch represents a central mechanism that governs stem cell self-renewal from worms to mammals.

**Molecular Mechanisms of Lin28 Function**

Following the discovery that Lin28a/b represses *let-7* biogenesis, several groups set about to determine the detailed biochemical mechanisms underlying *let-7* repression as a model for understanding miRNA biogenesis. Similar to the biogenesis of other miRNAs, *let-7* is first transcribed as part of long pri-*let-7* transcripts in the nucleus (Roush et al. 2008). Within the pri-*let-7* transcripts is a hairpin structure that is the precursor miRNA (pre-*let-7*). Drosha, in complex with its RNA-binding cofactor DGCR8, cleaves and releases the ~70 nt hairpin structure to produce pre-*let-7*. Like other pre-miRNAs, pre-*let-7* is then thought to be exported from the nucleus into the cytoplasm by exportin-5, although the majority of pre-*let-7* species lack the 3' two-nucleotide overhang that exportin-5 presumably needs to export pre-miRNAs (Heo et al. 2012; Yi et al. 2003), suggesting that another mechanism might serve this function. In the cytoplasm, pre-*let-7* is further processed by Dicer to produce a 22-nt double-stranded RNA duplex. Mature single-stranded *let-7* is then incorporated from the duplex into the RNA-induced silencing complex (RISC) to target mRNAs for translation inhibition and/or degradation in P-bodies (Figure 1.1).

In a multi-pronged fashion, Lin28a/b binds to both pri-*let-7* and pre-*let-7*, effectively sabotaging the post-transcriptional processing of *let-7* (Viswanathan et al. 2008; Rybak et al. 2008; Heo et al. 2008; Newman et al. 2008). X-ray crystallography studies further revealed that Lin28a binds pre-*let-7* at the terminal loop and at the bulge GGAG motif where Dicer cleaves (Nam et al. 2011). Lin28a also recruits Tut4 (Zcchc11), a cytoplasmic terminal uridylyl transferase, to oligo-uridylate pre-*let-7* and prevent its

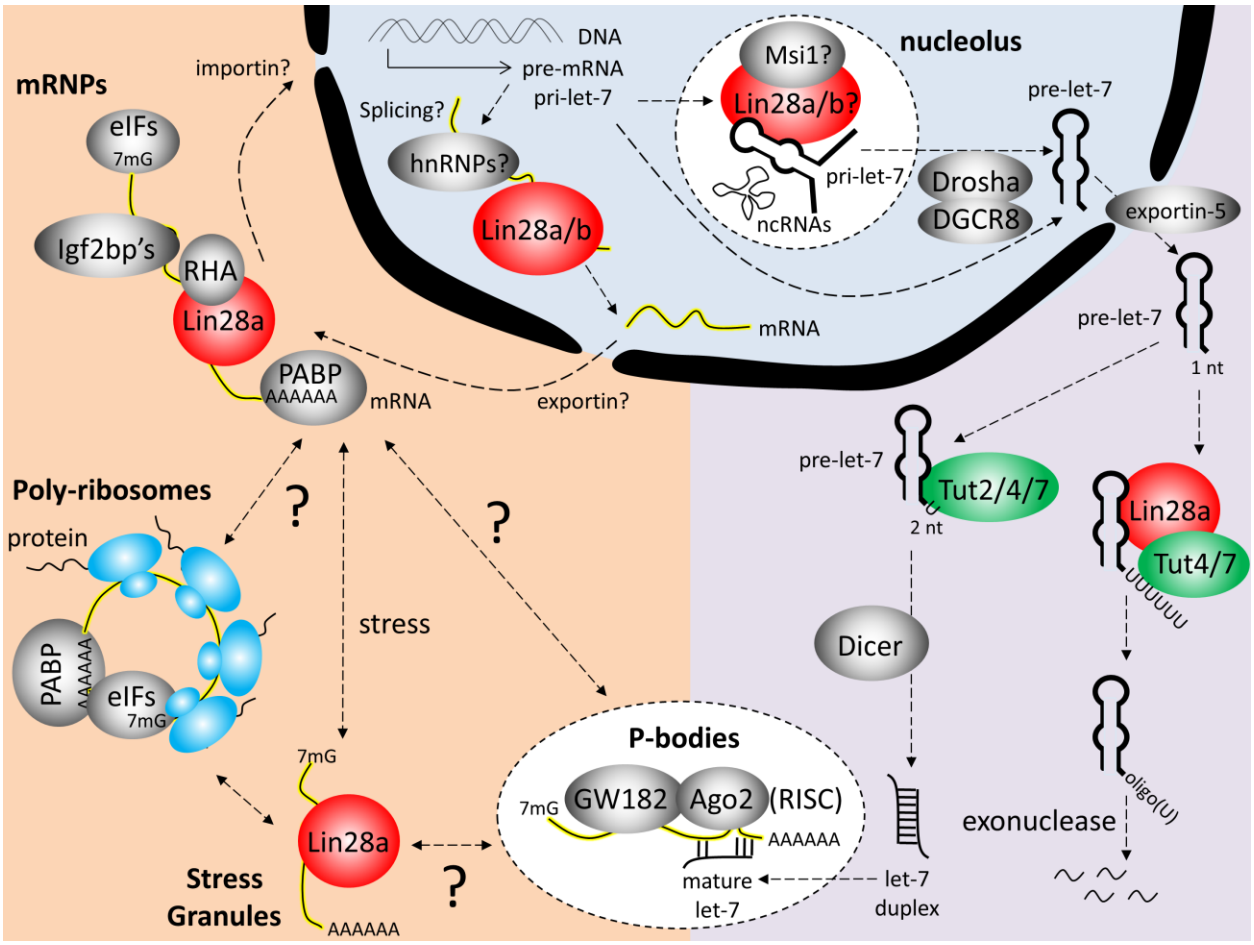


***Figure 1.1: Overview of Molecular Mechanisms Underlying Lin28 Function.***

Both Lin28a and Lin28b have been observed to shuttle between the nucleus and cytoplasm, binding both mRNAs and pri-/pre-*let-7*. In the nucleus, Lin28a/b could potentially work in tandem with the heterogeneous nuclear ribonucleoproteins (hnRNPs) to regulate splicing, or with Musashi-1 (Msi1) to block pri-*let-7* processing. In the cytoplasm, Lin28a recruits Tut4/7 to oligo-uridylate pre-*let-7*, and block Dicer processing to mature *let-7* miRNA (right, violet). Lin28a also recruits RNA helicase A (RHA) to regulate mRNA processing in messenger ribonucleoprotein (mRNP) complexes, in tandem with the Igf2bp's, poly(A)-binding protein (PABP), and the eukaryotic translation initiation factors (eIFs). In response to unknown signals and stimuli, the mRNAs are

***Figure 1.1 (continued)*** either shuttled into poly-ribosomes for translation, stress granules for temporary sequestering, or P-bodies for degradation, in part via miRNAs and the Ago2 endonuclease (left, orange).

processing by Dicer (Heo et al. 2009; Hagan et al. 2009). Recent studies have further elaborated on this mechanism, suggesting that Tut7 (Zcchc6) is a redundant homolog of Tut4 that can also oligo-uridylate pre-*let-7* in the presence of Lin28a (Thornton et al. 2012; Heo et al. 2012). In contrast, when Lin28a is absent, Tut4/7 or Tut2 (Papd4/Gld2) mono-uridylates pre-*let-7*'s at their 3' one-nucleotide overhang to generate a two-nucleotide overhang, thereby enabling their processing by Dicer (Heo et al. 2012). Thus, one would expect oligo-uridylated pre-*let-7* to accumulate when pri-*let-7,* Lin28a and Tut4/7 are present. But this is not observed, suggesting that an unknown nuclease must exist to degrade oligo-uridylated pre-*let-7*'s (Heo et al. 2008, 2009), and/or that Lin28 can sequester pri-*let-7*'s to prevent further processing (Viswanathan et al. 2008; Newman et al. 2008). Indeed, a study suggests that Lin28b is predominantly localized in the nucleolus where it can sequester pri-*let-7* away from Drosha/DGCR8 processing, whereas Lin28a is predominantly localized in the cytoplasm where it can recruit Tut4 to oligo-uridylate pre-*let-7* and prevent Dicer processing (Piskounova et al. 2011). However, mammalian Lin28a/b and *C. elegans* lin-28 can all enter the nucleus as well as the cytoplasm (Moss et al. 1997; Guo et al. 2006; Balzer and Moss 2007; Heo et al. 2008; Piskounova et al. 2011; Van Wynsberghe et al. 2011; Vogt et al. 2012; Hafner et al. 2013). Moreover, all three proteins possess a putative nucleolar localization signal, and all three proteins can bind to both pri- and pre-*let-7* (Viswanathan et al. 2008;

Rybak et al. 2008; Heo et al. 2008; Newman et al. 2008; Lehrbach et al. 2009; Van Wynsberghe et al. 2011). Thus, the mode of regulation of this division of labor between Lin28a and Lin28b remains unclear (Figure 1.1).

Under different conditions of metabolic stress in embryonal carcinoma cells and myoblasts, Lin28a localizes specifically to cytoplasmic stress granules where mRNAs are sequestered and mRNA translation is temporarily stalled (Balzer and Moss 2007; Polesskaya et al. 2007). Under normal growth conditions, cytoplasmic Lin28a can directly or indirectly associate with translation initiation factors eIF3B and eIF4E, elongation factors EF1α and EF1α2, ribosomal proteins, poly(A)-binding protein (PABP), Igf2bp1/2/3, Musashi1 (Msi1) and RNA helicase A (RHA) in messenger ribonucleoprotein (mRNP) complexes to regulate mRNA translation (Balzer et al. 2007; Polesskaya et al. 2007; Jin et al. 2011). When point mutations are introduced into the RNA-binding motifs, Lin28a localizes to the nucleus (Balzer and Moss 2007). These findings suggest a model in which Lin28a regulates the post-transcriptional processing of its mRNA targets, perhaps by first binding them in the nucleus and subsequently shuttling them between ribosomes, P-bodies or stress granules for translational regulation, depending on the environmental conditions. It would be interesting to know which factors sense the environmental conditions to regulate this shuttling of Lin28a, and whether these conditions alter the RNAs bound by Lin28a (Figure 1.1). One study, for example, suggests that retinoic acid-induced differentiation of ESCs triggers Msi1 expression, which recruits Lin28a to the nucleus to sequester and inhibit pri-*miR-98* but not pri-*let-7b* (Kawahara et al. 2011). But what else could Lin28a/b be doing in the nucleus? Nuclear Lin28 could also regulate the alternative splicing of pre-mRNAs, or

processing of small nucleolar RNAs (snoRNAs) and long non-coding RNAs (lincRNAs) to generate greater RNA diversity. The likelihood for this additional role is supported by the RNA-dependent association between Lin28a protein and nuclear splicing factors like hnRNP F and hnRNP H1 (Polesskaya et al. 2007), and its direct regulation of splicing factors and snoRNAs (Wilbert et al. 2012; Hafner et al. 2013). How these various RNA-processing mechanisms relate to stem cell self-renewal and plasticity in response to environmental changes remains an important avenue for future research.

**Regulatory Signals Upstream of Lin28**

Throughout their lifespan, stem cells must decide whether to self-renew, proliferate, differentiate or die. The regulation of stem cell homeostasis is a complex process that involves integrating intrinsic and extrinsic signals, so that stem cells can correctly adapt to the environment. The central role of the Lin28/*let-7* bistable switch in governing stem cell self-renewal raises the provocative question: what signaling pathways converge upstream to regulate the switch?

In *C. elegans*, an important intrinsic signal upstream of *lin-28* that regulates hypodermal progenitor self-renewal is the microRNA *lin-4*. In vertebrates, *lin-4* is conserved as *miR-125a* and *miR-125b* (Lagos-Quintana et al. 2002). Vertebrate *miR-125/lin-4* has been shown to be critical for regulating processes as disparate as neurogenesis, somitogenesis, hematopoiesis, myogenesis and epidermal stem cell self-renewal (Rybak et al. 2008; Le et al. 2009a; Le et al. 2009b; Klusmann et al. 2010; Bousquet et al. 2010; O'Connell et al. 2010; Ooi et al. 2010; Ge et al. 2011; Zhang et al. 2011; Guo

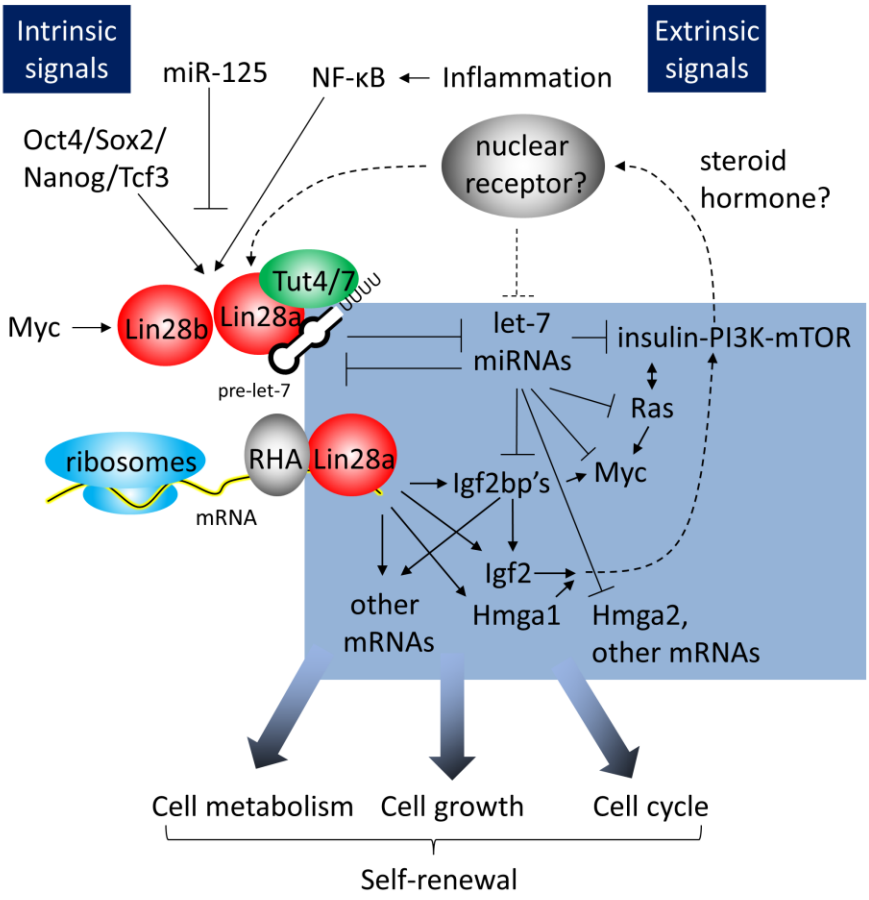


***Figure 1.2: Signals Upstream and Targets Downstream of Lin28.***

The *lin-4* homolog *miR-125a/b* represses both Lin28a and Lin28b during stem cell differentiation. The core pluripotency transcription factors Oct4, Sox2, Nanog and Tcf3 can activate *Lin28a* transcription in ESCs and iPSCs, whereas the growth regulator Myc and the inflammation-/stress-responsive NF-κB can transactivate *Lin28b*. A putative steroid hormone-activated nuclear receptor, conserved from *C. elegans daf-12*, might also regulate both Lin28a/b and *let-7* expression. Downstream of Lin28a/b, the *let-7* family represses a network of proto-oncogenes, including the insulin-PI3K-mTOR pathway, Ras, Myc, Hmga2, and the Igf2bp's. At the same time, Lin28a can also directly bind to and regulate translation of mRNAs, including Igf2bp's, Igf2, Hmga1, and mRNAs

***Figure 1.2 (continued)*** encoding metabolic enzymes, ribosomal peptides, and cell-cycle regulators. Together, this broad network of targets allows Lin28 to program both metabolism and growth to regulate self-renewal.

Guo et al. 2010; Chaudhuri et al. 2012). During these developmental processes, *miR-125/lin-4* appears to regulate stem cell self-renewal and progenitor differentiation by repressing a variety of different targets, including Lin28a/b, as well as the p53 network (Le et al. 2011). In mammalian ESCs, the pluripotency factors Oct4, Sox2, Nanog and Tcf3 have also been shown to regulate the transcription of *Lin28a* (Marson et al. 2008). Amongst these pluripotency factors, Sox2 appears to be the most critical for regulating *Lin28a* expression, based on Bayesian probabilistic network modeling of single-cell gene expression data during iPS reprogramming (Buganim et al. 2012). Interestingly, Sox2 directly binds to Lin28a in a nuclear protein-protein complex, suggesting a close relationship between Sox2 and Lin28a in pluripotency (Cox et al. 2010). Repression of the Dot1L H3K79 histone methyltransferase upregulates *Lin28a* during reprogramming, although the mechanism is indirect via mesenchymal regulators downstream of TGFβ signaling (Onder et al. 2012). Finally, c-Myc and NF-κB transactivate *Lin28b* in transformed cancer cells (Chang et al. 2009; Iliopoulos et al. 2009), suggesting that *Lin28a* and *Lin28b* possess distinct cis-regulatory elements to drive their transcription (Figure 1.2). Beyond these studies, relatively little is known about the transcription factors that regulate *Lin28a* and *Lin28b* expression during mammalian development, and further investigation is warranted.

The *C. elegans* nuclear receptor *daf-12* feeds extrinsic signals from steroid hormones to *lin-28* and *let-7*, to regulate diapause or dauer arrest (Antebi et al. 1998, 2000; Gerisch et al. 2007; Bethke et al. 2009; Hammell et al. 2009). Although this mechanism is well-characterized in *C. elegans* development, and a similar ecdysone-*let-7* mechanism operates in *Drosophila* metamorphosis (Sokol et al. 2008; Chawla et al. 2012), it is unclear if a similar mechanism exists to hormonally regulate the Lin28/*let-7* switch in mammals (Figure 1.2). Studies have shown that the homologous retinoic acid receptors and estrogen receptor α regulate *let-7* expression in vitro (Thomson et al. 2006; Wulczyn et al. 2007; Gehrke et al. 2010; Schulz et al. 2011; Bhat-Nakshatri et al. 2009), but both the directness and the physiological relevance of these mechanisms remain to be shown. It would also be interesting to test if any of the nuclear hormone receptors implicated in pluripotency and especially the naïve state (Feng et al. 2009; Heng et al. 2010; Guo and Smith 2010; Wang et al. 2011; Martello et al. 2012), a state associated with rodent diapause (Nichols et al. 2001, 2009), also regulates the Lin28/*let-7* switch (Figure 1.2).

**Coordinate Regulation of Metabolism and Cell Cycle by Targets of Lin28**

Given our wealth of understanding of the upstream regulators of *lin-28* in worms, it is surprising that relatively little was discerned about the downstream RNA targets in the *C. elegans* literature. It was only after the discovery that *lin-28* directly binds to and represses pre-*let-7*, that the more well-known *let-7* targets could be placed downstream of *lin-28.* Only some of these *let-7* targets are known to be conserved in mammals, including *lin-41* (Trim71), *let-60* (Ras), and Lin28 itself. The regulation of *NRAS* and *KRAS* by *let-7* in human cancer cells has led to the proposal that *let-7* functions as a

tumor suppressor in humans (Johnson et al. 2005). Indeed, a network of *let-7* targets involving numerous other proto-oncogenes has been uncovered in mammalian cells, including Myc, Hmga2, Igf2bp's, cyclins (Sampson et al. 2007; Mayr et al. 2007; Lee et al. 2007; Johnson et al. 2007; Yu et al. 2007; Boyerinas et al. 2008; Iliopoulos et al. 2009; Legesse-Miller et al. 2009; Chang et al. 2012), and components of the insulin-PI3K-mTOR pathway like Igf1r, Insr, Irs2, Akt2 and Rictor (Zhu et al. 2011; Frost and Olson 2011). These studies fit with the suggestion that Lin28a/b function as oncogenes in multiple cancers by repressing the *let-7* network (Viswanathan et al. 2009). A majority of these studies, however, were conducted in vitro and many of these claims still await validation in vivo through *Lin28a/b* or *let-7* mouse models.

Adding a second layer of complexity downstream of *Lin28*, some studies have shown that Lin28a directly binds to many mRNAs, including *Igf2* in myoblasts and neural progenitors, and *cyclin A/B* in ESCs, to directly enhance their translation independently of *let-7* (Polesskaya et al. 2007; Xu et al. 2009; Balzer et al. 2010). Genome-wide RNA-immunoprecipitation studies further reveal thousands of mRNA targets bound directly by Lin28. In human ESCs and cancer cells, LIN28A directly binds and promotes the mRNA translation of numerous metabolic enzymes, ribosomal peptides, cyclins as well as splicing factors (Peng et al. 2011; Li et al. 2012; Wilbert et al. 2012; Hafner et al. 2013). Curiously, in mouse ESCs, Lin28a was also recently found to bind and subtly repress the ribosomal occupancy of numerous membrane protein mRNAs (Cho et al. 2012). Given the plethora of mRNA targets that are emerging for Lin28a, including nearly 50% of the human transcriptome in one study (Cho et al. 2012), an important task lying ahead is to determine whether all these targets or only a subset contribute to the Lin28

phenotypes observed in vivo. Such an undertaking might require a return to the powerful genetics of *C. elegans* to search for conserved mRNA targets of *lin-28*. This idea is supported by the finding that *let-7*-independent mechanisms must account for the *lin-28* phenotype in *C. elegans* as well (Vadla et al. 2012).

Several key insights into Lin28 function are emerging from the small set of well-validated targets, most notably that Lin28 coordinates both proliferative growth and metabolism. Lin28a/b can upregulate a large number of cell-cycle regulators through *let-7* repression, including *Myc, Ras, cyclin D1/2, Cdk6, Cdc25a, Cdc34, Trim71* (which represses $p21^{Cip1}$), *Hmga2* (which represses $p16^{Ink4a}$ and $p19^{Arf}$) and PI3K/Akt signaling (Johnson et al. 2005; Sampson et al. 2007; Johnson et al. 2007; Chang et al. 2012; Mayr et al. 2007; Nishino et al. 2008; Zhu et al. 2011). A recent study even suggested that *let-7* can directly bind to and silence Rb1/E2F target genes via heterochromatin during senescence (Benhamed et al. 2012). Lin28a also directly binds and promotes the translation of mRNAs encoding *cyclin A/B/D, Cdk1/2/4*, *Cdc2* and *Cdc20,* thereby coordinating the cell-cycle at multiple checkpoints (Xu et al. 2009; Li et al. 2012; Hafner et al. 2013). Besides the cell-cycle, Lin28a/b might also control cellular growth by regulating ribosomal synthesis of proteins. Lin28a directly binds to the mRNAs of numerous ribosomal peptides in human ESCs (Peng et al. 2011). In addition, Lin28a/b increases mTOR signaling via *let-7* (Zhu et al. 2011; Frost and Olson 2011), which can activate ribosomal biogenesis and translation in many contexts. In parallel with its extensive control of cell-cycle and cell growth regulators, Lin28a/b appears to also coordinate cellular metabolism, both via *let-7* and by directly stimulating mRNA translation. Through *let-7*, Lin28a/b upregulates the insulin/PI3K, Ras and Myc

pathways – all of which are oncogenic regulators of metabolism (Vander Heiden et al. 2009; Dang 2011). By directly binding mRNAs and influencing translation of the Igf2bp's, Igf2, glycolysis enzymes, and mitochondrial enzymes, Lin28a can directly potentiate cellular metabolism (Zhu et al. 2011; Peng et al. 2011; Polesskaya et al. 2007; Janiszewska et al. 2012; Hafner et al. 2013). *Hmga1,* another mRNA target of Lin28a, can also upregulate insulin/PI3K signaling (Liau et al. 2006; Chiefari et al. 2011; Peng et al. 2011). Given how growth signaling pathways are intertwined with cellular metabolism, it is perhaps not surprising that Lin28 would have to program both arms of genes to regulate self-renewal. Thus a model is emerging, albeit an inchoate one, whereby Lin28 programs both metabolism and proliferative growth to regulate stem/progenitor cell self-renewal (Figure 1.2).

**Lin28 in Embryonic Stem Cell Metabolism**

The functional role of Lin28 in cellular metabolism is evidenced by recent studies in ESCs. Recent work has shown that aerobic glycolysis, akin to the Warburg effect in cancer, is critical to ESCs and iPSCs (Zhu et al. 2010b; Folmes et al. 2011). This is perhaps not surprising, given the high proliferative capacity of ESCs, and the importance of glycolysis in providing carbon intermediates for anabolic growth (Vander Heiden et al. 2009). What is surprising is that some studies have shown that mitochondrial oxidative metabolism is also critical to ESCs (Wang et al. 2009; Alexander et al. 2011; Zhang et al. 2011b), despite the immature morphology of ESC mitochondria. Interestingly, Lin28a binds to a large number of mRNAs encoding mitochondrial enzymes in human ESCs (Peng et al. 2011). One possibility is that ESC mitochondrial oxidation could be operating to recycle mitochondrial $NAD^+$ and keep the

Krebs cycle running in order to generate fatty acids and various amino acids for ESCs (Shyh-Chang et al. 2011). Curiously, mouse ESCs uniquely rely upon mitochondrial oxidation of threonine (Thr) into glycine (Gly), via threonine dehydrogenase (Tdh), to generate one carbon/folate intermediates to fuel rapid nucleotide synthesis (Wang et al. 2009). This seminal early work led to findings that the 5-methyl-THF generated by mitochondrial Thr oxidation also fuels the synthesis of S-adenosyl-methionine (SAM) to regulate histone H3K4 methylation and the pluripotency of ESCs (Shyh-Chang et al. 2013a). Surprisingly, *Lin28a* overexpression in ESCs leads to a dramatic accumulation of many metabolites in the Thr-Gly-SAM pathway, whereas overexpression of *let-7* reduces the abundance of these metabolites, suggesting that the Thr-Gly-SAM pathway is at least indirectly regulated by the Lin28/*let-7* switch to maintain ESC self-renewal. These findings might also have relevance to cancer, since lung cancer stem cells have been found to express and depend upon high levels of both Lin28b and glycine decarboxylase (Gldc) in the Thr-Gly pathway to initiate tumorigenesis (Zhang et al. 2012). In fact several enzymes in Gly metabolism have recently been implicated in human tumorigenesis (Locasale et al. 2011; Possemato et al. 2011; Jain et al. 2012). Lin28 could thus potentially regulate glucose and amino acid metabolism in a variety of stem and progenitor cells, both normal and malignant (Shyh-Chang et al. 2013b).

**Lin28 in Early Embryogenesis, Pluripotent Stem Cells and Reprogramming**

The earliest phases of embryogenesis feature high levels of Lin28a due to protein inheritance through the maternal oocyte. From the mouse zygote to the pre-implantation blastocyst, Lin28a is exclusively localized in the nucleolus where it is thought to regulate nucleolar maturation (Vogt et al. 2012). Morpholino knockdown of Lin28a in the zygote

produces defects in nucleolar morphology and developmental arrest at the 2-cell and 4-cell stages, suggesting that Lin28a is required for proper nucleolar genesis and function and early embryogenesis. Curiously, Lin28a is localized in the nucleolus of mouse ESCs as well, but not primate ESCs (Vogt et al. 2012). Given that Lin28a is an RNA-binding protein, these observations suggest that maternal Lin28a might also be involved in ribosomal RNA processing in the nucleolus to regulate zygotic genome activation during the maternal-zygotic transition, although this remains speculative.

After zygotic genome activation, mammalian blastocysts show high levels of *Lin28a* and *Lin28b* transcription in the pluripotent cells of the inner cell mass (ICM) and epiblast and their in vitro correlates – the indefinitely self-renewing ESCs. Studies suggest that Lin28a/b acts as a repressor of *let-7* microRNAs to prevent premature differentiation in the pluripotent ICM and epiblast (Suh et al. 2010; Melton et al. 2010). When the pluripotent ICM is cultured in vitro for ESC derivation, Lin28a is further upregulated, in parallel with acquisition of indefinite self-renewal capacity in vitro (Tang et al. 2010). Furthermore, overexpression of Lin28a with a cocktail of the core pluripotency-associated transcription factors Oct4, Sox2 and Nanog, helps promote reprogramming of human somatic fibroblasts into indefinitely self-renewing iPSCs (Yu et al. 2007; Hanna et al. 2009). These data suggest that Lin28a is critical to pluripotent stem cell self-renewal.

But is Lin28 also required for pluripotency? Lin28 knockout mouse models suggest the answer is no. *Lin28a* knockout mice progress through the blastocyst stage without obvious developmental defects in utero, although they weigh 20% less at birth (Zhu et

al. 2010). *Lin28b* knockout mice are viable and fertile. Thus Lin28a/b do not appear to be essential for pluripotency per se, in vivo.

Do pluripotent stem cells then require Lin28a/b for indefinite self-renewal? The answer depends on the context, since overexpression of mature *let-7* does not inhibit mouse ESC self-renewal unless DGCR8 is knocked out and miRNA biogenesis is prevented (Melton et al. 2010). Another class of miRNAs called the miR-290 family can respond to and compensate for the effects of *let-7* overexpression. Although the breadth of genes targeted by the miR-290 family, and the connections with Lin28a/b (if any) remain unclear, it is thought that *let-7* promotes ESC differentiation in the absence of DGCR8 by directly repressing *Sall4, Nmyc,* and *Lin28a*. Conversely, Lin28a or Lin28b knockout in the presence of DGCR8 should not lead to defects in self-renewal via *let-7* upregulation alone, even if we ignore the compensatory redundancy observed between Lin28a and Lin28b (Wilbert et al. 2012). RNAi against Lin28, however, does lead to proliferative defects in both mouse and human ESC (Xu et al. 2009; Peng et al. 2011), suggesting that Lin28a/b might synergistically promote ESC self-renewal through a combination of *let-7* repression and *let-7*-independent mechanisms such as direct binding of mRNAs involved in metabolism and growth. Thus it will also be interesting to see if Lin28a/b double knockout leads to defects in ESC self-renewal. On the other hand, *let-7* knockdown in fibroblasts promotes iPS reprogramming (Melton et al. 2010), suggesting that Lin28a might promote self-renewal via repression of *let-7* during iPS reprogramming, without compensatory effects from ESC-specific *miR-290*. Indeed, studies have shown that Lin28a can accelerate the early stochastic phase of iPS reprogramming by accelerating the cell-cycle, and that Lin28a is one of the earliest

markers of the deterministic phase of iPS reprogramming after endogenous Sox2 expression is induced (Hanna et al. 2009; Buganim et al. 2012; Golipour et al. 2012). It remains to be verified, however, whether *let-7* is the relevant target of Lin28a during reprogramming, and what downstream targets of *let-7* drive iPS reprogramming. It is also unknown whether Lin28/*let-7* is implicated in the much more rapid and deterministic process of reprogramming by somatic cell nuclear transfer (SCNT).

**Lin28 in Normal and Transformed Tissue Progenitors**

Contrary to popular belief, Lin28a/b's expression and influence on development is far from unique to pluripotent cells in the blastocyst ICM, but rather extends to a variety of tissues. For instance, the trophoblast and the resultant placental tissues show high levels of Lin28a/b. Studies suggest that the high Lin28a levels in trophoblast stem cells decrease to permit differentiation into trophoblast giant cells (Fromme et al. 2009; Winger et al. 2010), and Lin28a levels increase again during the invasive phase of placenta development to regulate cell migration (Seabrook et al., 2011). Moreover, the LIN28B locus shows imprinting and paternal monoallelic expression in the human placenta (Barbaux et al. 2012). However the placental function of Lin28 remains unclear in vivo.

Germline stem cells also retain high levels of Lin28 expression during mammalian development. Lin28a promotes primordial germ cell (PGC) specification via *let-7* regulation of the master regulator Blimp1 (West et al. 2009), and remains high specifically in the spermatogonial stem cells of adult male testes (Zheng et al. 2009). Both Lin28a knockout and *let-7* overexpression led to a reduction in PGCs during

embryogenesis, and a reduction in proliferating spermatogonia and germ cells before adulthood (Shinoda et al., 2013). Interestingly, aberrant overexpression of Lin28a/b is associated with the malignancy of human germ cell tumors, such as choriocarcinomas, embryonal carcinomas, seminomas, yolk-sac tumors, and mixed germ cell tumors (West et al. 2009; Cao et al. 2011a; Cao et al. 2011b; Gillis et al. 2011; Xue et al. 2011). Overexpression of Lin28a produces higher grade teratomas whereas Lin28a knockdown leads to smaller teratomas, suggesting that Lin28a acts as an oncogene in germ cell tumors by enhancing the self-renewal of PGCs and spermatogonial stem cells (West et al. 2009).

Although Lin28a/b declines rapidly upon implantation (Tang et al. 2010), high levels of Lin28 persist in the neural tube and neural crest (Yang and Moss 2003; Balzer et al. 2010). *miR-125* is thought to promote neural differentiation, in part by downregulating Lin28a in neural stem cells (Wulczyn et al. 2007; Rybak et al. 2008). Lin28a/b overexpression, in turn, regulates the balance of neurogenesis and gliogenesis in vitro (Balzer et al. 2010), and leads to an abundance of primitive neural tissue in teratomas formed by ESCs (West et al. 2009). By increasing Nmyc, conditional overexpression of Lin28b in neural crest progenitors in mice could inhibit neuronal differentiation and lead to neuroblastoma (Molenaar et al. 2012). Interestingly, a genome-wide association study (GWAS) also found that a Lin28b variant with higher expression is associated with higher neuroblastoma risk in humans (Diskin et al. 2012). This suggests that dysregulation of Lin28b in neural crest progenitors, which normally show only limited self-renewal, can provoke transformation into neuroblastoma. Lin28a is also highly expressed in aggressive primitive neuroectodermal brain tumors and medulloblastoma,

although its oncogenic role in these tumors remains less clear (Picard et al. 2012; Rodini et al. 2012).

Within the developing mesodermal tissues, fetal hematopoietic stem and progenitor cells (HSPCs) express high levels of Lin28b, whereas adult HSPCs do not (Yuan et al. 2012). Overexpression of Lin28a alone in adult $Lin^-$ bone marrow cells can reprogram some of them into fetal-like lymphoid progenitors (Yuan et al. 2012), which may be relevant to Lin28's oncogenic role in T-cell lymphoma and leukemia (Beachy et al. 2012; Rao et al. 2012). In acute myeloid leukemia (AML) however, Lin28a appears to act as an oncogene in MLL-driven AML on one end of the spectrum, and a tumor suppressor in *miR-125*-driven AML on the other (Jiang et al. 2012; Chaudhuri et al. 2012). It is especially interesting that *miR-125* overexpression alone can promote self-renewal of long-term adult HSCs, to cause a variety of myeloid and lymphoid malignancies in both mice and humans (Bousquet et al. 2008, 2010; Guo et al. 2010; O'Connell et al. 2010; Ooi et al. 2010; Chaudhuri et al. 2012), even though the *miR-125* homolog *lin-4* promotes differentiation in nematode stem cells. The unresolved questions surrounding *miR-125* and Lin28's roles in hematopoiesis indicate that our understanding of how the *miR-125-Lin28-let-7* pathway regulates hematopoiesis remains incomplete.

In another mesoderm-derived tissue, muscle stem cells or satellite cells have not been observed to express Lin28a/b, but proliferative myoblasts do upregulate Lin28a during muscle regeneration (Polesskaya et al. 2007). Loss of Lin28a by siRNA knockdown inhibits myogenesis, whereas Lin28a overexpression promotes myogenesis, at least in vitro. This process depends on direct stimulation of *Igf2* translation (Polesskaya et al. 2007), and probably other *Lin28a* targets in cellular growth and metabolism (Zhu et al.

2011). Although muscle development does not seem overtly affected in *Lin28a* transgenic or knockout mice (Zhu et al. 2010; Zhu et al. 2011), it remains to be tested whether *Lin28a/b* are functionally important in muscle regeneration upon injury, or in rhabdomyosarcoma growth in vivo.

Despite tremendous progress in our knowledge of Lin28 function in tissues of germline, ectodermal and mesodermal origin, little is known about Lin28 function in endodermal tissues. Lin28 expression has been detected in the fetal liver, kidney, intestines and lung by immunohistochemistry (Yang and Moss 2003). A variety of cancers involving these tissues express Lin28b, including hepatocellular carcinoma, Wilm's tumors, colorectal cancer and lung cancer – suggesting that Lin28a/b might play a role in both the normal development and malignancy of endodermal tissues (Guo et al. 2006; Viswanathan et al. 2009; King et al. 2011; Zhang et al. 2012). Given the limitations of immunohistochemistry in small cellular compartments, and the expectation that Lin28 may only be active in stem or progenitor cells, careful analysis using tissue specific Cre- or Cre-ER-driven mouse models are needed to rigorously address the role of Lin28a/b in tissue development by lineage-tracing.

**Lin28 in the Re-engineering of Mammalian Physiology**

It has been proposed that Lin28 is an oncofetal gene with little physiological relevance in normal adult tissues (Boyerinas et al. 2008; Peter 2009). Since Lin28a/b are primarily expressed during embryogenesis and largely silent in most adult tissues, one could argue that these proteins bear little relevance to normal adult human physiology except when reactivated in the setting of malignancy. Evolutionarily, this could be due to

Lin28's potency in promoting stem cell self-renewal, and hence tumorigenesis, if dysregulated. Another gene endowed with similar properties is the catalytic component of telomerase, Tert, which is likewise predominantly expressed during early embryogenesis, in small compartments of adult stem cells, and in cancers (Kolquist et al. 1998; Schaetzlein et al. 2004). Despite its apparent irrelevance to adult physiology initially – telomerase knockout mice are healthy and viable for the first few generations (Blasco et al. 1997; Yuan et al. 1999) – Tert has gained preeminence as an agent for re-engineering mammalian adult cells, by immortalizing cells and extending lifespan in vivo, along with being a potential target in cancer therapy (Sahin et al. 2010). Could Lin28 show similar potential in re-engineering adult human cells (Figure 1.3)?

The answer appears to be in the affirmative. Taken together, the demonstrations that Lin28a overexpression with Oct4, Sox2 and Nanog can help reprogram adult human fibroblasts into ESC-like iPSCs (Yu et al. 2007), that Lin28a overexpression can reprogram adult HSPCs into a fetal-like HSPCs (Yuan et al. 2012), and that Lin28b overexpression can expand neural crest progenitors (Molenaar et al. 2012), suggest that Lin28a/b overexpression might be useful for promoting stem cell or progenitor self-renewal in vitro. This is conceptually distinct from Tert-based immortalization of any somatic cell, since Lin28a/b appears to counteract cellular differentiation whereas Tert counteracts replicative senescence. If Lin28a/b can enhance self-renewal, what effects would it exert on adult tissue repair in vivo? Although Lin28's effects on mammalian tissue repair remains unexplored, a study has shown that zebrafish *Lin28* can promote retinal regeneration by repressing *let-7* (Ramachandran et al. 2010). This finding hints

at the possibility that Lin28 might also extend the limits of mammalian tissue repair upon injury – a hypothesis that awaits further testing (Figure 1.3).

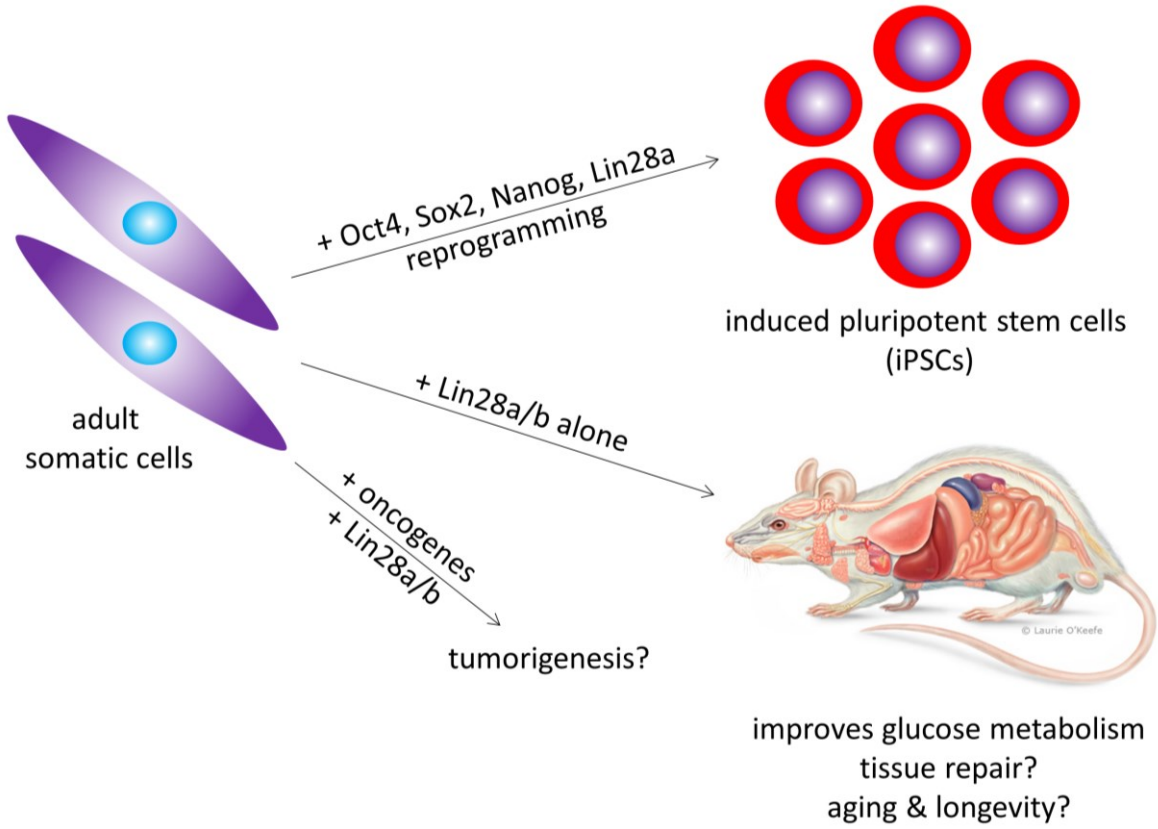


***Figure 1.3: Potential of Lin28 in Re-Engineering Adult Mammalian Physiology.*** Lin28a, in conjunction with the pluripotency factors Oct4, Sox2 and Nanog, can reprogram somatic cells into iPSCs. Alone, Lin28a/b can reprogram adult HSPCs into a fetal-like state, and enhance insulin sensitivity in the skeletal muscles to improve glucose homeostasis, resist obesity and prevent diabetes. Emergent clues suggest that optimal doses of Lin28a/b might have the potential to re-engineer adult mammalian tissue repair capacities and extend longevity, although Lin28a/b could also cooperate with oncogenes to initiate tumorigenesis. Future work might elucidate these mysteries.

In the same vein, the Lin28/*let-7* pathway could impact longevity, although it remains unclear whether Lin28 overexpression would promote or delay aging. Given that Lin28 upregulates and *let-7* downregulates insulin-PI3K signaling in mammals (Zhu et al. 2011), and insulin-PI3K signaling also regulates mammalian aging in an evolutionarily conserved fashion, one might expect Lin28 to promote and *let-7* to delay aging in mammals. This would concur with several studies showing that several long-lived mouse strains like the Ames, Snell, GHRKO and *Igfr1*$^{+/-}$ mice are all dwarfed (Bartke 2012), similar to mice overexpressing *let-7* (Zhu et al. 2011; Frost and Olson 2011). Yet improved insulin sensitivity, a prominent phenotype of mice overexpressing Lin28a/b, is associated with longevity (Barbieri et al. 2003), indicative of how longevity is regulated by a multifaceted network of factors. Adding to this complexity, deficiency in tissue repair can accelerate aging as shown in telomerase-deficient and p53-overexpressing mice (Rudolph et al. 1999; Tyner et al. 2002), but hyperactive tissue regeneration can also lead to stem cell exhaustion and shorter lifespans, as shown in models of *Pten*$^{-/-}$ myelodysplasias and muscular dystrophy (Yilmaz et al. 2006; Sacco et al. 2010). It could well be that only the precise dosage of Lin28/*let-7* that strikes an optimal equilibrium between insulin signaling and tissue repair would enhance mammalian longevity.

As is the case with telomerase, a wide variety of cancers reactivate Lin28 to re-engineer their cellular states (Viswanathan et al. 2009). Although the oncogenic role of Lin28a/b has only been demonstrated in vivo for a small subset of cancers including neuroblastoma, T-cell acute lymphoblastic leukemia and peripheral T-cell lymphoma (Molenaar et al. 2012; Beachy et al. 2012; Rao et al. 2012), the cancer stem cell model

seems to apply in all these cases, with Lin28 as a stem cell factor promoting self-renewal. The cancer stem cell model posits that cancers are maintained by a small population of tumor-sustaining cancer stem cells with self-renewal capacity (Rosen et al. 2009). Although the cancer stem cell model has engendered debate and does not apply universally to all cancers, as shown most convincingly in advanced melanoma and lymphoma (Quintana et al. 2008, 2010; Boiko et al. 2010), leukemias, germ cell tumors and some other solid cancers appear to follow the cancer stem cell model (Ishizawa et al. 2010). Irving Weissman and colleagues have proposed that in the earliest stages of melanoma, rare cancer stem cells differentiate into nonmalignant progeny to form the bulk of the tumor, whereas in the advanced stages cancer stem cell clones dominate and constitute the bulk of the tumor (Boiko et al. 2010). These findings suggest that targeting cancer cell heterogeneity may be a relevant approach for eradicating tumors only during a cancer's early stages. If Lin28's role in promoting stem cell and progenitor self-renewal is also its essential mechanism for promoting tumorigenesis, then Lin28 would represent a promising universal factor for therapeutic targeting in a wide variety of cancer stem cells. This exciting prospect warrants attempts to drug the Lin28 pathway.

## Conclusion

Seminal observations made nearly three decades ago by Victor Ambros and Robert Horvitz on the role of Lin28 in *C. elegans* heterochronic reiterations have spawned great leaps in our understanding of how post-transcriptional RNA processing can regulate stem cells. Recent advances are painting a detailed picture of how Lin28 regulates *let-7* microRNA biogenesis and mRNA translation, to coordinate both cellular metabolism

and proliferative growth pathways for the purpose of stem cell self-renewal. Although much effort has been expended to elucidate the *let-7* microRNA regulatory mechanism, it is imperative that we also understand how Lin28a/b regulates mRNA processing and trafficking between the nucleus, ribosomes, P-bodies and stress granules – a mystery that remains unresolved. And what conditions or pathways regulate the mechanism of Lin28a or Lin28b within the nucleolus, the cytoplasm, and P-bodies? How do these mechanisms affect Lin28a/b function in tissue stem cells and progenitors, especially those derived from the endoderm given its preponderance in colon, kidney, liver and lung cancers? And can we harness Lin28 to re-engineer and improve mammalian tissue repair and longevity? Or target it for cancer therapy? Hopefully we can answer these questions, and more, in the coming decade.

**Acknowledgements**

This chapter was published as Shyh-Chang and Daley (*Cell Stem Cell*, 2013b).

## Chapter 2: The *Lin28/let-7* axis regulates glucose metabolism in mammals

### Introduction

One rapidly emerging paradigm in cancer biology is that malignancy and metabolic disease share common biological mechanisms. Reprogramming towards glycolytic metabolism can increase a cancer cell's ability to generate biomass, a phenomenon termed the "Warburg Effect" (Denko, 2008; Engelman et al., 2006; Gao et al., 2009; Guertin and Sabatini, 2007; Laplante and Sabatini, 2009; Vander Heiden et al., 2009; Yun et al., 2009). Likewise, many genes identified in type 2 diabetes (T2D) genome wide association studies (GWAS) are proto-oncogenes or cell cycle regulators (Voight et al., 2010). MicroRNAs (miRNAs) are also emerging as agents of metabolic and malignant regulation in development and disease (Hyun et al., 2009; Peter, 2009). The *let-7* miRNA family members act as tumor suppressors by negatively regulating the translation of oncogenes and cell cycle regulators (Johnson et al., 2005; Lee et al., 2007; Mayr et al., 2007; Kumar et al., 2008). Widespread expression and redundancy among the well-conserved *let-7* miRNAs raise the question of how cancer and embryonic cells are able to suppress this miRNA family to accommodate rapid cell proliferation. In human cancers, loss of heterozygosity, DNA methylation, and transcriptional suppression have been documented as mechanisms to reduce *let-7* (Johnson et al., 2005; Lu et al., 2007). Another mechanism for *let-7* downregulation involves the RNA-binding proteins *Lin28a* and *Lin28b* (collectively referred to as *Lin28a/b*), which are highly expressed during normal embryogenesis and upregulated in some cancers to potently and selectively block the maturation of *let-7* (Heo et al., 2008; Newman et al., 2008; Piskounova et al., 2008; Rybak et al., 2008; Viswanathan et al.,

2008). By repressing the biogenesis of *let-7* miRNAs and in some cases through direct mRNA binding and enhanced translation (Polesskaya et al., 2007; Xu and Huang, 2009; Xu et al., 2009; Peng et al., 2011), *Lin28a/b* regulate an array of targets involved in cell proliferation and differentiation in the context of embryonic cells, stem cells, and cancer.

Little is known about the *in vivo* function of the *Lin28/let-7 axis*. The pathway was first revealed in a screen for heterochronic mutants in *C. elegans*, where loss of *lin-28* resulted in precocious vulval differentiation and premature developmental progression (Ambros and Horvitz, 1984; Moss et al., 1997; Nimmo and Slack, 2009), whereas loss of *let-7* led to reiteration of larval stages and delayed differentiation (Abbott et al., 2005; Reinhart et al., 2000). We previously showed that *Lin28a* gain of function promotes mouse growth and delays sexual maturation, recapitulating the heterochronic effects of *lin-28* and *let-7* in *C. elegans*, as well as the height and puberty phenotypes linked to human genetic variation at the *Lin28b* locus identified in GWAS (Zhu et al., 2010). The conservation of *Lin28* and *let-7's* biochemical and physiological functions throughout evolution suggests an ancient mechanism for *Lin28* and *let-7's* effects on growth and developmental timing.

In this report we found that both *Lin28a* and *LIN28B* transgenic mice were resistant to obesity and exhibited enhanced glucose tolerance. In contrast, muscle-specific *Lin28a* knockout and inducible *let-7* transgenic mice displayed glucose intolerance, suggesting that the *Lin28/let-7* pathway plays a specific and tightly regulated role in modulating glucose metabolism in mammals. *In vitro* experiments revealed that *Lin28a* enhances

glucose uptake via an increase in insulin-PI3K-mTOR signaling due in part to the derepression of multiple direct *let-7* targets in the pathway, including *IGF1R*, *INSR*, *IRS2*, *PIK3IP1, AKT2, TSC1* and *RICTOR*. Experiments with the mTOR-specific inhibitor rapamycin demonstrate that *Lin28a* regulates growth, glucose tolerance, and insulin sensitivity in an mTOR-dependent manner *in vivo*. In addition, analysis of T2D and fasting glucose whole genome associations suggests a genetic connection between multiple genes regulated by *let-7* and glucose metabolism in humans. These metabolic functions for *Lin28a/b* and *let-7 in vivo* provide a mechanistic explanation for how this pathway might influence embryonic growth, metabolic disease and cancer.

**Experimental Procedures**

***Mice.*** All animal procedures were based on animal care guidelines approved by the Institutional Animal Care and Use Committee. Mouse lines used in this study are described in Figure S2.5.

***Indirect Calorimetry****.* The apparatus used was a set of 16 OxyMax® Metabolic Activity Monitoring chambers (Columbus Instruments; Columbus, OH, USA). Each chamber consisted of a self-contained unit capable of providing continuous measurements of an individual mouse's total activity and feeding behavior. Monitoring occurred over a 3-day period. Each subject was placed into an individual chamber on day 1, with free access to food and water during the course of the experiment. Subjects were maintained under a normal 12:12 h light:dark cycle. All measurements were sampled periodically (at approximately 12-min intervals) and automatically recorded via the OXYMAX Windows V3.22 software. Activity measures over the final 24-h period were parceled into 2-h bins

and these were used to express diurnal activity levels.

***Quantitative RT-PCR.*** Performed with standard methods.

***Histology.*** Tissue samples were fixed in 10% buffered formalin or Bouin's solution and embedded in paraffin.

***Glucose and insulin tolerance tests***. Overnight-fasted mice were given i.p. glucose (2 mg/g body weight). For insulin tolerance test, 5 hour fasted mice were given 0.75 U insulin/kg body weight by i.p. injection (Humulin). Blood glucose was determined with a Lifescan One Touch glucometer. Insulin, GH, and Igf1 levels were measured by ELISA (Crystal Chem).

***Cloning.*** Murine *Lin28a* and human *LIN28B* cDNA was subcloned into pBabe.Puro and pMSCV.Neo retroviral vectors. *LIN28B* and Control shRNA in lentiviral plasmids were purchased from Sigma-Aldrich and previously reported in Viswanathan et al., 2009**.**

***Cell culture, viral production, and transfection.*** Performed using standard methods.

***Glucose uptake assay.*** In vitro glucose uptake assays were performed as described in Berti and Gammeltoft, 1999.

***Drug treatments***. Rapamycin was injected i.p. 3 times a week for mouse experiments. For cell culture, C2C12 myotubes differentiated for 3 days were incubated with inhibitors for 1 day prior to glucose uptake assays. See Extended Experimental Procedures for further details.

***Western blot assay.*** Performed using standard methods.

***Luciferase reporter assay.*** 10 ng of each construct was co-transfected with 10 nM miRNA duplexes or into HEK-293T cells in a 96-well plate using lipofectamin-2000

(Invitrogen). After 48 hours, the cell extract was obtained; firefly and *Renilla* luciferase activities were measured with the Promega Dual-Luciferase® reporter system.

***MAGENTA analysis.*** See Table 2.1 Legend.

***Statistical analysis****.* Data is presented as mean ± SEM, and Student's t-test (two-tailed distribution, two-sample unequal variance) was used to calculate *p* values. Statistical significance is displayed as $p < 0.05$ (one asterisk) or $p < 0.01$ (two asterisks). The tests were performed using Microsoft Excel where the test type is always set to two-sample equal variance.

## Results

### *Lin28a Tg mice are resistant to obesity and diabetes*

We previously described a tetracycline-inducible *Lin28a* transgenic mouse that showed leaky constitutive *Lin28a* expression in the absence of induction (See Experimental Procedures, "*Lin28a* Tg" mice: Zhu et al., 2010). In that study, we showed that these mice cleared glucose more efficiently during glucose and insulin tolerance testing (GTT and ITT), classic metabolic tests used for the characterization of whole animal glucose handling. Given that young *Lin28a* Tg mice exhibited enhanced glucose metabolism, we tested if old *Lin28a* Tg mice were also resistant to age-induced obesity. Compared to *Lin28a* Tg mice, wild-type mice fed a normal diet gained significantly more fat mass with age (Figure 2.1A). Dual Energy X-ray Absorptiometry scans showed increased percentage lean mass and reduced percentage body fat in the *Lin28a* Tg mice (Figure 2.1B,C). To rule out behavioral alterations, we measured activity over three days in

isolation cages and found no differences in horizontal activity, $O_2/CO_2$ exchange, and food/water intake between wild-type and Tg mice (Figure S2.1A,B in Appendix). To determine if these mice were resistant to HFD-induced obesity, we fed mice a diet containing 45% kcals from fat, and observed resistance to obesity in the *Lin28a* Tg mice (Figure 2.1D). *Lin28a* Tg mice consumed as much high-fat food as their wild-type littermates, ruling out anorexia (data not shown). Furthermore, we inquired if *Lin28a* Tg mice were resistant to HFD-induced diabetes and found that they had markedly improved glucose tolerance and insulin sensitivity under HFD conditions (Figure 2.1E,F). *Lin28a* Tg mice also showed resistance to HFD-induced hepatosteatosis (Figure 2.1G). Taken together, leaky *Lin28a* expression in the muscle, skin and connective tissues (Zhu et al., 2010) protected against obesity and diabetes in the context of aging and HFD.

***iLIN28B Tg mice are likewise resistant to diabetes***

Although *Lin28a* and *Lin28b* both block *let-7* miRNAs, they are differentially regulated, resulting in distinct expression patterns during normal development and malignant transformation (Guo et al., 2006; Viswanathan et al., 2009). Given that *LIN28B* is overexpressed more frequently than *LIN28A* in human cancer, we sought to determine if *LIN28B* exerts a similar effect on glucose metabolism. Thus, we generated a mouse strain with human *LIN28B* driven by a tetracycline transactivator *rtTA* placed under the control of the *Rosa26* locus (*iLIN28B* mouse) (See Experimental Procedures). After 14 days of treatment with the tetracycline analogue doxycycline (dox), high levels of *LIN28B* were induced and mature *let-7's* were repressed in metabolically important organs (Figure 2.1H,I), resulting in hypoglycemia with an average fasting glucose of <50

***Figure 2.1: Lin28a Tg and iLIN28B Tg mice are resistant to obesity and diabetes and Lin28a is physiologically required for normal glucose homeostasis.*** (**A**) Aged wild-type (left) and *Lin28a* Tg mice (right) fed a normal diet, at 20 weeks of age. (**B**) Percentage body fat and (**C**) lean mass as measured by DEXA. (**D**) Weight curve of mice fed a HFD containing 45% kcals from fat. (**E**) Glucose tolerance test (GTT) and (**F**) Insulin tolerance test (ITT) of mice on HFD. (**G**) Liver histology of mice fed HFD. (**H**) Human *LIN28B* mRNA expression in a mouse strain with dox inducible transgene expression (named *iLIN28B*). (**I**) Mature *let-7* expression in gut, spleen, liver, muscle and fat. (**J**) Kinetics of fed state glucose change after induction. (**K**) GTT and (**L**) ITT under normal diets. (**M**) *iLIN28B* growth curve under HFD. (**N**) GTT after 14 days of HFD and induction. (**O**) GTT and (**P**) ITT of *Myf5-Cre; Lin28a*$^{fl/fl}$ mouse. Controls for *Lin28a* Tg mice are WT. Controls for *iLIN28B* Tg mice carry only the *LIN28B* transgene. Controls for muscle knockout mice are *Lin28a*$^{fl/fl}$ mice. The numbers of experimental animals are listed within the charts.

## Figure 2.1 (continued)

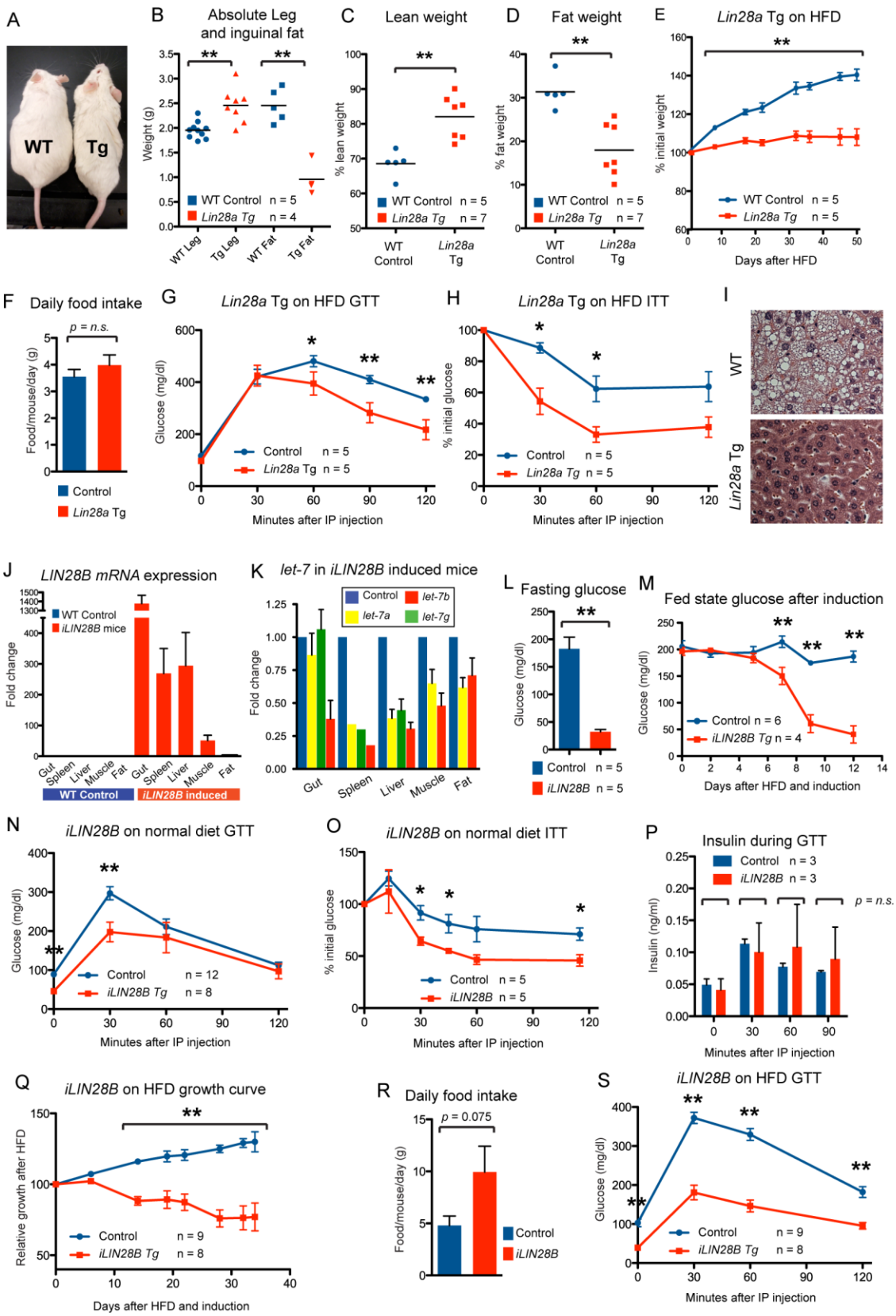

mg/dL in induced mice compared to >150 mg/dL in control mice ($p < 0.01$). To determine the kinetics of this effect, we measured fed state glucose daily and noted falling glucose levels after 5 days (Figure 2.1J). Glucose and insulin tolerance tests on dox-induced animals on normal diets showed considerable improvements in glucose tolerance and insulin sensitivity (Figure 2.1K,L). In checking for islet β cell hyperactivity, we found that *iLIN28B* mice produced no more insulin than control littermates during glucose challenge (data not shown). Under HFD, we found that induced *iLIN28B* mice were surprisingly resistant to weight gain (Figure 2.1M) despite a slight increase in food intake (9.9 vs. 4.8 g/mouse/day; $p = 0.075$). These mice continued to exhibit superior glucose tolerance after 14 days of dox induction under HFD (Figure 2.1N), when average weights were 33.5 ± 1.05 grams for controls and 27.1 ± 0.99 grams for *iLIN28B* mice, demonstrating that HFD had a strong obesogenic and diabetogenic effect on control but not on *LIN28B* induced animals. Unlike the *Lin28a* Tg mice, expression was not leaky in the *iLIN28B* mice (Figure 2.1H) and uninduced mice exhibited no growth or glucose phenotypes (Figure S2.1C,D), making this a better model for inducible *Lin28* hyperactivation. These data show that both *Lin28* homologues have similar effects on glucose metabolism and obesity, suggesting that these effects are mediated through common mRNA or miRNA targets of the *Lin28* family.

***Lin28a is physiologically required for normal glucose homeostasis***

We then asked if *Lin28a* is physiologically required for normal glucose metabolism in one specific adult tissue compartment, skeletal muscle, since previous studies have found low but significant levels of *Lin28a* expression in the muscle tissues of mice

(Yang and Moss, 2003; Zhu et al, 2010). We generated a skeletal muscle-specific knockout of *Lin28a* by crossing the mouse *myogenic factor 5 Cre* recombinase strain (*Myf5-Cre*) to the *Lin28a*$^{fl/fl}$ conditional loss of function mouse (See Experimental Procedures). These muscle-specific knockout mice showed impaired glucose tolerance (Figure 2.1O) and insulin resistance (Figure 2.1P) relative to wild-type littermates, demonstrating that *Lin28a* activity in skeletal muscles is required for normal glucose homeostasis. We analyzed miRNA expression in muscle tissue by qRT-PCR and found no significant difference in *let-7* levels during adult (data not shown) or embryonic stages (Figure S2.1E), suggesting that *Lin28a* loss of function affects glucose homeostasis either through *let-7*-independent mRNA binding or through changes in the spatiotemporal distribution of *let-7* miRNA. Together, these data show that *Lin28* isoforms are important and essential regulators of glucose homeostasis.

***iLet-7 mice are glucose intolerant***

In addition to their ability to suppress *let-7* biogenesis, *Lin28a* and *Lin28b* also regulate mRNA targets such as *Igf2*, *HMGA1, OCT4*, histones and cyclins through non-*let-7* dependent mechanisms of mRNA binding and enhanced translation (Polesskaya et al., 2007; Xu and Huang, 2009; Xu et al., 2009; Peng et al., 2011). To test if altered *let-7* expression might produce the opposite phenotypes of *Lin28a/b* gain of function, we generated a mouse strain in which *let-7g* can be induced with dox under the control of the *Rosa26* locus (*iLet-7* mouse, See Experimental Procedures). To ensure that endogenous *Lin28* would not block *pri- or pre-let-7g* biogenesis, we used a chimeric *let-*

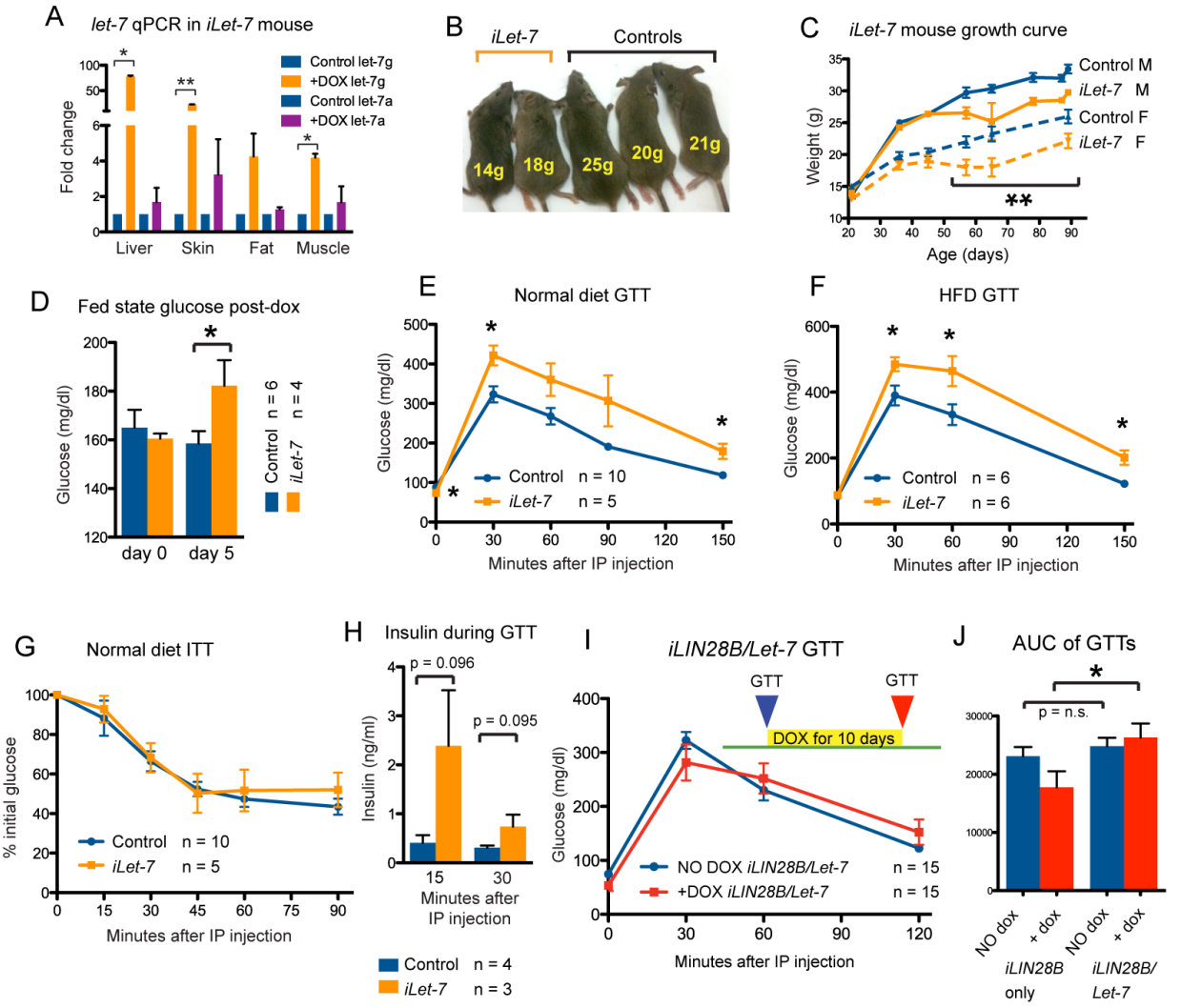


***Figure 2.2: iLet-7 mice are glucose intolerant***. (**A**) *let-7g* and *let-7a* qRT-PCR in tissues of dox induced *iLet-7* mice (n = 3) and controls (n = 3). (**B**) Reduced size of induced animals. (**C**) *iLet-7* growth curve for males and females. (**D**) Fed state glucose in *iLet-7* mice induced for 5 days. GTTs performed on mice fed with either (**E**) normal diet or (**F**) HFD. (**G**) ITT on normal diet. (**H**) Insulin production during a glucose challenge. (**I**) GTT of *LIN28B/Let-7* compound heterozygote mice before (blue) and after (red) induction with dox. (**J**) Area under the curve (AUC) analysis for this GTT. Controls for *iLet-7* Tg mice carry either the *Let-7* or *Rosa26-M2rtTa* transgene only. The numbers of experimental animals are listed within the charts.

*7g* species called *let-7S21L* (*let-7g* Stem, *mir-21 Loop*), in which the loop region of the precursor miRNA derives from *mir-21* and cannot be bound by *Lin28*, thus allowing for *let-7* processing despite *Lin28* expression (Piskounova et al., 2008). Global transgene induction from three weeks of age onwards increases mature *let-7g* levels in liver (>50-fold), skin (>20-fold), fat (~4-fold) and muscle (~4-fold) (Figure 2.2A). This level of *let-7* overexpression led to reduced body size and growth rates in induced animals (Figure 2.2B,C). Growth retardation was proportional and not manifested as preferential size reduction in any particular organs (Figure S2.2A). Similar to the *iLIN28B* mice, leaky expression was not detected and uninduced male mice exhibited no growth or glucose phenotypes (Figure S2.2B-D).

After 5 days of *let-7* induction, these *iLet-7* mice produced an increase in fed state glucose (Figure 2.2D). GTT revealed glucose intolerance in mice fed normal (Figure 2.2E) or HFD (Figure 2.2F). Surprisingly, ITT failed to detect a difference in insulin sensitivity (Figure 2.2G). The decreased glucose tolerance in the setting of comparable insulin sensitivity suggested either decreased insulin production from islet β cells in response to glucose, or higher insulin secretion to compensate for peripheral insulin resistance. Thus, we measured insulin production following glucose challenge, and found that *iLet-7* mice produced slightly more insulin than controls (Figure 2.2H). These results demonstrated that broad overexpression of *let-7* results in peripheral glucose intolerance and compensatory overproduction of insulin from islet β cells.

To test if *let-7* induction could abrogate the glucose uptake phenotype of *LIN28B* overexpression, we crossed the *iLIN28B* to the *iLet-7* inducible mice. After 10 days of induction, simultaneous induction of *LIN28B* and *let-7g* did not result in any differences in glucose tolerance (Figure 2.2I,J), in contrast to *LIN28B* or *let-7g* induction alone. Taken together, the opposing effects of *Lin28* and *let-7* expression on glucose regulation show that *Lin28* overexpression influences metabolism in part by suppressing *let-7*, and that *let-7* alone is sufficient to regulate glucose metabolism *in vivo.*

***Insulin-PI3K-mTOR signaling is activated by Lin28a/b and suppressed by let-7***

To dissect the molecular mechanism of the effects of *Lin28* and *let-7* on glucose regulation, we turned to the C2C12 cell culture system. Overexpression of *Lin28a* in C2C12 myoblasts resulted in protein levels of *Lin28a* similar to that observed in mouse embryonic stem cells (ESCs) (Figure 2.3A), and led to robust *let-7* suppression (Figure 2.3B). In C2C12 myotubes differentiated for 3 days, *Lin28a* promoted Ser473 phosphorylation of Akt and Ser235/236 phosphorylation of S6 ribosomal protein, suggesting activation of the PI3K-mTOR pathway (Figure S2.3A). In this setting, *Lin28a* increased myotube glucose uptake by 50% (Figure 2.3C). *Lin28a*-dependent glucose uptake was abrogated by 24hr treatment with the PI3K/mTOR inhibitor LY294002 or the mTOR inhibitor rapamycin (Figure 2.3C), but not the MAPK/ERK inhibitor PD98059 (Figure S2.3B), demonstrating that *Lin28a*-dependent glucose uptake requires the PI3K-mTOR pathway.

To exclude myotube differentiation-dependent phenomena, we tested the effects of *Lin28a* on PI3K-mTOR signaling in undifferentiated myoblasts under serum-fed, serum-

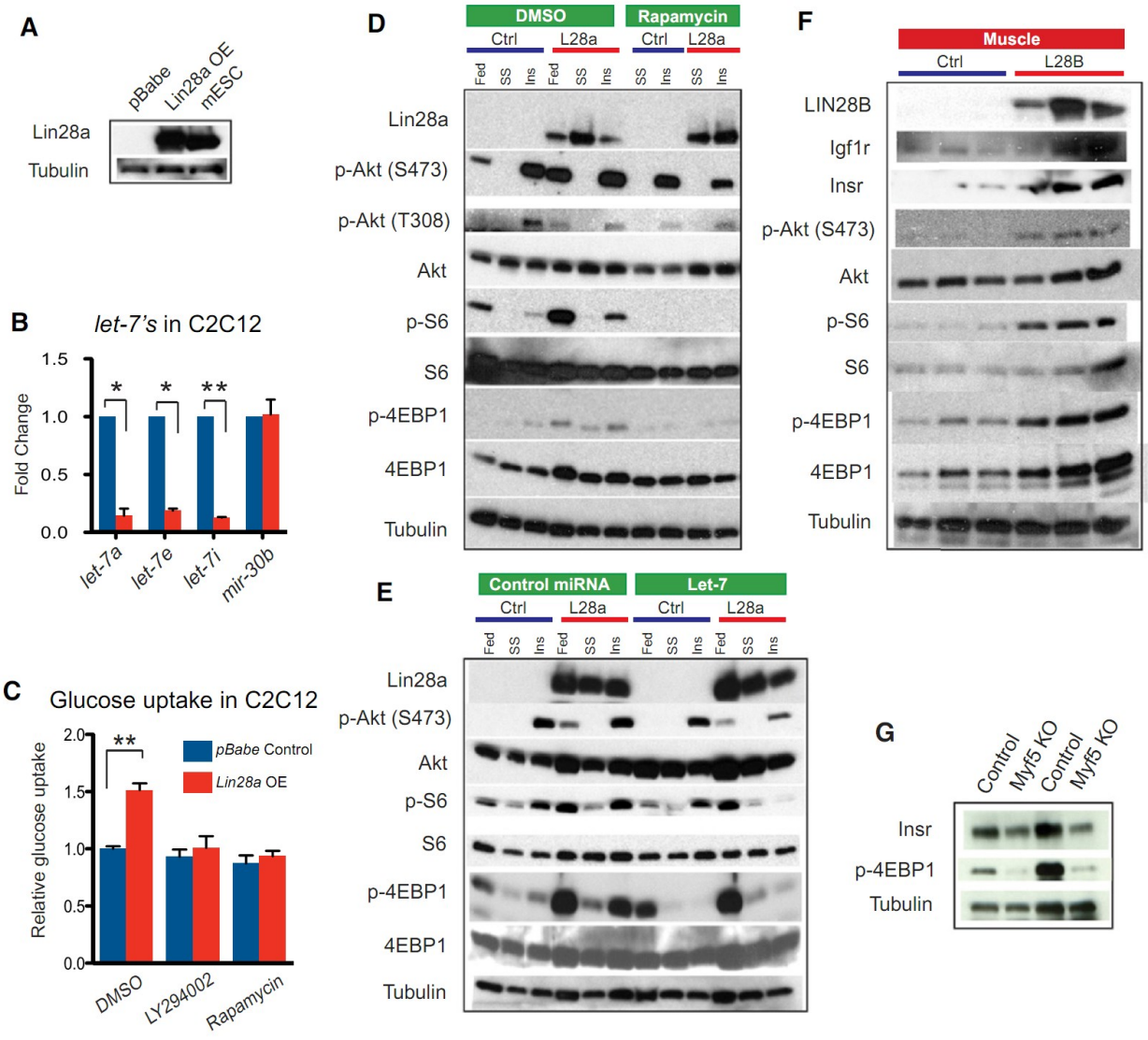


***Figure 2.3: Insulin-PI3K-mTOR signaling is activated by Lin28a/b and suppressed by let-7.*** (**A**) Western blot analysis of Lin28a protein expression in C2C12 myoblasts infected with control pBabe or *Lin28a* overexpression vector, and mouse ESCs, with tubulin as the loading control. (**B**) Quantitative PCR for *let-7* isoforms in C2C12 myoblasts, normalized to *sno142*, after *Lin28a* overexpression. (**C**) 2-deoxy-D-[$^{3}$H] glucose uptake assay on 3-day-differentiated C2C12 myotubes with and without *Lin28a* overexpression, treated with DMSO, the PI3K inhibitor LY294002, and the mTOR inhibitor rapamycin for 24 hrs. (**D**) Western blot analysis of the effects of *Lin28a*

***Figure 2.3 (continued)*** overexpression on PI3K-mTOR signaling in C2C12 myoblasts, under serum-fed (fed), 18 hr serum starved (SS) or insulin-stimulated (Ins) conditions. Insulin stimulation was performed in serum-starved myoblasts with 10 μg/mL insulin for 5 min. Prior to insulin stimulation, serum-starved myoblasts were treated with either DMSO or 20 ng/mL rapamycin for 1 hr. (**E**) Western blot analysis of the effects of *let-7f* or control miRNA on PI3K-mTOR signaling in C2C12 myoblasts under serum-fed (fed), 18 hr serum starved (SS) or insulin-stimulated (Ins) conditions. (**F**) Western blot analysis of the effects of *LIN28B* induction by dox on PI3K-mTOR signaling in quadriceps muscles *in vivo* (n = 3 *iLIN28B* Tg mice and 3 *LIN28B* Tg only mice). (**G**) Insr and p-4EBP1 protein levels in wild-type and *Lin28a* muscle-specific KO adults.

starved, and insulin-stimulated conditions (Figure 2.3D). In the serum-fed state, we found that *Lin28a* promoted the activation of PI3K/Akt signaling by increasing Akt phosphorylation at both Ser473 and Thr308, compared to the pBabe control.

Furthermore, we found that *Lin28a* robustly increased the phosphorylation of mTORC1 signaling targets S6 and 4EBP1 in the serum-fed state. Serum-starvation for 18 hours abrogated the phosphorylation of Akt, S6 and 4EBP1, indicating that *Lin28a*-induction of PI3K-mTOR signaling requires exogenous growth factor stimulation. Upon insulin stimulation, Akt phosphorylation increased dramatically and, both phospho-S6 and phospho-4EBP1 levels were increased even further by *Lin28a* overexpression, suggesting that *Lin28a* increases the insulin-sensitivity of C2C12 myoblasts. Importantly, we found that rapamycin abrogated the *Lin28a*-induction of phospho-S6

and phospho-4EBP1 upon insulin stimulation, but did not affect *let-7* levels (Figure S2.3C) or Lin28a itself (Figure 2.3D), indicating that the mTOR dependence is occurring downstream of *Lin28a*.

To test if the effects of *Lin28a* on insulin-PI3K-mTOR signaling are *let-7*-dependent, we transfected either mature *let-7f* duplex or a negative control miRNA into both *Lin28a*-overexpressing and pBabe control myoblasts (Figure S2.3D and Figure 2.3E). Because mature *let-7* duplexes cannot be bound and inhibited by Lin28a protein, this experiment tests if PI3K-mTOR activation is occurring downstream of *let-7*. Transfection with control miRNA did not affect *Lin28a*-induction of the phosphorylation of Akt, S6, or 4EBP1 in serum-starved myoblasts upon insulin stimulation. Transfection with *let-7f,* however, attenuated the *Lin28a*-induction of phospho-Akt (Ser473), and abrogated the increase in S6 and 4EBP1 phosphorylation upon insulin stimulation in *Lin28a*-overexpressing myoblasts (Figure 2.3E). In pBabe control myoblasts, *let-7* duplex still suppressed S6 and 4EBP1 phosphorylation in the serum-fed state, serum-starved, and insulin-stimulated conditions, relative to total S6 and 4EBP1 protein. The suppression of mTOR signaling by *let-7* even in the absence of *Lin28a* implies that *let-7* can act independently downstream of *Lin28a.* Together with data indicating that *let-7* abrogates *Lin28a*-specific induction of p-Akt, p-S6 and p-4EBP1 upon insulin stimulation, this demonstrates that the effects of *Lin28a* on PI3K-mTOR signaling are at least in part due to *let-7* and that *Lin28* and *let-7* exert opposing effects on PI3K-mTOR signaling.

To test if these effects of *Lin28* on insulin-PI3K-mTOR signaling are also relevant *in vivo*, we examined the quadriceps muscles of *iLIN28B* mice and found that dox-induction led to increases in the phosphorylation of Akt (S473), S6 and 4EBP1, the targets of PI3K-mTOR signaling (Figure 2.3F). Furthermore, the Insulin-like growth factor 1 receptor (Igf1r) and the Insulin receptor (Insr) proteins were also upregulated in the muscles upon *LIN28B* induction, reinforcing the fact that *Lin28a/b* drives insulin-PI3K-mTOR signaling in C2C12 myoblasts and within mouse tissues. On the other hand, similar analysis of the *Lin28a* muscle-specific knockout mice revealed reduced Insr and p-4EBP1 expression (Figure 2.3G), demonstrating that *Lin28a* is both necessary and sufficient to influence glucose metabolism through the regulation of insulin-PI3K-mTOR signaling *in vivo*.

*Lin28a/b and let-7 regulate genes in the insulin-PI3K-mTOR pathway*

On the RNA level, *Lin28a* overexpression in C2C12 myoblasts leads to an increase in mRNA levels of multiple genes in the insulin-PI3K-mTOR signaling pathway (Figure S2.4A). Although both *Lin28a* suppression of *let-7* and direct *Lin28a* binding to mRNAs could increase mRNA stability and thus increase mRNA levels, it is possible that these increases do not reflect direct interactions. To find direct targets, we performed a bioinformatic screen using the TargetScan 4.1 algorithm (Grimson et al., 2007), and found that 16 genes in the insulin-PI3K-mTOR pathway contained evolutionarily conserved *let-7* binding sites in their respective 3'UTRs (Figure 2.4A,B). Next, we performed 3' UTR luciferase reporter assays to determine if these genes were *bona fide* and direct targets of *let-7*. To do this, we generated luciferase reporters with twelve

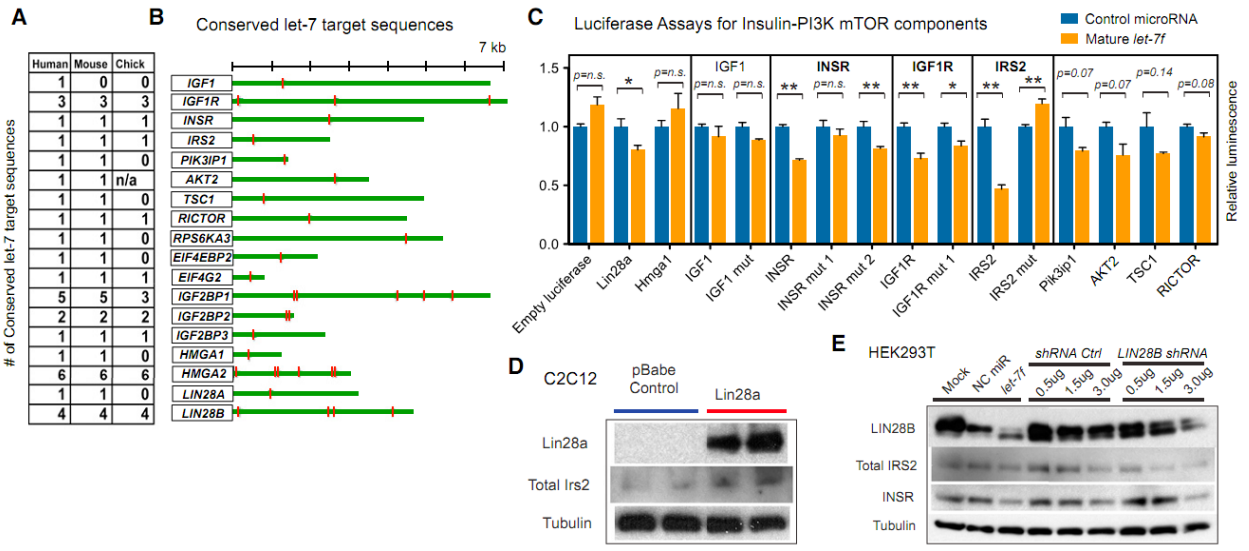


***Figure 2.4: Lin28a/b and let-7 regulate genes in the insulin-PI3K-mTOR pathway.*** (**A**) Shown are the numbers of conserved *let-7* binding sites within 3'UTRs found using the TargetScan algorithm. (**B**) Putative *let-7* binding sites in 16 genes of the insulin-PI3K-mTOR pathway and in *Lin28a/b*. (**C**) 3'UTR luciferase reporter assays performed to determine functional *let-7* binding sites. Bar graphs show relative luciferase reporter expression in human HEK293T cells after transfection of mature *let-7f* duplex normalized to negative control miRNA. Shown also are mutations in the seed sequence of the *let-7* binding sites for *INSR*, *IGF1R* and *IRS2*. (**D**) Western blot analysis of Lin28a, Irs2, and tubulin in C2C12 myoblasts with and without Lin28a overexpression. (**E**) Western blot analysis of LIN28B, total IRS2, INSR and TUBULIN in HEK293T cells with either *let-7f* transfection or shRNA knockdown of *LIN28B*.

human 3'UTR fragments containing conserved *let-7* sites. Luciferase reporter expression in human HEK293T cells after transfection of either mature *let-7f* duplex or a negative control miRNA demonstrated that the 3' UTRs of *INSR, IGF1R, IRS2*, *PIK3IP1,*

*AKT2, TSC1* and *RICTOR* were targeted by *let-7* for suppression in varying degrees (Figure 2.4C). Three-base mismatch mutations in the seed region of the *let-7* binding sites abrogated *let-7*'s suppression of *INSR*, *IGF1R* and *IRS2*. To confirm that the luciferase reporters predicted actual changes in protein expression mediated by *let-7*, we assayed the endogenous expression of some of these proteins upon *Lin28a/b* overexpression. We found that an increase in *Lin28a* upregulated Irs2 (Figure 2.4D) *in vitro*, and that an increase in *LIN28B* upregulated Igf1r and Insr protein in skeletal muscles *in vivo* (Figure 2.3F). Conversely, INSR and IRS2 are reduced upon both *let-7f* transfection and *LIN28B* shRNA knockdown in HEK293T, demonstrating that these regulatory mechanisms hold in both mouse and human cells, and in the setting of both LIN28B gain and loss of function (Figure 2.4E). This establishes a direct mechanism for *let-7*'s repression and *Lin28*'s derepression of multiple components in the insulin-PI3K-mTOR signaling cascade.

Previously, *Lin28a* has been shown to enhance *Igf2* translation independently of *let-7* (Polesskaya et al., 2007), offering an alternative mechanism by which *Lin28a* might activate the insulin-PI3K-mTOR pathway. To determine the relative contribution of this mechanism, we performed *in vitro* and *in vivo* loss of function experiments. Following siRNA knockdown of *Igf2* in C2C12 (the efficacy of knockdown is shown in Figure S2.4B), we found only minimal changes in S6 and 4EBP1 phosphorylation (Figure S2.4C). In these C2C12 myotubes, glucose uptake was unaffected by *Igf2* knockdown, but significantly decreased by *let-7a* (Figure S2.4D). In addition, we crossed the *Lin28a* Tg mice with *Igf2* knockout mice and found that the absence of *Igf2* did not abrogate

enhanced glucose uptake, insulin sensitivity, or the anti-obesity effect mediated by *Lin28a* (Figure S2.4E-H). Taken together, these data indicate that the metabolic phenotypes we have observed are not solely due to the ability of Lin28a/b to promote translation of *Igf2* mRNA, but do not rule out the possibility that Lin28a/b might modulate other mRNAs in the insulin-PI3K-mTOR signaling pathway.

***mTOR mediates Lin28a's enhancement of growth and glucose metabolism in vivo***

Given that *Lin28a* activates the insulin-PI3K-mTOR pathway both *in vitro* and *in vivo*, we asked whether the metabolic effects of *Lin28a in vivo* could be abrogated by pharmacological inhibition of the mTOR pathway. To do this, we injected *Lin28a* Tg and wild-type littermates with rapamycin 3 times per week beginning when mice were 18 days old. Rapamycin abrogated the growth enhancement in *Lin28a* Tg mice at doses that had minimal growth suppressive effects on wild-type mice (Figure 2.5A,B), suggesting that *Lin28a* promotes growth in an mTOR-dependent manner. Selective suppression of *Lin28a*-driven growth was observed using several parameters: weight (Figure 2.5B,C), crown-rump length (Figure 2.5D), and tail width (Figure 2.5E). We also tested if the enhanced glucose uptake phenotype *in vivo* was likewise dependent on mTOR. Indeed, glucose tolerance testing showed that short-term rapamycin reversed the enhanced glucose uptake effect of *Lin28a* (Figure 2.5F,G) and reduced the insulin-sensitivity of *Lin28a* Tg mice to wild-type levels (Figure 2.5H,I). These data indicate that the glucose uptake, insulin sensitivity and animal growth phenotypes of *Lin28a* overexpression *in vivo* are dependent on mTOR signaling.

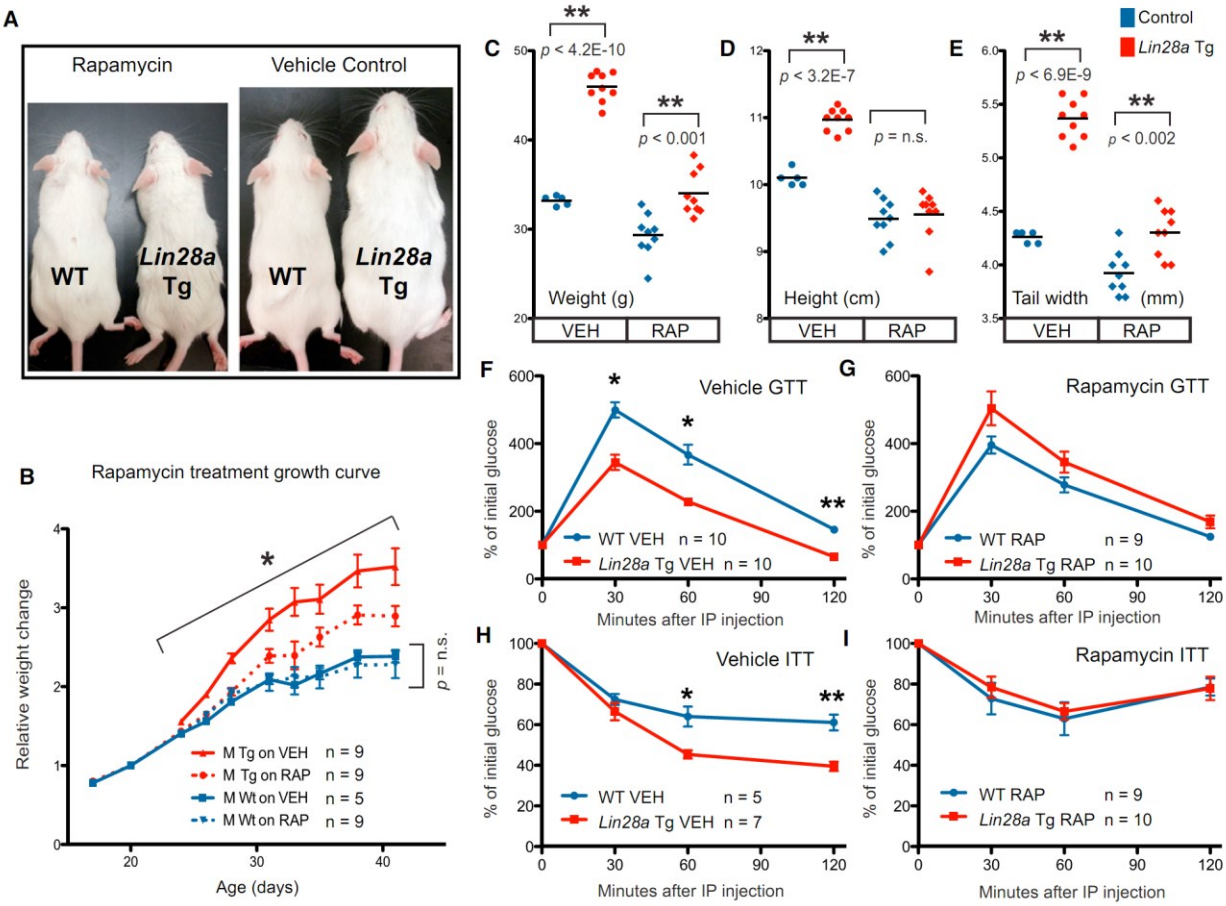


***Figure 2.5: mTOR is required for Lin28a's effects on growth and glucose metabolism in vivo***. (**A**) Rapamycin (left 2 mice) and vehicle (right 2 mice) treated wild-type and *Lin28a* Tg mice shows relative size differences. (**B**) Curves showing relative growth (normalized to weight on first day of treatment) for mice treated from 3 weeks to 5.5 weeks of age. Blue and red represent wild-type and *Lin28a* Tg mice, respectively. Solid and dotted lines represent vehicle and rapamycin treated mice, respectively. Growth was measured by several other parameters: (**C**) weight, (**D**) crown-rump length or height, and (**E**) tail width. (**F**) GTT performed after 2 doses of vehicle or (**G**) rapamycin. (**H**) ITT performed after 1 dose of vehicle or (**I**) rapamycin. Controls for Tg mice are WT. The numbers of experimental animals are listed within the charts.

***Let-7 target genes are associated with type 2 diabetes in human GWAS***

Finally, we sought to assess the relevance of the *Lin28*/*let-7* pathway to human disease and metabolism, using human genetic studies of T2D and fasting glucose levels. Because the *Lin28/let-7* pathway has not been previously implicated in T2D, we first asked whether any of the genes that lie in T2D association regions identified in T2D GWAS and meta-analyses (Voight et al., 2010) are known or predicted *let-7* targets. We used TargetScan 4.1 to computationally predict *let-7* targets (Grimson et al., 2007), and found that 14 predicted *let-7* target genes lie in linkage disequilibrium to 39 validated common variant associations with T2D, including *IGF2BP2*, *HMGA2*, *KCNJ11* and *DUSP9* (strength of T2D association signals $p < 4x10^{-9}$) (Table 2.1). Of the computationally predicted *let-7* targets associated with T2D, *IGF2BP1/2/3* and *Hmga2* have been verified as *let-7* targets in several studies (Boyerinas et al., 2008; Mayr et al., 2007). To validate the connection between *Lin28* and GWAS candidate genes, we analyzed the expression of *Igf2bp* and *Hmga* family members in C2C12 cells with and without *Lin28a* overexpression, and observed increases in *Igf2bp1*, *Igf2bp2*, and *Hmga2* mRNA following *Lin28a* overexpression (Figure 2.6A). To ensure that this was not a C2C12- or muscle-specific phenomenon, we confirmed the upregulation of these genes in 3T3 cells following human *LIN28A or LIN28B* overexpression on the mRNA (Figure 2.6B) and the protein level for the Igf2bp family (Figure 2.6C). We also observed increased expression of *Igf2bp2* and *Igf2bp3* (Figure 2.6D) in *Lin28a* Tg muscle, confirming this link *in vivo*.

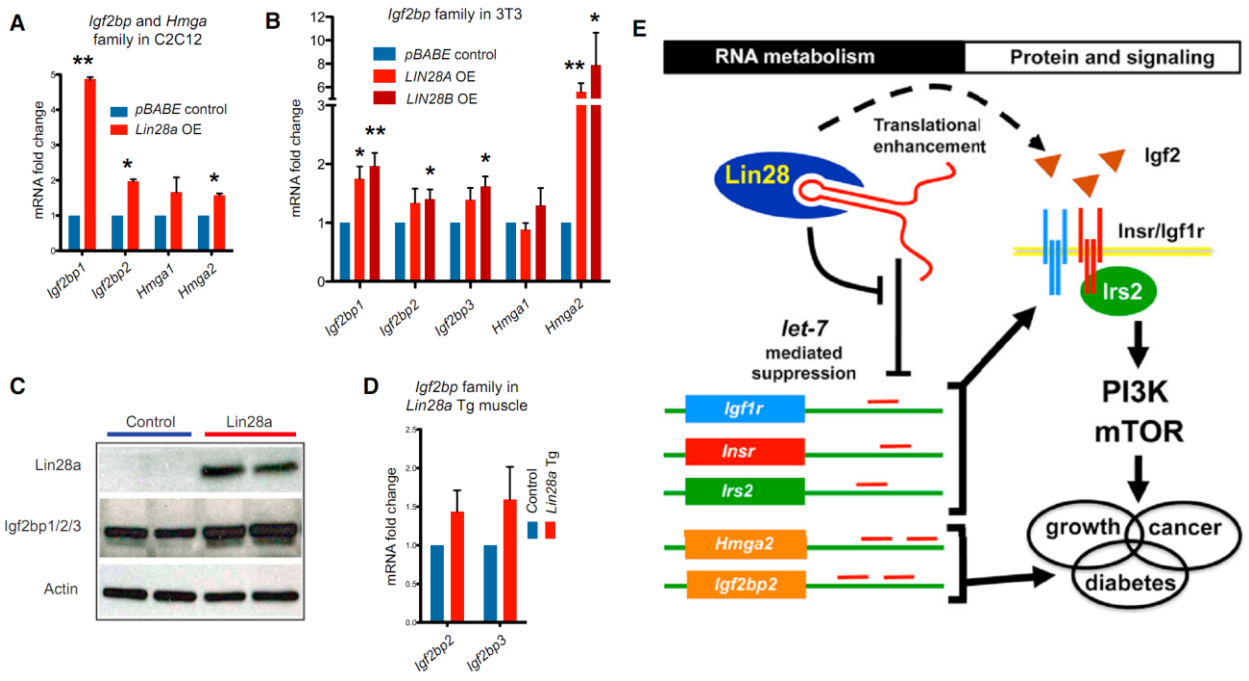


***Figure 2.6: Let-7 target genes are associated with Type 2 diabetes mellitus and a model of the Lin28/let-7 pathway in glucose metabolism.*** mRNA expression of *Igf2bp* and *Hmga* family members in (**A**) C2C12 with and without *Lin28a* overexpression and in (**B**) 3T3 cells with and without *LIN28A or LIN28B* overexpression. (**C**) Western blot of NIH 3T3 cells with Lin28a overexpression showing Lin28a and Igf2bp1/2/3 protein levels (n = 3 biological replicates). (**D**) *Igf2bp2* and *Igf2bp3* mRNA in *Lin28a* Tg muscle. (**E**) Model of *Lin28/let-7* pathway in glucose metabolism.

We next asked whether there is a more widespread connection between T2D susceptibility and *let-7* targets, in addition to the targets in validated T2D association regions ($p < 5x10^{-8}$). To address this, we applied a computational method called MAGENTA (Meta-Analysis Gene-set Enrichment of variaNT Associations) (Segre et al., 2010) to GWAS meta-analyses of T2D and fasting glucose blood levels, and tested whether the distributions of disease or trait associations in predefined *let-7* target gene

***Table 2.1: MAGENTA analysis of T2D and fasting glucose associations in different let-7 target gene sets.*** The statistical enrichment for genes associated with T2D and fasting glucose among *let-7* targets using the MAGENTA algorithm. The TargetScan algorithm was used to define the "All human let-7 targets" and the "Conserved let-7 targets" gene sets (http://www.targetscan.org/). mRNAs downregulation following *let-7* overexpression (OE) was measured in primary human fibroblasts (Legesse-Miller et al., 2009), and protein downregulation following *let-7* OE was measured in HeLa cells (Selbach et al., 2008). The enrichment cutoff used is the 75$^{th}$ percentile of all gene association scores in the genome. The enrichment fold is the ratio between the observed and expected number of genes above the enrichment cutoff. Genes linked to validated GWAS SNPs (39 SNPs for T2D and 14 SNPs for fasting glucose) were ordered according to the number of target gene sets they appear in and then alphabetically. † The following genes were removed from the analysis: (i) genes absent from the full human gene list used in the analysis, (ii) genes that had no SNPs within 110 kb upstream or 40 kb downstream to their most extreme transcript boundaries, or (iii) to correct for potential inflation of enrichment due to physical proximity of *let-7* target genes along the genome, subsets of proximal genes assigned the same best local SNP were collapsed to one gene and assigned the score of the most significant gene *p*-value in that subset. *gene sets that pass a Bonferroni corrected cutoff ($p < 0.004$).

**Table 2.1 (continued)**

| *let-7* Target Gene Set | Number of Genes Analyzed† | Nominal Enrichment *p* Value | Expected Number of Genes above Enrichment Cutoff | Observed Number of Genes above Enrichment Cutoff | Enrichment Fold | Number of Genes Linked to Validated GWAS SNPs | Genes Linked to Validated GWAS SNPs |
|---|---|---|---|---|---|---|---|
| Type 2 Diabetes (DIAGRAM+ Meta-Analysis) | | | | | | | |
| All targets predicted by *TargetScan* | 1763 | 0.036 | 441 | 462 | 1.05 | 14 | IGF2BP2, DUSP9, SLC5A6, TP53INP1, YKT6, ZNF512, HMGA2, KCNJ11, MAN2A2, MEST, NOTCH2, ZNF275, FAM72B, RCCD1 |
| Conserved targets predicted by *TargetScan* | 789 | 0.089 | 197 | 212 | 1.08 | 7 | IGF2BP2, DUSP9, SLC5A6, HMGA2, KCNJ11, MAN2A2, ZNF275 |
| Downregulated mRNAs following *let-7* OE | 795 | 0.055 | 199 | 216 | 1.09 | 9 | IGF2BP2, DUSP9, SLC5A6, TP53INP1, YKT6, ZNF512, HHEX, IRS1, TLE4 |
| Downregulated mRNAs following *let-7* OE + *TargetScan* | 502 | 0.061 | 126 | 140 | 1.11 | 6 | IGF2BP2, DUSP9, SLC5A6, TP53INP1, YKT6, ZNF512 |
| Downregulated proteins following *let-7* OE | 97 | 1.0E-06* | 24 | 46 | 1.92 | 2 | IGF2BP2, CDKAL1 |
| Downregulated proteins following *let-7* OE + *TargetScan* | 37 | 0.011 | 9 | 16 | 1.78 | 1 | IGF2BP2 |
| Fasting Glucose (MAGIC Meta-Analysis) | | | | | | | |
| All targets predicted by *TargetScan* | 1708 | 0.015 | 427 | 450 | 1.05 | 3 | CRY2, SLC2A2, GLIS3 |
| Conserved targets predicted by *TargetScan* | 759 | 0.042 | 190 | 207 | 1.09 | 1 | CRY2 |
| Downregulated mRNAs following *let-7* OE | 750 | 1.0E-04* | 188 | 226 | 1.20 | 2 | CRY2, FADS1 |
| Downregulated mRNAs following *let-7* OE + *TargetScan* | 484 | 0.013 | 121 | 141 | 1.17 | 1 | CRY2 |
| Downregulated proteins following *let-7* OE | 96 | 0.632 | 24 | 23 | 0.96 | 0 | - |
| Downregulated proteins following *let-7* OE + *TargetScan* | 35 | 0.245 | 9 | 11 | 1.22 | 0 | - |

sets are skewed towards highly ranked associations (including ones not yet reaching a level of genome-wide significance) compared to matched gene sets randomly sampled from the genome (Table 2.1). We tested three types of *let-7* target definitions with increasing levels of target validation, from *in silico* predicted *let-7* targets using TargetScan 4.1 (Grimson et al., 2007) to experimentally defined targets. For the latter, we used (i) a set of genes with at least one *let-7* site in their 3' UTR and whose mRNA was downregulated by *let-7b* overexpression in primary human fibroblasts (Legesse-

Miller et al., 2009), and (ii) a set of genes whose protein levels were most strongly downregulated by *let-7b* overexpression in HeLa cells (Selbach et al., 2008). We first tested the *let-7* target sets against the latest T2D meta-analysis of eight GWAS (called DIAGRAM+) (Voight et al., 2010), and found significant enrichment (Table 2.1). The enrichment rose from 1.05-fold for the broadest definition of *let-7* targets predicted using TargetScan (~1800 genes; $p = 0.036$) to 1.92-fold for the experimentally validated target set based on protein level changes in response to *let-7* overexpression (~100 genes; $p = 1x10^{-6}$). In the latter case, an excess of about 20 genes regulated by *let-7* at the protein level are predicted to contain novel SNP associations with T2D. Notably *IGF2BP2*, which is a canonical *let-7* target that lies in a validated T2D association locus, was found in all types of *let-7* target definitions in Table 2.1. Furthermore, the genes driving the T2D enrichment signals for the different *let-7* target sets include both functionally redundant homologues of T2D-associated genes, such as *IGF2BP1 (IGF2BP2), HMGA1 (HMGA2), DUSP12 and DUSP16 (DUSP9)*, and genes in the insulin-PI3K-mTOR pathway, including *IRS2, INSR, AKT2* and *TSC1* (best local SNP association $p = 10^{-4}$ to $4*10^{-3}$).

We next tested for enrichment of *let-7* target gene associations with fasting glucose levels, using data from the MAGIC (Meta-Analysis of Glucose and Insulin-related traits Consortium) study of fasting glucose levels (Dupuis et al., 2010). We observed an over-representation of multiple genes modestly associated with fasting glucose at different levels of significance for the different *let-7* target gene sets (Table 2.1). The strongest enrichment was found in the genes downregulated at the mRNA level by *let-7*, an

enrichment of 1.20 fold over expectation ($p$ = $1*10^{-4}$). Taken together, our human genetic results support the hypothesis that genes regulated by *let-7* influence human metabolic disease and glucose metabolism.

Recently it has also become clear that Lin28a/b has important *let-7*-independent roles in mRNA translation, as evidenced by numerous direct mRNA targets whose translation is enhanced by LIN28A (Peng et al., 2011). Using GSEA, we found that this list of direct mRNA targets is also significantly enriched for glucose, insulin and diabetes-related genes (Table S2.1). Thus, Lin28a/b may regulate metabolism through direct mRNA-binding as well as *let-7* targets.

## Discussion

### *Lin28 and let-7 are mutually antagonistic regulators of growth and metabolism*

Our work defines a new mechanism of RNA-mediated metabolic regulation. In mice, *Lin28a* and *LIN28B* overexpression results in insulin sensitivity, enhanced glucose tolerance, and resistance to diabetes. Our analysis of *iLet-7* Tg mice shows that *let-7* upregulation is also sufficient to inhibit normal glucose metabolism, supporting the idea that gain of *Lin28a/b* exerts effects on whole animal glucose metabolism at least in part through *let-7* suppression. Previously, we showed that transgenic overexpression of *Lin28a* causes enhanced growth and delayed puberty, phenotypes that mimicked human traits linked to genetic variation in the *Lin28/let-7* pathway in GWAS (Zhu et al., 2010). Given that *Lin28a/b* is downregulated in most tissues after embryogenesis, while *let-7* increases in adult tissues, lingering questions from our earlier report were first,

whether *let-7* was sufficient to influence organismal growth, and second, what function does *let-7* have in adult physiology? Our observation that the *iLin28a*, *iLIN28B*, and *iLet-7* Tg gain of function mice, as well as muscle-specific *Lin28a* loss of function mice manifest complementary phenotypes supports the notion that *Lin28a/b* and *let-7* are both regulators of growth and developmental maturation. We propose that different developmental time-points demand distinct metabolic needs, and that global regulators such as *Lin28* temporally coordinate growth with metabolism. The dynamic relationship between *Lin28*, *let-7* and metabolic states during major growth milestones in mammals is reminiscent of the heterochronic mutant phenotypes originally defined in *C. elegans* (Ambros and Horvitz, 1984; Moss et al., 1997; Boehm and Slack, 2005), and suggests that metabolism, like differentiation, is temporally controlled.

***Lin28a/b and let-7 influence glucose metabolism through the insulin-PI3K-mTOR pathway***

We have shown that *Lin28a/b* and *let-7* regulates insulin-PI3K-mTOR signaling, a highly conserved pathway that regulates growth and glucose metabolism throughout evolution. PI3K/Akt signaling is known to promote Glut4 translocation to upregulate glucose uptake, while mTOR signaling can promote glucose uptake and glycolysis by changing gene expression independently of Glut4 translocation (Brugarolas et al., 2003; Buller et al., 2008; Duvel et al., 2010). Previous studies have shown that Lin28a directly promotes Igf2 (Polesskaya et al., 2007) and HMGA1 translation (Peng et al., 2011), and that *let-7* suppresses IGF1R translation in hepatocellular carcinoma cells (Wang et al., 2010). Consistent with these findings, our results define a model whereby *Lin28a/b* and

*let-7* coordinately regulate the insulin-PI3K-mTOR pathway at multiple points (Figure 2.6E), a concept that is consistent with the hypotheses that miRNAs and RNA binding proteins regulate signaling pathways by tuning the production of a broad array of proteins rather than switching single components on or off (Kennell et al., 2008; Hatley et al., 2010; Small and Olson, 2011). Coordinated regulation is important because negative feedback loops exist within the insulin-PI3K-mTOR pathway. Loss-of-function and pharmacological inhibition studies have shown that the mTOR target S6K1, for instance, inhibits and desensitizes insulin-PI3K signaling by phosphorylating IRS1 protein and suppressing *IRS1* gene transcription (Harrington et al., 2004; Shah et al., 2004; Tremblay et al., 2007; Um et al., 2004). Conversely, TSC1-2 promotes insulin-PI3K signaling by suppressing mTOR signaling (Harrington et al., 2004; Shah et al., 2004). Although the effects of *let-7* and *Lin28a/b* on the expression of individual genes are modest, simultaneous regulation of multiple components such as *IGF2, IGF1R, INSR, IRS2, PIK3IP1, AKT2, TSC1, RICTOR* in the insulin-PI3K-mTOR signaling pathway could explain how this RNA processing pathway coordinately regulates insulin sensitivity and glucose metabolism by effectively bypassing these negative feedback loops.

Whereas our work has implicated *let-7* as a regulator of insulin-PI3K-mTOR signaling, we do not exclude a parallel role for direct mRNA targets of Lin28a/b in glucose metabolism, a hypothesis supported by the recent findings that *HMGA1* is translationally regulated by LIN28A and mutated in 5-10% of T2D patients (Peng et al., 2011; Chiefari et al., 2011). Such non-*let-7* functions are also suggested by the fact that muscle-

specific loss of *Lin28a* results in glucose derangement without significant *let-7* changes. Nevertheless, it remains likely that during other developmental stages or in other tissues, *let-7* suppression by *Lin28a* or *Lin28b* is required for normal glucose homeostasis. The effects of the *Lin28/let-7* pathway on glucose metabolism in our murine models, together with our observation that genes regulated by *let-7* are associated with T2D risk in humans, indicates important functional roles for both *Lin28a/b* and *let-7* in human metabolism.

***Let-7 targets are relevant to disparate human diseases: cancer and T2D***

Metabolic reprogramming in malignancy is thought to promote a tumor's ability to produce biomass and tolerate stress in the face of uncertain nutrient supplies (Vander Heiden et al., 2009). During their rapid growth phase early in development, embryos may utilize similar programs to maintain a growth-permissive metabolism. Dissecting the genetic underpinnings of embryonic metabolism would likely provide important insights into the nutrient uptake programs that are co-opted in cancer. While loss of function studies in the early embryo would help define the metabolic roles of oncofetal genes in their physiologic context, classical *in vivo* metabolic assays are difficult to perform in embryos. *Lin28a* and *Lin28b* are oncofetal genes, and thus highly expressed in early embryogenesis and then silenced in most adult tissues, but reactivated in cancer (Yang and Moss, 2003; Viswanathan et al., 2009). Cancer cells may utilize the embryonic function of *Lin28a/b* to drive a metabolic shift towards increased glucose uptake and glycolysis – a phenomenon termed the "Warburg effect." Previously, we showed that *Lin28a* expression promotes glycolytic metabolism in muscle *in vivo* and in

C2C12 myoblasts *in vitro* (Zhu et al., 2010). Though we cannot yet readily determine the metabolic effects of shutting off *Lin28a/b* within the embryo, we have dissected the potent effects of reactivating and inactivating this oncofetal program in adults. Conversely, in normal adult tissues that do not express high levels of *Lin28a* or *Lin28b*, one might ask if a role for the highly abundant *let-7* is to lock cells into the metabolism of terminally differentiated cells to prevent aberrant reactivation of embryonic metabolic programs. Further studies are required to understand how this pathway may link mechanisms of tumorigenesis and diabetogenesis.

Our report implicates *Lin28a/b* and *let-7* as important modulators of glucose metabolism through interactions with the insulin-PI3K-mTOR pathway and T2D-associated genes identified in GWAS. Although it is likely that additional mechanisms and feedback loops exist, our data suggests a model whereby *Lin28a/b* and *let-7* coordinate the GWAS identified genes and the insulin-PI3K-mTOR pathway to regulate glucose metabolism (Figure 2.6E). It also suggests that enhancing *Lin28* function or abrogating *let-7* may be therapeutically promising for diseases like obesity and diabetes. Likewise, results from this work might shed light on the physiology of aging and, specifically, how the accumulation of *let-7* in aging tissues may contribute to the systemic insulin resistance that accompanies aging.

**Acknowledgements**

This chapter was published in part as Zhu et al. (*Cell*, 2011). These studies were performed in close collaboration with Hao Zhu, who took primary responsibility for all

mouse work, while I focused on all the mechanistic experiments. Hao Zhu and I designed and performed the experiments, and wrote the manuscript. David Altshuler, Ayellet Segre and Jesse Engreitz performed bioinformatic analysis on targets in GWAS. Gen Shinoda, Samar Shah, Will Einhorn, and Ayumu Takeuchi aided with mouse strains and experiments. Michael Kharas helped to design some experiments. George Daley designed and supervised experiments, and wrote the manuscript. We also thank John Powers, Harith Rajagopalan, Jason Locasale, Abdel Saci, Akash Patnaik, Charles Kaufman, Christian Mosimann and Lewis Cantley for invaluable discussions and advice, Roderick Bronson and the Harvard Medical School Rodent Histopathology Core for mouse tissue pathology, and the Harvard Neurobehavior Laboratory for metabolic cage experiments.

## Chapter 3: *Lin28* enhances adult tissue regeneration by reprogramming cellular metabolism

### Introduction

Our prior studies linking Lin28 to juvenile programs of growth, development and metabolism led us to ask if reprogramming the developmental age of tissues with *Lin28* could influence their post-natal regenerative capacities. Across the evolutionary spectrum of organisms, the juvenile state is associated with superior tissue repair (defined as the partial or complete restoration of cellular content and tissue integrity after injury). *Drosophila* and *Tribolium* larvae repair robustly, but the adult insects do not (Smith-Bolton et al., 2009; Shah et al., 2011). Tadpoles, but not adult frogs, can repair multiple tissues (Sánchez Alvarado and Tsonis, 2006), and in *Ambystoma* salamanders, regenerative capacity declines with age (Young et al., 1983). Young fish repair their caudal fins better than older ones (Anchelin et al., 2011), and it is well-known that during gestation, fetal mammals repair their tissues more robustly than older mammals (Deuchar, 1976; Conboy et al., 2005; Nishino et al., 2008; Porrello et al., 2011). In contrast, insects like the *Apterygota*, which do not undergo complete metamorphosis, retain remarkable larval capacities for appendage repair throughout life (Pearson, 1984), and some hyper-regenerative urodeles such as the neotenic Axolotl fail to undergo metamorphosis and exhibit larval regenerative potential throughout their lifespan. These exceptions notwithstanding, the correlation between juvenility and tissue repair has long been discussed by Charles Darwin and others (Darwin, 1887; Pearson, 1984; Poss, 2010), but the causal mechanisms remain obscure.

Here we report that engineering the re-expression of Lin28 can enhance tissue repair in a variety of contexts. Surprisingly, *let-7* repression is necessary but alone insufficient to account for Lin28a's enhancement of tissue repair. Lin28a also binds and promotes the translation of the mRNAs for several metabolic enzymes, including *Pfkp, Pdha1, Idh3b, Sdha, Ndufb3* and *Ndufb8*, which as established through metabolomic profiling, enhance oxidative metabolism and promote an embryonic bioenergetic state. Pharmacologic studies with specific inhibitors shows that *Lin28a*-mediated tissue repair is significantly more sensitive to OxPhos inhibition by antimycin-A, than normal tissue repair. These data suggest that *Lin28a* promotes repair capacities in post-natal tissues by enhancing mitochondrial oxidative metabolism and promoting a bioenergetic state characteristic of embryonic cells.

**Experimental Procedures.**

***Mice.*** All animal procedures were based on animal care guidelines approved by the Institutional Animal Care and Use Committee.

***Digit amputation.*** A dissection microscope was used for all digit amputations. Neonatal mice were cryoanesthetized before the forelimb and hindlimb central digits 2, 3, and 4 were amputated at the distal interphalangeal joint using a no. 11 scalpel. In all animals, right limb digits were left un-amputated as controls. Digit regrowth was measured as % of the uninjured digit length. In adults, mice were anesthetized with ketamine/xylazine before 400μm of hindlimb digits 2 and 4 were amputated using a no. 11 scalpel. Digit 3 was left unamputated as a control. One dose of 0.05 mg/kg buprenorphine was given as

postsurgical analgesia.

***Ear hole punch assay.*** A 2-mm-diameter through-and-through hole was punched in the centre of each outer ear (pinna) by using a clinical biopsy punch (Roboz, Gaithersburg, MD). After wounding, the animals were killed at different time points to establish a time course. For profiling experiments, the entire pinna was punched throughout with 1-mm-diameter holes to maximize the amount of pinnal tissue undergoing tissue repair, then harvested 3 days after injury and frozen in liquid nitrogen before further processing.

***Quantitative RT-PCR, Western blot and Immunohistochemistry.*** All assessments of mRNA levels were performed by qRT-PCR, and all assessments of protein levels were performed by Western Immunoblotting, as previously described (Zhu et al. 2011). For immunohistochemistry, sections were incubated with anti-Lin28a (Cell Signaling), anti-Lin28b (Cell Signaling), anti-Ki-67 (Dako) or anti-BrdU (Cell Signaling), and visualized using the VECTASTAIN Elite ABC System (Vector Labs).

***RNA immunoprecipitation.*** Cells and tissues were lysed in M2 buffer with RNAse inhibitor, then incubated with anti-FLAG M2 affinity gel beads (Sigma Aldrich) according to the manufacturer's instructions, to pull-down FLAG-tagged Lin28a. After 4 washes with M2 buffer, RNA bound to the M2 affinity gel beads was isolated using Trizol (Invitrogen).

***Metabolomics, and Seahorse Analyzer.*** Metabolomics analysis was performed as previously described (Shyh-Chang et al., 2013). Seahorse data analysis was performed as previously described (Wu et al., 2007).

***Drug treatments***. For the pinnal repair experiments, drug inhibitors were applied topically using 25uL of 5mM 2-deoxy-D-glucose, 100uM 3-bromopyruvate, 500nM antimycin-A, or 10mM N-acetyl-cysteine, per ear 3 times a week, with 1 g/L dox dissolved in DMSO as the vehicle control. *Let-7* antimiR (Exiqon, Denmark) was injected subcutaneously once weekly as previously described (Frost and Olson, 2011), or applied topically with 25ug LNA per ear using jetPEI according to manufacturer instructions (Polyplus, France).

***Histology.*** Tissue samples were fixed in 10% buffered formalin or Bouin's solution and embedded in paraffin.

***Statistical analysis***. Data is presented as mean ± SEM, and Student's t-test (two-tailed distribution, two-sample unequal variance) was used to calculate *p* values. Statistical significance is displayed as $p < 0.05$ (one asterisk) or $p < 0.01$ (two asterisks) unless specified otherwise. The tests were performed using Microsoft Excel where the test type is always set to two-sample equal variance.

## Results

### *Lin28a promotes epidermal hair regrowth*

*Lin28a* is expressed in the embryonic epidermis, but disappears by birth (Yang and Moss, 2003). We previously described a doxycycline (dox)-inducible *Lin28a* transgenic mouse ("iLin28a Tg") with constitutively low levels of leaky *Lin28a* expression in the absence of induction (Zhu et al., 2010). Relative to non-transgenic wild type littermates (WT), iLin28a Tg mice displayed thicker hair coats and increased skin thickness (Figure 4.1A and Figure S3.1A), correlating with *Lin28a* overexpression and *let-7* repression in

the epidermis (Figure 3.1B-D). The hair appearance was not explained by greater hair follicle density or follicle bulb diameter (Figure S3.1B,C). Given these observations, we analyzed the response to shaving to determine if *Lin28a* overexpression might influence hair regrowth.

In mice, the hair follicle cycle is normally synchronized for the first 10 weeks of life (Muller-Rover et al. 2001). The first post-natal growth phase (anagen) ends at approximately post-natal day 16 (p16), followed by the first resting phase (telogen). The second anagen begins at p28 and is followed by a second protracted telogen phase between p42 and p70 (Muller-Rover et al. 2001). We shaved the hair of mice expected to be in the first and second telogen phases (p21 and p70), and found that iLin28a Tg mice displayed enhanced dorsal hair regrowth at both of these time points (Figure 3.1E). To explore the mechanism of this growth difference, we performed a full 10-week hair cycle survey and found that while WT mice conform to the expected timing of the anagen-telogen phases, iLin28a Tg mice have extended periods of anagen and shortened telogen periods (Figure 3.1F). Specifically, WT mice were in telogen at p20, 24, 42, 47, 49, 56 and 69, while iLin28a Tg mice manifested only a brief resting phase at p42 and p47. We then asked if hair regrowth occurs differently in WT and iLin28a Tg mice when both are in anagen. We synchronized hair cycling using wax depilation, which removes the entire hair follicle and thus induces anagen in both genotypes, and found no differential in hair regrowth during anagen (Figure S3.1D), which was corroborated by equivalent cell proliferation in anagen hair follicles (Figure S3.1E). Additionally, we inquired if *Lin28a* induction could induce anagen during a telogen

***Figure 3.1: Lin28a reactivation promotes hair regrowth.*** (**A**) Uninduced iLin28a Tg mice possess a thicker fur coat than WT mice. (**B**) *Lin28a* expression in the skin of WT or iLin28a Tg mice as determined by immunohistochemistry. (**C**) *Lin28a* mRNA levels as determined by qRT-PCR. (**D**) Mature *let-7* expression as determined by qRT-PCR in tail epidermis of WT and uninduced iLin28a Tg mice. (**E**) Hair regrowth in mice shaved at p21 was observed 1 week post-shaving in 0/6 WT vs. 6/6 Lin28a Tg littermates (Left image). Hair regrowth in mice shaved at p70 was observed 3 weeks post-shaving in 0/6 WT vs. 5/5 iLin28a Tg littermates (Right image). (**F**) Histologic hair cycle analysis over 10 weeks. All sections are 10x and H+E stained. (**G**) Hair regrowth on dorsal skin in topical dox-treated p47 WT and iLin28a Tg littermates, 1 and 2 weeks after shaving. Ectopic hair regrowth was observed in 0/4 WT dox treated vs. 0/3 DMSO treated Tg vs. 3/4 dox induced Tg mice.

**Figure 3.1 (continued)**

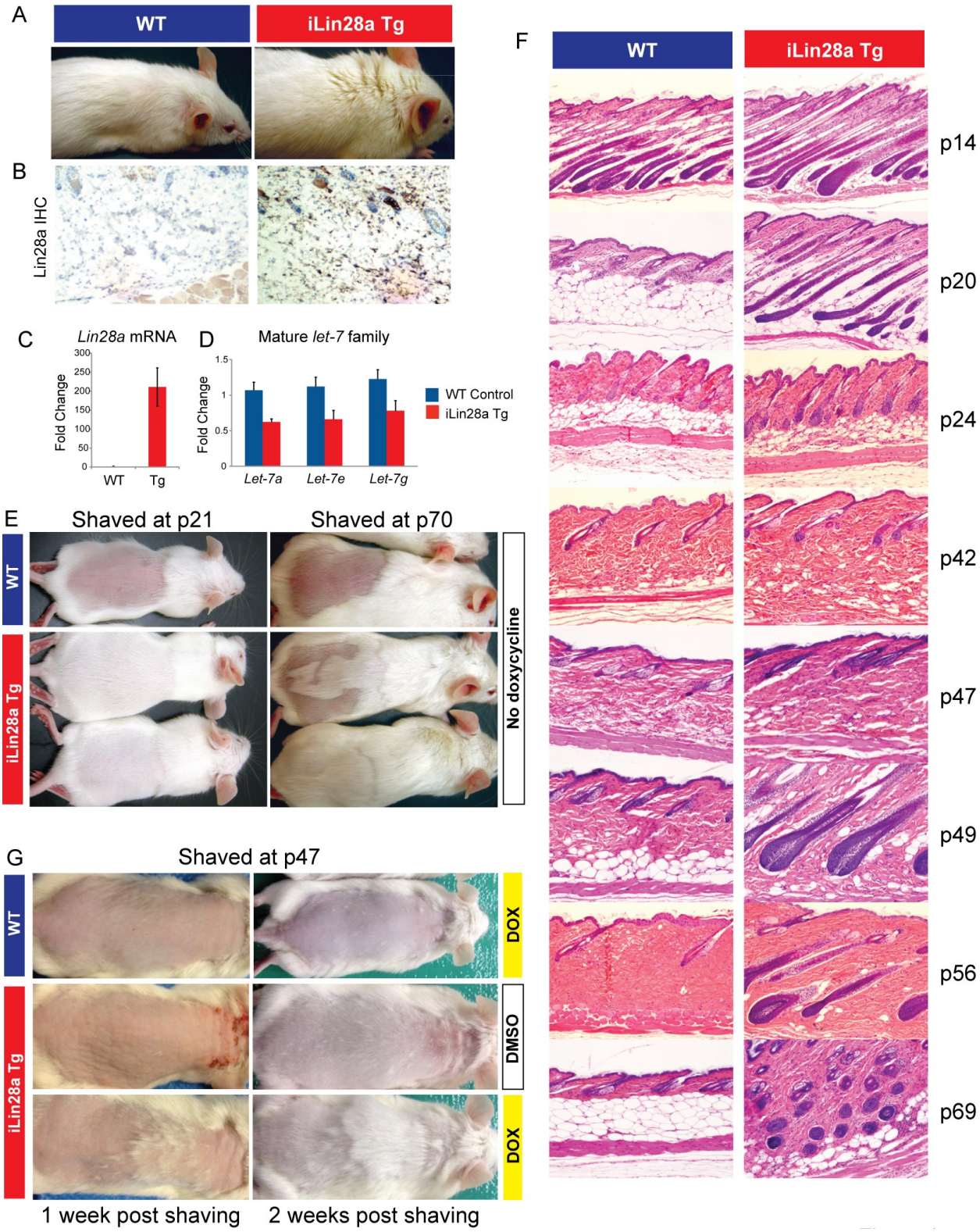

phase. We induced *Lin28a* by topical application of dox at p47, when both WT and iLin28a Tg mice were in telogen. Dox treated WT or DMSO treated iLin28a Tg mice showed no hair regrowth, whereas iLin28a Tg mice with topical dox showed patchy hair regrowth after 7 and 14 days, indicating that *Lin28a* overexpression during telogen is sufficient to induce anagen in hair follicles (Figure 3.1G). Thus, *Lin28a* overexpression promotes hair regrowth by promoting anagen. Findings from this tissue context suggested that ectopic reactivation of *Lin28a* might be capable of promoting regeneration in other post-natal tissues as well.

***Lin28a promotes digit regeneration***

*Lin28a* mRNA is expressed in the embryonic limb buds of E9.5 – E11.5 embryos, but declines sharply by birth (Yokoyama et al. 2008). Limb digits consist of multiple tissue types and show limited regenerative capacity after amputation in neonatal mammals. To assess regeneration, mouse digits were amputated at the distal interphalangeal joint on day 2 after birth, and digit length was measured at 3 weeks of age. Relative to WT neonates, iLin28a Tg neonates displayed significantly enhanced soft tissue and bone regrowth in amputated digit tips (Figure 3.2A-C). Even after normalizing for the greater body growth in iLin28a Tg mice, *Lin28a* accelerated the regrowth of injured digits over time (Figure 3.2D). Whereas *Lin28a* showed no significant increase in expression in WT digits following amputation, *Lin28a* expression was elevated in iLin28a Tg digits before and after amputation (Figure 3.2E-F). Consistent with this pattern, only *let-7b* dropped after digit amputation in WT mice, whereas several *let-7* species were repressed both before and after injury in iLin28a Tg mice (Figure 3.2G).

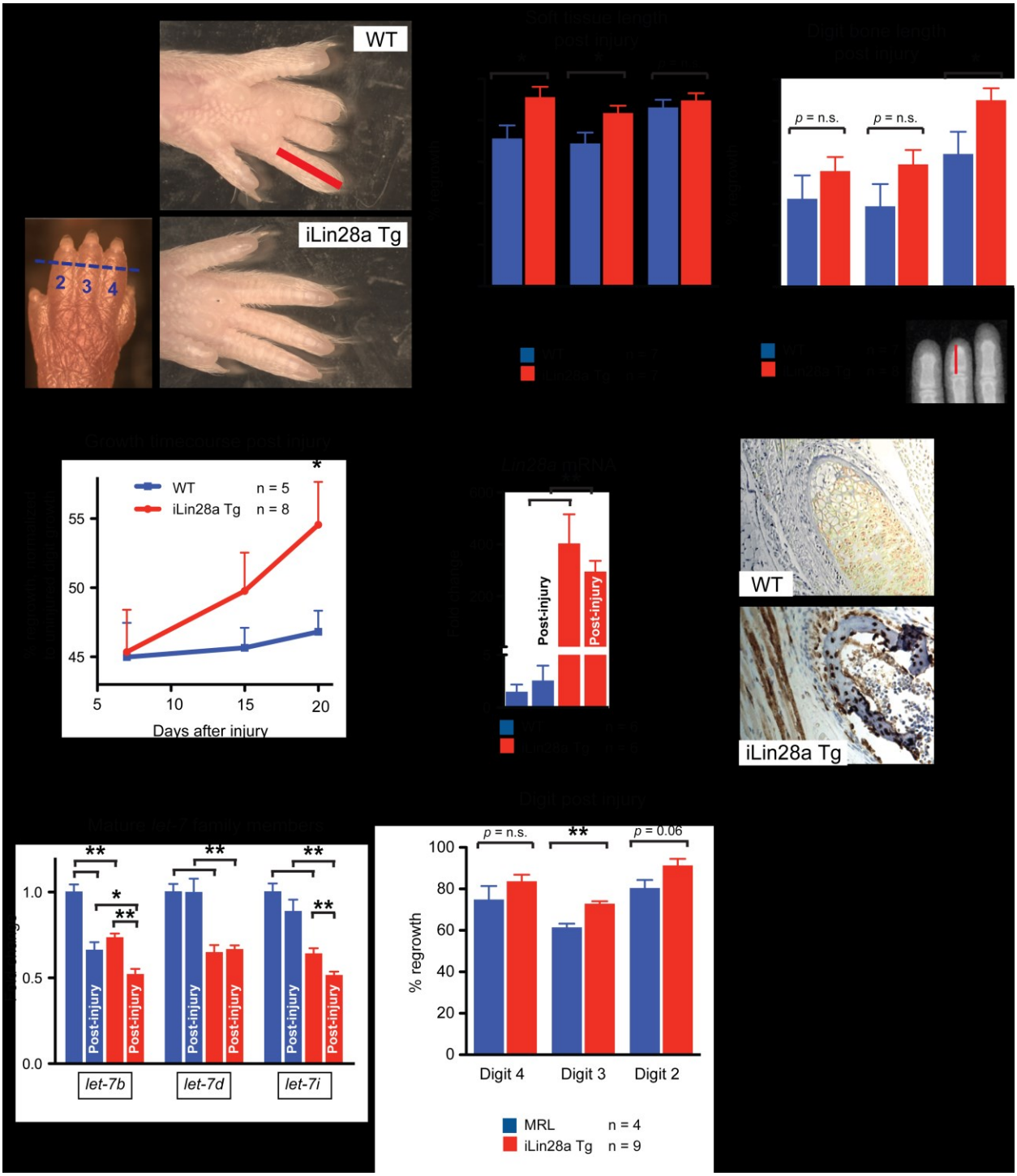


***Figure 3.2: Lin28a reactivation promotes digit regrowth after amputation.*** For all digit measurements, % regrowth is quantified by dividing the length of the regrowing digit in the injured limb with the length of the normal digit on the opposite uninjured limb.

***Figure 3.2 (continued)*** (**A**) Left image shows p1 digits and the amputation site (blue hash mark). Right images show digits 21 days after neonatal digit amputation. Red bar depicts the soft tissue dimension measured between the digit tip and the proximal interphalangeal joint. (**B**) Quantification of soft tissue regrowth 21 days after neonatal digit amputation. (**C**) Quantification of bone regrowth 21 days after neonatal digit amputation. X-ray film with red bar showing that bone length was measured from the proximal interphalangeal joint. (**D**) Post-injury growth kinetics (as % of uninjured digit length) over 21 days. (**E**) *Lin28a* mRNA expression in WT, injured WT, iLin28a Tg, and injured iLin28a Tg digits, as determined by qRT-PCR. (**F**) Immunohistochemistry indicating Lin28a protein expression in Tg and WT bone from the neonatal skeleton. (**G**) Mature *let-7* expression in WT, injured WT, iLin28a Tg, and injured iLin28a Tg digits, as determined by qRT-PCR. (**H**) Digit tip regrowth in iLin28a Tg mice backcrossed onto the hyper-regenerative MRL strain background. Control mice are WT MRL littermates. * $P<0.05$, ** $P< 0.01$.

We next asked if *Lin28a* overexpression could further improve tissue regeneration in MRL mice, a well-known hyper-regenerative strain (Clark et al. 1998; Chadwick et al. 2007; Gourevitch et al. 2009). After backcrossing iLin28a Tg mice onto the MRL strain for 5 generations, *Lin28a* overexpression further enhanced digit tip regeneration relative to WT MRL controls, suggesting non-overlapping, additive mechanisms of enhanced repair. This supports the idea that even the enhanced regeneration of the MRL strain could be augmented by genetic reactivation of *Lin28a* (Figure 3.2H).

Because *Lin28a* improved neonatal digit regeneration, we hypothesized that *Lin28a* overexpression might also improve adult digit tip regeneration. In 5-week old mice, we amputated hindlimb digit tips, but found that reactivation of *Lin28a* expression conferred no significant enhancement of regeneration (Figure S3.2), suggesting that *Lin28a* alone is insufficient to enhance adult repair in this context.

***Lin28a promotes pinnal tissue repair***

We assayed repair in the adult pinnal tissues of the outer ear, another complex tissue that fails to regenerate completely upon injury (Goss et al. 1975; McBrearty et al. 1998; Liu et al. 2011). Low-level leaky *Lin28a* overexpression in the iLin28a Tg mice enhanced wound healing after 2mm full-thickness punch biopsy (Figure 3.3A), as indicated by smaller wound sizes detected at 5, 8, and 11 days (Figure 3.3B). In WT mice, 28% of the wounds could not be evaluated quantitatively because of poor healing and severe tearing of the wounds, whereas only 2% of wounds in iLin28a Tg mice displayed such severe damage (Figure 3.3C). Similar to the digits, we observed a transient drop in *let-7b* following injury (Figure 3.4A), but did not observe an increase in *Lin28a* during WT tissue repair (Figure 3.3D, E). To determine if direct activation of *Lin28a* at the site of injury would promote pinnal repair, we applied dox topically onto wounds after punch biopsy.

We detected local induction of *Lin28a* protein (Figure 3.3D) and mRNA (Figure 3.3E), and measured 50% greater wound closure after 11 days relative to uninduced iLin28a Tg ears (Figure 3.3F). *Hmga2*, a prominent *let-7* target, was also induced in iLin28a Tg

***Figure 3.3: Lin28a reactivation promotes pinnal tissue repair.*** (**A**) WT and iLin28a Tg wound healing 8 days after 2mm-diameter ear hole punches. (**B**) Wound area size at day 5, 8, and 11, during the course of wound healing. (**C**) Proportion of WT and iLin28a Tg ear holes torn by mice after ear hole punching. (**D**) Western blot indicating Lin28a protein levels in topical dox-treated iLin28a Tg ears, before (n=2) and 3 days after (n=2) injury, compared to WT ears. (**E**) mRNA levels of *Lin28a* and the *let-7* target *Hmga2* in topical dox-treated iLin28a Tg ears, as determined by qRT-PCR. (**F**) Wound area size after 10 days of local topical treatment with dox. (**G**) H+E, trichrome, Lin28a, and Ki-67 staining in WT, iLin28a Tg and induced iLin28a Tg mice.

**Figure 3.3 (continued)**

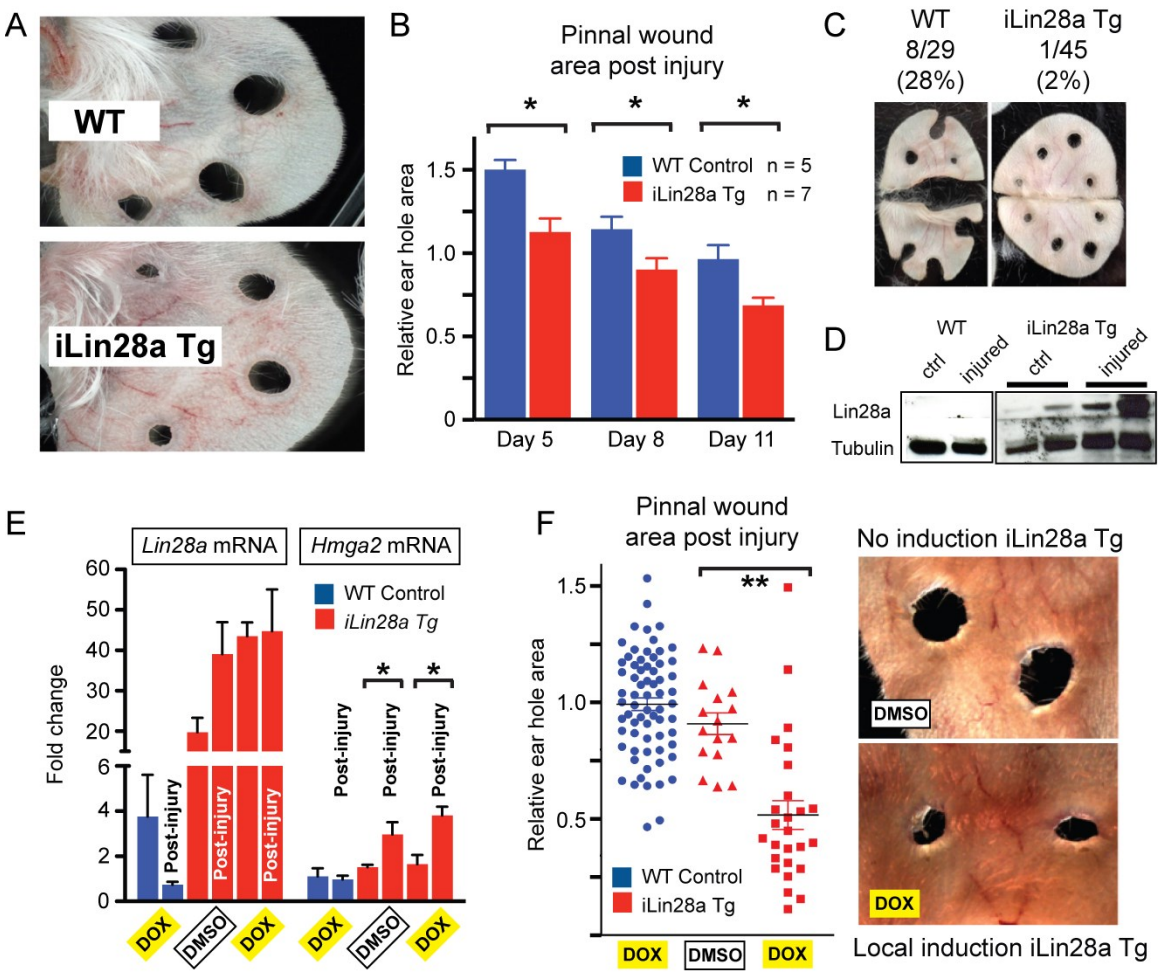

but not in WT ears (Figure 3.3E). Histologically, there was an increase in mesenchymal connective tissue after local *Lin28a* induction, and an increase in proliferation according to Ki67 staining (Figure 3.3G), indicating that *Lin28a* induction promotes mesenchymal cell proliferation and tissue repair in pinnae. Interestingly, local dox induction of *LIN28B* in iLIN28B Tg mice (Zhu et al. 2011) was not sufficient to promote ear wound healing, suggesting a *Lin28a*-specific mechanism for this process (Figure S3.3).

***Repression of let-7 is necessary but insufficient for promoting tissue repair***

A major downstream effect of *Lin28* is the repression of *let-7* microRNAs. Because a subset of *let-7* miRNAs decreased after digit and pinnal injury in WT animals (Figure 3.2G, 3.4A), we hypothesized that suppression of *let-7* might be essential to tissue repair, and that enforced expression of *let-7* would antagonize wound healing. We therefore assessed tissue repair in a transgenic mouse that expresses a dox-inducible form of the *let-7* miRNA ("iLet-7 mice"; Zhu et al. 2011). Indeed, induction of *let-7* after ear punch biopsy inhibited wound closure and pinnal repair relative to uninduced mice (Figure 3.4B). To test if *let-7* repression would be sufficient to phenocopy the enhanced tissue repair observed with overexpression of *Lin28a*, we used a locked nucleic acid (LNA)-modified antimiR to antagonize *let-7* function. Previously, *let-7* antimiRs successfully reduced mature *let-7* levels and promoted an anti-diabetic phenotype in mice, thus phenocopying *Lin28a* overexpression (Frost and Olson 2011; Zhu et al. 2011).

***Figure 3.4: Let-7 repression is necessary but insufficient for tissue repair.*** (**A**) Expression of mature *let-7g* and *let-7b* in WT and iLet-7 ears, before and after injury, as determined by qRT-PCR. (**B**) Ear hole wound area size after whole animal *let-7g* induction in iLet-7 mice. (**C**) Mature *let-7* miRNA expression in MEFs after *let-7* antimiR treatment, as determined by qRT-PCR. (**D**) Mature *let-7* miRNA expression in vivo after 2 subcutaneous injections of *let-7* antimiR. (**E**) Northern blot indicating *let-7a* levels in the liver and skin of control and *let-7* antimiR-treated WT mice. (**F**) Ear hole wound size after subcutaneous *let-7* antimiR treatment of WT mice. (**G**) Ear hole wound size after local topical *let-7* antimiR treatment of WT mice. (**H**) Hair regrowth after *let-7* antimiR treatment of WT mice.

**Figure 3.4 (continued)**

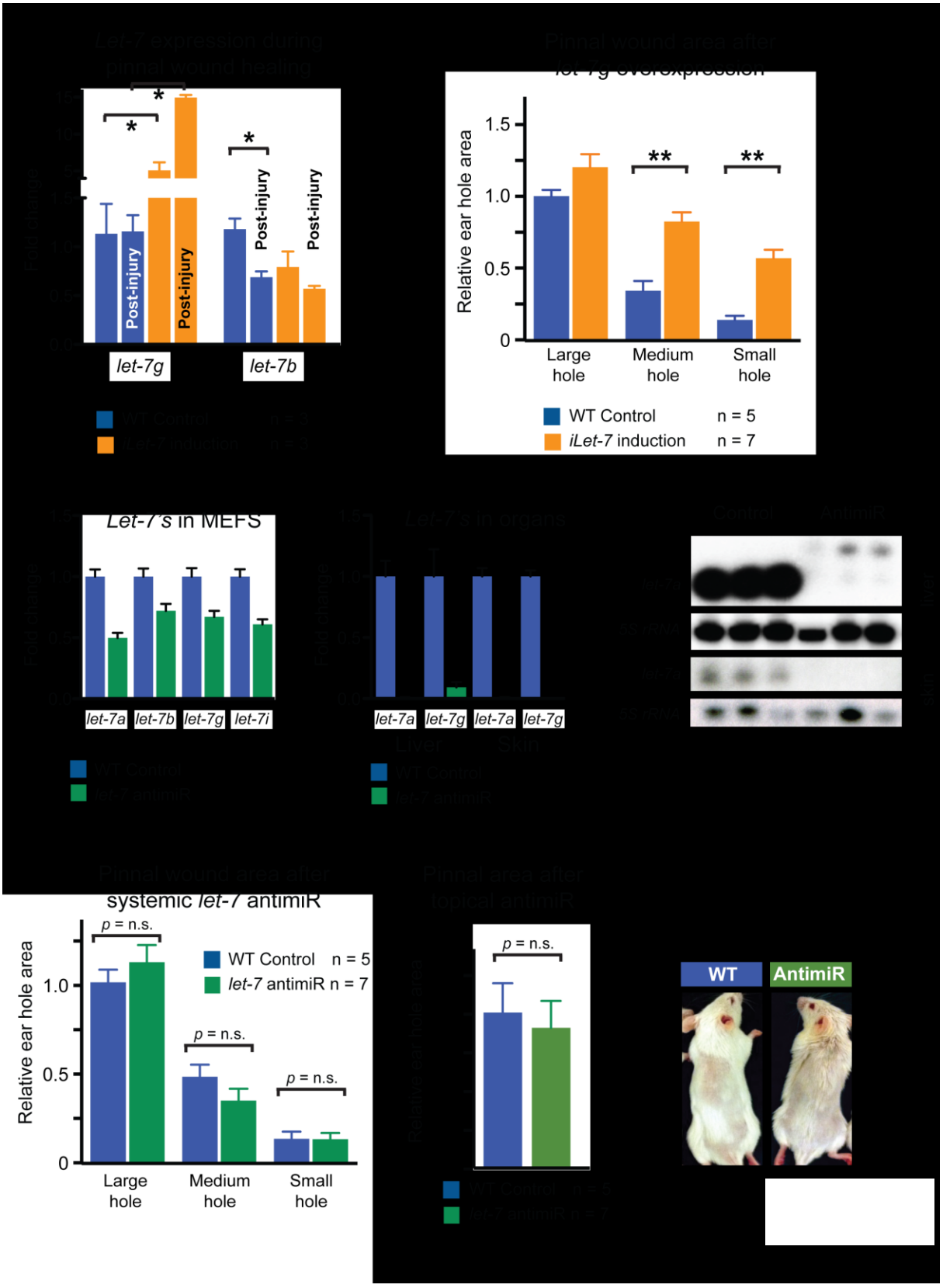

In our experiments, the *let-7* antimiR repressed a wide range of mature *let-7*'s in MEFs and in vivo (Figure 3.4C-E), to a greater extent than achieved by *Lin28a* overexpression. However, despite an efficient knockdown of *let-7*, neither systemic nor topical delivery of *let-7* antimiR enhanced pinnal tissue repair (Figure 3.4F,G) nor hair regrowth (Figure 3.4H). These data indicate that *let-7* antagonizes normal tissue repair, but also suggest that *let-7* repression is necessary but not alone sufficient to explain the mechanism of enhanced tissue repair by Lin28a.

***Lin28a alters the bioenergetic state during tissue repair***

Although Lin28a is most well-known as a repressor of *let-7* microRNA biogenesis, Lin28a also regulates mRNA translation independently of *let-7* (Polesskaya et al., 2007; Peng et al., 2011; Wilbert et al., 2012; Cho et al., 2012). Transcripts encoding metabolic enzymes in mitochondrial oxidative phosphorylation (OxPhos) and glycolysis are among the top mRNAs bound specifically by *Lin28a* (Peng et al., 2011; Zhu et al., 2011). To test if these findings are consistent with the embryonic metabolic state influenced by *Lin28a*, we profiled metabolism in whole *Lin28a*$^{-/-}$ *Lin28b*$^{-/-}$ embryos vs. *Lin28a*$^{+/+}$ *Lin28b*$^{-/-}$ embryos at E10.5, using Liquid Chromatography/Tandem Mass Spectrometry metabolomics (Shyh-Chang et al., 2013). *Lin28a* deficiency led to lower levels of some glycolytic intermediates (Figure S3.4A), lower ATP/AMP and NADH/NAD ratios, and higher levels of reduced glutathione (higher GSH/GSSG ratio, which indicates lower levels of reactive oxygen species - ROS; Figure S3.4B). These data demonstrate that *Lin28a* is physiologically required for normal embryonic bioenergetics, and are consistent with our previous study which compared *Lin28a*$^{+/-}$ to *Lin28a*$^{-/-}$ embryos and

***Figure 3.5: Lin28a alters the bioenergetic state during tissue repair.*** (**A**) LC-MS/MS selected reaction monitoring (SRM) analysis of abundance in glycolysis intermediates in WT and iLin28a Tg pinnal tissue after injury (inj), relative to WT uninjured pinnae. G3P, D-glyceraldehyde-3-phosphate. DHAP, dihydroxyacetone-phosphate. BPG, 1,3-bisphosphoglycerate. 3PG, 3-phosphoglycerate. PEP, phosphoenolpyruvate. (**B**) SRM analysis of several metabolic indicators in WT and iLin28a Tg pinnal tissue after injury (inj), relative to WT uninjured pinnae. ATP, adenosine-5'-triphosphate. AMP, adenosine-5'-monophosphate. GTP, guanosine-5'-triphosphate. GMP, guanosine-5'-monophosphate. GSH/GSSG, glutathione/glutathione disulfide. (**C**) Fraction of glycolytic intermediates labeled by $^{13}C$, derived from [U-$^{13}C$]glucose in MEFs over 30 minutes, as measured by SRM analysis (n=3). (**D**) Fraction of Krebs cycle intermediates labeled at 2 carbons by $^{13}C$, derived from [U-$^{13}C$]glucose in MEFs over 8 hours, as measured by SRM analysis (n=3). (**E**) SRM analysis of the ATP/AMP and GSH/GSSG ratios in WT and iLin28a Tg MEFs (n=3). (**F**) Mitochondrial biogenesis, glycolytic enzyme, and *let-7* target mRNAs, analyzed by qRT-PCR. *Lin28a,* and the *let-7* targets *Imp1* and *Imp2* served as positive controls. Relative expression levels were normalized to WT MEFs. (**G**) Oxygen consumption rate (OCR) of WT and iLin28a Tg MEFs, as measured by the Seahorse Analyzer (n=4 each). Oligomycin treatment inhibits ATP synthase-dependent OCR, the proton gradient uncoupler FCCP then induces maximal OCR, and antimycin/rotenone finally inhibits all OxPhos-dependent OCR. (**H**) Extracellular acidification rate (ECAR) of WT and iLin28a Tg MEFs, as measured by the Seahorse Analyzer (n=4 each). Addition of glucose induces glycolysis-dependent lactic acid production and ECAR, oligomycin then induces maximal ECAR, and 3BP partially

***Figure 3.5 (continued)*** inhibits glycolysis-dependent ECAR. (**I**) Mature *let-7* expression in WT and iLin28a Tg MEFs, after transfection with a scrambled (scr) control, *let-7* LNA antimiR, or *let-7a* duplex, as determined by qRT-PCR. (**J**) Expression of the *let-7* targets *Hmga2* and *Imp2* in WT and iLin28a Tg MEFs, after transfection with a scrambled (scr) control, *let-7* LNA antimiR, or *let-7a* duplex, as determined by qRT-PCR. (**K**) Fraction of the glycolytic intermediate 3-phosphoglycerate (3PG) and the glycolytic side-product serine, labeled by $^{13}C$ derived from [U-$^{13}C$]glucose over 30 minutes, in MEFs after transfection with a scrambled (scr) control, *let-7* LNA antimiR, or *let-7a* duplex (n=3). (**L**) Fraction of the Krebs cycle intermediates citrate, malate and oxaloacetate-derived aspartate, labeled at 2 carbons by $^{13}C$ derived from [U-$^{13}C$]glucose over 8 hours, in MEFs after transfection with a scrambled (scr) control, *let-7* LNA antimiR, or *let-7a* duplex (n=3). (**M**) SRM analysis of several metabolic indicators in WT and iLin28a Tg MEFs after transfection with a scrambled (scr) control, *let-7* LNA antimiR, or *let-7a* duplex (n=3).

**Figure 3.5 (continued)**

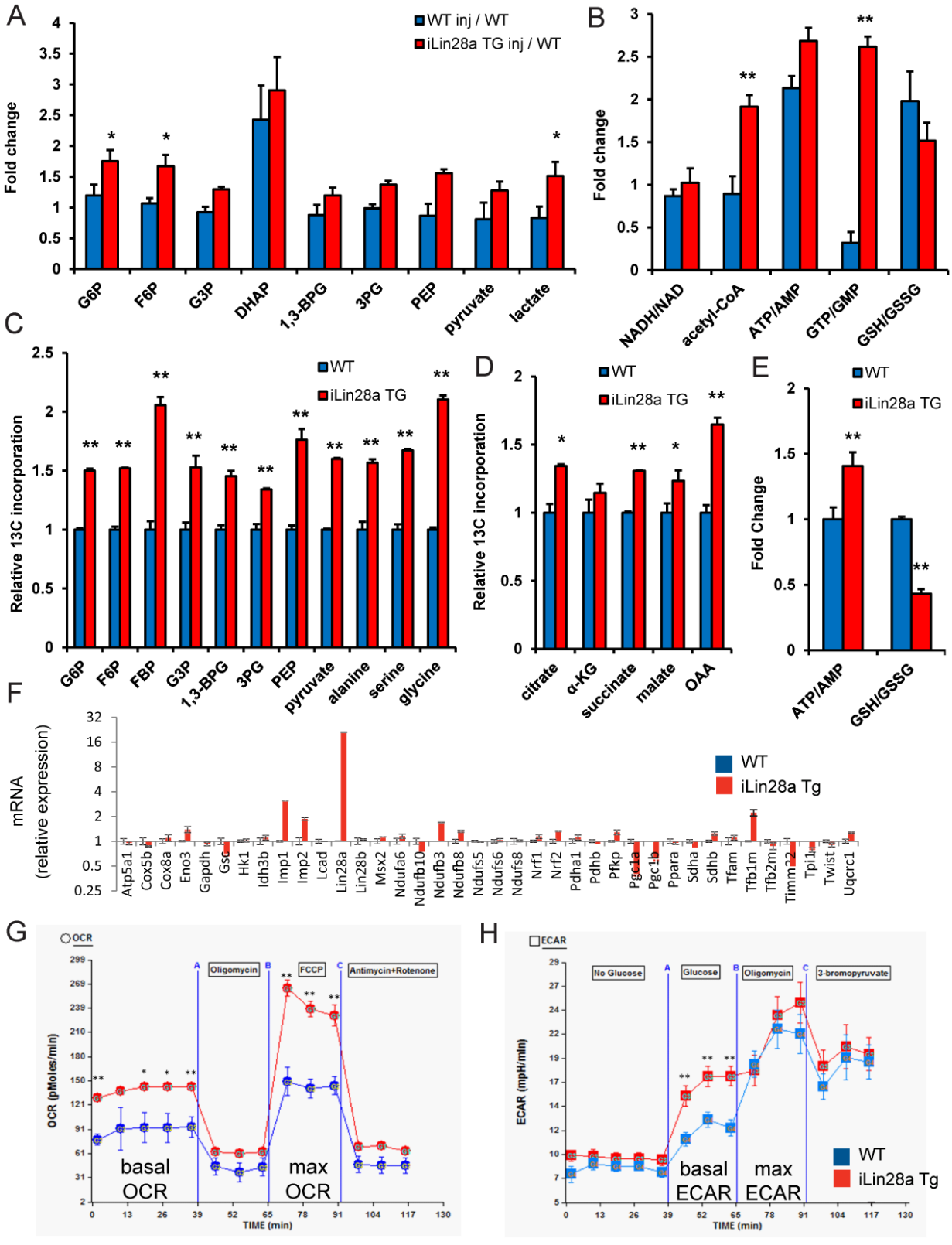

**Figure 3.5 (continued)**

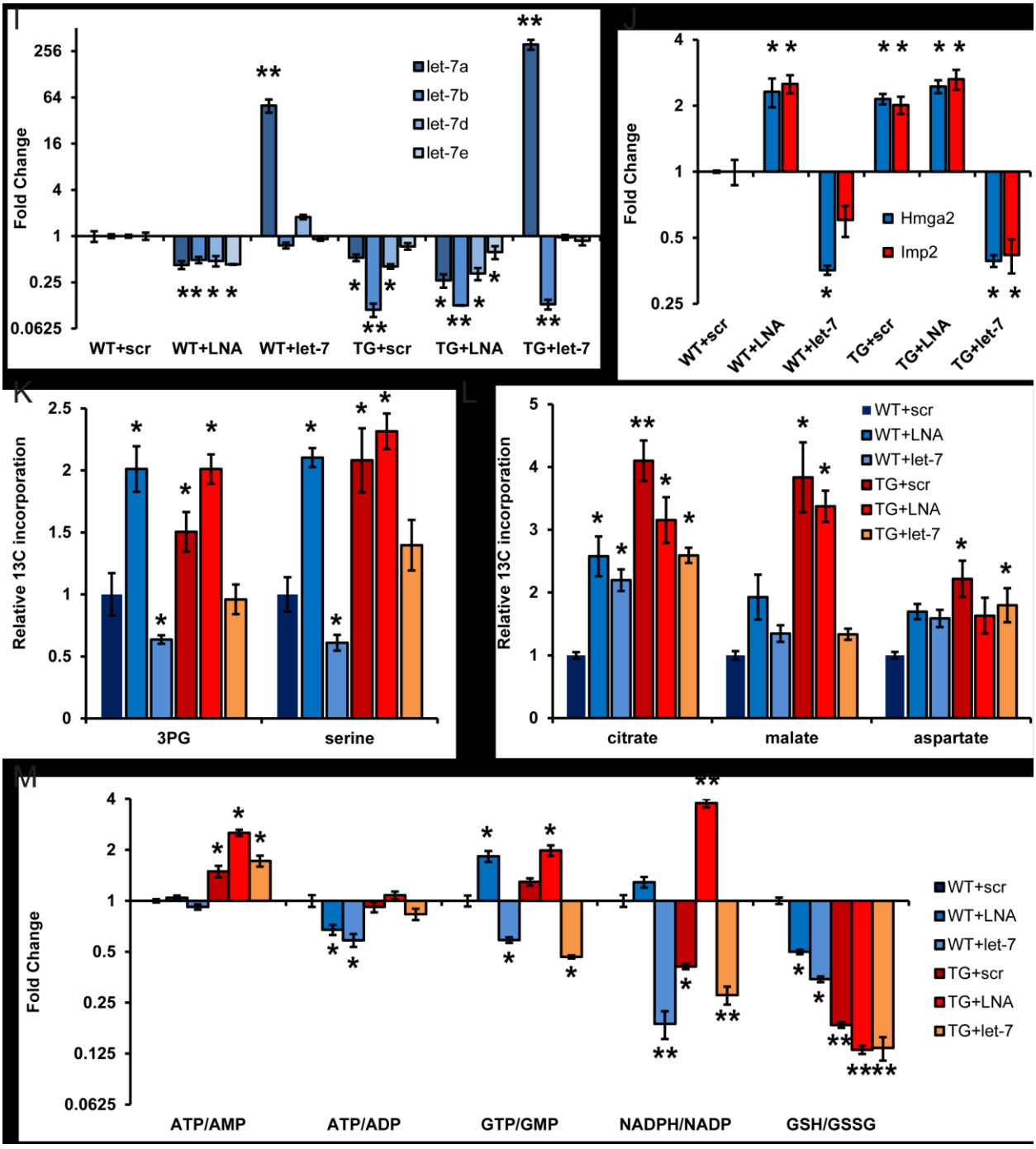


likewise concluded that *Lin28a* is essential for normal embryonic metabolism (Shinoda et al., 2013).

These precedents prompted us to profile the metabolomic effects of *Lin28a* reactivation during tissue repair. We found that *Lin28a* induction led to an increase in several glycolytic intermediates in pinnal tissues after injury (e.g., glucose-6-phosphate, fructose-6-phosphate as well as lactate), suggesting a general increase in glucose oxidation, whereas WT ears exhibited few changes (Figure 3.5A). *Lin28a* induction also enhanced the bioenergetic state during tissue repair in vivo, as indicated by the increase in acetyl-CoA biosynthesis, and the increased ATP/AMP and GTP/GMP bioenergetic ratios (Figure 3.5B).

Using $^{13}$C-glucose, we measured the flux of glucose through glycolysis and the Krebs cycle in MEFs, and found that *Lin28a* increased $^{13}$C-glucose flux into glycolytic intermediates (Figure 3.5C), as well as Krebs cycle intermediates (Figure 3.5D), consistent with our observations in vivo. Furthermore, we found that the ATP/AMP ratio increased by 40% whereas the GSH/GSSG ratio decreased significantly with *Lin28a* overexpression (Figure 3.5E), consistent with our observations that Lin28a enhances glucose oxidation to produce more ATP and ROS during tissue repair.

To determine if *Lin28a* was promoting the bioenergetic state by simply increasing mitochondrial biogenesis, we measured mitochondrial markers. We failed to detect increases in the mRNA levels of mitochondrial biogenesis markers and enzymes (Figure 3.5F); there was no change in mitochondrial DNA (Figure S3.4C); and CMXRos staining revealed no significant changes in the mitochondrial density and distribution (Figure S3.4D). These data indicate that *Lin28a* enhances mitochondrial OxPhos

activity rather than mass. We confirmed this using the Seahorse analyzer to measure the $O_2$ consumption rates of primary MEFs from iLin28a Tg mice. Relative to WT control MEFs, *Lin28a* increased both the basal and maximal OxPhos capacity, as indicated by the increases in $O_2$ consumption (Figure 3.5G). *Lin28a* also increased the basal glycolytic capacity (Figure 3.5H), consistent with findings from $^{13}$C-glucose flux metabolomics.

To assess if *Lin28a* was causing metabolic changes in a *let-7*-dependent manner, we transfected a *let-7* mimic and/or the *let-7* antimiR into WT and iLin28a Tg MEFs. As expected, the *let-7* LNA antimiR led to *let-7* repression (Figure 3.5I) and increased expression of the canonical *let-7* targets *Hmga2* and *Imp2* (Figure 3.5J), whereas the *let-7* mimic led to the converse (Figure 3.5I-J). $^{13}$C-glucose flux metabolomic profiling of these transfected MEFs then revealed that *let-7* repression phenocopied Lin28a's enhancement of glycolytic flux (into 3-phosphoglycerate and serine biosynthesis), whereas *let-7* overexpression suppressed WT glycolysis and partially abrogated Lin28a's enhancement of glycolysis (Figure 3.5K). These data are consistent with previous studies showing that *let-7* regulates insulin-PI3K-mTOR signaling, which promotes glycolysis (Zhu et al., 2011; Frost and Olson, 2011). However, *let-7* repression failed to fully phenocopy Lin28a's enhancement of Krebs cycle flux, and *let-7* overexpression failed to reduce WT Krebs cycle flux, although it did partially abrogate Lin28a's enhancement of Krebs cycle flux (Figure 3.5L). Most importantly, *let-7* repression failed to phenocopy Lin28a's enhancement of OxPhos, and *let-7* overexpression failed to block Lin28a's enhancement of OxPhos (Figure 3.5M). These

results show that Lin28a acts on OxPhos in ways that do not involve *let-7*, and support our conclusion that *let-7* regulation is necessary but insufficient to phenocopy Lin28a's effects on tissue repair.

***Lin28a promotes the expression of mitochondrial oxidation enzymes***

We used RNA immunoprecipitation (RIP) to determine which of the mRNAs for metabolic enzymes previously shown to be bound by Lin28a in human ESCs (Peng et al., 2011) are likewise bound and regulated by Lin28a in primary MEFs and tissues in vivo. FLAG-tagged Lin28a bound to mRNAs for *Pfkp, Pdha1, Idh3b, Sdha, Ndufb3* and *Ndufb8*, both in MEFs (Figure 3.6A) and pinnal tissues (Figure 3.6B). Western blots further revealed that Lin28a overexpression correlated with increased expression of Pfkp, Pdha1, Idh3b, Sdha, Ndufb3 and Ndufb8 proteins in primary MEFs and pinnal tissues in vivo (Figure 3.6C), consistent with previous studies showing that Lin28a can directly enhance mRNA translation (Polesskaya et al., 2007). Interestingly, phosphofructokinase (Pfkp) and pyruvate dehydrogenase (Pdha1) are the rate-limiting enzymes that fuel glycolysis and the Krebs cycle respectively (Figure S3.5A). Isocitrate dehydrogenase (Idh3b) is the mitochondrial enzyme that catalyzes the first oxidative decarboxylation step in the Krebs cycle to produce α-ketoglutarate, NADH and $CO_2$, whereas succinate dehydrogenase (Sdha) oxidizes succinate to produce fumarate and $FADH_2$, and also serves as Complex II in the electron transport chain. NADH dehydrogenases (Ndufb3/8) constitute the rate-limiting Complex I in the electron transport chain that oxidizes NADH for ATP synthesis during OxPhos. Hence, Lin28a

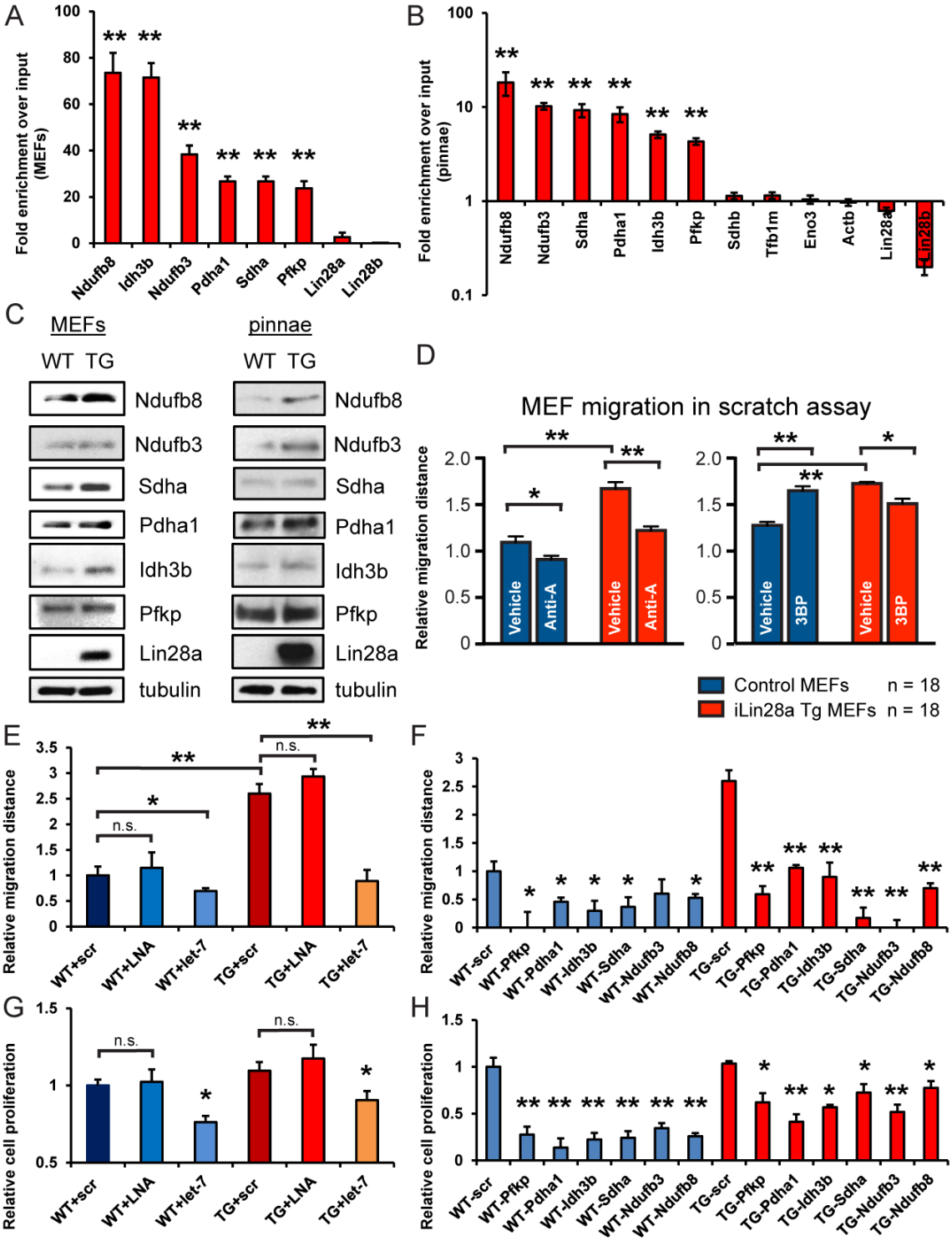


***Figure 3.6: Lin28 promotes wound healing by enhancing bioenergetic metabolism.*** (**A**) RNA immunoprecipitation (RIP) using FLAG-tagged Lin28a and subsequent RT-PCR shows the metabolic enzyme mRNAs bound by Lin28a in MEFs in

***Figure 3.6 (continued)*** vitro. (**B**) RNA immunoprecipitation (RIP) using FLAG-tagged Lin28a and subsequent RT-PCR shows the metabolic enzyme mRNAs bound by Lin28a in pinnal tissues in vivo. (**C**) Western blots for Lin28a mRNA targets in primary MEFs and pinnal tissues in vivo. (**D**) Distance traveled by WT and iLin28a Tg MEFs, 18 hours after a defined scratch was made on equal-numbered monolayers (n=18). MEFs were treated with 50nM Anti-A, 100uM 3BP, or DMSO vehicle control immediately after the scratch. (**E**) Distance traveled by WT and iLin28a Tg MEFs treated with a scrambled (scr) control, *let-7* LNA antimiR, or *let-7a* duplex. (**F**) Distance traveled by WT and iLin28a Tg MEFs treated with siRNAs against metabolic enzymes. (**G**) Cell proliferation of WT and iLin28a Tg MEFs treated with a scrambled (scr) control, *let-7* LNA antimiR, or *let-7a* duplex. (**H**) Cell proliferation of WT and iLin28a Tg MEFs treated with siRNAs against metabolic enzymes.

directly binds and promotes translation of multiple rate-limiting enzyme components in both glycolysis and OxPhos (Figure 3.6A-C).

To determine if *Lin28a*-mediated metabolic enhancements might influence cell migration or proliferation, two processes that are critical for tissue repair (Guo and DiPietro, 2010), we subjected MEFs to in vitro migration and proliferation assays. Indeed, iLin28a Tg MEFs migrated more than WT MEFs (Figure 3.6D). We then tested if pharmacological inhibition of glycolysis or OxPhos could influence MEF migration (see Figure S3.5A forsummary of inhibitor targets). OxPhos inhibition by antimycin-A, a specific electron transport chain Complex III inhibitor, reduced iLin28a Tg MEF migration more than WT MEFs (Figure 3.6D). The glycolysis inhibitor 3-bromopyruvate (3BP) also reduced

iLin28a Tg MEF migration more than WT MEFs (Figure 3.6D), together suggesting that Lin28a promotes cell migration by enhancing glycolysis and OxPhos.

To determine if Lin28a was influencing cell migration in a *let-7*-dependent manner, we transfected the *let-7* LNA antimiR and *let-7* mimic into Tg and WT MEFs. Neither *let-7* repression nor overexpression had significant effects on WT MEF migration, whereas *let-7* overexpression significantly inhibited iLin28a Tg MEF migration (Figure 3.6E). These data are consistent with our observations that *let-7* repression is necessary but insufficient to recapitulate Lin28a's effects, suggesting that the mRNA targets of Lin28a play critical roles. Indeed, siRNA knockdown of *Pfkp, Pdha1, Idh3b, Sdha, Ndufb3* or *Ndufb8* (Figure S3.5A-E) all impaired cell migration for WT and Tg MEFs (Figure 3.6F), indicating that these metabolic enzymes contribute to cell migration.

Cell proliferation is critical for tissue repair as well, but the necessity for OxPhos in this process is unclear. In vitro, OxPhos inhibition by antimycin-A impaired the proliferation of both WT and iLin28a Tg MEFs (Figure S3.5F), with no changes in apoptosis, suggesting that normal OxPhos is essential for cell proliferation. Overexpression of *let-7* inhibited cell proliferation in both WT and iLin28a Tg MEFs, whereas *let-7* repression did not significantly affect proliferation in either MEFs (Figure 3.6G). These data are, again, consistent with our observations that *let-7* repression alone is necessary but insufficient to recapitulate Lin28a's effects, suggesting that the mRNA targets of Lin28a are also important. Depletion of *Pfkp, Pdha1, Idh3b, Sdha, Ndufb3* or *Ndufb8* (Figure S3.5A-E), led to a defect in cell proliferation for both WT and iLin28a Tg MEFs (Figure

3.6H), showing that these metabolic enzymes are also involved in cell proliferation. Over the course of passaging, *Lin28a* suppressed MEF proliferation in vitro (Figure S3.5F) while in vivo, *Lin28a* promoted cell proliferation in hair follicles (Figure 3.1) and pinnal tissues (Figure 3.3G). Lin28a is therefore likely to be inducing senescence in vitro after long-term passage, via pyruvate dehydrogenase-dependent oxidative stress (Kaplon et al., 2013). This counter-intuitive effect is also observed when other oncogenes like Kras, Braf and PI3K are over-expressed in cells cultured in vitro, even when these oncogenes are known to promote cell proliferation in vivo.

To assess the importance of *Lin28a*-mediated metabolic changes in vivo, we applied specific pharmacologic inhibitors of glycolysis and OxPhos in the setting of hair regrowth (Figure 3.7A). As shown in Figure 3.1, topical induction of Lin28a in the epidermis improves hair regrowth during telogen. OxPhos inhibition with topical antimycin-A (+dox) suppressed hair regrowth specifically in iLin28a Tg mice, with no effect on WT mice (Figure 3.7A). Glycolysis inhibition with topical 3BP (+dox) also suppressed hair growth specifically in iLin28a Tg mice, without influencing WT mice. When the drugs were discontinued for 10 days, WT mice showed partial hair regrowth whereas iLin28a Tg mice showed complete regrowth, indicating that hair follicle cycling was only transiently, and not irreversibly inhibited by this dosing regimen (Figure 3.7A). These results imply that *Lin28a* promotes hair regrowth by enhancing both glycolysis and OxPhos.

***Figure 3.7: Lin28 promotes tissue repair in vivo by enhancing bioenergetic metabolism.*** (**A**) Hair regrowth of dorsal skin in p42 iLin28a Tg mice and WT littermates, at the time of shaving, and 3 weeks after local topical treatment with 3BP, or Anti-A, dissolved in 1g/L dox in DMSO (Ctrl). Mice were then taken off all treatment for 1 week. (**B**) Pinnal wound size after 10 days of local topical treatment with Anti-A, dissolved in 1g/L dox in DMSO (Ctrl), on both iLin28a Tg and WT littermate ear holes. (**C**) Pinnal wound size after 10 days of local topical treatment with the antioxidant N-acetyl-cysteine (NAC) dissolved in 1g/L dox in DMSO (Ctrl), on both iLin28a Tg and WT littermate ear holes. (**D**) Pinnal wound size after 10 days of local topical treatment with the glycolysis inhibitors 3BP or 2-deoxy-D-glucose (2DG) dissolved in 1g/L dox in DMSO (Ctrl), on both iLin28a Tg and WT littermate ear holes. (**E**) Metabolomic profiling on WT ears 1 and 7 days after daily 3BP treatment. Shown are glycolytic intermediates and the bioenergetics ratios NADH/NAD, ATP/AMP, ATP/ADP, and GTP/GMP (n=4). (**F**) Fraction of the Krebs cycle intermediates isocitrate, succinate, and malate, labeled at 2 carbons by $^{13}C$ derived from [U-$^{13}C$]glucose over 8 hours, in WT MEFs after continuous incubation in 3BP for 3 days (n=3). (**G**) Maximal $O_2$ consumption rate in WT MEFs after continuous incubation in 3BP for 3 days (n=6).

**Figure 3.7 (continued)**

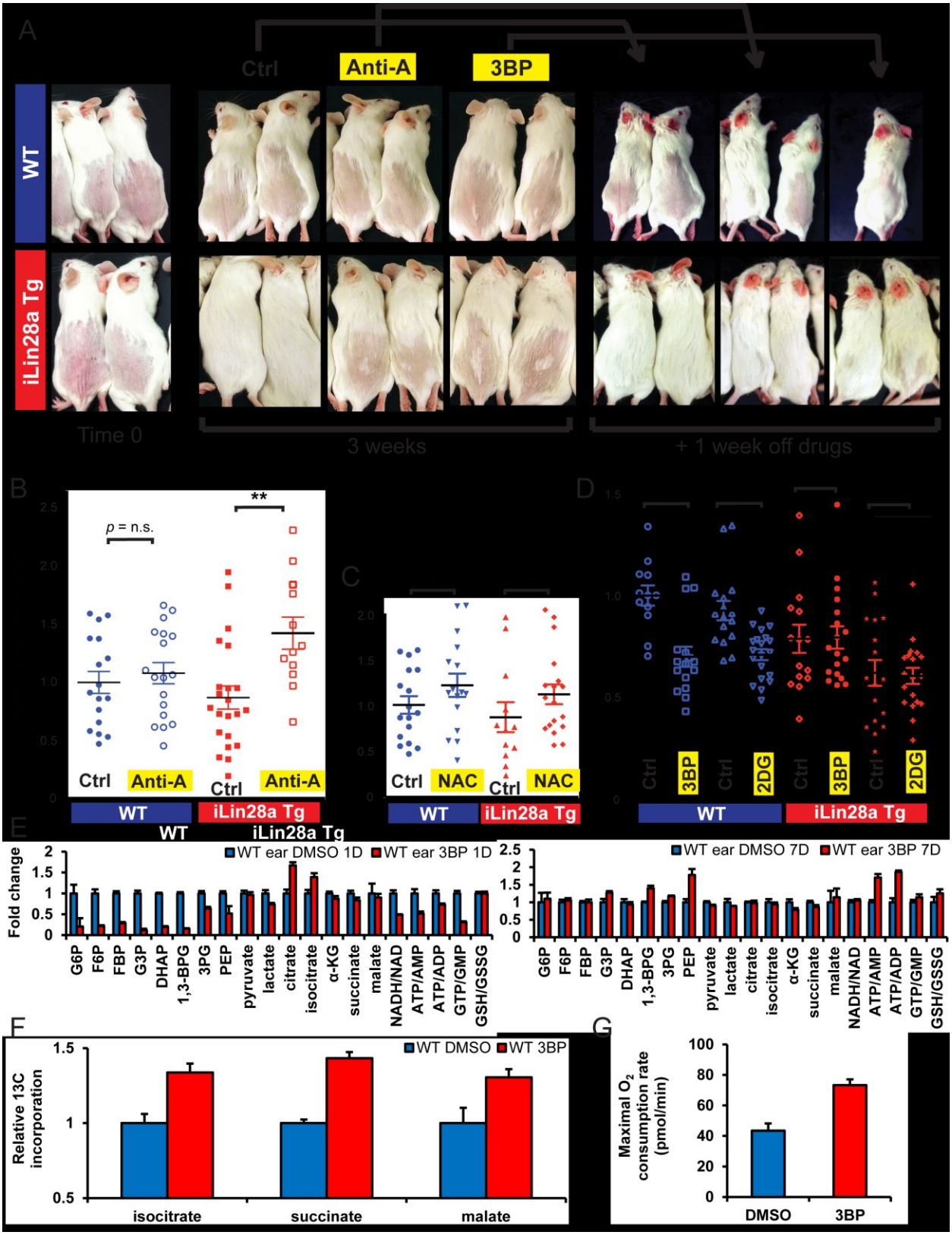

We sought to confirm this mechanism in another tissue context. Hence, we blocked OxPhos by topically applying antimycin-A daily on ears following pinnal injury. Consistent with the results in hair regrowth, antimycin-A specifically abrogated *Lin28a*'s enhancement of pinnal repair, with no significant effects on WT pinnae (Figure 3.7B). This implies that iLin28a Tg tissue repair is more sensitive to OxPhos inhibition than WT tissue repair. In contrast, the antioxidant N-acetyl-cysteine had only a small effect on pinnal repair in both WT and iLin28a Tg mice (Figure 3.7C), thus excluding a role for ROS or ROS-induced macrophage recruitment in the *Lin28a* mechanism.

Surprisingly, daily topical application of glycolysis inhibitors (3BP or 2-deoxy-D-glucose (2DG)), induced a substantial enhancement in WT tissue repair, comparable to the *Lin28a*-mediated enhancement (Figure 3.7D). Interestingly, 3BP also enhanced migration in WT MEFs (Figure 3.6D). One possible result of glycolysis inhibition is a compensatory increase in OxPhos activity, a phenomenon frequently observed in cancer cells (Wu et al. 2007). To test if a compensatory increase in OxPhos explains how glycolysis inhibition in WT ears enhances tissue repair similarly to *Lin28a* overexpression (Figure 3.7D), we performed metabolomic profiling on WT ears 1 and 7 days after daily 3BP treatment. 1 day after topical treatment, we found that 3BP drastically reduced glycolytic intermediates and significantly decreased the NADH/NAD, ATP/AMP, ATP/ADP, and GTP/GMP bioenergetic ratios (Figure 3.7E), as expected with glycolysis inhibition. After 7 days of daily 3BP treatment, however, the levels of glycolytic intermediates and the NADH/NAD ratio returned to normal, and there was a significant increase in the ATP/AMP and ATP/ADP ratios (Figure 3.7E), indicating a

compensatory increase in OxPhos activity in vivo. In WT MEFs, continuous incubation in 3BP for 3 days also led to an increase in $^{13}$C-glucose flux through the Krebs cycle (Figure 3.7F), and an increase in the maximal $O_2$ consumption rate (Figure 3.7G), further confirming that chronic glycolysis inhibition by 3BP induces a compensatory increase in OxPhos to enhance tissue repair. Together with our results on Lin28a's enhancement of OxPhos (Figure 3.5A-M), and the necessity for increased OxPhos in Lin28a's enhancement of tissue repair in vivo (Figure 3.7A-G), these results demonstrate that the enhancement of oxidative metabolism by *Lin28a* can confer the higher bioenergetic capacities needed to activate adult cells out of quiescence to enhance tissue repair.

**Discussion**

Our work demonstrates that the highly conserved heterochronic gene and juvenility regulator *Lin28a*, first described in a genetic screen for *C. elegans* mutants with altered developmental timing (Ambros and Horvitz, 1984), promotes mammalian tissue repair by altering cellular metabolism. *Lin28a* is normally highly expressed in the early embryo, downregulated during mid-gestation, and silenced in most tissues after birth. We have shown that engineering its reactivation in post-natal tissues reactivates an embryonic metabolic state that confers on post-natal tissues the enhanced regenerative potential of embryonic tissues. In another model organism, the zebrafish, *lin-28* reactivation has also been found to promote retinal regeneration (Ramachandran et al., 2010).

Collectively, our results demonstrate that *Lin28a* can promote tissue repair through

mechanisms independent of *let-7, a* result that was unexpected. Although overexpression of *let-7* could inhibit tissue repair, *let-7* repression alone failed to promote it. One possibility is that *let-7*-dependent and independent functions of *Lin28* synergize to regulate tissue homeostasis in a context-dependent manner; thus *let-7* repression is necessary but alone insufficient to promote tissue repair. There is accumulating evidence that *Lin28a*, like other RNA-binding proteins, enhances the translation of thousands of mRNAs and thus operates at the systems level (Peng et al., 2011; Wilbert et al., 2012; Cho et al., 2012). Our findings that specific inhibition of OxPhos can reversibly abrogate the effects of *Lin28a* on tissue repair, without detriment to WT tissue repair, provides strong evidence that *Lin28a* is promoting tissue repair by enhancing oxidative metabolism and bioenergetics, with pleiotrophic effects. For example, enhanced ATP and GTP levels could supply the higher energetic needs of anabolic biosynthesis, mitosis, and migration during tissue repair, or promote growth signaling pathways like mTOR, all of which are enhanced by *Lin28a.* Our results suggest that *Lin28a*-mediated enhancement of mitochondrial oxidation, independently of *let-7*, is one important mechanism by which *Lin28a* executes its functions.

We have shown here that altering oxidative metabolism can modulate repair capacities in several different post-natal somatic tissues. It is still possible that the effects of *Lin28a* on metabolism and tissue repair might differ in other contexts. For example, adult digits and the adult heart do not show improved tissue repair after injury in iLin28a Tg mice (Figure S3.2 and S3.6), indicating that even general metabolic pathways have injury- or tissue-specific activities. It is interesting to note that prior studies have linked PPARs

(peroxisome proliferator-activated receptors), master regulators of mitochondrial biogenesis and oxidative metabolism, to tissue repair in the mammalian skin, liver, muscles, and cornea (Michalik et al., 2001; Anderson et al., 2002; Angione et al., 2011; Nakamura et al., 2012). ATP-powered ion gradients and ROS have also been found to be critical in other regenerative animal models, such as *Xenopus* tail and planarian regeneration (Adams et al., 2007; Beane et al., 2011; Love et al., 2013). Clinically, the utility of topical oxygen for chronic wound therapy (Schreml et al., 2010), might also be partially related to the metabolic mechanisms that we have uncovered for *Lin28a*. Our findings support a novel use for *Lin28a* and the enhancement of oxidative metabolism for treating injuries and diseases related to tissue degeneration.

**Acknowledgements**

This chapter will be published in part in Shyh-Chang et al. (*Cell*, 2013d). These studies were performed in close collaboration with Hao Zhu. I took primary responsibility for all ear, skin and mechanistic experiments, while Hao Zhu focused on all digit and liver experiments, although we also helped each other on every aspect. Hao Zhu and I designed and performed the experiments, and wrote the manuscript. Yvanka de Soysa, Gen Shinoda, Marc Seligson, Kaloyan Tsanov, and Liem Nguyen aided with various mouse strains and experiments. John Asara and Lewis Cantley helped to design and supervised all metabolic experiments. George Daley designed and supervised all experiments. We also thank John Powers, Costas Lyssiotis, Charles Kaufman, Jessica Lehoczky, and Cliff Tabin for invaluable discussions and advice, Jin Zhang and the lab of Marcia Haigis for technical help with the Seahorse Analyzer, Min Yuan and Susanne

Breitkopf for technical help with the metabolomics, Samar Shah and Akiko Yabuuchi for help with mouse work, Asher Bomer for help with scratch assays, James Thornton for help with Northern blots, Roderick Bronson and the Harvard Medical School Rodent Histopathology Core for mouse tissue pathology.

## Chapter 4: *Lin28* promotes threonine metabolism to regulate S-adenosyl-methionine levels and histone methylation in pluripotent stem cells

### Introduction

Recent advances had improved our understanding of cellular mechanisms that underlie mESC pluripotency (Ng and Surani, 2011), yet the connections between the particular metabolic states of ESCs and pluripotency were only beginning to come into focus (Tahiliani et al., 2009). Metabolically, mESCs show a high glycolytic flux and high sensitivity to glucose restriction in the culture media (Facucho-Oliveira et al., 2007; Kondoh et al., 2007). It was also recently shown that mESCs possess a distinct mode of amino acid catabolism. Thr abundance is particularly low in mESCs and increases upon mESC differentiation (Wang et al., 2009). Threonine dehydrogenase (Tdh), which catalyzes the first step of threonine (Thr) metabolism, is expressed at over 200-fold greater levels in mESCs and induced pluripotent stem cells (iPSCs) relative to mouse embryonic fibroblasts (MEFs) (Wang et al., 2009; Mikkelsen et al., 2008). Furthermore, Thr restriction in the culture media or pharmacological inhibition of Tdh abolishes growth of mESCs (Wang et al., 2009; Alexander et al., 2011). Although Thr catabolism appears to be critical for mESCs, the functions of the downstream metabolites and the mechanisms connecting amino acid metabolism to the pluripotent state had remained unclear.

My interest in the central principles of stem cell metabolism led us to map the metabolomic changes associated with *Lin28/let-7* perturbation in ESCs and induced pluripotent stem cell (iPS) reprogramming. Instead of glycolysis and OxPhos, we found

that Thr and S-adenosylmethionine (SAM) metabolism consistently showed the most dramatic changes during both *Lin28/let-7* perturbation and iPS reprogramming.

We demonstrate that Thr and methionine (Met) metabolism are coupled in pluripotent stem cells, resulting in regulation of SAM levels and histone methylation. Isotope labeling of mESCs revealed that Thr provides a significant fraction of both the cellular glycine (Gly) and the acetyl-CoA needed to regulate SAM synthesis. Depleting Thr from the culture medium or knocking down expression of Tdh in mESCs resulted in decreased SAM levels, reduced tri-methylation of lysine 4 of histone H3 (H3K4me3), slowed growth, and increased differentiation. Ectopic expression of Tdh in human fibroblasts, which lack a functional Tdh gene, increased SAM and H3K4me3 levels and enhanced reprogramming to the pluripotent state. These findings demonstrate that metabolic regulation of cellular SAM levels play a critical role in determining the extent of H3K4 methylation, and illustrate a novel mechanism by which modulation of a metabolic pathway influences cell fate.

**Experimental Procedures**

***Cell Culture.*** iOSKM-MEFs were obtained and cultured according to previously published methods (12,15). For consistency, iOSKM-MEFs (no dox, dox 4D, or dox 18D) and mESCs were cultured in feeder-free conditions and fed fresh mESC media 2 hours prior to harvesting for metabolomics. E14Tg2a, Ainv-15, iLin28a and iLet-7mESCs were maintained on gelatinized plates and irradiated MEFs in mESC media (MEF media plus LIF: DMEM (Gibco) plus 10% FBS (Hyclone), 100 uM MEM non-

essential amino acids (Gibco), 2 mM glutamine, 200 ug/ml penicillin, 100 ug/ml streptomycin (Gibco), 50 uM 2-mercaptoethanol and 1000 U/ml LIF (Chemicon)). iLin28a and iLet-7 mESCs were generated according to the methods of H. Zhu et al., (*Cell,* 147, 81, 2011). Irradiated MEFs were omitted during feeder-free culture for metabolomics, qRT-PCR, immunoblotting, and metabolite-rescue experiments. Pluripotent colonies were visualized with alkaline phosphatase staining (Sigma). Amino acid restriction media were prepared by omitting the indicated amino acids from amino acid-free DMEM powder, and reconstituting the media in ultra-pure embryo-tested water. The pH of the mESC media was adjusted using $NaHCO_3$. All component chemicals were obtained from Sigma. Embryoid body (EB) differentiation was performed according to the methods of M. Kyba et al., (*Cell,* 109, 29, 2002). Briefly, mESCs were trypsinized, collected in EBD media (IMDM plus 15% FBS, 200 µg/mL iron-saturated transferrin (Sigma), 3.5 mM monothiolglycerol (Sigma), 50 µg/mL ascorbic acid (Sigma), and 2 mm glutamine), and plated for 45 min to allow MEFs to adhere. Nonadherent cells were collected and plated in hanging drops at 100 cells per 10 µl drop in an inverted bacterial petri dish. EBs were collected from the hanging drops at day 2 and transferred into 10 ml EBD media in slowly rotating 10 cm petri dishes.

***$^{14}$C-Thr labeling, amino acid derivatization and reverse-phase HPLC analysis.*** At ~50% confluence, feeder-free mESCs were grown in complete media supplemented with 2.5 uCi/ml of [U-$^{14}$C]Thr [Moravek]. After 24 hours, mESCs were quickly washed with ice-cold PBS twice, and then snap-frozen in liquid nitrogen. Polar metabolites including amino acids were extracted using 80% methanol, as described above. Primary amino acids readily react with ortho-phthalaldehyde (OPA) and the resulting derivatives

can be analyzed by reversed phase HPLC with UV detection. Dried 80% methanol extract from one well of a 6-well plate was dissolved in 100 ul of distilled water. A 20-ul aliquot was mixed with 60 ul of OPA reagent [Sigma] at room temperature for 1 min, and then immediately injected onto HPLC, according to the methods of R. Schuster (*J. Chromatogr.*, 431, 271, 1988). Derivatized amino acids were analyzed on an Agilent 1200 quaternary HPLC system equipped with a multiple wavelength UV detector, connected on-line to a Flo-One A510 radioactive detector. Reversed phase HPLC analysis was performed using an Agilent ZORBAX Eclipse Plus C18 column (0.46 cm × 15 cm), a linear gradient program from 98% mobile phase A, 2% mobile phase B to 50% mobile phase A, 50% mobile phase B in 60 min, and a flow rate of 1 ml/min. Mobile phase A was 10 mM $Na_2HPO_4$ : 10 mM $Na_2B_4O_7$ pH 8.2 : 5 mM NaN3 and mobile phase B was acetonitrile/methanol/water (45:45:10 v/v/v). UV detection was set at 338 nm. Peaks were assigned by measuring the retention times of pure standards (Sigma). NADH/NAD and NADPH/NADP ratios were measured using colorimetric enzyme-based assay kits, according to the manufacturer's instructions (Biovision).

***Targeted liquid-chromatography mass spectrometry (LC/MS/MS).*** LC/MS/MS-based metabolomics analysis was performed according to the methods of J.W. Locasale et al., (*Nat. Genet.,* 43, 869, 2011). $10^6$ cells were harvested in 80% (v/v) methanol at -78$^oC$. Insoluble material in lysates was centrifuged at 2,000g for 15 min, and the resulting supernatant was evaporated using a refrigerated speed vac. Samples were resuspended using 20 µL LC/MS grade water. 7 µL was injected and analyzed using a 5500 QTRAP triple quadrupole mass spectrometer (AB/SCIEX) coupled to a Prominence HPLC system (Shimadzu) using selected reaction monitoring (SRM) of a

total of 252 endogenous water soluble metabolites for analyses of samples. Some metabolites were targeted in both the positive and negative ion mode for a total of 292 SRM transitions. ESI voltage was +4,900 V in the positive ion mode and −4,500 V in the negative ion mode using positive/negative switching. The dwell time was 4ms per SRM transition, and the total cycle time was 1.82 sec producing 9-12 data points per metabolite peak. Samples were delivered to the MS using hydrophilic interaction chromatography(HILIC) using a 3.6 mm internal diameter × 10 cm Amide XBridge column (Waters) at 300 µL/min. Mobile phase gradients were run startingfrom 85% buffer B (LC/MS grade acetonitrile) to 35% buffer B from 0–3 min; 35% buffer B to 0% buffer B from 3–12 min; 0% buffer B held from 12–17 min; 0% buffer B to 85% buffer B from 17–18 min; and 85% B held for 7 min tore-equilibrate the column. Buffer A was comprised of 20 mM ammonium hydroxide and 20 mM ammonium acetate in 95:5water:acetonitrile (pH=9.0). Peak areas from the total ion current for each metabolite SRM transition were integrated using MultiQuant v2.0 software (AB/SCIEX). For $^{13}$C-Thr, -Ser, -Gln, and -glucose flux metabolomics, complete mESC media was deprived of the relevant nutrients and supplemented with the equivalent concentration of [U-$^{13}$C]Thr, [U-$^{13}$C]Ser, [U-$^{13}$C]Gln, or [U-$^{13}$C]glucose (Cambridge Isotopes), and cells were quickly harvested at the given time points using the above mentioned protocol. Samples were prepared as described above, and run with 153 total SRM transitions for expected $^{13}$C incorporation (93 transitions in positive ion mode and 60 in negative ion mode). All data was normalized to total biomass, and analyzed using MATLAB.

***Antibodies.*** Immunoblot analysis for H3K4me3 (Millipore), H3K4me2 (Millipore), H3K4me1 (Millipore), H3K27me3 (Millipore), H3K9me3 (Millipore), H3K36me3 (Abcam),

H3K79me3 (Abcam), pan-methyl-lysine (Abcam), acetyl-histone H3 (Millipore), total histone H3 (Abcam), Tdh (Millipore), Gldc (Abcam), Mat2a (Abcam), tubulin (Santa-Cruz), actin (Santa Cruz), was performed according to the methods of H. Zhu et al., (*Cell,* 147, 81, 2011).

***Gene knockdown by shRNA.*** The Tdh-targeting short hairpin RNA (shRNA) sequences used were ACTGGCCCATGATTCTAGATGATAGTGAAGCCACAGAT GTATCATCTAGAATCATGGGCCAGC (shTdh-1) and ACACCAGAGTTGCCCA AGTGAATAGTGAAGCCACAGATGTATTCACTTGGGCAACTCTGGTGC (shTdh-2). The Gldc-targeting short hairpin RNA (shRNA) sequences used were TGCTGTTGACAGTGAGCGATAGGGTCTTCATTCAAGAGAATAGTGAAGCCACAGAT GTATTCTCTTGAATGAAGACCCTAGTGCCTACTGCCTCGGA (shGldc-1) and TGCTGTTGACAGTGAGCGACCACAGAAATCGCCATTCTAATAGTGAAGCCACAGAT GTATTAGAATGGCGATTTCTGTGGCTGCCTACTGCCTCGGA (shGldc-2). The Mat2a-targeting short hairpin RNA (shRNA) sequences used were TGCTGTTGACAGTGAGCGATAGGTGTTTTGTTCACCATTATAGTGAAGCCACAGAT GTATAATGGTGAACAAAACACCTAGTGCCTACTGCCTCGGA (shMat2a-1) and TGCTGTTGACAGTGAGCGACCAGATAAGATTTGTGACCAATAGTGAAGCCACAGAT GTATTGGTCACAAATCTTATCTGGGTGCCTACTGCCTCGGA (shMat2a-2). An shRNA in the pTRIPZ vector that targeted firefly luciferase (shLuc) was used as a control. The shRNA constructs were cut from the pGIPZ vector (Open Biosystems) using the restriction enzymes MluI and XhoI and ligated into the precut (MluI/XhoI) doxycycline-inducible pTRIPZ vector (Open Biosystems) and sequence-verified. To generate shRNA virus, HEK293T cells were transfected during log-growth with 2 μg of

the pTRIPZ-shRNA vector, 2 μg of the Δ8.9 lenti-viral packaging construct and 0.2 μg the VSV-g envelope vector using PEI (3-to-1 ratio: PEI-to-DNA in 800 μL Opti-MEM). 12 hours post-transfection, HEK293T supernatant containing the transfection mixture was replaced with fresh growth media (DMEM plus 10% FBS). Viral supernatant was collected and passed through a 0.22 μm filter 36 and 60 hours after transfection. mESCs at 40% confluence growing on a MEF-feeder layer were transduced with viral supernatant from HEK293T cells 1-to-1 with growth media. Polybrene hexabromide (Sigma) was added to a final concentration of 6 ug/mL. mESCs were transduced 2 times, 24 hours apart. 12 hours after the second transduction, virus-depleted media was replaced with growth media. Virus-transduced mouse mESCs were subjected to selection with 1 μg/mL puromycin 48 hours later. Inducible shRNA mESC lines were maintained in 1 μg/mL puromycin. For experiments, the shRNA was induced with 1 μg/mL of doxycycline. The kinetics of shRNA expression was readily observed by RFP expression upstream of the shRNA and downstream of the doxycycline-inducible promoter.

***Gene overexpression and human iPSC reprogramming.*** Mouse Tdh was cloned from mESC cDNA libraries using the forward primer CGTAGGAATTCGCCGCCACCATGCTATTCCTTGGGATGCTAAAACAGG and the reverse primer CCGGCCGGATCCGTTCACTTGGGCAACTCTGG, and inserted into the pCDH-MCS-T2A-copGFP-MSCV vector (System Biosciences). Tdh and empty vector lentivirus was generated and transduced into H1-derived differentiated human fibroblasts, according to the above-mentioned protocol for lenviral shRNA. Tdh-T2A-copGFP and empty-T2A-GFP human fibroblasts were sorted by FACS, and expanded

in DMEM plus 10% FBS and 100uM MEM non-essential amino acids. Mouse Gldc, Ahcy, Wdr5, Rbbp5, Ash2l, Dpy30, Setd1a, Setd1b, and GFP cDNA constructs in the pCMV-SPORT6 vector were obtained from Open Biosystems. 1 µg of each construct was transfected into feeder-free mESCs with Fugene 6.0 (Roche), according to the manufacturer's instructions. Fresh medium was replaced after 24 hours. 2 days later, the mESCs were assayed for gene expression by qRT-PCR and duplicate wells were subjected to Thr restriction. Human iPSC reprogramming with OSKM lentivirus was performed according to the methods of I.H. Park et al., (*Nature,* 451, 141, 2008). Proviral silencing was used to identify properly reprogrammed human iPSC colonies and Tra-160 immunohistochemistry (eBioscience) was used to evaluate human iPSC reprogramming efficiency, according to E.M. Chan et al., (*Nat. Biotech.*, 27, 1033, 2009).

**Results**

To investigate how metabolism is altered upon reprogramming to pluripotency, we used the liquid chromatography-based tandem mass spectrometry (LC-MS/MS) platform based on selected reaction monitoring (Locasale et al., 2011) to profile metabolomic changes during murine iPSC reprogramming. We utilized MEFs expressing inducible Oct4, Sox2, Klf4, and Myc (OSKM; Mikkelsen et al., 2008) and profiled metabolism without doxycycline (dox)-induction (no dox), 4 days after dox (dox 4D), and 18 days after dox (dox 18D), whereupon iPSC clones were isolated and compared to mESCs. Hierarchical clustering revealed that iPSCs are similar to mESCs, while MEFs form a

***Figure 4.1: Pluripotency factors upregulate Threonine-Methionine metabolism.*** (**A**) Hierarchical clustering of metabolomic profiles of mouse embryonic fibroblasts with doxycycline-inducible *Oct4, Sox2, Klf4,* and *Myc* (iOSKM-MEFs) in the absence of doxycycline (no dox) and 4 days after dox (dox 4D), compared to iPSC clones isolated 18 days after dox (dox 18D) and mESCs, profiled in triplicate (n=3) using selected reaction monitoring (SRM) and a liquid-chromatography based mass spectrometry platform. (**B**) Scatter plot of mESC (x-axis) metabolites vs. iPSC (y-axis) of raw metabolite intensities obtained from the integrated total ion current from a single SRM transition. Correlation coefficient $r = 0.99$. (**C**) Relative levels (Fold Change) of glycolytic intermediates in iOSKM-MEFs in the absence of doxycycline (no dox) and 4 days after dox (dox 4D), compared to iPSC clones isolated 18 days after dox (dox 18D) and mESCs (n=3).**$P < 0.01$, * $P < 0.05$. (**D**) Relative levels (Fold Change) of threonine-glycine and cysteine-methionine metabolites in iOSKM-MEFs in the absence of doxycycline (no dox) and 4 days after dox (dox 4D), compared to iPSC clones isolated 18 days after dox (dox 18D) and mESCs (n=3). ** $P < 0.01$. (**E**) Most significant metabolite changes in dox-inducible *let-7* (iLet-7) and dox-inducible *Lin28a* (iLin28a) mESCs, after dox treatment ($P < 0.05$). Overlap shows metabolites that are reciprocally downregulated by *let-7* plus upregulated by *Lin28a*, and vice versa. (**F**) Relative levels (Fold Change) of threonine-glycine and cysteine-methionine metabolites in iLet-7 and iLin28a mESCs after dox (n=3). All error bars represent the s.e.m. from three independent measurements.

**Figure 4.1 (continued)**

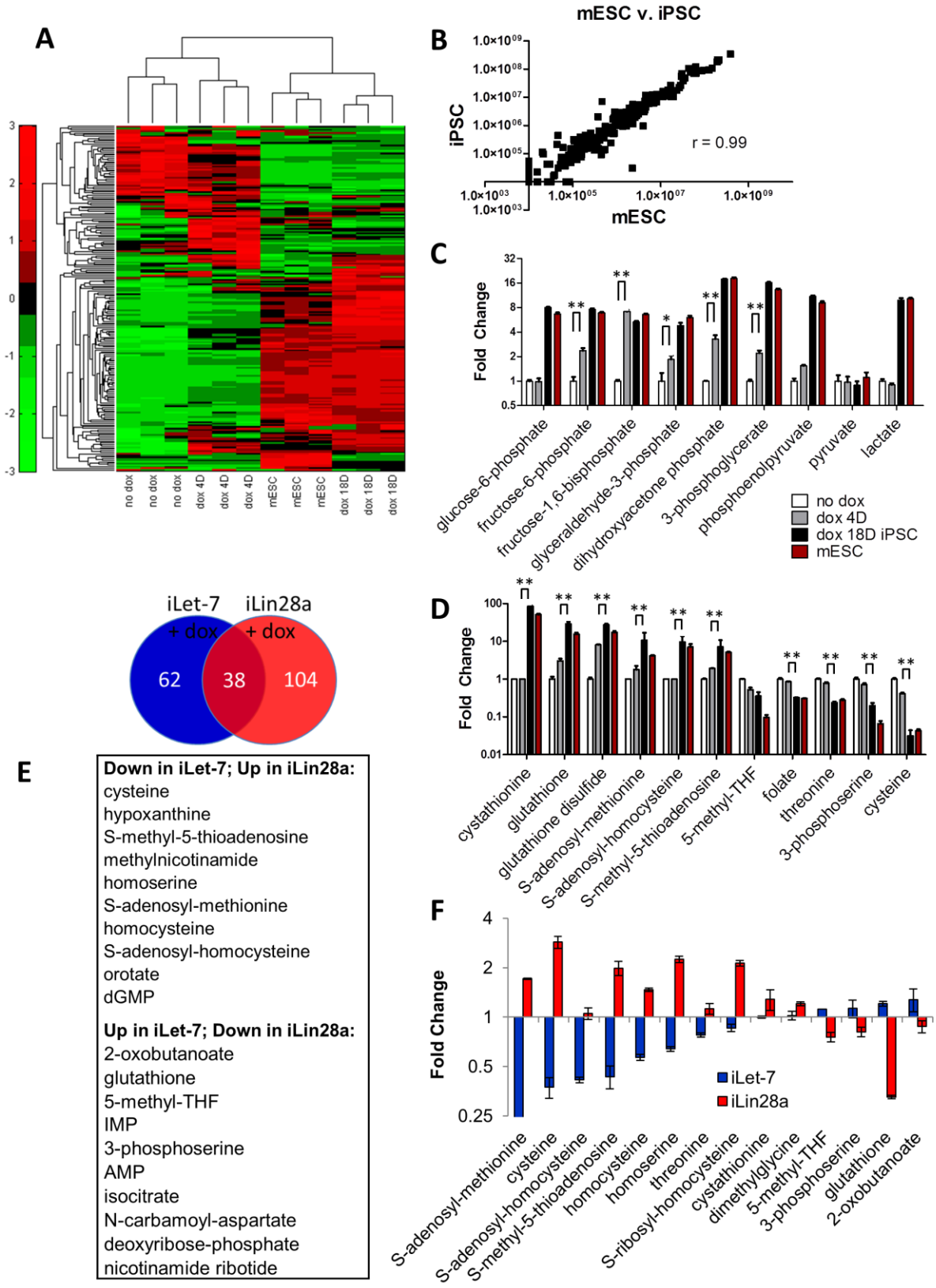

distinct cluster. The dox 4D cells form a cluster intermediate to the MEFs and the iPSC/mESC clusters (Figure 4.1A). A scatter plot indicated that mESCs are largely indistinguishable from iPSCs based on their overall metabolic profiles ($r$ = 0.99, Figure 4.1B). Inspection of the top metabolites regulated by OSKM induction revealed a large number of glycolytic intermediates (Figure S4.1A). Glycolytic intermediates like fructose-6-phosphate, fructose-1,6-bisphosphate, glyceraldehyde-3-phosphate, dihydroxyacetone phosphate, and 3-phosphoglycerate, were already significantly upregulated within 4 days of reprogramming ($P < 0.05$). This coincides with the time frame in which MEF proliferation is accelerating, but well before the cells become pluripotent (Mikkelsen et al., 2008), and suggests that the upregulation of glycolytic intermediates in reprogramming occurs prior to the acquisition of the pluripotent state (Figure 4.1C).

Most of the remaining prominent metabolites regulated by OSKM induction are involved in Thr and Met metabolism. In contrast to glycolytic intermediates, cystathionine, glutathione, S-adenosyl-methionine (SAM), S-adenosyl-homocysteine (SAH), S-methyl-5-thioadenosine (SMTA), folate, 3-phosphoserine, cysteine and threonine are only significantly altered after 18 days of dox treatment ($P < 0.01$), suggesting that enhanced Thr/Met metabolism occurs later in the process of reprogramming (Figure 4.1D). Some of the largest changes were in threonine (down 5-fold), cysteine (down 33-fold), SAM (up 11-fold), SMTA (up 7-fold) and cystathionine (up 85-fold). These observations suggest that reprogramming to the pluripotent state is correlated with significant

changes in Thr/Met metabolism, consistent with observations of high SAM and SMTA levels in human iPSCs (Panapoulos et al., 2012).

To study metabolic changes associated with the switch between mESC pluripotency and differentiation, we profiled the metabolites of mESCs after dox induction of a *let-7* or *Lin28a* transgene (iLet-7 or iLin28a; Figure 4.1E). In the context of mESCs, the *let-7* microRNA promotes differentiation by targeting the pluripotency network, while *Lin28a* helps promote pluripotency by repressing the maturation of endogenous *let-7* (Yu et al., 2007; Viswanathan et al., 2008; Melton et al., 2009). We profiled metabolic changes in iLet-7 and iLin28a mESCs upon acute dox-induction, while the cell-cycle was relatively unperturbed (Figure S4.1B). *Lin28a* and *let-7* regulated 38 metabolites in a reciprocal fashion (Figure 4.1E), amongst which were a large number of Thr/Met metabolites (Figure 4.1E-F). These data further support the idea that Thr/Met metabolism is tightly regulated by the pluripotent state.

We then integrated our metabolomics data on mESCs with cDNA microarray data on mESCs (Mikkelsen et al., 2008), within the KEGG database of metabolic networks. This analysis showed that many of the metabolic enzymes that channel Thr metabolism into Met metabolism are highly expressed in mESCs relative to MEFs (Figure 4.2A). Consistent with the enzyme expression patterns, several Thr/Met pathway inputs like Thr, Cys, and folate are lower in mESCs than in MEFs, while downstream outputs like SAM, SAH, SMTA and cystathionine are higher in mESCs than MEFs (Figure 4.1D). Collectively, these findings suggest that Thr fuels Met metabolism in mESCs.

***Figure 4.2: Threonine is catabolized to maintain the SAM/SAH ratio in mESCs.*** (**A**) Schematic of glycolysis, threonine-glycine and cysteine-methionine metabolism, with levels of metabolites and metabolic enzymes in mESCs/iPSCs vs. MEFs indicated (red: up >3-fold; pale red: up 1.5 – 3-fold; black: no significant change; pale green: down 1.5 – 3-fold; green: down >3-fold). Tdh, threonine dehydrogenase. Sdhl, serine/threonine dehydratase. Gcat, glycine C-acetyltransferase. Gldc, glycine decarboxylase or glycine cleavage system protein P. TCA, tricarboxylic acid. Shmt1, serine hydroxymethyltransferase 1. Folr1, folate receptor 1. Dhfr, dihydrofolate reductase. THF, tetrahydrofolate. Mthfr, methylene tetrahydrofolate reductase. Cth, cystathionase. Cbs, cystathionine-beta-synthase. Mtr, 5-methyltetrahydrofolate-homocysteine methyltransferase. Mat2a/b, methionine adenosyltransferase II, alpha and beta. SAM, S-adenosyl-methionine. SMTA, S-methyl-5-thioadenosine. SAH, S-adenosyl-homocysteine. AHCY, adenosyl-homocysteinase or SAH hydrolase. (**B**) HPLC analysis of radioactive $^{14}$C-labeled amino acids derived from [U-$^{14}$C]Thr in mESCs, after 24h. Thr, threonine. Gly, glycine. Ser, serine. Glu, glutamate. GSH, glutathione. Scintillation counts per minute (CPM) are plotted against retention time in minutes (time/min). Peaks were identified from the retention time of internal standards of the corresponding compounds. (**C**) Isotopic tracing of $^{13}$C-labeled metabolites derived from [U-$^{13}$C]Thr in mESCs. Media was replaced with [U-$^{13}$C]Thr and monitored over a 5h time-course (n=3). The fraction of $^{13}$C incorporation ($^{13}$C / total C ratio) is plotted against time in minutes (Time/min). (**D**) Isotopic tracing of $^{13}$C-labeled metabolites derived from [U-$^{13}$C]Thr in mESCs. The fraction of $^{13}$C incorporation ($^{13}$C / total C ratio) is plotted after 24h of incubation (n=3). (**E**) SRM analysis of metabolites in mESCs during 6h of Thr

***Figure 4.2 (continued)*** restriction (n=3). Metabolite levels (Fold change) relative to the zero time point are plotted over time across a 6h time course. (**F**) Levels (Fold change) relative to the zero time point are plotted for several metabolic ratios over time across a 6h time course. (**G**) Threonine restriction and re-feeding in mESCs. Feeder-free mESCs were deprived of threonine in the media for 12h, then supplemented for 36h with the indicated metabolites at the given concentrations. Alkaline phosphatase-positive colonies were quantified and normalized to mESC colony numbers in normal mESC media (% colonies recovered) and plotted across all conditions. X denotes a relative concentration with respect to the concentration in the standard mESC media. Thr, threonine. Gly, glycine. Ser, serine. Met, methionine. Cys, cysteine. Glu, glutamate. Gln, glutamine. NAC, N-acetyl-cysteine. Py, pyruvate. DMG, dimethylglycine. Bet, betaine. Hypo, hypoxanthine. Thy, thymidine. HT, hypoxanthine and thymidine. All error bars represent the s.e.m. from three independent measurements.

**Figure 4.2 (continued)**

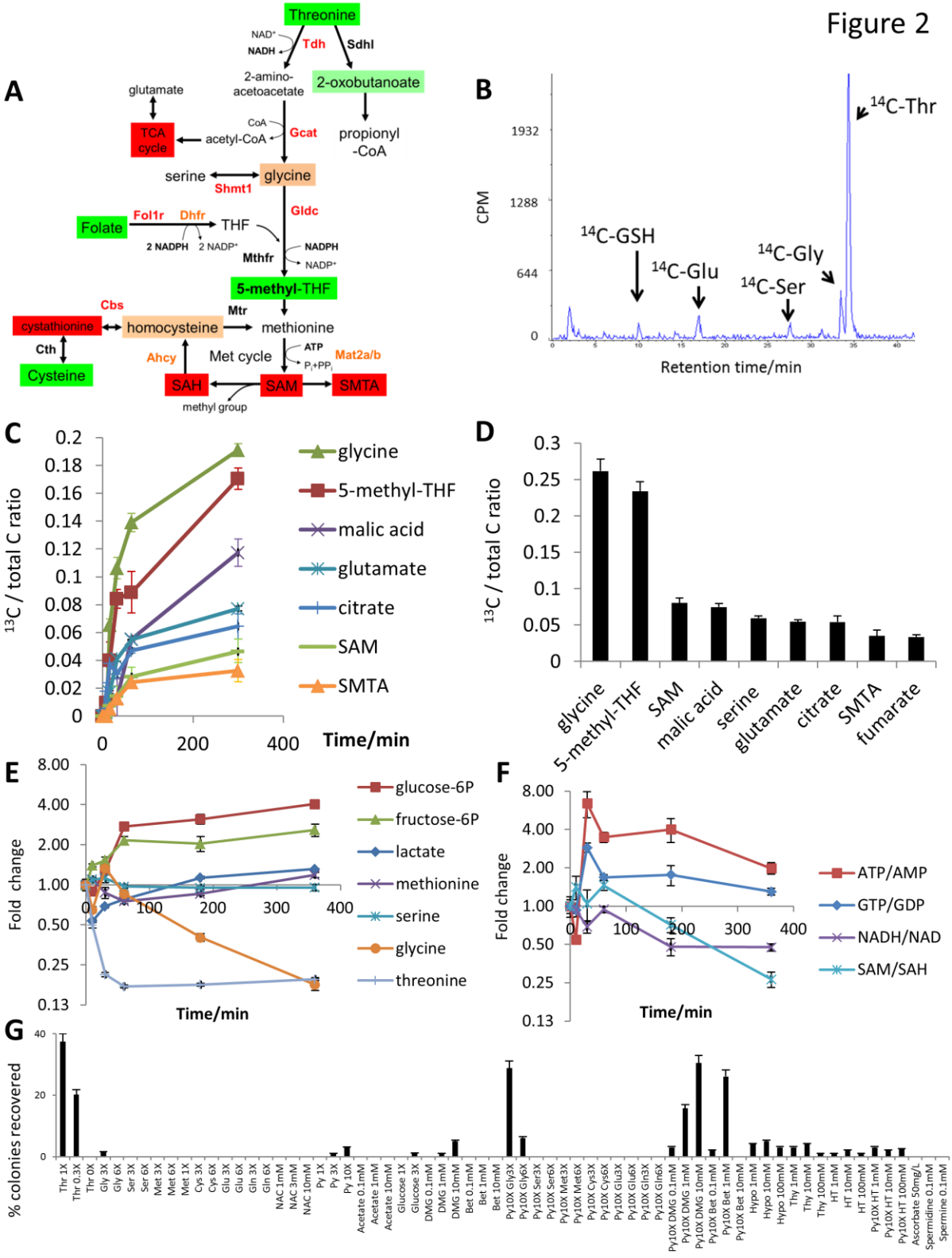

To test this pathway, we traced the metabolic fate of $^{14}$C-Thr in mESCs with HPLC. $^{14}$C-isotope was incorporated into Gly and Glu, indicating that Thr was used to synthesize these amino acids (Figure 4.2B). In contrast, MEFs incubated with $^{14}$C-Thr did not exhibit Thr catabolism (Figure S4.2A). We also traced the fate of $^{13}$C-Thr in mESCs with LC-MS/MS metabolomics (Figure S2B-F, Table S1). mESCs used Thr to synthesize acetyl-CoA-derived TCA cycle intermediates (Figure 4.2C-D). At steady-state, $^{13}$C-Thr contributed ~20% of the citrate via acetyl-CoA, whereas $^{13}$C-glucose contributed ~35% via acetyl-CoA (+2 isotopomer). Thus Thr contributes significantly to the acetyl-CoA pool in mESCs (Figure 4.2D). Extracellular $^{13}$C-Thr-derived $^{13}$C-Gly also donated its $^{13}$C-methyl group to ultimately generate 5-methyl-tetrahydrofolate (5mTHF) and SAM (+1 isotopomer), whereas extracellular $^{13}$C-Ser-derived $^{13}$C-Gly contributed little to the synthesis of these metabolites (Figure 4.2C-D). Although only ~25% of intracellular Gly and 5mTHF, and ~10% of SAM were labeled by $^{13}$C-Thr at steady state, these numbers underestimate the contribution of Thr to the synthesis of these intermediates due to rapid 1-for-1 antiport of intracellular $^{13}$C-Gly and $^{13}$C-Met for extracellular $^{12}$C-Gly and $^{12}$C-Met. Evidence for rapid antiport-mediated $^{13}$C-isotope dilution was provided by the appearance of large quantities of $^{13}$C-Gly and $^{13}$C-Met in the media - 6% of extracellular Gly and 13% of extracellular Met was $^{13}$C-labeled within 1 hour of $^{13}$C-Thr addition to the media - with no significant consumption of Gly or Met from the media. These data suggest that the rapid conversion of Thr to Gly by Tdh provides a major fraction of 5mTHF needed for recycling SAH to SAM.

Although we observed flux of Thr into the activated Met cycle, it was unclear whether Thr was necessary to regulate Met metabolism, as other metabolites can also be used to support the activated Met cycle and the fraction of SAM labeled by $^{13}$C-Thr was small. Thus we profiled metabolic changes upon Thr restriction in mESCs. We first observed that Thr restriction kills mESCs even when protein synthesis is inhibited by cycloheximide, indicating that Thr restriction affects cell viability independently of protein synthesis (Figure S4.2G-H). Concordant with the rapid drop in cellular Thr following Thr restriction, Gly also steadily decreased over 6 hours after Thr restriction (Figure 4.2E), suggesting an imbalance in Gly synthesis and consumption. In addition, the SAM/SAH ratio dropped rapidly and steadily over 6 hours (Figure 4.2F). In contrast, the ATP/AMP ratio increased, as did glucose-6-phosphate and fructose-6-phosphate (Figure 4.2E), consistent with a compensatory increase in ATP synthesis due to increased glycolysis, whereas the total NADH/NAD ratio decreased over time (Figure S4.2K-L). This suggests that Thr is also necessary to provide the acetyl-CoA needed to regulate the pool of reducing equivalents and SAM synthesis (Figure 4.2A). It is difficult to measure NADPH and NADH levels in the mitochondrial matrix, but the drop in total NADH might be due to a drop in mitochondrial acetyl-CoA, which fuels the production of reducing equivalents. Thus, the drop in SAM/SAH after Thr restriction is consistent with the metabolites of Thr contributing not only to the methyl group of SAM (from Thr-derived Gly), but also to the supply of acetyl-CoA needed to regulate SAM synthesis.

To test this model, we subjected mESCs to 12 hours of Thr restriction, and then supplemented the culture media with metabolites identified from our metabolomics

analysis. Titration with varying concentrations of Gly and pyruvate (to supply acetyl-CoA) showed that only a combination of 3X Gly and 10X pyruvate can rescue Thr restriction in mESCs to levels comparable to re-feeding of 1X Thr (Figure 4.2G). Given that Thr contributes a significant portion of the mitochondrial acetyl-CoA at steady-state (Figure S4.2I), our working model is that glucose-derived pyruvate is limiting in producing the higher levels of mitochondrial acetyl-CoA needed by mESCs, and that supplying extracellular pyruvate can meet the demand that is normally met by Thr. Glucose, acetate, Ser, Met, Cys, Glu, Gln, N-acetyl-Cys, or combinations with pyruvate, all failed to rescue Thr restriction. However a combination of pyruvate with the methyl donors dimethylglycine and betaine also rescued Thr restriction in mESCs (Figure 4.2G), suggesting that Thr-derived 5-methyl-THF and its main product SAM (Figure 4.2C-D) are essential for viability of mESCs. SAM was not used to rescue the mESCs because it is not transported efficiently across the mammalian plasma membrane (McMillan et al., 2005). Conversely the addition of an inhibitor of SAH, hydrolase 3-deaza-adenosine (DZA, Backlund et al., 1986), which raises the SAH levels and decreases the SAM/SAH ratio, led to mESC death, thereby phenocopying Thr restriction (Figure S4.2M). In contrast, the two main products of formyl-THF and methylene-THF, hypoxanthine and thymidine respectively, failed to rescue Thr restriction, although they can enter mESCs (Valancius et al., 1991). A side-product of SAM and SMTA catabolism, the polyamine spermidine (Zhang et al., 2012), also failed to rescue Thr restriction. An alternative hypothesis is that Thr is also necessary for suppressing reactive oxygen species and maintaining redox balance in ESCs, but two different antioxidants ascorbate and N-acetyl-Cys failed to rescue Thr restriction.

Altogether, these experiments demonstrate that Thr is necessary to generate an optimal balance of Gly and acetyl-CoA, at least in part to maintain the SAM/SAH ratio in mESCs.

SAM is the universal substrate for all protein methylation reactions in the cell. After transferring the methyl group in SAM, protein methyltransferases are competitively inhibited by the downstream product SAH (Luka et al., 2009); thus the SAM/SAH ratio is important for regulating methylation of proteins, including the abundant histones (Figure 4.3A). To test if Thr restriction affects histone methylation, we used a pan-methyl-lysine antibody to probe which proteins show differential lysine methylation upon restriction of Thr, Gly, and Ser, relative to complete growth media. Amongst the most abundant methylated proteins (Iwabata et al., 2005), the 17 kDa histone H3 showed a significant drop in methylation upon Thr restriction, whereas the 71 kDa heat shock protein 8, the 50 kDa elongation factor-1a and the 41 kDa actins showed no changes (Figure 4.3B). Because ESCs possess an open euchromatin conformation crucial for epigenetic plasticity, and given the importance of histone H3 lysine 4 methylation and H3 acetylation in maintaining open euchromatin (Azuara et al., 2006; Gaspar-Maia et al., 2011), we tested if Thr catabolism is required to regulate H3K4 tri-methylation (H3K4me3) and H3 acetylation (H3ac) in mESCs. We checked H3 modifications in mESCs under conditions of Thr restriction (0.3X) that do not lead to mESC death (Figure S4.3A). H3K4me3, the prevalent H3 methylation mark in ESCs (Azuara et al., 2006; Pan et al., 2007; Zhao et al., 2007; Gaspar-Maia et al., 2011), was dramatically reduced in mESCs after 48 hours of 0.3X Thr restriction, whereas H3ac was relatively

**Figure 4.3*: Threonine-methionine metabolism controls H3K4 methylation levels.*** (**A**) Schematic of relevant methyl-transferase reactions. Histone lysine methylation requires S-adenosyl-methionine (SAM) as a methyl donor, and is competitively-inhibited by S-adenosyl-homocysteine (SAH). (**B**) Immunoblot analysis of mESCs using an antibody against methyl-lysine, after restriction (0X) of Thr, Gly, or Ser for 24h. Total tubulin is used as a loading control. (**C**) Immunoblot analysis of mESCs and MEFs for histone H3 lysine 4 tri-methylation (H3K4me3), and H3 acetylation (H3ac), when exposed to 3X and 0.3X relative threonine concentrations in the media for 48h. Total tubulin is used as a loading control. (**D**) Immunoblot analysis of mESCs for H3K4me3 levels, total histone H3, and tubulin after Thr restriction (0X) for 6 hours, then re-fed for 6 hours with 0X Thr, 1X Thr, 10X Py + 3X Gly, 3X Gly or 10X Py + 3X Gly + 20μM DZA. DZA, 3-deaza-adenosine. (**E**) Relative levels of the SAM/SAH ratio after Thr restriction (0X) for 6h, then re-fed for 6h with 0X Thr, 1X Thr, 3X Gly, 10X Py + 3X Gly, or 10X Py + 3X Gly + 20μM DZA. (**F**) Rescue of threonine restriction with pyruvate and glycine. Feeder-free mESCs were deprived of threonine in the media for 12h, then supplemented for 36h with 10X Py + 3X Gly, with or without 20μM DZA. Pluripotent mESC colonies were stained for alkaline phosphatase. (**G**) Immunoblot analysis of mESCs for the levels of H3K4me3, K4me2, K4me1, K27me3, K9me3, K36me3, and K79me3, after restriction (0X) of threonine (Thr), glycine (Gly), serine (Ser), methionine (Met) or leucine (Leu) for 24h. (**H**) Model of how threonine catabolism regulates the SAM/SAH ratio and H3K4 methylation.

**Figure 4.3 (continued)**

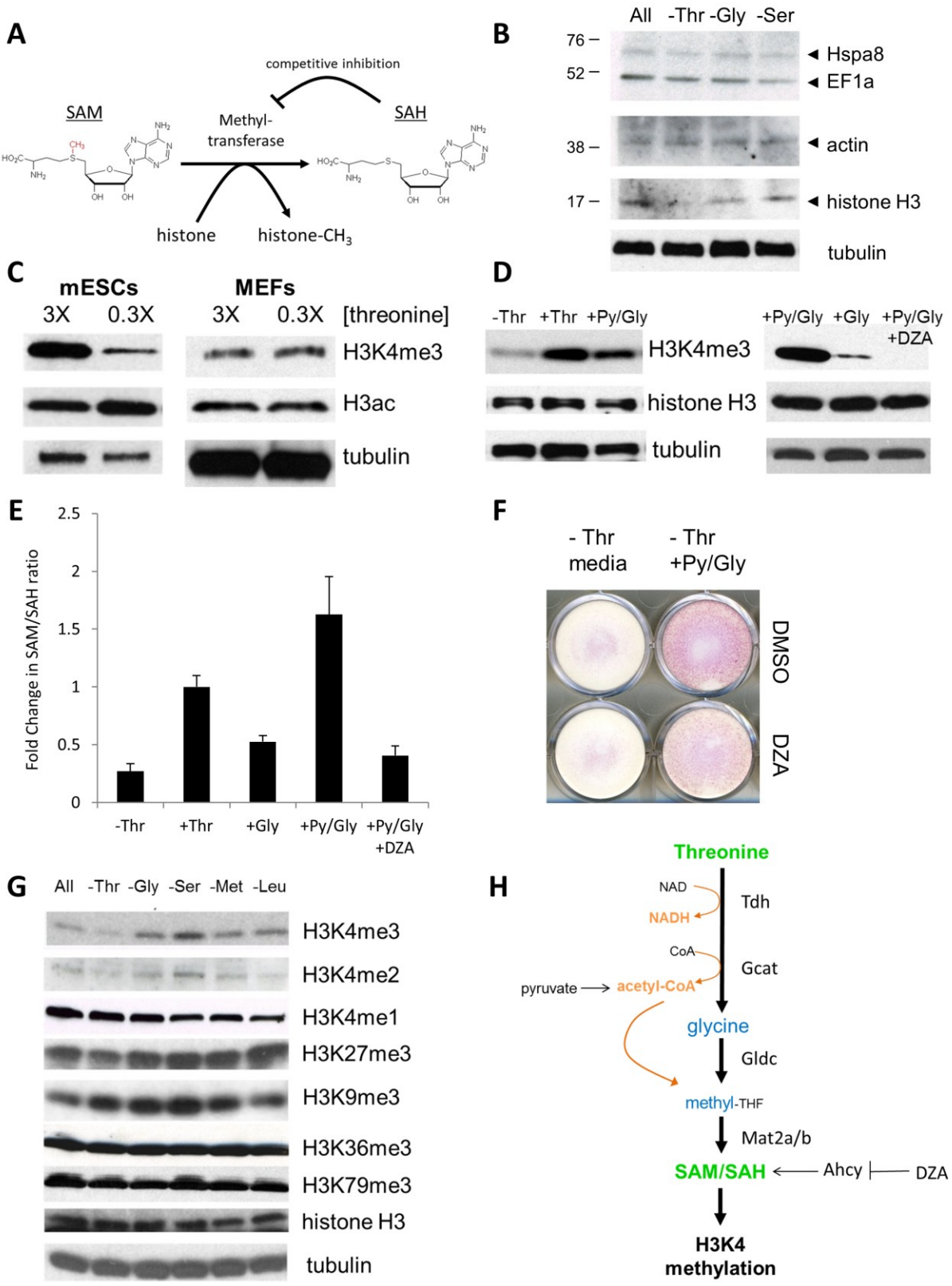

unaltered (Figure 4.3C), although both epigenetic modifications mark open euchromatin and activated gene expression (Azuara et al., 2006; Gaspar-Maia et al., 2011). These results indicate that Thr metabolism regulates the SAM/SAH ratio and H3K4me3 in mESCs, without affecting H3ac. In comparison, MEFs did not show significant changes in H3ac nor H3K4me3 upon 0.3X Thr restriction (Figure 4.3C), consistent with our observations that MEFs do not utilize Thr for Gly or Met synthesis (Figure S4.2A) and with our finding that Thr/Met metabolism changes correlate with pluripotency (Figure 4.1).

To test the sensitivity and reversibility of H3K4me3, we supplemented Thr-restricted mESCs with increasing doses of Thr. While mESCs had lost most of the H3K4me3 mark after just 6 hours of Thr restriction, re-feeding with increasing concentrations of Thr for 6 hours reversed the drop in H3K4me3 levels (Figure S4.3B). Furthermore, we were also able to rescue the drop in H3K4me3 levels by adding high levels of Gly and pyruvate to the medium (Figure 4.3D). Addition of both pyruvate and Gly was necessary to restore the SAM/SAH ratio to normal levels, consistent with the idea that Thr-derived acetyl-CoA and Gly are regulating H3K4me3 by modulating the SAM/SAH ratio (Figure 4.3E). Conversely DZA, which decreases the SAM/SAH ratio by raising SAH levels led to a rapid extinction of H3K4me3 (Figure 4.3D), and over-rode the rescue by pyruvate and Gly (Figure 4.3F), suggesting that the SAM/SAH ratio lies downstream of acetyl-CoA and Gly. We then tested H3 methylation on lysines 4, 9, 27, 36, and 79 in mESCs after restriction of a variety of individual amino acids. H3K4me3 and H3K4me2 were dramatically decreased by Thr restriction, while H3K27me3 decreased slightly following

Thr restriction (Figure 4.3G). H3K9me3 was increased by restriction of every amino acid tested, suggesting that changes in H3K9me3 are regulated independently of Thr restriction. H3K4me1, H3K36me3 and H3K79me3 did not change significantly with restriction of any amino acid. These results suggest that the SAM/SAH ratio maintained by Thr catabolism is not required to regulate all protein lysine methylation in mESCs, but rather certain specific lysines such as H3K4me3 and H3K4me2 (Figure 4.3H). Assays of H3K4 methyltransferase activity from nuclear lysates further indicated that this change in H3K4 methylation with Thr levels is not due to a change in the total amount of methyltransferase activity (Figure S4.3C), suggesting that it is changes in the substrate/product ratio (SAM/SAH) and/or the exposure of H3K4 to the methyltransferase that influences the extent of methylation at this site.

To test if the Thr/Met metabolic flux (Figure 4.3H) has functional consequences on mESC pluripotency, we knocked down the Tdh enzyme. Thr restriction was less suitable for this purpose because it induces cell death very rapidly. We used an inducible RFP-shRNA against Tdh, and observed a substantial dox-dependent downregulation of Tdh protein (Figure S4.3D). In the presence of 0.3X Thr media, Tdh knockdown led to a dramatic decrease in the growth of mESCs (Figure 4.4A). Partial knockdown of Tdh led to mESC differentiation and death, as revealed by staining for alkaline phosphatase. This phenotype could be rescued by higher levels of Thr in the media, further supporting the notion that Thr metabolism is required for mESC self-renewal (Figure 4.4B). More robust knockdown of Tdh abrogated the ability of Thr supplementation to rescue cell viability. Importantly, the presence of Thr did not affect

Tdh expression in surviving cells (Figure S4.3F-G). Tdh knockdown led to a slower flux of $^{13}$C-Thr to Gly, Met and SAM, as well as to acetyl-CoA-derived TCA intermediates (Figure 4C). At steady state, Tdh knockdown also led to lower levels of Gly and citrate, and a lower SAM/SAH ratio (Figure 4.4D). Again, we observed a compensatory upregulation of glycolysis (Figure 4.4D), consistent with our analysis of Thr restriction (Figure 4.2E-F). Tdh knockdown also led to a downregulation of H3K4me3 (Figure S4.3E). Expression profiling by qRT-PCR revealed that Tdh knockdown led to a decrease in expression of pluripotency factors, including *Oct4, Sox2, Nanog, Rex1,* and *Blimp1,* and increased expression of the differentiation markers *Foxa2* and *Sox17* (Fig. S4.4A). Embryoid body differentiation of the mESCs for 3 days showed that Tdh knockdown leads to more rapid extinction of the pluripotency factor *Sox2*, and an aberrantly rapid induction of the differentiation markers *Gata4* and *Sox17* (Figure S4.4B). These data provide evidence that Thr catabolism by Tdh is required for maintenance of the pluripotent epigenetic state.

We then tested if enzymes downstream of Tdh in Thr/Met metabolism are genetically required by mESCs in a similar fashion. In particular we tested mitochondrial glycine decarboxylase (Gldc) which produces methylene-THF from Gly, and the methionine adenosyltransferase Mat2a, which produces SAM from Met. Dox-inducible knockdown of Gldc led to a drop in H3K4me3 (Figure S4.4C). Like Tdh knockdown, Gldc knockdown also led to a growth defect in mESCs (Figure S4.4D), and a general decrease in Thr/Met metabolic flux (Figure S4.4G). In contrast, transient overexpression of Gldc rescued mESCs from Thr restriction (Figure S4.4H-I), suggesting that Thr-

***Figure 4.4: Threonine dehydrogenase regulates the pluripotency of mESCs.*** (**A**) Effects of Tdh shRNA (shTdh) on mESC growth, before (No dox) and after 48 hours dox treatment (Dox) in 0.3X Thr media, relative to a control shRNA against luciferase (shLuc). Images are taken at 4X magnification. (**B**) Feeder-free mESC colonies with dox-induced shTdh or shLuc, seeded at clonal density, after 48h of culture in 0.1X, 0.3X, and 1X relative concentrations of Thr, as visualized by alkaline phosphatase staining. (**C**) $^{13}$C-labeled metabolites derived from [U-$^{13}$C]Thr in mESCs, after 24h incubation in [U-$^{13}$C]Thr and 48h dox-induction of shTdh or shLuc (n=3). The fraction of $^{13}$C incorporation ($^{13}$C / total C ratio) is plotted. (**D**) Relative metabolite levels of mESCs after 48h dox-induction of shTdh or shLuc (n=3). (**E**) Human iPSC colonies reprogrammed from human fibroblasts overexpressing mouse Tdh-T2A-GFP, relative to empty vector, for 18 days with *Oct4/Sox2/Klf4/Myc* lentivirus. Colonies were immunohistochemically stained for the hESC marker Tra-160. (**F**) Efficiency of human iPSC reprogramming from human fibroblasts overexpressing mouse Tdh-T2A-GFP, relative to empty vector (n = 5 replicates, 3 independent experiments). (**G**) Quantitative RT-PCR analysis for relative gene expression of threonine-glycine metabolic enzymes and endogenous pluripotency factors in human fibroblasts overexpressing Tdh-T2A-GFP, relative to empty vector (fold change), after 6 days of iPSC reprogramming (n=3). (**H**) Immunoblot analysis of human fibroblasts overexpressing Tdh-T2A-GFP, relative to empty vector, for Tdh, H3K4me3, H3K27me3, and pan-methyl-lysine levels, prior to iPS reprogramming. (**I**) Metabolite profiles of human fibroblasts overexpressing Tdh-T2A-GFP, relative to empty vector (fold change), prior to iPSC reprogramming (n=3). (**J**) $^{13}$C-labeled metabolites derived from [U-$^{13}$C]Thr after 24h of incubation in human fibroblasts

***Figure 4.4 (continued)*** overexpressing Tdh-T2A-GFP, prior to iPSC reprogramming (n=3). The fraction of $^{13}C$ incorporation ($^{13}C$ / total C ratio) is plotted across several metabolites. All error bars represent the s.e.m. from three independent measurements.

**Figure 4.4 (continued)**

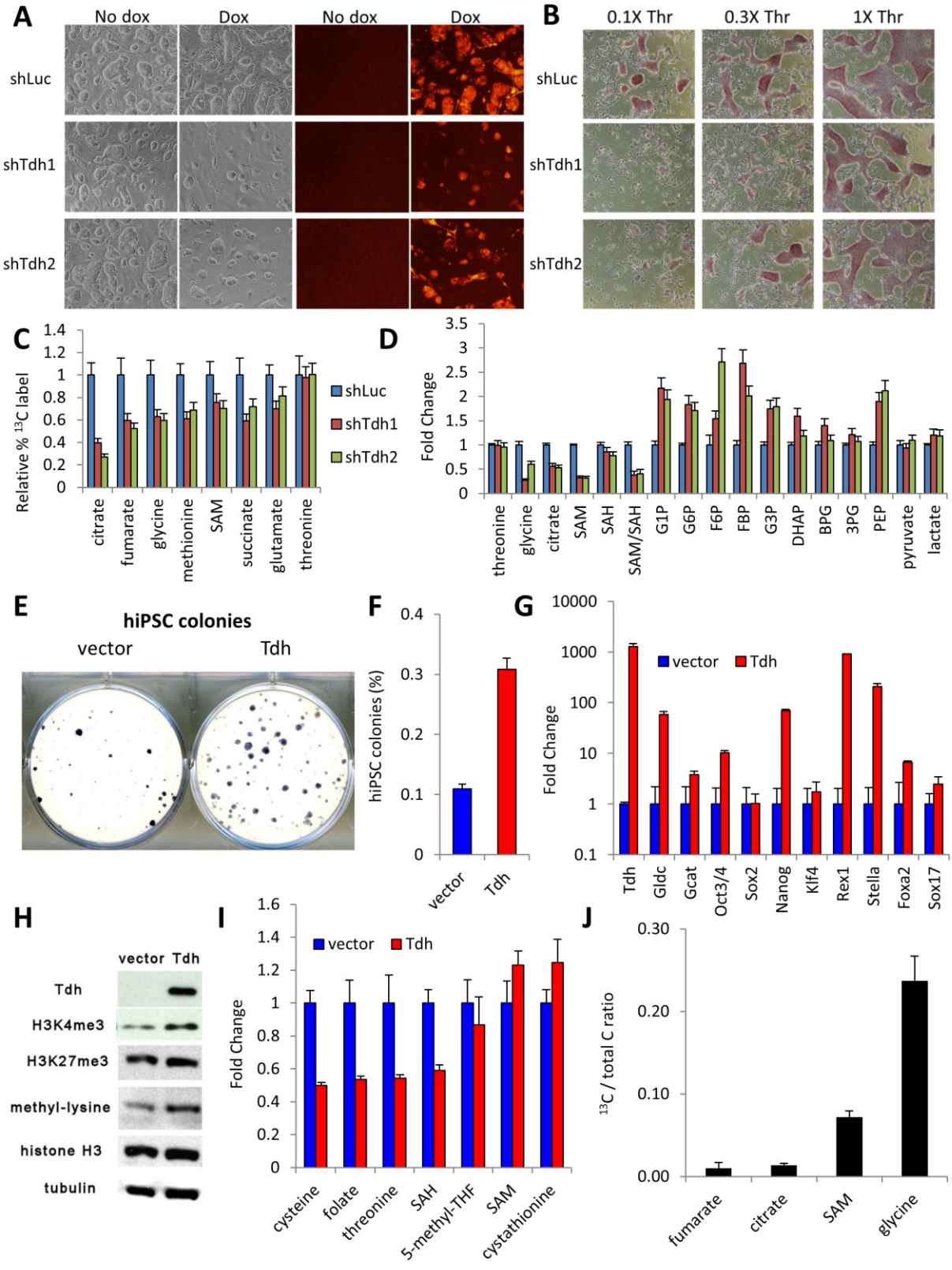

derived 5-methyl-THF and SAM are necessary for mESC pluripotency. Dox-inducible knockdown of the downstream Mat2a also led to a drop in H3K4me3 (Figure S4.4E) due to a lower flux of SAM synthesis (Figure S4.4G), with an accompanying growth defect in mESCs (Figure S4.4F). Conversely, transient overexpression of the SAH hydrolase Ahcy, which is known to decrease SAH and increase the SAM/SAH ratio, rescued mESCs from Thr restriction (Figure S4.4H-I). Finally components of the H3K4 methyltransferase complexes, like Wdr5, Dpy30, and Setd1a also partially rescued mESCs from Thr restriction, suggesting that Thr/Met metabolism is affecting mESCs at least in part through effects on H3K4me3. These data provide further evidence that Thr/Met metabolism regulates pluripotency in mESCs.

In contrast to mice, humans lack a functional form of Tdh (Edgar et al., 2002; Wang et al., 2009) and thus, human ESCs must utilize other metabolic pathways to maintain the SAM/SAH ratio. We examined the possibility that introduction of murine Tdh into human fibroblasts might promote the epigenetic changes that maintain or establish the pluripotent state. We expressed murine Tdh in a lentiviral vector with a self-cleaving T2A tag followed by GFP, and observed high levels of GFP fluorescence and Tdh expression in human fibroblasts following viral transduction, similar to levels in mESCs (Figure S4.4J-L). Cell proliferation was not affected (Figure S4.4M). Tdh-overexpressing and empty-vector control fibroblasts were then subjected to iPSC reprogramming with OSKM lentivirus. By 18 days, *Tdh*-overexpressing human fibroblasts extinguished most of their GFP fluorescence due to the silencing of provirus that is characteristic of

pluripotent stem cells. This indicated that *Tdh*-overexpressing fibroblasts were properly reprogrammed into human iPSCs (Figure S4.4L). Immunohistochemical staining with the definitive human iPSC and ESC marker Tra-160 showed that Tdh overexpression led to 3-fold more human iPSC colonies than control fibroblasts (Figure 4.4E-F). Expression profiling by qRT-PCR revealed that the *Tdh*-overexpressing fibroblasts showed a more rapid upregulation of endogenous pluripotency markers *Oct4, Nanog, Rex1* and *Stella* than control fibroblasts after 6 days of iPSC reprogramming (Figure 4.4G).To further understand Tdh's mechanism for promoting iPSC reprogramming, we assayed the effects of ectopic Tdh expression on histone methylation and the metabolome. Immunoblotting showed that Tdh leads to higher H3K4me3 and pan-methyl-lysine levels relative to control fibroblasts, even before iPSC reprogramming was initiated; moreover, pluripotency factor expression was not significantly changed over background levels (Figure 4.4H, S4.4N). The steady-state metabolome of Tdh-expressing fibroblasts revealed a resemblance to mESCs, with lower levels of Thr, Cys, folate and 5-methyl-THF, and higher levels of cystathionine and a higher SAM/SAH ratio, relative to control fibroblasts (Figure 4.4I). $^{13}$C-Thr isotope labeling further revealed that Tdh-expressing fibroblasts were converting Thr to Gly and SAM, as well as acetyl-CoA-derived TCA intermediates (Figure 4.4J). Thus, Thr/Met metabolism driven by Tdh regulates epigenetic changes to promote changes in cellular identity.

**Discussion**

We have demonstrated that in mESCs, Thr/Met metabolism regulates changes in SAM and SAH, amongst other metabolites. Alterations in the SAM/SAH ratio directly

influenced the maintenance of ESC/iPSCs, in part by regulating tri-methylation of H3K4, thus revealing a novel mechanistic link between cellular metabolism and pluripotency. Previous studies have shown that Thr is uniquely required to generate both acetyl-CoA and Gly in mESCs, but it was unclear why Thr was uniquely required (Wang et al., 2009) - since both acetyl-CoA and Gly are available from other nutrients. The data we present here suggests that the unique ability of Tdh to convert Thr into both Gly and acetyl-CoA in the mitochondrial matrix optimizes the ability of cells to synthesize SAM and deplete SAH to maintain high SAM/SAH ratios. Besides providing reducing equivalents for the synthesis of 5-methyl-THF, Thr-derived acetyl-CoA could also be directly activating the Gly cleavage system by increasing synthesis of its rate-limiting cofactor lipoate (Brody et al., 1997) or, as proteomics profiling studies suggest (Schwer et al., 2009), by directly acetylating proteins in the Gly cleavage complex, like Gldc. Future work will resolve these possibilities. We also found that H3K4me3 is more sensitive to changes in Thr metabolism than methylation of other histone H3 lysines, possibly due to the high abundance of this H3 methylation mark in the euchromatin of mESCs (Azuara et al., 2006; Pan et al., 2007; Zhao et al., 2007; Gaspar-Maia et al., 2011) and its rapid turnover (Deal et al., 2010; Zee et al., 2010). While previous findings have suggested that H3K4me3 is necessary for mESC pluripotency and self-renewal (Ang et al., 2011), here we provide an explanation for how the Thr/Met pathway, by modulating the SAM/SAH ratio amongst other changes in metabolism, regulates murine ESC self-renewal and promotes fibroblast reprogramming to iPSCs at least in part through changes in H3K4me3. It is also interesting to note that, since human ESCs lack a functional Tdh gene (Edgar et al., 2002; Wang et al., 2009), they must rely on other

metabolic enzymes to maintain optimal SAM/SAH ratios for histone methylation. The high levels of Tdh in mouse ESCs could explain why these cells are relatively easy to isolate and maintain in the pluripotent state compared with human ESCs that lack Tdh. Indeed, we have shown that ectopic expression enhances reprogramming, suggesting that adding Tdh to the reprogramming cocktail may facilitate the isolation of human iPSCs from cells that appear refractory to reprogramming.

Collectively, our results establish a metabolic signaling pathway that controls epigenetic identity in stem cells, supporting an emerging appreciation of the role of intermediary metabolism in controlling histone acetylation (Wellen et al., 2009; Cai et al., 2011), and making a novel link between regulation of metabolite levels and maintenance of the stem cell state. Since other enzymes that regulate Gly metabolism have also been implicated in the development of cancer (Locasale et al., 2011; Possemato et al., 2011; Jain et al., 2012; Zhang et al., 2012), our findings provide a framework for the study of a metabolic signaling mechanism that might also be dysregulated in the pathogenesis of other diseases.

**Acknowledgements**

This chapter was published in part in Shyh-Chang et al. (*Science,* 2013a). I designed and performed the experiments, performed the data analysis and wrote the manuscript. Jason Locasale helped greatly with experimental design, metabolomic analysis and helped to write the manuscript. Costas Lyssiotis, Yuxiang Zheng, Ren Yi Teo, Sutheera Ratanasirintrawoot, Tamer Onder, and Juli Unternaehrer helped with various ESC and iPSC experiments. Hao Zhu helped to design some experiments. John Asara

supervised the metabolomic experiments. George Daley and Lewis Cantley designed and supervised experiments, and wrote the manuscript. We also thank all other members of the Daley and Cantley labs for helpful discussions.

## Chapter 5: Epilogue - Stem cell metabolism in tissue development and aging

As the zygote develops into a multicellular organism, the evolving demands for rapid cell growth, tissue formation, and organogenesis place drastically different metabolic requirements on embryos, early pluripotent stem cells, tissue-resident adult stem cells, transient amplifying tissue progenitors, and ultimately mature adult tissues.

During the 1960-70s, advances in our understanding of the metabolism of embryos led to techniques for in vitro culture of blastocysts and the development of in vitro fertilization (IVF). More recently, advances in cancer cell metabolism have led to an explosion in our understanding of how aerobic glycolysis (the “Warburg effect), rather than normal glycolysis linked to OxPhos supports rapid cellular growth. This understanding has led to new drug targets for cancer therapy. Within the last decade, studies of metabolism in various stem cell populations have also highlighted a role for cell-specific metabolic pathways that are modulated during differentiation or during reprogramming to pluripotency. These novel insights have challenged the long-held assumption that all metabolic enzymes perform the same housekeeping functions in all cells, and have provoked a resurgence of interest in metabolism. Overall, these results paint a picture of tissue- and cell-specific metabolic pathways and isoenzymes, which are tightly regulated during development and perform unique functions in specific contexts. Such cell- and tissue-specific isoenzymes provide a therapeutic window for pharmacological manipulation. Hence, the application of metabolomics to the study of stem cells during development could lead to new breakthroughs in our understanding of embryogenesis and adult tissue homeostasis, with implications for ongoing efforts in stem cell biology, tissue regeneration, and therapies for degenerative diseases.

In this Epilogue, we review the specific metabolic pathways active in mammalian totipotent stem cells, pluripotent stem cells before and after differentiation, quiescent adult stem cells, and proliferative stem/progenitor cells during mammalian tissue development. We will also discuss the role of stemness factors in governing stem cell metabolism, and examine the role of stem cell metabolism during aging using insights gleaned from invertebrate models.

**Metabolism in totipotent stem cells and the early (pre-blastocyst) embryo**

Before the morula stage of development in mammalian embryos, each individual early blastomere is totipotent and retains the ability to generate an entire organism and its placenta. Despite differences between mammalian species in the time spent in gestation, the amount of time required to develop to the blastocyst stage is remarkably conserved (Brinster, 1974). In the first week, blastomeres, which are considered here as totipotent stem cells (TSCs), undergo a few self-renewing cell divisions and rounds of DNA replication, but the embryo as a whole experiences no net growth (Leese, 1995). TSCs likely autophagize their protein reserves, which drop by 26% by the 8-cell stage (Brinster, 1967).

Metabolic studies indicate that TSCs have a block at the rate-limiting glycolysis enzymes hexokinase (HK) and phosphofructokinase-1 (PFK1), thus glycolysis rates are initially low (Figure 5.1A; Barbehenn et al., 1978). Instead, the only energy and carbon sources that TSCs can use are pyruvate analogs, a fact that is also true for primordial germ cells, oocytes and spermatocytes, which utilize pyruvate secreted by ovarian follicle cells and lactate secreted by testicular Sertoli cells. The advantages of this

preference for pyruvate in TSCs remain unknown. Early embryo development is actually inhibited by high concentrations of glucose (Brinster and Troike, 1973). Only at the morula stage does the relative rate of glucose oxidation rival that of pyruvate (Leese and Barton, 1984). Pyruvate oxidation in the mitochondria fuels the Krebs cycle, which in turn generates carbon intermediates and fuels OxPhos.

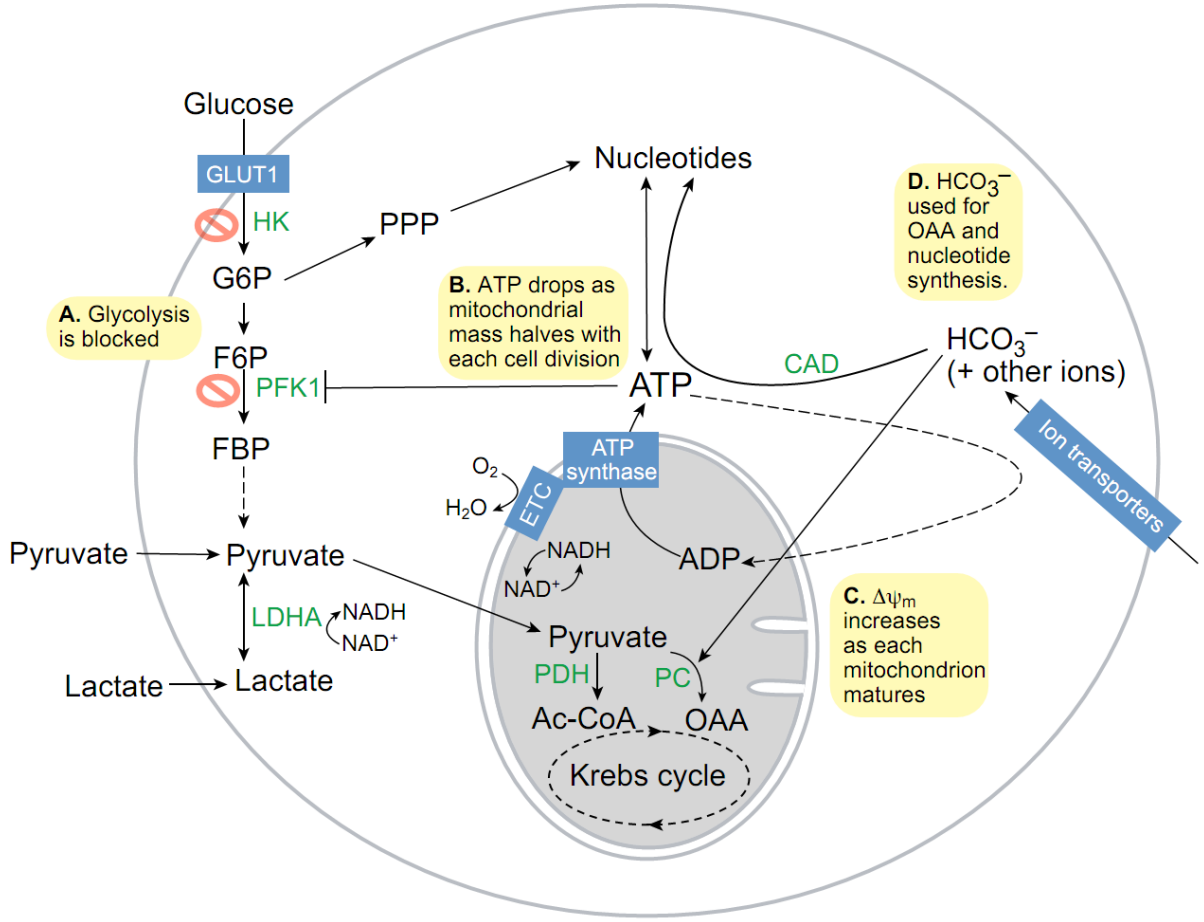


***Figure 5.1: Totipotent stem cell (TSC) metabolism.*** (**A**) Glycolysis is impaired due to the low activities of the rate-limiting enzymes hexokinase (HK) and phosphofructokinase (PFK). TSCs use pyruvate as their major energy and carbon source instead, via pyruvate dehydrogenase (PDH) to generate acetyl-CoA (Ac-CoA) and pyruvate

***Figure 5.1 (continued)*** carboxylase (PC) to generate oxaloacetate (OAA) for anaplerosis or gluconeogenesis. (**B**) ATP synthesis is dependent on mitochondrial OxPhos driven by the electron transport chain (ETC) and ATP synthase. However, as mitochondrial replication has not yet initiated, the halving of mitochondrial mass with each round of mitosis leads to a drop in ATP levels during embryo cleavage. (**C**) Simultaneously, each mitochondrion matures and the inner mitochondrial membrane potential ($\Delta\Psi_m$) increases steadily, thus turning the exponential drop in ATP into a linear drop. (**D**) Bicarbonate $HCO_3^-$ is needed to buffer the pH and also contributes as a carbon source to OAA in the Krebs cycle for anaplerosis via PC, or nucleotide synthesis for DNA and RNA via carbamoyl phosphate synthetase (CAD).

Despite the preference for pyruvate oxidation, the $O_2$ consumption rate of TSCs is relatively low, comparable to that of adult skin or bone (Brinster and Troike, 1973). Consistent with the low $O_2$ consumption rate, mitochondria are structurally immature in TSCs. Oocyte and TSC mitochondria are typically spherical elements ≤1 μM in diameter with few truncated cristae, which contain a matrix of high-electron density. By the end of early embryogenesis, mitochondria elongate and develop networks of cristae containing a matrix of low-electron density (Van Blerkom, 2009). The inner mitochondrial membrane potential ($\Delta\Psi_m$) per mitochondrion also increases with embryo cleavage. However, prior to blastocyst implantation and mitochondrial replication, mitochondrial numbers are halved with each cell division. Accordingly, total ATP levels and the ATP/ADP ratio are high initially in TSCs but decrease linearly with time during development (Figure 5.1B-C), whereas the $NADH/NAD^+$ ratio remains relatively high throughout (Quinn and Wales, 1971; Wales, 1974). Considering that ATP is a potent

allosteric inhibitor of PFK1, the decrease in ATP may play a role in activating glycolysis at the blastocyst stage (Johnson et al., 2003).

The ATP generated by mitochondrial OxPhos is also used to actively transport ions into the early embryo. For example, the pH inside the early embryo is kept alkaline by importing high levels of bicarbonate from the oviduct and uterine fluid (Vishwakarma, 1962). Bicarbonate is important not just for pH buffering and membrane potential - it also contributes significantly to the carbon pool within TSCs (Graves and Biggers, 1970; Brinster, 1973). TSCs might utilize bicarbonate for carbon fixation via mitochondrial pyruvate carboxylase (PC) to generate oxaloacetate for anaplerosis or gluconeogenesis, or via carbamoyl phosphate synthetase (CAD) to generate nucleotides for DNA and RNA synthesis (Figure 5.1D).

**Metabolism in pluripotent stem cells and the blastocyst**

During morula compaction, blastomeres undergo the first round of differentiation to segregate into trophectoderm (which becomes the placenta) and the pluripotent inner cell mass (ICM, which becomes the embryo proper). Accompanying this transformation is a sharp increase in net growth and metabolic activity (Figure 5.2). Firstly, glucose uptake rises sharply as the embryo upregulates the expression of the glucose transporters GLUT1 and GLUT3 (Pantaleon and Kaye, 1998). Glycolytic flux hence rises sharply, leading to increased lactate synthesis (Figure 5.2A; Leese and Barton, 1984). The importance of glycolysis to blastocysts is evident in vivo, since mutations in 4 glycolytic enzymes – glucose-6-phosphate isomerase (GPI), glyceraldehyde-3-phosphate dehydrogenase (GAPDH), triosephosphate isomerase (TPI1) and lactate

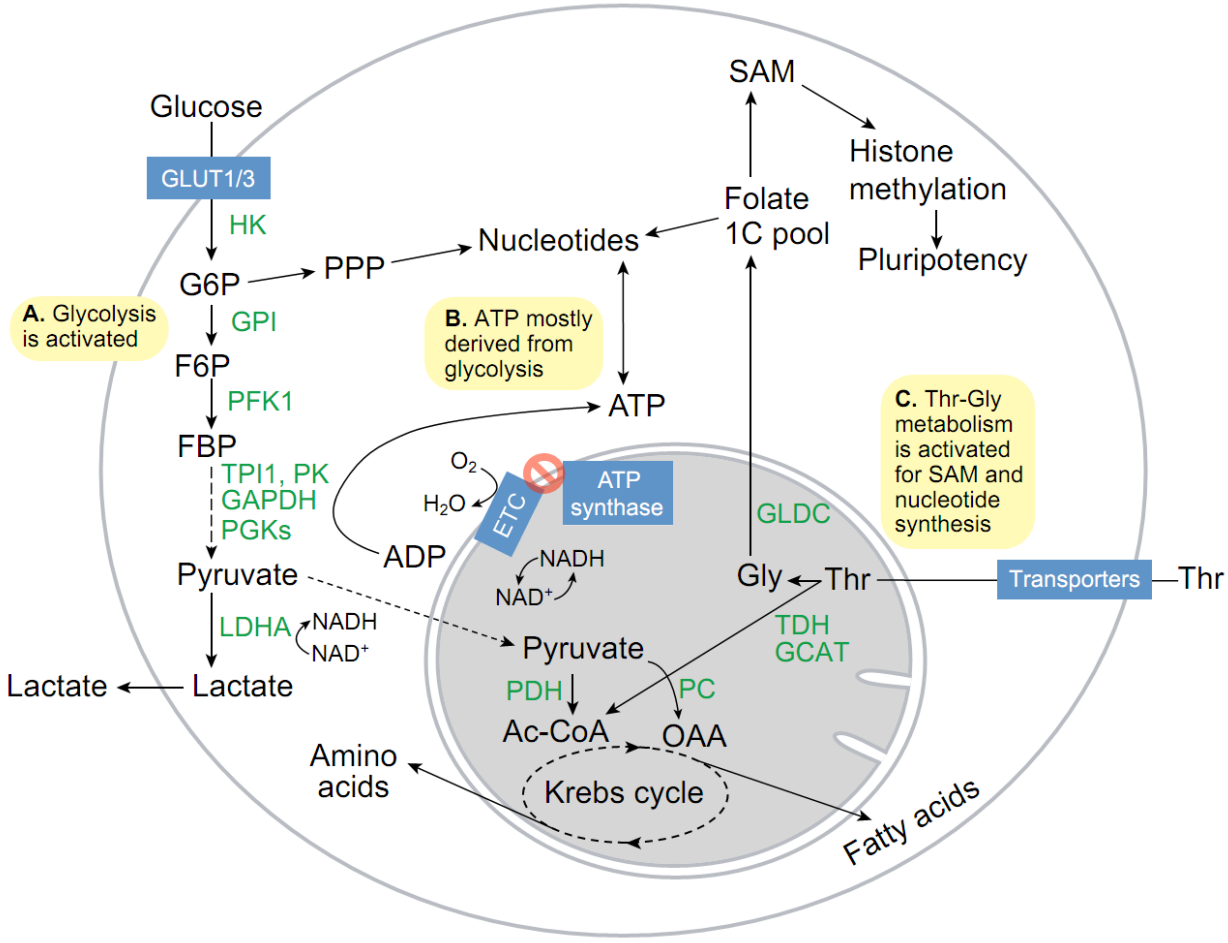


***Figure 5.2: Metabolism in pluripotent stem cells.*** (**A**) Glucose flux increases with the increase in GLUT1/3 expression, and the HK and PFK1 enzymes become activated to sharply increase glycolytic flux. As a result, flux into the pentose phosphate pathway (PPP) for nucleotide synthesis increases. (**B**) ATP synthesis is more dependent on the reactions carried out by glycolytic phosphoglycerate kinases (PGK) and pyruvate kinases (PK), and is decoupled from $O_2$ consumption by the mitochondrial ETC. (**C**) Activation of threonine dehydrogenase (TDH), glycine C-acetyltransferase (GCAT), and glycine decarboxylase (GLDC) promotes Thr-Gly catabolism to feed the folate one-carbon (1C) pool, which in turn fuels S-adenosyl-methionine (SAM) and nucleotide synthesis to maintain pluripotency and proliferation.

dehydrogenase A (LDHA) - result in early postimplantation lethality (West et al., 1990; Pretsch, 2000; Merkle and Pretsch, 1989; Merkle et al., 1992). OxPhos rates also increase, and $O_2$ consumption in blastocysts rises to a high rate, comparable to that observed in the adult brain (Brinster, 1974). However, this increase is largely due to mitochondria of the trophectoderm, which have a high $\Delta\Psi_{m.}$ In contrast, mitochondria in the ICM, which is not involved in organizing the blastocyst cavity, have a lower $\Delta\Psi_m$ (Van Blerkom et al., 2009).

Consistent with the lower $\Delta\Psi_m$ in ICM mitochondria, pluripotent embryonic stem cells (ESCs) derived from in vitro culture of the ICM show high rates of glycolysis (Chung et al., 2007; Kondoh et al., 2007; Prigione et al., 2010; Varum et al., 2011; Zhang et al., 2011a; Panopoulos et al., 2012; Shyh-Chang et al., 2013). A switch from OxPhos back to glycolysis is also seen during the conversion of differentiated cells into induced pluripotent stem cells (iPSCs), and reflects metabolic reprogramming (Folmes et al., 2011; Shyh-Chang et al., 2013). However, the upregulation of glycolysis precedes the reactivation of pluripotency markers (Hansson et al., 2012; Shyh-Chang et al., 2013). This indicates that the activation of glycolysis is not necessarily specific to pluripotency but, rather, represents the preferred metabolic state of rapidly proliferating cells. Furthermore, cell proliferation enhances iPSC reprogramming stochastically (Hanna et al., 2009), further confounding the relationship between glycolysis, proliferation, and pluripotency. That said, promotion of glycolysis enhances iPSC reprogramming, whereas pharmacological inhibition of glycolysis or stimulation of OxPhos impairs iPSC reprogramming (Yoshida et al., 2009; Zhu et al., 2010; Folmes et al., 2011). In the Warburg effect, cancer cells are thought to shunt glycolytic intermediates into amino

acid, lipid, and nucleotide biosynthesis for cell proliferation (Vander Heiden et al., 2009). Similarly, mouse ESCs show increased activity in the pentose phosphate pathway (PPP), which allows rapid nucleotide synthesis (Filosa et al., 2003; Manganelli et al., 2012; Varum et al., 2011). Thus, anabolic glycolysis is a common feature of the metabolism in both ESCs and cancer cells.

Despite the low levels of OxPhos occurring in undifferentiated ESCs, $O_2$ consumption is still important. However, ATP synthesis appears to be decoupled from $O_2$ consumption, and depends on glycolysis instead (Figure 5.2B; Zhang et al., 2011a). Although the mechanism and reasons for this decoupling remain unclear, it is possible that ESCs consume $O_2$ through the electron transport chain to oxidize NADH into $NAD^+$ and maintain the Krebs cycle flux. This might also allow ESCs to maintain an optimal redox potential for lipid synthesis from citrate, and amino acid synthesis from OAA or α-ketoglutarate (Shyh-Chang et al., 2011). In line with this, ESCs with high $\Delta\Psi_m$ form teratomas more efficiently than ESCs with low $\Delta\Psi_m$ (Schieke et al., 2008), and blastocysts deficient in mitochondrial oxidation enzymes, including the pyruvate dehydrogenase (PDH) complex, show developmental defects (Johnson et al., 1998, 2001).

Mouse ESCs also utilize a unique mode of amino acid metabolism to maintain their pluripotent epigenetic state (Figure 5.2C). In a screen for dependence on each of the 20 amino acids, restriction of Thr alone (and to a lesser extent, Met or Cys) uniquely abolished mouse ESC growth. In contrast, other proliferative cell lines such as HeLa, 3T3 or MEFs were sensitive to restriction of other amino acids but not Thr restriction (Wang et al., 2009). Consistent with these findings, expression of the Thr catabolizing

enzyme threonine dehydrogenase (TDH) is dramatically upregulated in early blastocysts and ESCs, and after iPSC reprogramming, relative to differentiated cells (Wang et al., 2009; Shyh-Chang et al., 2013). TDH is a mitochondrial enzyme that serves as the rate-limiting step in the metabolism of Thr into Gly and acetyl-CoA. Gly can be subsequently used by the mitochondrial enzyme glycine decarboxylase (GLDC) to generate 1-carbon equivalents for the folate pool. Like TDH, GLDC is also upregulated in pluripotent cells relative to differentiated cells (Shyh-Chang et al., 2013). Furthermore, pharmacological inhibition or knockdown of TDH disrupts mESC colony growth (Alexander et al., 2011; Shyh-Chang et al., 2013). Collectively, these findings suggest that the metabolites generated by Thr degradation may be utilized specifically for the self-renewal of pluripotent ESCs. Indeed, it was recently demonstrated that TDH and GLDC regulate the synthesis of 5-methyl-tetrahydrofolate (5mTHF), thereby modulating S-adenosylmethionine (SAM) metabolism and histone H3K4 tri-methylation (Shyh-Chang et al., 2013; Box 2). H3K4 tri-methylation is associated with open euchromatin, which is critical for the epigenetic plasticity of pluripotent ESCs and their self-renewal (Azuara et al., 2006; Gaspar-Maia et al., 2011; Ang et al., 2011). TDH regulation of the folate pool was also found to promote rapid proliferation in mESCs (Wang et al., 2009), consistent with findings that GLDC regulates the folate pool to promote nucleotide synthesis and proliferation in cancer stem cells (Zhang et al., 2012).

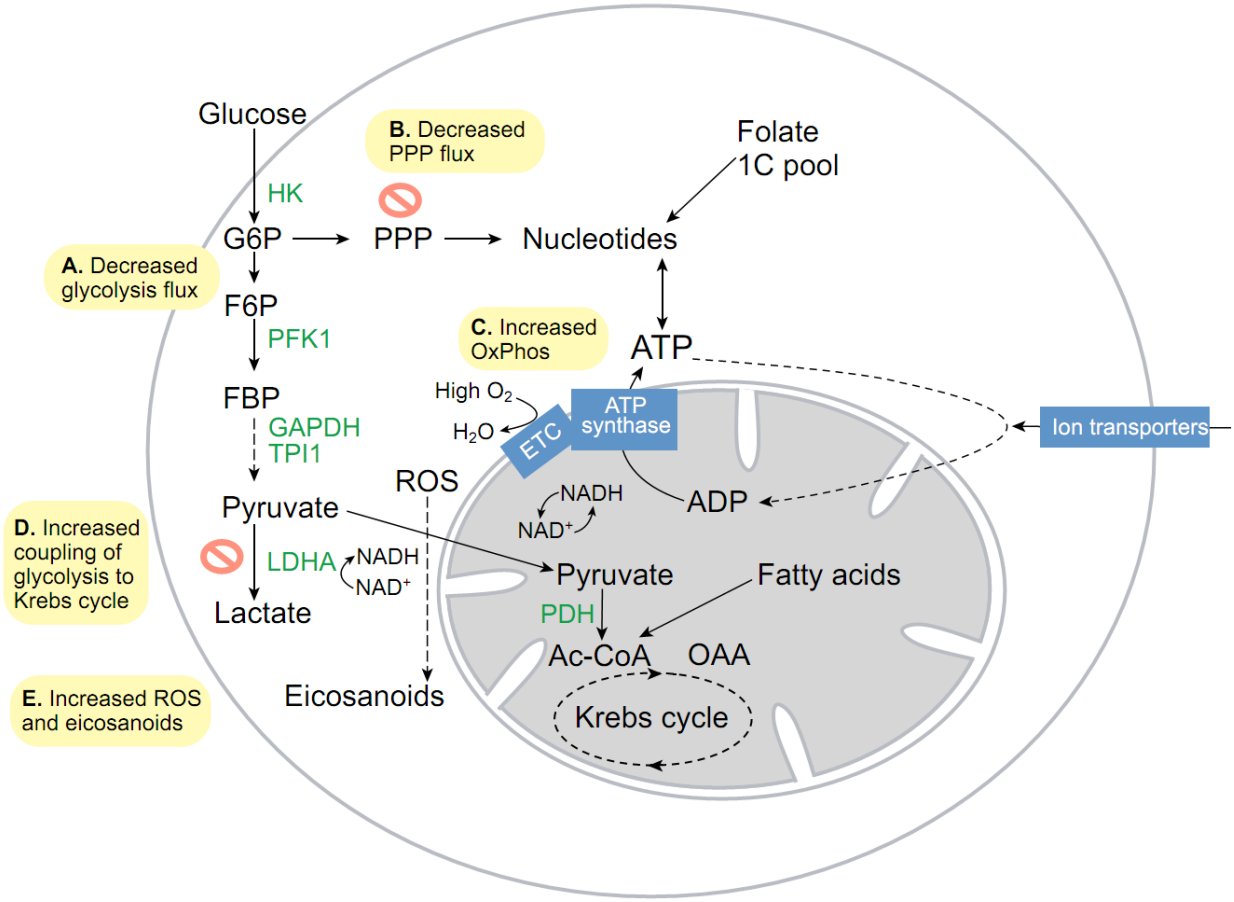


***Figure 5.3: Metabolism in differentiating ESCs.*** (**A**) Glycolytic flux and lactate production drop rapidly upon ESC differentiation. (**B**) Flux into the PPP decreases as a result. (**C**) $O_2$ consumption increases sharply as the ETC again becomes coupled to ATP synthase, to fulfill the needs of cell differentiation. (**D**) Glycolysis also becomes more coupled to the Krebs cycle, as pyruvate is transported more efficiently into mitochondria. (**E**) Increased ETC activity leads to increased reactive oxygen species (ROS) and eicosanoid signaling, which promote cell differentiation.

**Metabolism in differentiating ESCs**

When ESCs differentiate, glycolytic flux decreases dramatically (Figure 5.3A-B), Thr-Gly metabolism is extinguished, and mitochondrial OxPhos fueled by glucose and fatty acids increases (Figure 5.3C-D; Cho et al., 2006; Chung et al., 2007; Facucho-Oliveira et al., 2007; Wang et al., 2009). Thus cells acquire an even more oxidized state. Furthermore, pluripotent ESCs are enriched with unsaturated lipids such as omega-3 and omega-6 fatty acids that contain readily oxidizable carbon-carbon double bonds (Yanes et al., 2010). These unsaturated lipids prime ESCs to differentiate after oxidation by reactive oxygen species (ROS) to form eicosanoids (Figure 5.3E). In support of this concept, pharmacological inhibition of enzymes in the eicosanoid synthesis pathway, which oxidizes these unsaturated lipids, preserves ESC pluripotency (Yanes et al., 2010).

**Metabolism in quiescent adult stem cells**

Unlike the proliferative ESCs, most adult stem cells are quiescent. Such quiescent adult stem cells reside in various tissues and include long-term hematopoietic stem cells (LT-HSCs) and mesenchymal stem cells (MSCs) in the bone marrow, neural stem cells (NSCs) in the brain, epidermal stem cells in the hair follicle bulge, and satellite cells in the skeletal muscles. It is thought that quiescent adult stem cells generally maintain a slow-cycling state to avoid cellular damage from ROS and to ensure life-long tissue renewal capacity (Rossi et al., 2008; Suda et al., 2011). One largely unanswered question is whether the metabolic program in adult stem cells is an intrinsic feature required for stem cell self-renewal, or an adaptive response to the hypoxic environment.

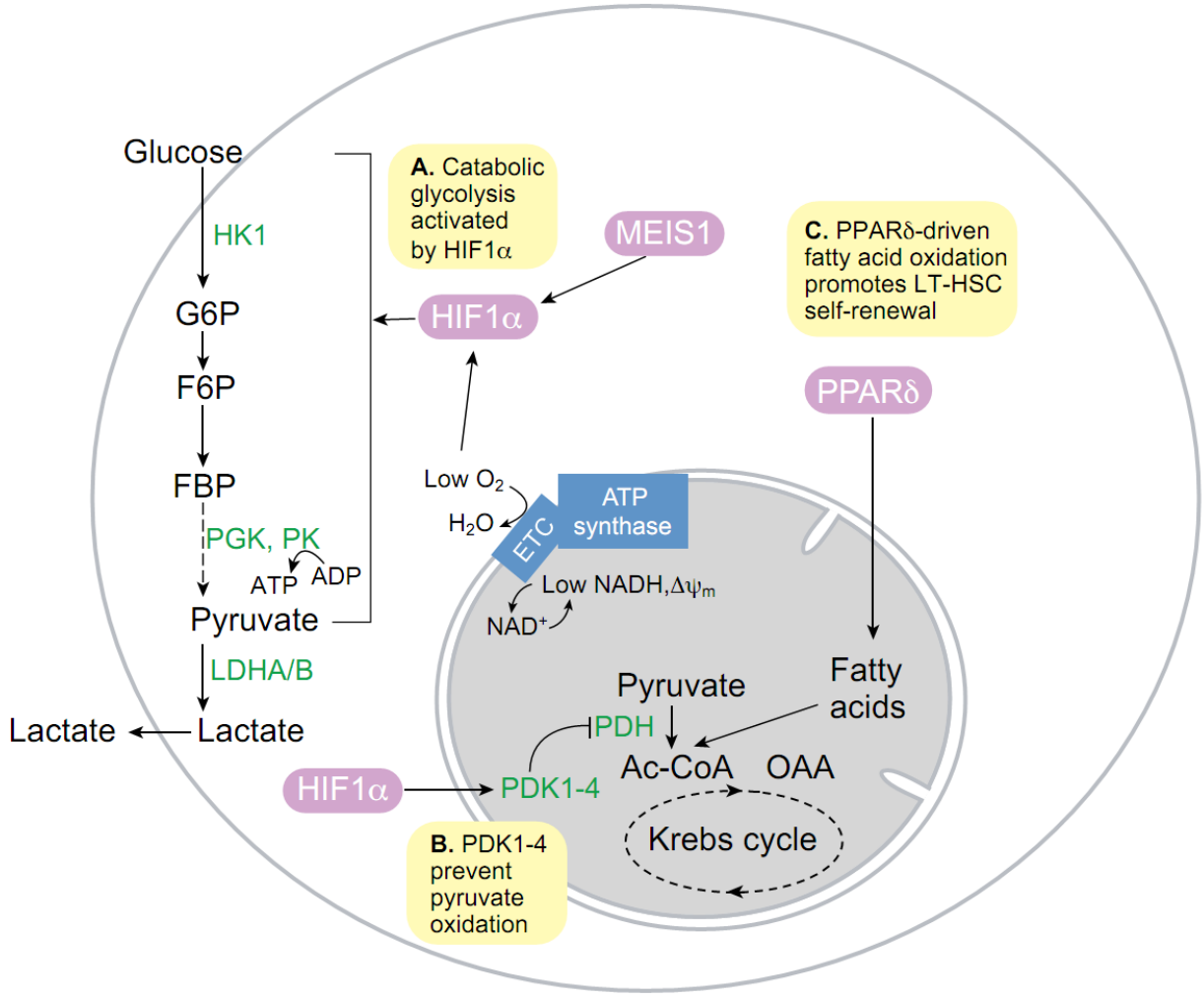


***Figure 5.4: Metabolism in quiescent long-term hematopoietic stem cells (LT-HSCs).*** (**A**) The HSC transcription factor MEIS1 and low $O_2$ levels combine to activate HIF1a activity, which in turn promotes glycolysis in quiescent LT-HSCs. (**B**) HIF1a-dependent pyruvate dehydrogenase kinases (PDK1-4) prevent pyruvate oxidation by suppressing PDH. (**C**) PPARδ-driven fatty acid oxidation in the mitochondria is required for LT-HSC self-renewal and quiescence. Inhibition of fatty acid oxidation leads to LT-HSC proliferation and differentiation.

It is known that adult LT-HSCs prefer to utilize glycolysis (Figure 5.4A), a phenotype that some have argued to be an adaptation to the hypoxic environment of the bone

marrow niche (Suda et al., 2011). One potential advantage of hypoxia-induced glycolysis in LT-HSCs is the associated reduction in ROS production from mitochondria, that leads to LT-HSC differentiation (Figure 5.5). LT-HSCs are sensitive to ROS, and they either undergo differentiation or apoptosis in the presence of excessive ROS when the stress response is defective (Tothova et al., 2007). NSCs in the hypoxic brain exhibit similar responses to ROS (Figure 5.6A; Renault et al., 2009). This suggests that glycolysis is not simply an environmental adaptation but an intrinsic necessity for quiescent adult stem cells. In line with this, the pro-glycolytic phenotype of LT-HSCs appears to be programmed by the HSC transcription factor MEIS1 via its target hypoxia-inducible factor 1-alpha (HIF1a; Simsek et al., 2010), which upregulates many glycolytic enzymes. Similar to embryonic TSCs and ESCs, adult HSCs possess low mitochondrial mass and immature mitochondrial morphology (Chung et al., 2007). In fact, the majority of LT-HSCs can be metabolically sorted by gating for low $\Delta\Psi_m$ and low endogenous NADH, and the resultant cells have greater hematopoietic capacity in vivo (Simsek et al., 2010). The low $\Delta\Psi_m$ could be partly because LT-HSCs express higher levels of the pyruvate dehydrogenase kinases PDK1 and PDK3, which inhibit PDH and mitochondrial pyruvate oxidation (Figure 5.4B; Klimmeck et al., 2012). Interestingly, another pair of PDKs regulated by HIF1a, PDK2 and PDK4, are also required by LT-HSCs, demonstrating that PDK-regulated OxPhos generally acts as a switch for LT-HSC function (Takubo et al., 2013). Overall, it appears that OxPhos capacity is reduced in LT-HSCs. However, PPARδ-driven fatty acid β-oxidation has been shown to promote LT-HSC self-renewal (Figure 5.4C; Ito et al., 2012), suggesting that it is not the absolute quantity per se, but the efficiency of OxPhos that might also be important.

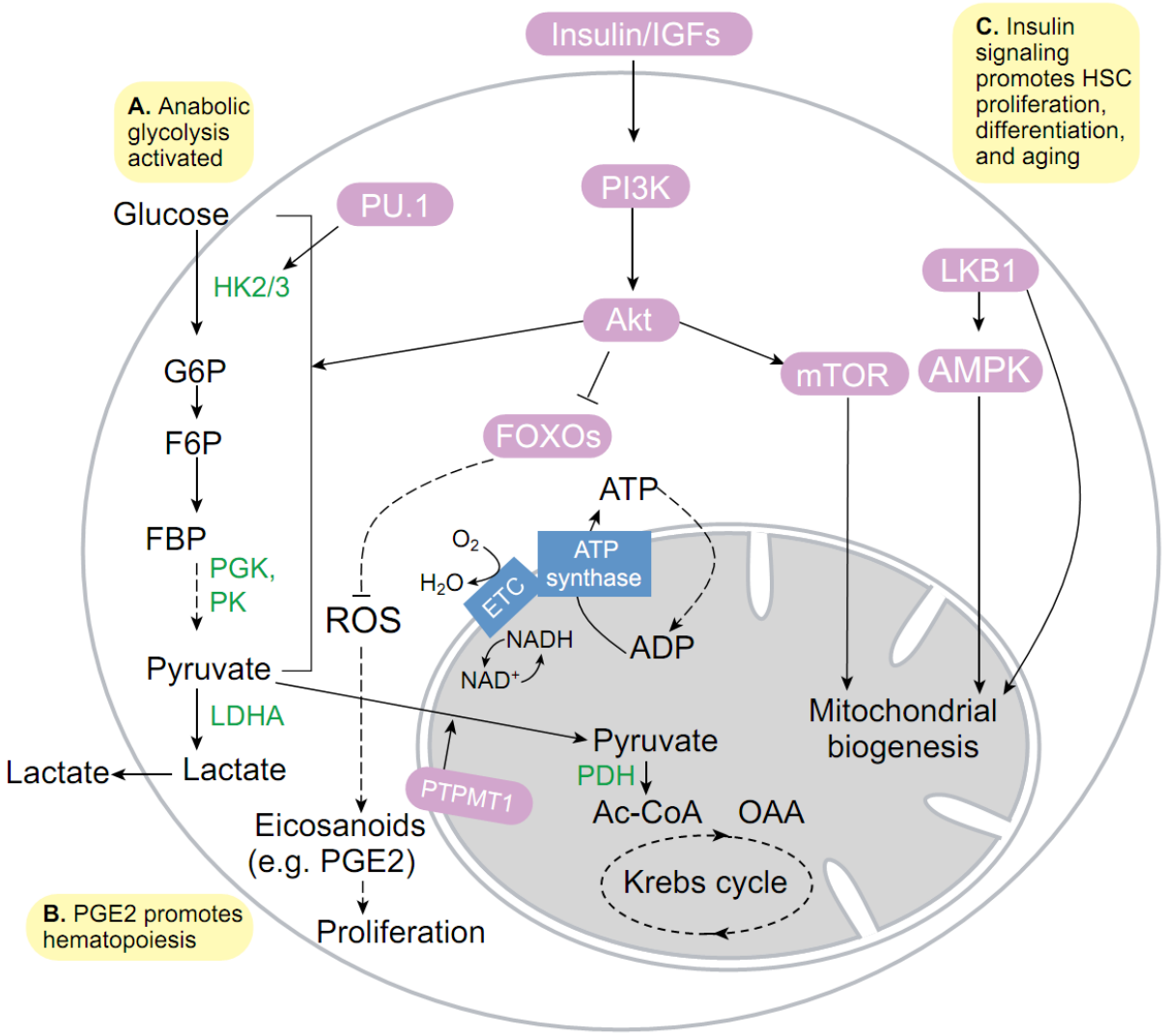


***Figure 5.5: Proliferative hematopoietic stem and progenitor cell metabolism.*** (**A**) Anabolic glycolysis is driven in part by the myeloid transcription factor PU.1 and the Akt kinase. (**B**) Increased ROS production during OxPhos, fueled by PTPMT1-driven pyruvate oxidation, might lead to increased synthesis of eicosanoids, e.g. prostaglandin E2 (PGE2), which promote hematopoiesis. (**C**) Insulin-PI3K-Akt signaling activates glycolysis, promotes ROS production by repressing the FoxO-mediated stress response, and promotes mitochondrial biogenesis by activating mTOR signaling. This leads to HSC proliferation, differentiation, and aging.

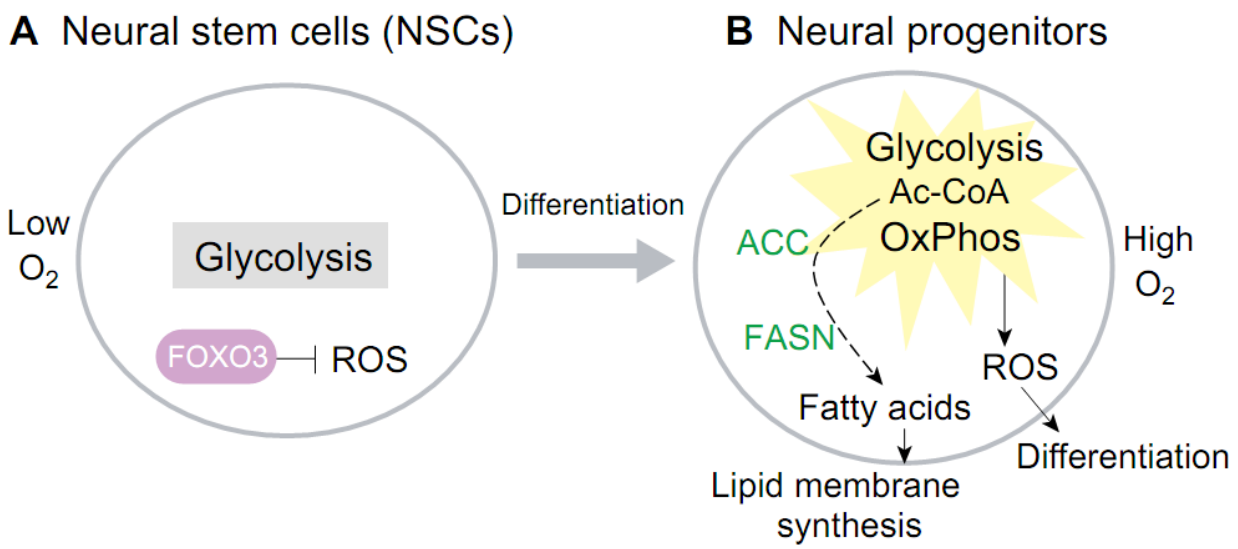


***Figure 5.6: Metabolism in neural stem cells and progenitors.*** (**A**) Neural stem cells (NSCs) remain quiescent in a hypoxic niche with low $O_2$. NSCs require FoxO3 to suppress ROS. (**B**) Neural progenitors, which exist under normoxia, upregulate both glycolysis and OxPhos. In normoxia, FoxO3 is repressed and leads to increased ROS, which prime NSCs for differentiation. Activation of acetyl-CoA carboxylase (ACC) and fatty acid synthase (FASN) increase fatty acid synthesis from Ac-CoA to fuel phospholipid membrane synthesis.

MSCs also reside in hypoxic conditions in vivo (Figure 5.7A). Relative to the more differentiated osteoblasts within the bone marrow niche, MSCs express higher levels of glycolytic enzymes and lower levels of OxPhos proteins, suggesting that MSCs rely more on glycolysis than do osteoblasts (Chen et al., 2008a). Nevertheless, MSCs expanded under normoxia can still utilize OxPhos with a high $O_2$ consumption rate, suggesting that glycolysis may be an environmental adaptation for MSCs (Pattappa et

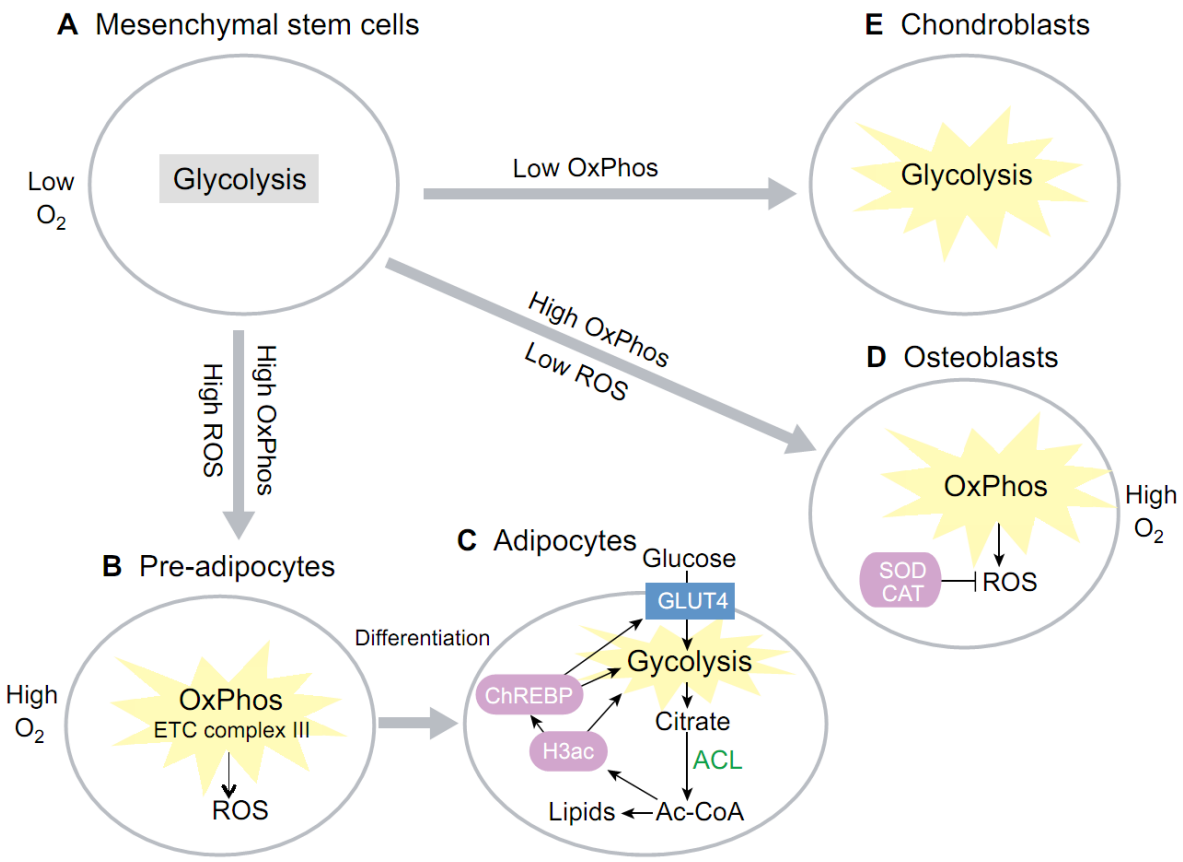


***Figure 5.7: Metabolism in mesenchymal stem cell (MSCs) and progenitors.*** (**A**) Bone marrow MSCs remain quiescent in a hypoxic niche, and utilize glycolysis. (**B**) Pre-adipocytes upregulate OxPhos, and ROS production from the ETC complex III is highly active, to prime adipocyte differentiation. (**C**) Adipocytes upregulate glycolysis and ATP citrate lyase (ACL), which leads to increased cytosolic acetyl-CoA synthesis and hence an increase in histone H3 acetylation (H3ac) and also lipid synthesis. H3ac, in turn, leads to activation of the ChREBP transcription factor to promote GLUT4-mediated glucose uptake and glycolysis in order to generate the acetyl-CoA needed. (**D**) In osteoblasts, which give rise to bone, OxPhos and $O_2$ consumption are upregulated, but ROS is suppressed via superoxide dismutase (SOD) and catalase (CAT). (**E**) Glycolysis is further upregulated in chondroblasts during chondrogenesis, which give rise to cartilage.

al., 2011). In fact, MSC proliferative and colony formation capacity is significantly increased in normoxia (Pattappa et al., 2013). The switch to OxPhos comes at a cost however, since MSCs expanded under normoxia show a 3-4 fold increase in senescence, suggesting that hypoxia-induced glycolysis limits MSC proliferation to prevent oxidative stress-induced senescence and preserve MSC long-term self-renewal (Pattappa et al., 2013). Thus, in at least three types of adult stem cells, namely LT-HSCs (Tothova et al., 2007), MSCs (Chen et al., 2008a), and NSCs (Renault et al., 2009), the induction of ROS forces adult stem cells out of quiescence in hypoxia, and into a more proliferative state in normoxia. This may be a common mechanism for priming stem cell differentiation.

**Metabolism in proliferative adult stem/progenitor cells**

In addition to long-lived quiescent stem cells, a number of adult tissues contain proliferative stem and progenitor cells that contribute to tissue homeostasis and renewal. These include hematopoietic progenitors, neural progenitors, mesenchymal progenitors, skeletal myoblasts, cardiomyocyte progenitors, intestinal stem cells (ISCs), and germline stem cells (GSCs). As we discuss below, these are all highly proliferative undifferentiated cells that rely on different combinations of glycolysis and OxPhos for proliferation (summarized in Table 5.1).

*Hematopoietic progenitors*

The metabolic switch from anaerobic glycolysis under hypoxia for quiescent adult stem cells, to a mixture of aerobic glycolysis and OxPhos for proliferative adult stem/progenitor cells is well exemplified in hematopoiesis. A proteomics study of the

***Table 5.1: Summary of Metabolic Pathways in Various Stem and Progenitor Cells***

**Table 1. Summary of metabolism in respective stem and progenitor cells**

| Mammalian cell type | Active metabolic pathways |
|---|---|
| Totipotent stem cells/blastomeres | Pyruvate oxidation, bicarbonate fixation |
| Pluripotent stem cells/embryonic stem cells | Anabolic glycolysis, PPP, Thr-Gly metabolism |
| Differentiating embryonic stem cells | OxPhos, ROS, eicosanoids |
| Long-term hematopoetic stem cells | Catabolic glycolysis, fatty acid oxidation |
| Hematopoietic progenitors | Anabolic glycolysis, OxPhos, ROS, eicosanoids |
| Neural stem cells | Low glycolysis |
| Neural progenitors | High glycolysis, OxPhos, ROS, eicosanoids, fatty acid synthesis |
| Mesenchymal stem cells | Low glycolysis |
| Chondroblasts | High glycolysis |
| Osteoblasts | OxPhos |
| Pre-adipocytes | OxPhos, ROS |
| Myoblasts | Anabolic glycolysis, PPP |
| Myotubes | Glycolysis, OxPhos |
| Cardiomyocyte progenitors | Lactate oxidation |
| Intestinal stem cells (*Drosophila*) | OxPhos |

OxPhos, oxidative phosphorylation; PPP, pentose phosphate pathway; ROS, reactive oxygen species.

transition from HSCs to myeloid progenitors showed that among the hexokinase isoforms, HK1 expression is higher in HSCs, whereas HK2 and HK3 expression levels were higher in myeloid progenitors (Klimmeck et al. 2012). HK1 is primarily associated with catabolism, whereas HK2 and HK3 have anabolic roles (Wilson, 2003), suggesting that HSCs rely on glycolysis for energy whereas myeloid progenitors use glycolysis for anabolic growth (Figure 5.5A). In fact, myeloid cells express high levels of the transcription factor PU.1, which transactivates HK3 to drive myeloid differentiation and maintain myeloid identity (Federzoni et al., 2012). Myeloid progenitors also express lower levels of PDKs, suggesting that PDK-mediated suppression of OxPhos in HSCs is relieved upon myeloid commitment (Klimmeck et al., 2012; Takubo et al., 2013). In addition, the mitochondrial phosphatase PTPMT1, which dephosphorylates phosphatidylglycerol phosphate during cardiolipin synthesis (Zhang et al., 2011b), appears to be another master regulator of the OxPhos switch (Figure 5.5B; Yu et al., 2013).

Concomitant with the increase in OxPhos activity as HSCs differentiate, ROS also increases (Figure 5.5B; Tothova et al., 2007). In the *Drosophila* larval lymph gland, hematopoietic cells resembling mammalian myeloid progenitors require ROS to differentiate into mature blood cells (Owusu-Ansah and Banerjee, 2009). The targets of ROS that prime HSC differentiation still remain unknown, but it is possible that components of the eicosanoid biosynthesis pathway, which oxidizes lipids in ESCs (Yanes et al., 2010), may be involved. In fact, the eicosanoid product prostaglandin-E2 has been shown to significantly enhance HSC proliferation, hematopoietic colony formation, and hematopoiesis in vivo by activating Wnt signaling (Goessling et al., 2009), suggesting that eicosanoids might be important for HSC proliferation and differentiation.

*Neural progenitors*

Like hematopoietic progenitors, proliferative neural progenitors show high levels of glycolysis mediated by HK2 (Gershon et al., 2013). And like hematopoietic progenitors, the directed differentiation of ESCs into neural progenitors is stimulated by the eicosanoid pathway, and also fatty acid metabolism (Yanes et al., 2010). However, it is unclear if these effects of fatty acids are due to mitochondrial fatty acid β-oxidation, or fatty acid utilization in lipogenesis, or both. On one hand, the oxidative stress response mediated by FoxO3 becomes rapidly deactivated upon NSC differentiation, suggesting that mitochondrial oxidation-induced ROS is required in neural progenitors (Figure 5.6A; Renault et al., 2009). In fact, deficiency in FoxO3 causes depletion of adult brain NSCs, and an expansion of oligodendrocytes in the corpus callosum (Renault et al., 2009). On the other hand, $Nestin^{+}$ neural progenitors require lipogenesis, mediated by fatty acid

synthase (FASN) and acetyl-CoA carboxylase (ACC), for lipid membrane synthesis and neural progenitor proliferation (Knobloch et al., 2013). These results suggest that both fatty acid synthesis and oxidation-induced ROS might be critical for neural progenitors (Figure 5.6B). Alternatively, it is possible that fatty acid β-oxidation is only required in quiescent NSCs, resembling the situation observed in LT-HSCs (Ito et al. 2012). Upon differentiation into neural progenitors, the ACC-mediated increase in malonyl-CoA could then allosterically inhibit fatty acid β-oxidation and promote fatty acid synthesis. Yet another possibility is that fatty acid-derived lipids are oxidized via the eicosanoid pathway to promote neurogenesis. More work is required to resolve these questions.

*Mesenchymal progenitors*

During adipogenesis, mesenchymal pre-adipocytes activate a lipogenic program involving ATP citrate lyase (ACL) to increase glucose metabolism and to synthesize lipids for fat storage. Adipocytes also rely upon ACL to increase their supply of acetyl-CoA for increased histone acetylation during adipogenesis (Figure 5.7B-C). This is necessary for transactivation of key metabolic proteins such as the glucose transporter GLUT4, HK2, PFK1, LDHA, and the carbohydrate-responsive element-binding protein (ChREBP) in the lipogenic program (Wellen et al., 2009). Directed adipogenesis of MSCs also increases mTORC1-dependent mitochondrial biogenesis, OxPhos and ROS (Figure 5.7B). Endogenous ROS generated from the mitochondrial ETC complex III is required to initiate adipogenesis, suggesting that OxPhos and ROS are not simply a consequence of adipogenesis but are a causal factor in promoting it (Tormos et al., 2011). Similarly, directed osteogenesis of MSCs leads to an increase in mitochondrial biogenesis and OxPhos in osteoblasts (Chen et al., 2008a). Unlike adipogenesis,

however, osteogenesis cannot tolerate ROS (Figure 5.7D). In fact, antioxidant enzymes such as superoxide dismutase (SOD) and catalase (CAT) are simultaneously upregulated with OxPhos in osteoblasts to prevent ROS accumulation (Chen et al., 2008a). In contrast to adipogenesis and osteogenesis, MSCs undergoing chondrogenesis have significantly reduced $O_2$ consumption and OxPhos, indicating a shift towards increased glycolysis (Figure 5.7E; Pattappa et al., 2011). Furthermore, hypoxia inhibits MSC osteogenesis, while chondrogenesis is unaffected (Pattappa et al. 2013). Taken together, these studies demonstrate that careful manipulation of oxidative metabolism can direct the differentiation of MSCs either into adipocytes, osteoblasts or chondroblasts.

*Skeletal myoblasts*

Myogenesis during muscle regeneration is mediated by the proliferation of myoblasts derived from satellite cells, which undergo fusion to form myotubes. The expression of glucose transporters is tightly regulated during this process. GLUT1, for example, is expressed only in satellite cells and myoblasts (Figure 5.8A). The higher affinity transporter GLUT3 increases markedly in myoblasts during myogenesis, and decreases in myotubes. In contrast, the high affinity and insulin-sensitive GLUT4 is expressed only in myotubes (Figure 5.8B). Accordingly, the rate of glucose transport rises significantly during myogenesis, suggesting a switch in glucose metabolism during this process (Guillet-Deniau et al., 1994). This switch is supported by findings that myoblast differentiation leads to a dramatic switch in the expression of pyruvate kinase isoforms, mediated by RNA-binding proteins, from the pro-glycolytic PKM2 to the pro-OxPhos PKM1 (Figure 5.8A-B; Clower et al., 2010; David et al., 2010). In fact, myoblasts require

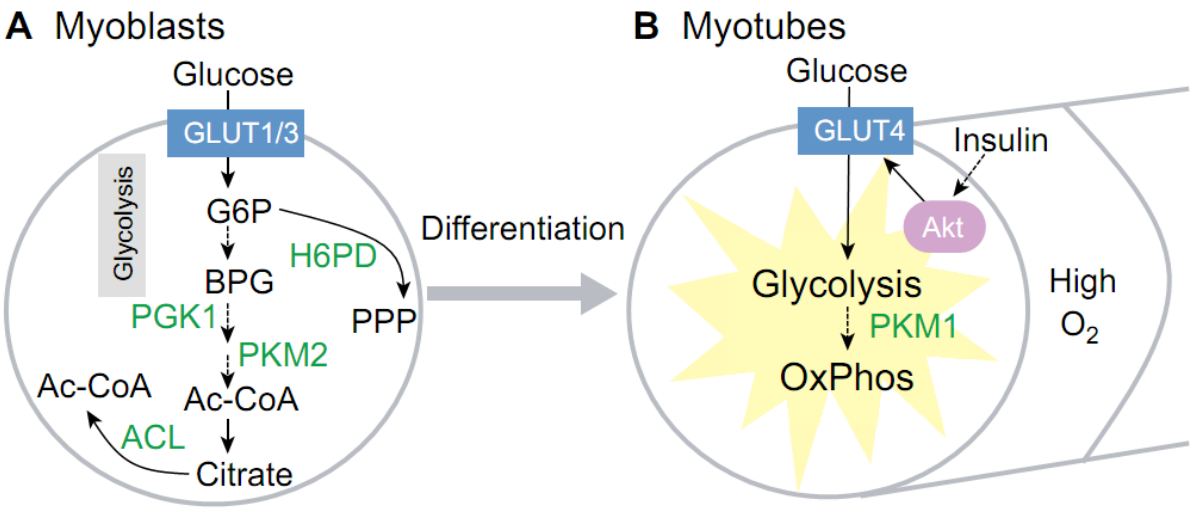


***Figure 5.8: Metabolism in skeletal myoblasts and myotubes.*** (**A**) Myoblasts utilize GLUT1 and GLUT3 for glucose uptake. Glycolysis mediated by PGK1 is necessary for myoblast self-renewal. The low activity pyruvate kinase isoform M2 (PKM2) then facilitates accumulation of glycolytic intermediates for anabolic metabolism in myoblasts. For example the pentose phosphate pathway (PPP), mediated by hexose-6-phosphate dehydrogenase (H6PD), shunts glucose-6-phosphate (G6P) into ribose and NADPH synthesis. ACL, which generates acetyl-CoA from citrate, is also necessary for myoblast self-renewal. (**B**) Upon cell fusion and differentiation into myotubes, glucose uptake and glycolysis are increased by GLUT4, which is sensitive to regulation by insulin-PI3K-Akt signaling. Mitochondrial OxPhos increases as well, partly due to the switch to the high activity pyruvate kinase isoform M1 (PKM1).

glycolytic phosphoglycerate kinase-1 (PGK1) for self-renewal (Bracha et al., 2010). Hexose-6-phosphate dehydrogenase (H6PD) in the pentose phosphate pathway, and

ACL-driven acetyl-CoA synthesis also appear to be required for myoblast self-renewal in vitro (Bracha et al., 2010).

*Cardiomyocyte progenitors*

In the fetal heart, cardiomyocyte progenitors prefer to use lactate to fuel OxPhos (Werner and Sicard, 1987). Knowledge of these metabolic features has aided the efficient derivation of cardiomyocytes from ESCs and iPSCs during directed differentiation. Lactate media without glucose effectively eliminates human ESCs and iPSCs from differentiating embryoid bodies, while stimulating the rapid proliferation of cardiomyocyte progenitors. The resultant human cardiomyocytes showed physiologically relevant action-potential configurations and drug responses, and can be transplanted without forming tumors (Tohyama et al., 2013). These results demonstrate how understanding stem cell metabolism can lead to effective strategies for directed differentiation and mass production of functional cells and tissues.

**Metabolism and "stemness" factors: establishing a link**

After decades of research in stem cell biology, candidate factors that define "stemness" across the myriad of tissue lineages and stem cells are emerging. One outstanding question in stem cell biology is whether such a stemness factor, if it exists, drives particular cellular functions such as metabolism in a specific manner to maintain stemness. One such candidate factor is Lin28, an RNA-binding protein first identified in *C. elegans* through mutagenesis screens for regulators of developmental timing, or heterochrony (Ambros and Horvitz, 1984; Shyh-Chang and Daley, 2013). In mammals, Lin28a/b have been found to be regulators of pluripotent ESCs and iPSCs, fetal HSCs,

neural crest progenitors, skeletal myoblasts during muscle regeneration, and spermatogonia (Viswanathan et al., 2008; Yu et al., 2007; Yuan et al., 2012; Molenaar et al., 2012; Polesskaya et al., 2007; Zheng et al., 2009). Interestingly, Lin28a/b regulate glucose metabolism in vivo by modulating insulin-PI3K-mTOR signaling via the *let-7* microRNA (Zhu et al., 2011). Furthermore, transcripts encoding glycolysis and mitochondrial enzymes are amongst the top mRNA targets directly bound by Lin28a in human ESCs (Peng et al., 2011). These findings suggest that the effects of Lin28 on stem/progenitor cell self-renewal across multiple lineages might be mediated in part by metabolic programming – a hypothesis that awaits testing.

**Stem cell metabolism and aging**

Several lines of evidence support the notion that enhanced tissue regeneration by adult stem cells can delay aging, whereas a decline in adult stem cell numbers and function drives aging-related syndromes (Sahin and DePinho, 2010). Accumulating damage from ROS, for example, can compromise stem cell self-renewal and promote aging (Rossi et al., 2008; Sahin and DePinho, 2010). Nutrient-sensitive signaling pathways that regulate organismal aging, such as the insulin-PI3K, Akt-FoxO, mTOR, and AMPK pathways, also regulate the balance between quiescence and proliferation of stem cells during aging (Chen et al., 2009; Jasper and Jones, 2010; Kharas et al., 2010; Kalaitzidis et al., 2012; Magee et al., 2012). As one example of the cross-talk between nutrient-sensitive signaling and ROS in mammals, deficiency in the FoxO transcription factors dampens the oxidative stress response and depletes mouse LT-HSCs (Tothova et al., 2007). Likewise, deletion of the AMPK regulator LKB1 leads to loss of mouse LT-HSC quiescence, depletion of LT-HSC pools, and impaired hematopoiesis, likely due to

mitochondrial defects (Gan et al., 2010; Gurumurthy et al., 2010; Nakada et al., 2010). The mTOR signaling pathway also plays a major role in governing stem cell fate. For example, deletion of the metabolic sensor TSC1, which upregulates mTORC1 signaling, drives mouse LT-HSCs into proliferation due to increased mitochondrial biogenesis, ultimately depleting the LT-HSCs and impairing hematopoiesis (Chen et al., 2008b). Consistently, mTORC1 inhibition with rapamycin delays mouse LT-HSC aging by preserving adult LT-HSC self-renewal and hematopoietic capacity (Chen et al., 2009). Excessive mTOR signaling also leads to adult epidermal stem cell exhaustion and progressive hair loss in mice – a phenomenon that rapamycin can delay (Castilho et al., 2009). Perhaps more strikingly, rapamycin treatment late in adulthood can extend organismal longevity in mice (Harrison et al., 2009). These mechanisms appear to be well-conserved in *Drosophila* too, since insulin-PI3K signaling also regulates the proliferative capacity of fruit fly hematopoietic progenitors (Shim et al., 2012), neuroblasts (Chell and Brand, 2010; Sousa-Nunes et al., 2011), intestinal stem cells (ISCs; Biteau et al., 2010; Choi et al., 2011; O'Brien et al., 2011), and germline stem cells (GSCs; McLeod et al., 2010). Thus, metabolic signaling pathways that regulate aging might do so via stem cell metabolism, by acting as nutrient-sensors that modulate regenerative capacity during aging (Figure 5.5C).

*Drosophila* models of ISCs provide strong evidence that efficient oxidative metabolism can enhance stem cell self-renewal during aging and contribute to organismal longevity. One example is the demonstration that intestine-specific upregulation of the *Drosophila* PGC-1 homolog (*dPGC-1/spargel*), a master regulator of mitochondrial biogenesis, can delay ISC aging and the consequent accumulation of mis-differentiated cells during

aging by enhancing the efficiency of OxPhos. Moreover, *dPGC-1* upregulation in ISCs improves intestinal integrity and extends adult organismal longevity in old flies (Rera et al., 2011). In the same vein, it is well-known that redox balance regulates ISC proliferation. In the *Drosophila* intestine, high levels of ROS are produced by enterocytes to control bacterial populations. ISCs respond to this oxidative stress by proliferating, as part of a regenerative response. But over time, this can lead to hyperproliferation, stem cell exhaustion and epithelial degeneration in the aging animal. In fact, ROS-induced hyperproliferation can be prevented with antioxidants (Hochmuth et al., 2011). Moreover, organismal longevity can be increased upon gain-of-function of *NRF2* or its *C. elegans* homolog *SKN1*, master regulators of the oxidative stress response (Hochmuth et al., 2011). In contrast, tissue-specific loss of *NRF2* in ISCs causes accumulation of ROS and accelerates aging-related degeneration of the intestine (Hochmuth et al., 2011). Interestingly, loss of the NRF2 regulator, KEAP1, leads to hyperkeratosis in the gastrointestinal tract in mice (Wakabayashi et al., 2003), suggesting that NRF2 might also control ISC proliferation and aging in mammals.

Although very little is known regarding GSC metabolism, GSC proliferation is known to be regulated by the availability of various nutrients. GSCs in the *Drosophila* ovary adjust their proliferation rates to nutritional conditions (Drummond-Barbosa and Spradling, 2001), and the nutrient-sensitive insulin/IGF1 and TOR signaling pathways are required for this response (LaFever and Drummond-Barbosa, 2005; Hsu et al., 2008; Ueishi et al., 2009; LaFever et al., 2010). Given that studies in *C. elegans* have shown GSCs regulate *C. elegans* longevity (Arantes-Oliveira et al. 2002; Wang et al., 2008), it will be

interesting to see if GSC metabolism plays a role in regulating *C. elegans* and mammalian longevity.

Calorie restriction might also promote longevity in part by promoting the self-renewal of stem cells. Calorie restriction not only extends longevity but also prolongs the health of organisms, ranging from worms and flies to rodents and primates, by improving metabolic homeostasis and decreasing the incidence of degenerative diseases and cancer (Barger et al., 2003). However, the detailed mechanisms underlying the benefits of calorie restriction in specific tissues had remained unclear until recently. In *Drosophila*, calorie restriction conditions that extend longevity also delay the loss of male GSCs over the course of aging (Mair et al., 2010). In mammalian muscles, calorie restriction boosts the number and myogenic function of skeletal satellite cells, by increasing mitochondrial biogenesis and enhancing OxPhos (Cerletti et al., 2012). In fact, the pro-myogenic effect of calorie restriction can be recapitulated in vitro by replacing glucose in satellite cell media with galactose to force the use of fatty acid oxidation and OxPhos. In the intestinal villus crypts, calorie restriction leads to upregulation of cyclic ADP-ribose (cADPR) signaling in the intestinal niche Paneth cells by inhibiting mTOR signaling. As a result, cADPR signaling induces the proliferation of $Lgr5^{+}$ ISCs during calorie restriction (Yilmaz et al., 2012). Thus, calorie restriction can lead to complex effects in niche and stem cells to promote stem cell function and counteract aging-related degeneration.

## Conclusion

By the end of the 20th century, early seminal discoveries of metabolism in early embryos led to the perfection of techniques in blastocyst culture and IVF. More recent insights into the metabolism in human ESCs have also led to rapid advances in chemically-defined conditions for human ESC culture, iPSC reprogramming, and their use in human disease models. As we move forward, a deeper understanding of human stem and progenitor cell metabolism could lead to similar breakthroughs in our efforts to define conditions to culture functional human tissues in vitro via directed differentiation of human ESCs. Furthermore, it is clear that our understanding of stem cell metabolism could also be useful in fighting aging-related degeneration in patients. Studies of metabolism in stem cells thus harbor enormous potential for the field of regenerative medicine. One recent example is the mass production of functional human cardiomyocytes from human ESCs achieved by changing the primary carbon source in growth media from glucose to lactate (Tohoyama et al. 2012), thus yielding a source of cells that could help treat degenerative heart diseases in the future. But progress is slow elsewhere. Much remains unclear about metabolism in quiescent adult stem cells. This gap in our knowledge represents a critical barrier in our ability to grow, study, and utilize adult stem cells ex vivo, and to derive transplantable adult stem cells from human ESCs. A case in point is that highly desired methods for long-term culture and expansion of LT-HSCs do not yet exist. Similarly, much remains unknown about the metabolic requirements of various adult progenitor cells and their differentiated progeny, such that we are still unable to properly differentiate many adult stem and progenitor cells into fully functional, terminally differentiated cells that we can grow or maintain in

vitro (Lyssiotis et al., 2011; Lairson et al., 2013). Although the traditional focus in this regard has been on growth factors and transcription factors, it would be critical to discover the necessary metabolic conditions as well. In fact, optimal metabolic conditions need not just be permissive for the directed differentiation of cells, but could also serve as instructive regulatory signals (see Box 1). Drugs could even be developed to pharmacologically manipulate the relevant enzymes, which have historically proven to be one of the most druggable classes of proteins in humans.

To achieve these goals, further advances in metabolomic technologies might be necessary. Much of the extant literature on stem cell metabolism is based on steady-state measurements of lysed cells. Given the rapid kinetics of metabolic reactions, it will be critical to measure metabolic fluxes inside cells. Isotope-tracing methods in gas or liquid chromatography mass spectrometry (GC-MS or LC-MS) represent the state-of-the-art in this area with their high levels of sensitivity, but still suffer from the inability to track real-time changes in vivo. Nuclear magnetic resonance (NMR) detection methods could potentially overcome this barrier, but they currently show poorer sensitivity compared to mass spectrometry. Another important barrier to advances in stem cell metabolism is the current lack of reliable methods for metabolomic profiling at a single-cell level. Current methods are limited to single fluorescent reporters of a few metabolic indicators, such as the ATP/AMP ratio, the NADH/NAD ratio, or ROS abundance, instead of the hundreds of metabolites measurable by metabolomics. In addition, the intercellular metabolism and subcellular metabolism of stem cell niches in vivo also await further exploration. Therefore, we emphasize the need to explore beyond the

current paradigm of in vitro stem cell metabolism to one that also encompasses the real-time changing metabolic needs of stem cells in vivo.

**Box 1: Metabolic regulation of epigenetics during stem/progenitor cell differentiation**

Acetyl-CoA, besides being a Krebs cycle substrate, is important for protein acetylation (Choudhary et al. 2009; Kaelin and McKnight, 2013) - which is known to impact protein function and gene expression. In particular, histone H3 acetylation leads to an open euchromatin conformation that regulates gene expression in stem cells. Reduction of acetyl-CoA by knockdown of ATP citrate lyase (ACL, the enzyme responsible for acetyl-CoA synthesis) induces myoblast differentiation (Bracha et al., 2010), whereas inhibition of histone deacetylases promotes iPSC reprogramming (Huangfu et al., 2008). In addition, glycolysis fuels the rise in acetyl-CoA and histone acetylation required for pre-adipocyte differentiation (Wellen et al., 2009).

Akin to the role of acetyl-CoA in histone acetylation, S-adenosylmethionine (SAM) is critical for histone methylation (Shyh-Chang et al., 2013). Like histone acetylation, histone H3K4 di- or tri-methylation leads to euchromatin formation. Reduction in the ratio of SAM to S-adenosylhomocysteine (SAH), induced by the SAH hydrolase inhibitor DZA, leads to rapid loss of H3K4 tri-methylation in ESCs and causes ESCs to differentiate and die (Shyh-Chang et al., 2013). Thr-Gly-Ser metabolism was shown to fuel SAM synthesis in mouse ESCs, thus maintaining the high levels of H3K4 tri-methylation critical to mouse ESC pluripotency and reprogramming. This demonstrates that changes in amino acid metabolism can regulate histone methylation via SAM, thereby influencing epigenetic control of stem cell fate (Shyh-Chang et al., 2013).

The Krebs cycle intermediate α-ketoglutarate (αKG) is also an important cofactor for the $Fe^{2+}$-dependent Jumonji (JmjC) family of dioxygenases, which mediate histone demethylation, and the TET family of dioxygenases, which mediate DNA demethylation. Somatic mutations in isocitrate dehydrogenases IDH1/2 lead to reduced αKG, thus disrupting normal histone demethylation and consequently HSC differentiation (Figueroa et al., 2010; Sasaki et al., 2012), as well as pre-adipocyte and neural progenitor differentiation (Lu et al., 2012). This leads to cellular transformation and cancer. Interestingly, another cofactor for $Fe^{2+}$-dependent dioxygenases, ascorbate or vitamin C, has also been shown to improve iPSC reprogramming, thereby promoting DNA and H3K36 demethylation (Chung et al., 2010; Stadtfeld et al., 2012; Wang et al., 2011).

Another tradition among extant metabolic studies is the focus on the carbon and energy source of cells. This focus has led to numerous studies on key common pathways in glucose metabolism, i.e. glycolysis, OxPhos and ROS. However, insufficient attention

has been dedicated to amino acid and lipid metabolism. Recent studies are just beginning to show that Thr-Gly-Ser metabolism is important to the folate pool and SAM/Met metabolism, with implications for nucleotide synthesis during proliferation and histone methylation for epigenetic regulation in stem cells (see Box 1). Acetyl-CoA metabolism is also beginning to emerge as a major regulator of protein (including histone) acetylation to regulate stem cells epigenetically. Furthermore, lipogenesis is emerging as a key pathway that sustains membrane synthesis and proliferation, whereas lipid oxidation via the eicosanoid pathway might generate a diversity of tissue-specific signaling molecules necessary to guide stem cell differentiation. An entire universe of cell- or tissue-specific metabolic pathways might be awaiting future discovery – with the potential to revolutionize regenerative medicine.

**Acknowledgments**

This chapter was published in part in Shyh-Chang, Daley and Cantley (*Development,* 2013c). We thank Costas Lyssiotis, Hao Zhu and the three anonymous reviewers for thoughtful and constructive feedback on our manuscript.

## Bibliography

Abbott, A. L., Alvarez-Saavedra, E., Miska, E. A., Lau, N. C., Bartel, D. P., Horvitz, H. R., and Ambros, V. (2005). The let-7 microRNA family members mir-48, mir-84, and mir-241 function together to regulate developmental timing in Caenorhabditis elegans. Dev. Cell 9, 403–14.

Adams, D. S., Masi, A., and Levin, M. (2007). H+ pump-dependent changes in membrane voltage are an early mechanism necessary and sufficient to induce Xenopus tail regeneration. Development 1335, 1323–1335.

Alexander, P. B., Wang, J. and McKnight, S. L. (2011). Targeted killing of a mammalian cell based upon its specialized metabolic state. Proceedings of the National Academy of Sciences of the United States of America 108, 15828-15833.

Alexander, P. B., Wang, J., and McKnight, S. L. (2011). Targeted killing of a mammalian cell based upon its specialized metabolic state. Proc Natl Acad Sci USA. 108, 15828-33.

Ambros, V. and Horvitz, H. R. (1984). Heterochronic mutants of the nematode Caenorhabditis elegans. Science 226, 409-416.

Anchelin, M., Murcia, L., Alcaraz-Pérez, F., García-Navarro, E. M., and Cayuela, M. L. (2011). Behaviour of telomere and telomerase during aging and regeneration in zebrafish. PloS One 6, e16955.

Anderson, S. P. et al. (2002). Delayed liver regeneration in peroxisome proliferator-activated receptor-α-null mice. Hepatology 36, 544-54.

Ang, Y.-S., Tsai, S.-Y., Lee, D.-F., Monk, J., Su, J., Ratnakumar, K., Ding, J., Ge, Y., Darr, H., Chang, B., et al. (2011). Wdr5 Mediates Self-Renewal and Reprogramming via the Embryonic Stem Cell Core Transcriptional Network. Cell 145, 183-197.

Angione, A. R. et al. (2011). PPARδ regulates satellite cell proliferation and skeletal muscle regeneration. Skelet. Muscle 1, 1-33.

Antebi, A., Culotti, J. G., and Hedgecock, E. M. (1998). Daf-12 regulates developmental age and the dauer alternative in Caenorhabditis elegans. Development 125, 1191–205.

Antebi, A., Yeh, W. H., Tait, D., Hedgecock, E. M., and Riddle, D. L. (2000). Daf-12 encodes a nuclear receptor that regulates the dauer diapause and developmental age in C. elegans. Genes Dev. 14, 1512–27.

Arantes-Oliveira, N., Apfeld, J., Dillin, A. and Kenyon, C. (2002). Regulation of life-span by germ-line stem cells in Caenorhabditis elegans. Science 295, 502-505.

Azuara, V., Perry, P., Sauer, S., Spivakov, M., Jorgensen, H. F., John, R. M., Gouti, M., Casanova, M., Warnes, G., Merkenschlager, M., et al. (2006). Chromatin signatures of pluripotent cell lines. Nature Cell Biology 8, 532-8.

Backlund, P.S. et al., Eur. J. Biochem. 160, 245 (1986)

Balzer, E., and Moss, E. G. (2007). Localization of the developmental timing regulator Lin28 to mRNP complexes, P-bodies and stress granules. RNA Biol. 4, 16–25.

Balzer, E., Heine, C., Jiang, Q., Lee, V. M., and Moss, E. G. (2010). LIN28 alters cell fate succession and acts independently of the let-7 microRNA during neurogliogenesis in vitro. Stem Cells 900, 891–900.

Barbaux, S., Gascoin-Lachambre, G., Buffat, C., Monnier, P., Mondon, F., Tonanny, M. B., Pinard, A., Auer, J., Bessières, B., Barlier, A., et al. (2012). A genome-wide approach reveals novel imprinted genes expressed in the human placenta. Epigenetics 7, 1079-90.

Barbehenn, E. K., Wales, R. G. and Lowry, O. H. (1978). Measurement of metabolites in single pre-implantation embryos. Journal of Embryology and Experimental Morphology 43, 29-46.

Barbieri, M., Rizzo, M. R., Manzella, D., Grella, R., Ragno, E., Carbonella, M., Abbatecola, A. M., and Paolisso, G. (2003). Glucose regulation and oxidative stress in healthy centenarians. Exp. Gerontol. 38, 137–43.

Barger, J. L., Walford, R. L. and Weindruch, R. (2003). The retardation of aging by caloric restriction: its significance in the transgenic era. Experimental Gerontology 38, 1343-1351.

Bartke, A. (2012). Healthy aging: is smaller better? - a mini-review. Gerontology 58, 337–43.

Beachy, S. H., Onozawa, M., Chung, Y. J., Slape, C., Bilke, S., Francis, P., Pineda, M., Walker, R. L., Meltzer, P., and Aplan, P. D. (2012). Enforced expression of Lin28b leads to impaired T-cell development, release of inflammatory cytokines, and peripheral T-cell lymphoma. Blood 120, 1048–59.

Beane, W. S., Morokuma, J., Adams, D. S., and Levin, M. (2011). A Chemical Genetics Approach Reveals H, K-ATPase-Mediated Membrane Voltage Is Required for Planarian Head Regeneration. Chem. Biol. 18, 77–89.

Beard, C., Hochedlinger, K., Plath, K., Wutz, A., and Jaenisch, R. (2006). Efficient method to generate single-copy transgenic mice by site-specific integration in embryonic stem cells. Genesis 44, 23-28.

Benhamed, M., Herbig, U., Ye, T., Dejean, A., and Bischof, O. (2012). Senescence is an endogenous trigger for microRNA-directed transcriptional gene silencing in human cells. Nat. Cell Biol. 14, 266–75.

Berti, L., and Gammeltoft, S. (1999). Leptin stimulates glucose uptake in C2C12 muscle cells by activation of ERK2. Mol Cell Endocrinol 157, 121-130.

Bethke, A., Fielenbach, N., Wang, Z., Mangelsdorf, D. J., and Antebi, A. (2009). Nuclear hormone receptor regulation of microRNAs controls developmental progression. Science 324, 95–98.

Bhat-Nakshatri, P., Wang, G., Collins, N. R., Thomson, M. J., Geistlinger, T. R., Carroll, J. S., Brown, M., Hammond, S., Srour, E. F., Liu, Y., et al. (2009). Estradiol-regulated microRNAs control estradiol response in breast cancer cells. Nucleic Acids Res. 37, 4850–4861.

Biteau, B., Karpac, J., Supoyo, S., Degennaro, M., Lehmann, R. and Jasper, H. (2010). Lifespan extension by preserving proliferative homeostasis in Drosophila. PLoS Genetics 6: e1001159.

Blasco, M. A., Lee, H. W., Hande, M. P., Samper, E., Lansdorp, P. M., DePinho, R. A., and Greider, C. W. (1997). Telomere shortening and tumor formation by mouse cells lacking telomerase RNA. Cell 91, 25–34.

Boehm, M., and Slack, F. (2005). A developmental timing microRNA and its target regulate life span in C. elegans. Science 310, 1954-1957.

Boiko, A. D., Razorenova, O. V., van de Rijn, M., Swetter, S. M., Johnson, D. L., Ly, D. P., Butler, P. D., Yang, G. P., Joshua, B., Kaplan, M. J., et al. (2010). Human melanoma-initiating cells express neural crest nerve growth factor receptor CD271. Nature 466, 133–7.

Bousquet, M., Harris, M. H., Zhou, B., and Lodish, H. F. (2010). MicroRNA miR-125b causes leukemia. Proc Natl Acad Sci USA. 107, 21558-63.

Bousquet, M., Quelen, C., Rosati, R., Mansat-De Mas, V., La Starza, R., Bastard, C., Lippert, E., Talmant, P., Lafage-Pochitaloff, M., Leroux, D., et al. (2008). Myeloid cell differentiation arrest by miR-125b-1 in myelodysplastic syndrome and acute myeloid leukemia with the t(2;11)(p21;q23) translocation. J Exp Med. 205, 2499–506.

Boyerinas, B., Park, S.M., Shomron, N., Hedegaard, M.M., Vinther, J., Andersen, J.S., Feig, C., Xu, J., Burge, C.B., and Peter, M.E. (2008). Identification of let-7-regulated oncofetal genes. Cancer Res 68, 2587-2591.

Bracha, A. L., Ramanathan, A., Huang, S., Ingber, D. E. and Schreiber, S. L. (2010). Carbon metabolism-mediated myogenic differentiation. Nature Chemical Biology 6, 202-204.

Brinster, R. L. (1967). Protein content of the mouse embryo during the first five days of development. Journal of Reproduction and Fertility 13, 413-420.

Brinster, R. L. (1973). Nutrition and metabolism of the ovum, zygote and blastocyst. Greep, Roy O. (Ed.). Handbook of Physiology, Section 7. Endocrinology, Vol. 2. Female Reproductive System. Part 2. V+375p. Illus. American Physiological Society: Washington, D.C., U.S.A., 165-185.

Brinster, R. L. (1974). Embryo development. Journal of Animal Science 38, 1003-1012.

Brinster, R. L. and Troike, D. E. (1979). Requirements for blastocyst development in vitro. Journal of Animal Science 49 Suppl 2, 26-34.

Brody, S.C. et al. FEBS Lett. 408, 217 (1997)

Brugarolas, J.B., Vazquez, F., Reddy, A., Sellers, W.R., and Kaelin, W.G., Jr. (2003). TSC2 regulates VEGF through mTOR-dependent and -independent pathways. Cancer Cell 4, 147-158.

Buganim, Y., Faddah, D. A., Cheng, A. W., Itskovich, E., Markoulaki, S., Ganz, K., Klemm, S. L., van Oudenaarden, A., and Jaenisch, R. (2012). Single-cell expression analyses during cellular reprogramming reveal an early stochastic and a late hierarchic phase. Cell 150, 1209–22.

Buller, C.L., Loberg, R.D., Fan, M.H., Zhu, Q., Park, J.L., Vesely, E., Inoki, K., Guan, K.L., and Brosius, F.C., 3rd (2008). A GSK-3/TSC2/mTOR pathway regulates glucose uptake and GLUT1 glucose transporter expression. Am J Physiol Cell Physiol 295, C836-843.

Cai, L. et al. Mol. Cell 42, 426 (2011)

Cao, D., Allan, R. W., Cheng, L., Peng, Y., Guo, C. C., Dahiya, N., Akhi, S., and Li, J. (2011b). RNA-binding protein LIN28 is a marker for testicular germ cell tumors. Hum. Pathol. 42, 710-8.

Cao, D., Liu, A., Wang, F., Allan, R. W., Mei, K., Peng, Y., Du, J., Guo, S., Abel, T. W., Lane, Z., et al. (2011a). RNA-binding protein LIN28 is a marker for primary extragonadal germ cell tumors: an immunohistochemical study of 131 cases. Mod. Pathol. 24, 288-96.

Castilho, R. M., Squarize, C. H., Chodosh, L. A., Williams, B. O. and Gutkind, J. S. (2009). mTOR Mediates Wnt-Induced Epidermal Stem Cell Exhaustion and Aging. Cell Stem Cell 5, 279-289.

Cerletti, M., Jang, Y. C., Finley, L. W. S., Haigis, M. C. and Wagers, A. J. (2012). Short-Term Calorie Restriction Enhances Skeletal Muscle Stem Cell Function. Cell Stem Cell 10, 515-519.

Chadwick, R. B., Bu, L., Yu, H., Hu, Y., Wergedal, J. E., Mohan, S., and Baylink, D. J. (2007). Digit tip regrowth and differential gene expression in MRL/Mpj, DBA/2, and C57BL/6 mice. Wound Repair Regen. 15, 275–84.

Chalfie, M., Horvitz, H. R., and Sulston, J. E. (1981). Mutations that lead to reiterations in the cell lineages of C. elegans. Cell 24, 59–69.

Chang, H.M., Martinez, N. J., Thornton, J. E., Hagan, J. P., Nguyen, K. D., and Gregory, R. I. (2012). Trim71 cooperates with microRNAs to repress Cdkn1a expression and promote embryonic stem cell proliferation. Nat. Commun. 3, 923.

Chang, T. C., Zeitels, L. R., Hwang, H. W., Chivukula, R. R., Wentzel, E. A., Dews, M., Jung, J., Gao, P., Dang, C. V., Beer, M. A., et al. (2009). Lin-28B transactivation is necessary for Myc-mediated let-7 repression and proliferation. Proc Natl Acad Sci USA. 106, 3384–9.

Chaudhuri, A. A., So, A. Y., Mehta, A., Minisandram, A., Sinha, N., Jonsson, V. D., Rao, D. S., O'Connell, R. M., and Baltimore, D. (2012). Oncomir miR-125b regulates hematopoiesis by targeting the gene Lin28A. Proc Natl Acad Sci USA. 109, 4233–8.

Chawla, G., and Sokol, N. S. (2012). Hormonal activation of let-7-C microRNAs via EcR is required for adult Drosophila melanogaster morphology and function. Development 139, 1788–1797.

Chell, J. M. and Brand, A. H. (2010). Nutrition-responsive glia control exit of neural stem cells from quiescence. Cell 23, 1161-73.

Chen, C.-T., Shih, Y.-R. V., Kuo, T. K., Lee, O. K. and Wei, Y.-H. (2008a). Coordinated changes of mitochondrial biogenesis and antioxidant enzymes during osteogenic differentiation of human mesenchymal stem cells. Stem Cells 26, 960-968.

Chen, C., Liu, Y., Liu, R., Ikenoue, T., Guan, K. L., Liu, Y. and Zheng, P. (2008b). TSC-mTOR maintains quiescence and function of hematopoietic stem cells by repressing mitochondrial biogenesis and reactive oxygen species. Journal of Experimental Medicine 205, 2397-408

Chen, C., Liu, Y., Liu, Y. and Zheng, P. (2009). mTOR regulation and therapeutic rejuvenation of aging hematopoietic stem cells. Science Signaling 2, ra75

Chiefari, E., Tanyolaç, S., Paonessa, F., Pullinger, C. R., Capula, C., Iiritano, S., Mazza, T., Forlin, M., Fusco, A., Durlach, V., et al. (2011). Functional variants of the HMGA1 gene and type 2 diabetes mellitus. JAMA 305, 903–12.

Cho, J., Chang, H., Kwon, S. C., Kim, B., Kim, Y., Choe, J., Ha, M., Kim, Y. K., and Kim, V. N. (2012). LIN28A Is a Suppressor of ER-Associated Translation in Embryonic Stem Cells. Cell 151, 765-77.

Cho, Y. M., Kwon, S., Pak, Y. K., Seol, H. W., Choi, Y. M., Park, D. J., Park, K. S. and Lee, H. K. (2006). Dynamic changes in mitochondrial biogenesis and antioxidant enzymes during the spontaneous differentiation of human embryonic stem cells. Biochemical and Biophysical Research Communications 348, 1472-1478.

Choi, N. H., Lucchetta, E. and Ohlstein, B. (2011). Nonautonomous regulation of Drosophila midgut stem cell proliferation by the insulin-signaling pathway. Proceedings of the National Academy of Sciences of the United States of America 108, 18702-7.

Choudhary, C., Kumar, C., Gnad, F., Nielsen, M. L., Rehman, M., Walther, T. C., Olsen, J. V. and Mann, M. (2009). Lysine Acetylation Targets Protein Complexes and Co-Regulates Major Cellular Functions. Science 325, 834-840.

Chung, S., Dzeja, P. P., Faustino, R. S., Perez-Terzic, C., Behfar, A. and Terzic, A. (2007). Mitochondrial oxidative metabolism is required for the cardiac differentiation of stem cells. Nature Clinical Practice Cardiovascular medicine 4 Suppl 1, S60-67.

Chung, T.-L., Brena, R. M., Kolle, G., Grimmond, S. M., Berman, B. P., Laird, P. W., Pera, M. F. and Wolvetang, E. J. (2010). Vitamin C Promotes Widespread Yet Specific DNA Demethylation of the Epigenome in Human Embryonic Stem Cells. Stem Cells 28, 1848-1855.

Clark, L. D., Clark, R. K., and Heber-Katz, E (1998). A new murine model for mammalian wound repair and regeneration. Clin. Immunol. Immunopathol. 88, 35–45.

Clower, C. V., Chatterjee, D., Wang, Z., Cantley, L. C., Vander Heiden, M. G. and Krainer, A. R. (2010). The alternative splicing repressors hnRNP A1/A2 and PTB influence pyruvate kinase isoform expression and cell metabolism. Proceedings of the National Academy of Sciences of the United States of America 107, 1894-9.

Conboy, I. M., Conboy, M. J., Wagers, A. J., Girma, E. R., Weissman, I. L., and Rando, T. a (2005). Rejuvenation of aged progenitor cells by exposure to a young systemic environment. Nature 433, 760–4.

Cox, J. L., Mallanna, S. K., Luo, X., and Rizzino, A. (2010). Sox2 uses multiple domains to associate with proteins present in Sox2-protein complexes. PloS One 5, e15486.

Dang, C. V. (2011). Therapeutic targeting of Myc-reprogrammed cancer cell metabolism. Cold Spring Harb Symp Quant Biol. 76, 369-74.

Darwin, C. (1887). The Variation of Animals and Plants Under Domestication (Forgotten Books Classic Reprint Series).

David, C. J., Chen, M., Assanah, M., Canoll, P. and Manley, J. L. (2010). HnRNP proteins controlled by c-Myc deregulate pyruvate kinase mRNA splicing in cancer. Nature 463, 364-8.

Deal, R.B., Henikoff, J. G. and Henikoff, S. (2010). Genome-Wide Kinetics of Nucleosome Turnover Determined by Metabolic Labeling of Histones. Science 328, 1161-4.

Denko, N.C. (2008). Hypoxia, HIF1 and glucose metabolism in the solid tumour. Nat Rev Cancer 8, 705-713.

Deuchar, B. E. M. (1976). Regeneration of amputated limb-buds in early rat embryos. J. Embryol. Exp. Morphol. 35, 345–354.

Diskin, S. J., Capasso, M., Schnepp, R. W., Cole, K. A., Attiyeh, E. F., Hou, C., Diamond, M., Carpenter, E. L., Winter, C., Lee, H., et al. (2012). Common variation at 6q16 within HACE1 and LIN28B influences susceptibility to neuroblastoma. Nat. Genet. 44, 1126–30.

Drummond-Barbosa, D. and Spradling, A. C. (2001). Stem cells and their progeny respond to nutritional changes during Drosophila oogenesis. Developmental Biology 231, 265-278.

Dupuis, J., Langenberg, C., Prokopenko, I., Saxena, R., Soranzo, N., Jackson, A.U., Wheeler, E., Glazer, N.L., Bouatia-Naji, N., Gloyn, A.L., et al. New genetic loci implicated in fasting glucose homeostasis and their impact on type 2 diabetes risk. Nat Genet 42, 105-116.

Duvel, K., Yecies, J.L., Menon, S., Raman, P., Lipovsky, A.I., Souza, A.L., Triantafellow, E., Ma, Q., Gorski, R., Cleaver, S., et al. Activation of a metabolic gene regulatory network downstream of mTOR complex 1. Mol Cell 39, 171-183.

Edgar, A.J. BMC Genet. 3, 18 (2002)

Engelman, J.A., Luo, J., and Cantley, L.C. (2006). The evolution of phosphatidylinositol 3-kinases as regulators of growth and metabolism. Nat Rev Genet 7, 606-619.

Facucho-Oliveira, J. M., Alderson, J., Spikings, E. C., Egginton, S. and John, J. C. S. (2007). Mitochondrial DNA replication during differentiation of murine embryonic stem cells. Journal of Cell Science 120, 4025-4034.

Federzoni, E. A., Valk, P. J. M., Torbett, B. E., Haferlach, T., Lowenberg, B., Fey, M. F. and Tschan, M. P. (2012). PU.1 is linking the glycolytic enzyme HK3 in neutrophil differentiation and survival of APL cells. Blood 119, 4963-4970.

Feng, B., Jiang, J., Kraus, P., Ng, J. H., Heng, J. C., Chan, Y. S., Yaw, L. P., Zhang, W., Loh, Y. H., Han, J., et al. (2009). Reprogramming of fibroblasts into induced pluripotent stem cells with orphan nuclear receptor Esrrb. Nat. Cell Biol. 11, 197–203.

Figueroa, M. E., Abdel-Wahab, O., Lu, C., Ward, P. S., Patel, J., Shih, A., Li, Y., Bhagwat, N., Vasanthakumar, A., Fernandez, H. F., et al. (2010). Leukemic IDH1 and

IDH2 Mutations Result in a Hypermethylation Phenotype, Disrupt TET2 Function, and Impair Hematopoietic Differentiation. Cancer Cell 18, 553-567.

Filosa, S., Fico, A., Paglialunga, F., Balestrieri, M., Crooke, A., Verde, P., Abrescia, P., Bautista, J. M. and Martini, G. (2003). Failure to increase glucose consumption through the pentose-phosphate pathway results in the death of glucose-6-phosphate dehydrogenase gene-deleted mouse embryonic stem cells subjected to oxidative stress. Biochemical Journal 370, 935-943.

Folmes, C. D. L., Nelson, T. J., Martinez-Fernandez, A., Arrell, D. K., Lindor, J. Z., Dzeja, P. P., Ikeda, Y., Perez-Terzic, C. and Terzic, A. (2011). Somatic Oxidative Bioenergetics Transitions into Pluripotency-Dependent Glycolysis to Facilitate Nuclear Reprogramming. Cell Metabolism 14, 264-271.

Frost, R. J. A., and Olson, Eric N (2011). Control of glucose homeostasis and insulin sensitivity by the Let-7 family of miRNAs. Proc. Natl. Acad. Sci. USA 108, 21075-80.

Gan, B., Hu, J., Jiang, S., Liu, Y., Sahin, E., Zhuang, L., Fletcher-Sananikone, E., Colla, S., Wang, Y. A., Chin, L., et al. (2010). Lkb1 regulates quiescence and metabolic homeostasis of haematopoietic stem cells. Nature 468, 701-4.

Gao, P., Tchernyshyov, I., Chang, T.C., Lee, Y.S., Kita, K., Ochi, T., Zeller, K.I., De Marzo, A.M., Van Eyk, J.E., Mendell, J.T., et al. (2009). c-Myc suppression of miR-23a/b enhances mitochondrial glutaminase expression and glutamine metabolism. Nature 458, 762-765.

Gaspar-Maia, A., Alajem, A., Meshorer, E. and Ramalho-Santos, M. (2011). Open chromatin in pluripotency and reprogramming. Nature Reviews Molecular Cell Biology 12, 36-47.

Ge, Y., Sun, Y., and Chen, J. (2011). IGF-II is regulated by microRNA-125b in skeletal myogenesis. J. Cell Biol. 192, 69–81.

Gehrke, S., Imai, Y., Sokol, N., and Lu, B. (2010). Pathogenic LRRK2 negatively regulates microRNA-mediated translational repression. Nature 466, 637–41.

Gerisch, B., Rottiers, V., Li, D., Motola, D. L., Cummins, C. L., Lehrach, H., Mangelsdorf, D. J., and Antebi, A. (2007). A bile acid-like steroid modulates Caenorhabditis elegans lifespan through nuclear receptor signaling. Proc Natl Acad Sci USA. 104, 5014–9.

Gershon, T. R., Crowther, A. J., Tikunov, A., Garcia, I., Annis, R., Yuan, H., Miller, C. R., MacDonald, J., Olson, J. and Deshmukh, M. (2013). Hexokinase-2-mediated aerobic glycolysis is integral to cerebellar neurogenesis and pathogenesis of medulloblastoma. Cancer and Metabolism 1:2.

Gillis, A. J., Stoop, H., Biermann, K., van Gurp, R. J., Swartzman, E., Cribbes, S., Ferlinz, A., Shannon, M., Oosterhuis, J. W., and Looijenga, L. H. (2011). Expression

and interdependencies of pluripotency factors LIN28, OCT3/4, NANOG and SOX2 in human testicular germ cells and tumours of the testis. Int. J. Androl. 34, e160-74.

Goessling, W., North, T. E., Loewer, S., Lord, A. M., Lee, S., Stoick-Cooper, C. L., Weidinger, G., Puder, M., Daley, G. Q., Moon, R. T., et al. (2009). Genetic Interaction of PGE2 and Wnt Signaling Regulates Developmental Specification of Stem Cells and Regeneration. Cell 136, 1136-1147.

Golipour, A., David, L., Liu, Y., Jayakumaran, G., Hirsch, C. L., Trcka, D., and Wrana, J. L. (2012). A late transition in somatic cell reprogramming requires regulators distinct from the pluripotency network. Cell Stem Cell. 11, 769-82.

Goss, R. J. (1992). The evolution of regeneration: adaptive or inherent? J. Theor. Biol. 159, 241–60.

Goss, R. J., and Grimes, L. N. (1975). Epidermal downgrowths in regenerating rabbit ear holes. J. Morphol. 146, 533–42.

Gourevitch, D. L., Clark, L., Bedelbaeva, K., Leferovich, J., and Heber-Katz, Ellen (2009). Dynamic changes after murine digit amputation: the MRL mouse digit shows waves of tissue remodeling, growth, and apoptosis. Wound Repair Regen. 17, 447–55.

Graves, C. N. and Biggers, J. D. (1970). Carbon dioxide fixation by preimplantation mouse embryos. Science 167, 1506-1507.

Grimson, A., Farh, K.K., Johnston, W.K., Garrett-Engele, P., Lim, L.P., and Bartel, D.P. (2007). MicroRNA targeting specificity in mammals: determinants beyond seed pairing. Mol Cell 27, 91-105.

Guertin, D.A., and Sabatini, D.M. (2007). Defining the role of mTOR in cancer. Cancer Cell 12, 9-22.

Guilletdeniau, I., Leturque, A. and Girard, J. (1994). Expression and cellular-localization of glucose transporters (GLUT1, GLUT3, GLUT4) during differentiation of myogenic cells isolated from rat fetuses. Journal of Cell Science 107, 487-496.

Guo, G., and Smith, A. (2010). A genome-wide screen in EpiSCs identifies Nr5a nuclear receptors as potent inducers of ground state pluripotency. Development 137, 3185–92.

Guo, S. and DiPietro, L. A. (2010). Factors Affecting Wound Healing. J Dent Res. 89, 219–229.

Guo, S., Lu, J., Schlanger, R., Zhang, H., Wang, J. Y., Fox, M. C., Purton, L. E., Fleming, H. H., Cobb, B., Merkenschlager, M., et al. (2010). MicroRNA miR-125a controls hematopoietic stem cell number. Proc Natl Acad Sci USA 107, 14229-34.

Guo, Y., Chen, Y., Ito, H., Watanabe, A., Ge, X., Kodama, T., and Aburatani, H. (2006). Identification and characterization of lin-28 homolog B (LIN28B) in human hepatocellular carcinoma. Gene 384, 51–61.

Gurumurthy, S., Xie, S. Z., Alagesan, B., Kim, J., Yusuf, R. Z., Saez, B., Tzatsos, A., Ozsolak, F., Milos, P., Ferrari, F., et al. (2010). The Lkb1 metabolic sensor maintains haematopoietic stem cell survival. Nature 468, 659-63.

Hafner, M., Max, K. E., Bandaru, P., Morozov, P., Gerstberger, S., Brown, M., Molina, H., and Tuschl, T. (2013). Identification of mRNAs bound and regulated by human LIN28 proteins and molecular requirements for RNA recognition. RNA, Epub ahead of print.

Hagan, J. P., Piskounova, E., and Gregory, R. I. (2009). Lin28 recruits the TUTase Zcchc11 to inhibit let-7 maturation in mouse embryonic stem cells. Nat. Struct. Mol. Biol. 16, 1021–5.

Hammell, C. M., Karp, X., and Ambros, V. (2009). A feedback circuit involving let-7-family miRNAs and DAF-12 integrates environmental signals and developmental timing in Caenorhabditis elegans. Proc Natl Acad Sci USA. 106, 18668–73.

Hanna, J., Saha, K., Pando, B., van Zon, J., Lengner, C. J., Creyghton, M. P., van Oudenaarden, A. and Jaenisch, R. (2009). Direct cell reprogramming is a stochastic process amenable to acceleration. Nature 462, 595-601.

Hansson, J., Rafiee, M. R., Reiland, S., Polo, J. M., Gehring, J., Okawa, S., Huber, W., Hochedlinger, K. and Krijgsveld, J. (2012). Highly Coordinated Proteome Dynamics during Reprogramming of Somatic Cells to Pluripotency. Cell Reports 2, 1579-1592.

Harrington, L.S., Findlay, G.M., Gray, A., Tolkacheva, T., Wigfield, S., Rebholz, H., Barnett, J., Leslie, N.R., Cheng, S., Shepherd, P.R., et al. (2004). The TSC1-2 tumor suppressor controls insulin-PI3K signaling via regulation of IRS proteins. J Cell Biol 166, 213-223.

Harrison, D. E., Strong, R., Sharp, Z. D., Nelson, J. F., Astle, C. M., Flurkey, K., Nadon, N. L., Wilkinson, J. E., Frenkel, K., Carter, C. S., et al. (2009). Rapamycin fed late in life extends lifespan in genetically heterogeneous mice. Nature 460, 392-5.

Hatley, M.E., Patrick, D.M., Garcia, M.R., Richardson, J.A., Bassel-Duby, R., van Rooij, E., and Olson, E.N. Modulation of K-Ras-dependent lung tumorigenesis by MicroRNA-21. Cancer Cell 18, 282-293.

Heiden, M. G. Vander, Cantley, L. C., and Thompson, C. B. (2009). Understanding the Warburg effect: the metabolic requirements of cell proliferation. Science 324, 1029–33.

Heng, J. C., Feng, B., Han, J., Jiang, J., Kraus, P., Ng, J. H., Orlov, Y. L., Huss, M., Yang, L., Lufkin, T., et al. (2010). The nuclear receptor Nr5a2 can replace Oct4 in the reprogramming of murine somatic cells to pluripotent cells. Cell Stem Cell 6, 167–74.

Heo, I., Ha, M., Lim, J., Yoon, M. J., Park, J. E., Kwon, S. C., Chang, H., and Kim, V. N. (2012). Mono-uridylation of pre-microRNA as a key step in the biogenesis of group II let-7 microRNAs. Cell 151, 521–32.

Heo, I., Joo, C., Cho, J., Ha, M., Han, J., and Kim, V. N. (2008). Lin28 mediates the terminal uridylation of let-7 precursor MiRNA. Mol. Cell 32, 276–84.

Heo, I., Joo, C., Kim, Y.-K., Ha, M., Yoon, M.-J., Cho, J., Yeom, K.-H., Han, Jinju, and Kim, V. N. (2009). TUT4 in concert with Lin28 suppresses microRNA biogenesis through pre-microRNA uridylation. Cell 138, 696–708.

Hochmuth, C. E., Biteau, B., Bohmann, D. and Jasper, H. (2011). Redox Regulation by Keap1 and Nrf2 Controls Intestinal Stem Cell Proliferation in Drosophila. Cell Stem Cell 8, 188-199.

Horvitz, H. R., and Sulston, J. E. (1980). Isolation and genetic characterization of cell-lineage mutants of the nematode Caenorhabditis elegans. Genetics 96, 435-54.

Hsu, H.-J., LaFever, L. and Drummond-Barbosa, D. (2008). Diet controls normal and tumorous germline stem cells via insulin-dependent and -independent mechanisms in Drosophila. Developmental Biology 313, 700-712.

Huangfu, D., Maehr, R., Guo, W., Eijkelenboom, A., Snitow, M., Chen, A. E. and Melton, D. A. (2008). Induction of pluripotent stem cells by defined factors is greatly improved by small-molecule compounds. Nature Biotechnology 26, 795-797.

Hyun, S., Lee, J.H., Jin, H., Nam, J., Namkoong, B., Lee, G., Chung, J., and Kim, V.N. (2009). Conserved MicroRNA miR-8/miR-200 and its target USH/FOG2 control growth by regulating PI3K. Cell 139, 1096-1108.

Iliopoulos, D., Hirsch, H. a, and Struhl, K. (2009). An epigenetic switch involving NF-kappaB, Lin28, Let-7 microRNA, and IL6 links inflammation to cell transformation. Cell 139, 693–706.

Ishizawa, K., Rasheed, Z. A., Karisch, R., Wang, Q., Kowalski, J., Susky, E., Pereira, K., Karamboulas, C., Moghal, N., Rajeshkumar, N. V., et al. (2010). Tumor-initiating cells are rare in many human tumors. Cell Stem Cell 7, 279–282.

Ito, K., Carracedo, A., Weiss, D., Arai, F., Ala, U., Avigan, D. E., Schafer, Z. T., Evans, R. M., Suda, T., Lee, C.-H., et al. (2012). A PML-PPAR-delta pathway for fatty acid oxidation regulates hematopoietic stem cell maintenance. Nature Medicine 18, 1350-8.

Iwabata, H. et al. Proteomics. 5, 4653 (2005)

Jain, M. et al. Science 336, 1040 (2012)

Jain, M., Nilsson, R., Sharma, S., Madhusudhan, N., Kitami, T., Souza, A. L., Kafri, R., Kirschner, M. W., Clish, C. B., and Mootha V. K. (2012). Metabolite profiling identifies a key role for glycine in rapid cancer cell proliferation. Science 336, 1040–4.

Janiszewska, M., Suvà, M. L., Riggi, N., Houtkooper, R. H., Radovanovic, I., Rheinbay, E., Auwerx, J., and Cle, V. (2012). Imp2 controls oxidative phosphorylation and is crucial for preserving glioblastoma cancer stem cells. Genes Dev. 26, 1926-44.

Janzen, V. et al. (2006). Stem-cell ageing modified by the cyclin-dependent kinase inhibitor p16INK4a. Nature 443, 421–6.

Jasper, H. and Jones, D. L. (2010). Metabolic Regulation of Stem Cell Behavior and Implications for Aging. Cell Metabolism 12, 561-565.

Jiang, X., Huang, H., Li, Z., Li, Y., Wang, X., Gurbuxani, S., Chen, P., He, C., You, D., Zhang, S., et al. (2012). Blockade of miR-150 maturation by MLL-fusion/MYC/LIN-28 is required for MLL-associated leukemia. Cancer Cell 22, 524–35.

Jin, J., Jing, W., Lei, X. X., Feng, C., Peng, S., Boris-Lawrie, K., and Huang, Y. (2011). Evidence that Lin28 stimulates translation by recruiting RNA helicase A to polysomes. Nucleic Acids Res. 39, 3724–34.

Johnson, M. T., Yang, H. S., Magnuson, T. and Patel, M. S. (1997). Targeted disruption of the murine dihydrolipoamide dehydrogenase gene (Dld) results in perigastrulation lethality. Proceedings of the National Academy of Sciences of the United States of America 94, 14512-14517.

Johnson, M. T., Mahmood, S., Hyatt, S. L., Yang, H. S., Soloway, P. D., Hanson, R. W. and Patel, M. S. (2001). Inactivation of the murine pyruvate dehydrogenase (Pdha1) gene and its effect on early embryonic development. Molecular Genetics and Metabolism 74, 293-302.

Johnson, M. T., Mahmood, S. and Patel, M. S. (2003a). Intermediary metabolism and energetics during murine early embryogenesis. Journal of Biological Chemistry 278, 31457-31460.

Johnson, S. M., Lin, S. Y., and Slack, F. J. (2003b). The time of appearance of the C. elegans let-7 microRNA is transcriptionally controlled utilizing a temporal regulatory element in its promoter. Dev. Biol. 259, 364–379.

Johnson, S.M., Grosshans, H., Shingara, J., Byrom, M., Jarvis, R., Cheng, A., Labourier, E., Reinert, K.L., Brown, D., and Slack, F.J. (2005). RAS is regulated by the let-7 microRNA family. Cell 120, 635-647.

Johnson, C. D., Esquela-Kerscher, A., Stefani, G., Byrom, M., Kelnar, K., Ovcharenko, D., Wilson, M., Wang, X., Shelton, J., Shingara, J., et al. (2007). The let-7 microRNA represses cell proliferation pathways in human cells. Cancer Res. 67, 7713–22.

Kaelin, W. G. and McKnight, S. L. (2013). Influence of Metabolism on Epigenetics and Disease. Cell 153, 56-69.

Kalaitzidis, D., Sykes, S. M., Wang, Z., Punt, N., Tang, Y., Ragu, C., Sinha, A. U., Lane, S. W., Souza, A. L., Clish, C. B., et al. (2012). mTOR Complex 1 Plays Critical Roles in Hematopoiesis and Pten-Loss-Evoked Leukemogenesis. Cell Stem Cell 11, 429-439.

Kaplon, J. et al. (2013). A key role for mitochondrial gatekeeper pyruvate dehydrogenase in oncogene-induced senescence. Nature 498, 109-112.

Kawahara, H., Okada, Y., Imai, T., Iwanami, A., Mischel, P. S., and Okano, H. (2011). Musashi1 cooperates in abnormal cell lineage protein 28 (Lin28)-mediated let-7 family microRNA biogenesis in early neural differentiation. J. Biol. Chem. 286, 16121–30.

Kennell, J.A., Gerin, I., MacDougald, O.A., and Cadigan, K.M. (2008). The microRNA miR-8 is a conserved negative regulator of Wnt signaling. Proc Natl Acad Sci U S A 105, 15417-15422.

Kharas, M. G., Okabe, R., Ganis, J. J., Gozo, M., Khandan, T., Paktinat, M., Gilliland, D. G. and Gritsman, K. (2010). Constitutively active AKT depletes hematopoietic stem cells and induces leukemia in mice. Blood 115, 1406-1415.

King, C., Cuatrecasas, M., Castells, A., Sepulveda, A., Lee, J. S., and Rustgi, A. K. (2011). Lin28b promotes colon cancer progression and metastasis. Cancer Res. 71, 4260-8

Klimmeck, D., Hansson, J., Raffel, S., Vakhrushev, S. Y., Trumpp, A. and Krijgsveld, J. (2012). Proteomic Cornerstones of Hematopoietic Stem Cell Differentiation: Distinct Signatures of Multipotent Progenitors and Myeloid Committed Cells. Molecular & Cellular Proteomics 11, 286-302.

Klusmann, J. H., Li, Z., Böhmer, K., Maroz, A., Koch, M. L., Emmrich, S., Godinho, F. J., Orkin, S. H., and Reinhardt, D. (2010). miR-125b-2 is a potential oncomiR on human chromosome 21 in megakaryoblastic leukemia. Genes Dev. 24, 478–90.

Knobloch, M., Braun, S. M. G., Zurkirchen, L., von Schoultz, C., Zamboni, N., Arauzo-Bravo, M. J., Kovacs, W. J., Karalay, O., Suter, U., Machado, R. A. C., et al. (2013). Metabolic control of adult neural stem cell activity by Fasn-dependent lipogenesis. Nature 493, 226-230.

Knopf, F. et al. (2011). Bone Regenerates via Dedifferentiation of Osteoblasts in the Zebrafish Fin. Dev. Cell 20, 713–24.

Kolquist, K. A., Ellisen, L. W., Counter, C. M., Meyerson, M., Tan, L. K., Weinberg, R. A., Haber, D. A., and Gerald, W. L. (1998). Expression of TERT in early premalignant lesions and a subset of cells in normal tissues. Nat. Genet. 19, 182–6.

Kondoh, H., Lleonart, M. E., Nakashima, Y., Yokode, M., Tanaka, M., Bernard, D., Gil, J. and Beach, D. (2007). A high glycolytic flux supports the proliferative potential of murine embryonic stem cells. Antioxidants & Redox Signaling 9, 293-299.

Kragl, M., Knapp, D., Nacu, E., Khattak, S., Maden, M., Epperlein, H. H., and Tanaka, E. M. (2009). Cells keep a memory of their tissue origin during axolotl limb regeneration. Nature 460, 60–5.

Krishnamurthy, J., Ramsey, M. R., Ligon, K. L., Torrice, C., Koh, A., Bonner-Weir, S., and Sharpless, N. E. (2006). p16INK4a induces an age-dependent decline in islet regenerative potential. Nature 443, 453–7.

Kumar, M.S., Erkeland, S.J., Pester, R.E., Chen, C.Y., Ebert, M.S., Sharp, P.A., and Jacks, T. (2008). Suppression of non-small cell lung tumor development by the let-7 microRNA family. In Proc Natl Acad Sci USA, pp. 3903-3908.

LaFever, L. and Drummond-Barbosa, D. (2005). Direct control of germline stem cell division and cyst growth by neural insulin in Drosophila. Science 309, 1071-1073.

LaFever, L., Feoktistov, A., Hsu, H.-J. and Drummond-Barbosa, D. (2010). Specific roles of Target of rapamycin in the control of stem cells and their progeny in the Drosophila ovary. Development 137, 2117-2126.

Lagos-Quintana, M., Rauhut, R., Yalcin, A., Meyer, J., Lendeckel, W., and Tuschl, T. (2002). Identification of tissue-specific microRNAs from mouse. Curr. Biol. 12, 735–9.

Lairson, L. L., Lyssiotis, C. A., Zhu, S. and Schultz, P. G. (2013). Small molecule-based approaches to adult stem cell therapies. Annual Review of Pharmacology and Toxicology 53, 107-125.

Laplante, M., and Sabatini, D.M. (2009). An emerging role of mTOR in lipid biosynthesis. Curr Biol 19, R1046-1052.

Le, M. T., Xie, H., Zhou, B., Chia, P. H., Rizk, P., Um, M., Udolph, G., Yang, H., Lim, B., and Lodish, H. F. (2009a). MicroRNA-125b promotes neuronal differentiation in human cells by repressing multiple targets. Mol. Cell. Biol. 29, 5290–305.

Le, M. T., Teh, C., Shyh-Chang, N., Xie, H., Zhou, B., Korzh, V., Lodish, H. F., and Lim, B. (2009b). MicroRNA-125b is a novel negative regulator of p53. Genes Dev. 23, 862–76.

Le, M. T., Shyh-Chang, N., Khaw, S. L., Chin, L., Teh, C., Tay, J., O'Day, E., Korzh, V., Yang, H., Lal, A., et al. (2011). Conserved regulation of p53 network dosage by microRNA-125b occurs through evolving miRNA-target gene pairs. PLoS Genet. 7, e1002242.

Lee, Y. S., and Dutta, A. (2007). The tumor suppressor microRNA let-7 represses the HMGA2 oncogene. Genes Dev. 21, 1025–30.

Leese, H. J. (1995). Metabolic control during preimplantation mammalian development. Human Reproduction Update 1, 63-72.

Leese, H. J. and Barton, A. M. (1984). Pyruvate and glucose uptake by mouse ova and preimplantation embryos. Journal of Reproduction and Fertility 72, 9-13.

Legesse-Miller, A., Elemento, O., Pfau, S. J., Forman, J. J., Tavazoie, S., and Coller, H. A. (2009). Let-7 overexpression leads to an increased fraction of cells in G2/M, direct down-regulation of Cdc34, and stabilization of Wee1 kinase in primary fibroblasts. J. Biol. Chem. 284, 6605–9.

Lehrbach, N. J., Armisen, J., Lightfoot, H. L., Murfitt, K. J., Bugaut, A., Balasubramanian, S., and Miska, E. A. (2009). LIN-28 and the poly(U) polymerase PUP-2 regulate let-7 microRNA processing in Caenorhabditis elegans. Nat. Struct. Mol. Biol. 16, 1016–20.

Leinonen, J. T., Surakka, I., Havulinna, A. S., Kettunen, J., Luoto, R., Salomaa, V., and Widén, E. (2012). Association of LIN28B with Adult Adiposity-Related Traits in Females. PloS One 7, e48785.

Lettre, G. et al. (2008). Identification of ten loci associated with height highlights new biological pathways in human growth. Nat. Genet. 40, 584–91.

Li, N., Zhong, X., Lin, X., Guo, J., Zou, L., Tanyi, J. L., Shao, Z., Liang, S., Wang, L. P., Hwang, W. T., et al. (2012). Lin-28 homologue A (LIN28A) promotes cell cycle progression via regulation of cyclin-dependent kinase 2 (CDK2), cyclin D1 (CCND1), and cell division cycle 25 homolog A (CDC25A) expression in cancer. J. Biol. Chem. 287, 17386–97.

Li, X., Zhang, J, Gao, L., McClellan, S., Finan, M. A., Butler, T. W., Owen, L. B., Piazza, G. A., and Xi, Y. (2011). MiR-181 mediates cell differentiation by interrupting the Lin28 and let-7 feedback circuit. Cell Death Differ. 19, 378-86.

Liau, S. S., Jazag, A., and Whang, E. E. (2006). HMGA1 is a determinant of cellular invasiveness and in vivo metastatic potential in pancreatic adenocarcinoma. Cancer Res. 66, 11613–22.

Liu, J. et al. (2011). Regenerative phenotype in mice with a point mutation in transforming growth factor β type I receptor (TGFBR1). Proc. Natl. Acad. Sci. USA 108, 14560–5.

Locasale, J. W., Grassian, A. R., Melman, T., Lyssiotis, C. A., Mattaini, K. R., Bass, A. J., Heffron, G., Metallo, C. M., Muranen, T., Sharfi, H., et al. (2011). Phosphoglycerate dehydrogenase diverts glycolytic flux and contributes to oncogenesis. Nat Genet. 43, 869-74.

Locasale, J. W., and Cantley, L. C. (2011). Metabolic flux and the regulation of mammalian cell growth. Cell Metab. 14, 443–451.

Love, N. R. et al. (2013). Amputation-induced reactive oxygen species are required for successful Xenopus tadpole tail regeneration. Nat Cell Biol. 15, 222-8.

Lu, C., Ward, P. S., Kapoor, G. S., Rohle, D., Turcan, S., Abdel-Wahab, O., Edwards, C. R., Khanin, R., Figueroa, M. E., Melnick, A., et al. (2012). IDH mutation impairs histone demethylation and results in a block to cell differentiation. Nature 483, 474-8.

Lu, L., Katsaros, D., de la Longrais, I.A., Sochirca, O., and Yu, H. (2007). Hypermethylation of let-7a-3 in epithelial ovarian cancer is associated with low insulin-like growth factor-II expression and favorable prognosis. Cancer Res 67, 10117-10122.

Luka, Z. et al. J. Biol. Chem. 284, 22507 (2009)

Lyssiotis, C. A., Lairson, L. L., Boitano, A. E., Wurdak, H., Zhu, S. and Schultz, P. G. (2011). Chemical Control of Stem Cell Fate and Developmental Potential. Angewandte Chemie-International Edition 50, 200-242.

Magee, J. A., Ikenoue, T., Nakada, D., Lee, J. Y., Guan, K.-L. and Morrison, S. J. (2012). Temporal Changes in PTEN and mTORC2 Regulation of Hematopoietic Stem Cell Self-Renewal and Leukemia Suppression. Cell Stem Cell 11, 415-428.

Mair, W., McLeod, C. J., Wang, L. and Jones, D. L. (2010). Dietary restriction enhances germline stem cell maintenance. Aging Cell 9, 916-918.

Manganelli, G., Fico, A., Masullo, U., Pizzolongo, F., Cimmino, A. and Filosa, S. (2012). Modulation of the Pentose Phosphate Pathway Induces Endodermal Differentiation in Embryonic Stem Cells. PloS One 7.

Marson, A., Levine, S. S., Cole, M. F., Frampton, G. M., Brambrink, T., Johnstone, S., Guenther, M. G., Johnston, W. K., Wernig, M., Newman, J., et al. (2008). Connecting microRNA genes to the core transcriptional regulatory circuitry of embryonic stem cells. Cell 134, 521–33.

Martello, G., Sugimoto, T., Diamanti, E., Joshi, A., Hannah, R., Ohtsuka, S., Göttgens, B., Niwa, H., and Smith, A. (2012). Esrrb is a pivotal target of the Gsk3/Tcf3 axis regulating embryonic stem cell self-renewal. Cell Stem Cell 11, 491–504.

Mayr, C., Hemann, M. T., and Bartel, D. P. (2007). Disrupting the pairing between let-7 and Hmga2 enhances oncogenic transformation. Science 315, 1576–9.

McBrearty, B. a, Clark, L. D., Zhang, X. M., Blankenhorn, E. P., and Heber-Katz, E (1998). Genetic analysis of a mammalian wound-healing trait. Proc. Natl. Acad. Sci. USA 95, 11792–7.

McLeod CJ, Wang L, Wong C, Jones DL. (2010). Stem cell dynamics in response to nutrient availability. Current Biology 20, 2100-5.

McMillan, J.M. et al. J. Pharm. Pharmacol. 57, 599 (2005)

Melton, C., Judson, R. L., and Blelloch, R. (2010). Opposing microRNA families regulate self-renewal in mouse embryonic stem cells. Nature 463, 621–6.

Merkle, S. and Pretsch, W. (1989). Characterization of triosephosphate isomerase mutants with reduced enzyme-activity in Mus musculus. Genetics 123, 837-844.

Merkle, S., Favor, J., Graw, J., Hornhardt, S. and Pretsch, W. (1992). Hereditary lactate dehydrogenase A-subunit deficiency as cause of early postimplantation death of homozygotes in Mus musculus. Genetics 131, 413-421.

Michalik, L. et al. (2001). Impaired skin wound healing in peroxisome proliferator receptor (PPAR)α and PPARβ mutant mice. J. Cell Biol. 154, 799–814.

Mikkelsen, T.S. et al. Nature 454, 49 (2008)

Molenaar, J. J., Domingo-Fernández, R., Ebus, M. E., Lindner, S., Koster, J., Drabek, K., Mestdagh, P., van Sluis, P., Valentijn, L. J., van Nes, J., et al. (2012). LIN28B induces neuroblastoma and enhances MYCN levels via let-7 suppression. Nat Genet. 44, 1199-206.

Molenaar, J. J., Domingo-Fernandez, R., Ebus, M. E., Lindner, S., Koster, J., Drabek, K., Mestdagh, P., van Sluis, P., Valentijn, L. J., van Nes, J., et al. (2012). LIN28B induces neuroblastoma and enhances MYCN levels via let-7 suppression. Nature Genetics 44, 1199-1206.

Molofsky, A. V, Slutsky, S. G., Joseph, N. M., He, S., Pardal, R., Krishnamurthy, J., Sharpless, N. E., and Morrison, S. J. (2006). Increasing p16INK4a expression decreases forebrain progenitors and neurogenesis during ageing. Nature 443, 448–52.

Morita, K., and Han, M. (2006). Multiple mechanisms are involved in regulating the expression of the developmental timing regulator lin-28 in Caenorhabditis elegans. EMBO J. 25, 5794–804.

Moss, E G, Lee, R. C., and Ambros, V. (1997). The cold shock domain protein LIN-28 controls developmental timing in C. elegans and is regulated by the lin-4 RNA. Cell 88, 637–46.

Moss, E. G., and Tang, L. (2003). Conservation of the heterochronic regulator Lin-28, its developmental expression and microRNA complementary sites. Dev. Biol. 258, 432–442.

Moss, E. G., Lee, R. C., and Ambros, V. (1997). The cold shock domain protein LIN-28 controls developmental timing in C. elegans and is regulated by the lin-4 RNA. Cell 88, 637–46.

Muller-Rover, S., Handjiski, B., Veen, C. Van Der, Eichmuller, S., Foitzik, K., Mckay, I. A., Stenn, K. S., and Paus, R. (2001). A Comprehensive Guide for the Accurate

Classification of Murine Hair Follicles in Distinct Hair Cycle Stages. J. Invest. Dermatol. 117, 3–15.

Nakada, D., Saunders, T. L. and Morrison, S. J. (2010). Lkb1 regulates cell cycle and energy metabolism in haematopoietic stem cells. Nature 468, 653-8.

Nakamura, Y. et al. (2012). Functional role of PPARδ in corneal epithelial wound healing. Am. J. Pathol. 180, 583–598.

Nam, Y., Chen, C., Gregory, R. I., Chou, J. J., and Sliz, P. (2011). Molecular basis for interaction of let-7 microRNAs with Lin28. Cell 147, 1080–1091.

Newman, M. A., Thomson, J. M., and Hammond, S. M. (2008). Lin-28 interaction with the Let-7 precursor loop mediates regulated microRNA processing. RNA 14, 1539–49.

Newman, M., Thomson, J. M., and Hammond, S. M. (2008). Lin-28 interaction with the Let-7 precursor loop mediates regulated miRNA processing. RNA 14, 1539–49.

Ng, H.H. & Surani, M.A. Nat. Cell Biol. 13, 490 (2011)

Nichols, J., and Smith, A. (2009). Naive and primed pluripotent states. Cell Stem Cell 4, 487–92.

Nichols, J., Chambers, I., Taga, T., and Smith, A. (2001). Physiological rationale for responsiveness of mouse embryonic stem cells to gp130 cytokines. Development 128, 2333-9.

Nimmo, R.A., and Slack, F.J. (2009). An elegant miRror: microRNAs in stem cells, developmental timing and cancer. Chromosoma 118, 405-418.

Nishino, J., Kim, I., Chada, K., and Morrison, S. J. (2008). Hmga2 promotes neural stem cell self-renewal in young but not old mice by reducing p16Ink4a and p19Arf Expression. Cell 135, 227–39.

Nishino, J., Kim, I., Chada, K., and Morrison, S. J. (2008). Hmga2 promotes neural stem cell self-renewal in young but not old mice by reducing p16Ink4a and p19Arf Expression. Cell 135, 227–39.

O'Connell, R. M., Chaudhuri, A. A., Rao, D. S., Gibson, W. S. J., Balazs, A. B., and Baltimore, D. (2010). MicroRNAs enriched in hematopoietic stem cells differentially regulate long-term hematopoietic output. Proc Natl Acad Sci USA. 107, 14235–40.

O'Brien, L. E., Soliman, S. S., Li, X. and Bilder, D. (2011). Altered modes of stem cell division drive adaptive intestinal growth. Cell 147, 603-14.

Onder, T. T., Kara, N., Cherry, A., Sinha, A. U., Zhu, N., Bernt, K. M., Cahan, P., Marcarci, B. O., Unternaehrer, J., Gupta, P. B., et al. (2012). Chromatin-modifying enzymes as modulators of reprogramming. Nature 483, 598–602.

Ong, K. K. et al. (2009). Genetic variation in LIN28B is associated with the timing of puberty. Nat. Genet. 41, 729–33.

Ong, K. K., Elks, C. E., Wills, A. K., Wong, A., Wareham, N. J., Loos, R. J. F., Kuh, D., and Hardy, R. (2011). Associations between the pubertal timing-related variant in LIN28B and BMI vary across the life course. J. Clin. Endocrinol. Metab. 96, E125–9.

Ooi, A. G., Sahoo, D., Adorno, M., Wang, Y., Weissman, I. L., and Park, C. Y. (2010). MicroRNA-125b expands hematopoietic stem cells and enriches for the lymphoid-balanced and lymphoid-biased subsets. Proc Natl Acad Sci USA. 107, 21505-10.

Owusu-Ansah, E. and Banerjee, U. (2009). Reactive oxygen species prime Drosophila haematopoietic progenitors for differentiation. Nature 461, 537-41.

Pan, G. et al. Cell Stem Cell 1, 299 (2007)

Panopoulos, A. D., Yanes, O., Ruiz, S., Kida, Y. S., Diep, D., Tautenhahn, R., Herrerias, A., Batchelder, E. M., Plongthongkum, N., Lutz, M., et al. (2012). The metabolome of induced pluripotent stem cells reveals metabolic changes occurring in somatic cell reprogramming. Cell Research 22, 168-177.

Pantaleon, M. and Kaye, P. L. (1998). Glucose transporters in preimplantation development. Reviews of Reproduction 3, 77-81.

Pasquinelli, A. E., Reinhart, B. J., Slack, F., Martindale, M. Q., Kuroda, M. I., Maller, B., Hayward, D. C., Ball, E. E., Degnan, B., Müller, P., et al. (2000). Conservation of the sequence and temporal expression of let-7 heterochronic regulatory RNA. Nature 408, 86–9.

Pattappa, G., Heywood, H. K., De Bruijn, J. D. and Lee, D. A. (2011). The Metabolism of Human Mesenchymal Stem Cells During Proliferation and Differentiation. Journal of Cellular Physiology 226, 2562-2570.

Pattappa, G., Thorpe, S. D., Jegard, N. C., Heywood, H. K., de Bruijn, J. D. and Lee, D. A. (2013). Continuous and Uninterrupted Oxygen Tension Influences the Colony Formation and Oxidative Metabolism of Human Mesenchymal Stem Cells. Tissue Engineering Part C-Methods 19.

Pearson, R. D. (1984). Neotenic blastemal morphogenesis. Acta Biotheoretica 33, 51–59.

Peng, S., Chen, L. L., Lei, X. X., Yang, L., Lin, H., Carmichael, G. G., and Huang, Y. (2011). Genome-wide studies reveal that Lin28 enhances the translation of genes important for growth and survival of human embryonic stem cells. Stem Cells 29, 496–504.

Perry, J. R. B. et al. (2009). Meta-analysis of genome-wide association data identifies two loci influencing age at menarche. Nat. Genet. 41, 648–50.

Peter, M. E. (2009). Let-7 and miR-200 microRNAs: Guardians against pluripotency and cancer progression. Cell Cycle 8, 843–852.

Picard, D., Miller, S., Hawkins, C. E., Bouffet, E., Rogers, H. A., Chan, T. S., Kim, S. K., Ra, Y. S., Fangusaro, J., Korshunov, A. et al. (2012). Markers of survival and metastatic potential in childhood CNS primitive neuro-ectodermal brain tumours: an integrative genomic analysis. Lancet Oncol. 13, 838–48.

Piskounova, E., Polytarchou, C., Thornton, J. E., Lapierre, R. J., Pothoulakis, C., Hagan, J. P., Iliopoulos, D., and Gregory, R. I. (2011). Lin28A and Lin28B inhibit let-7 microRNA biogenesis by distinct mechanisms. Cell 147, 1066–1079.

Piskounova, E., Viswanathan, S.R., Janas, M., LaPierre, R.J., Daley, G.Q., Sliz, P., and Gregory, R.I. (2008). Determinants of microRNA processing inhibition by the developmentally regulated RNA-binding protein Lin28. J Biol Chem 283, 21310-21314.

Polesskaya, A., Cuvellier, S., Naguibneva, I., Duquet, A., Moss, E. G., and Harel-Bellan, A. (2007). Lin-28 binds IGF-2 mRNA and participates in skeletal myogenesis by increasing translation efficiency. Genes Dev. 21, 1125–38.

Porrello, E. R., Mahmoud, A. I., Simpson, E., Hill, J. A., Richardson, J. A., Olson, E. N., and Sadek, H. A. (2011). Transient Regenerative Potential of the Neonatal Mouse Heart. Science 331, 1078–1080.

Poss, K. D. (2010). Advances in understanding tissue regenerative capacity and mechanisms in animals. Nat. Rev. Genet. 11, 710–721.

Possemato, R., Marks, K. M., Shaul, Y. D., Pacold, M. E., Kim, D., Birsoy, K., Sethumadhavan, S., Woo, H. K., Jang, H. G., Jha, A. K., et al. (2011). Functional genomics reveal that the serine synthesis pathway is essential in breast cancer. Nature 476, 346-50.

Pretsch, W. (2000). Enzyme-activity mutants in Mus musculus. I. Phenotypic description and genetic characterization of ethylnitrosourea-induced mutations. Mammalian Genome 11, 537-542.

Prigione, A., Fauler, B., Lurz, R., Lehrach, H. and Adjaye, J. (2010). The Senescence-Related Mitochondrial/Oxidative Stress Pathway is Repressed in Human Induced Pluripotent Stem Cells. Stem Cells 28, 721-733.

Quinn, P. and Wales, R. G. (1971). Adenosine triphosphate content of preimplantation mouse embryos. Journal of Reproduction and Fertility 25, 133-135.

Quintana, E., Shackleton, M., Foster, H. R., Fullen, D. R., Sabel, M. S., Johnson, T. M., and Morrison, S. J. (2010). Phenotypic heterogeneity among tumorigenic melanoma

cells from patients that is reversible and not hierarchically organized. Cancer Cell 18, 510–23.

Quintana, E., Shackleton, M., Sabel, M. S., Fullen, D. R., Johnson, T. M., and Morrison, S. J. (2008). Efficient tumour formation by single human melanoma cells. Nature 456, 593-8.

Ramachandran, R. et al. (2010). Ascl1a regulates Muller glia dedifferentiation and retinal regeneration through a Lin-28-dependent, let-7 microRNA signalling pathway. Nat. Cell Biol. 12, 1101-7.

Ramachandran, R., Fausett, B. V, and Goldman, D. (2010). Ascl1a regulates Müller glia dedifferentiation and retinal regeneration through a Lin-28-dependent, let-7 microRNA signalling pathway. Nat. Cell Biol. 12, 1101-7

Rao, S., Lee, S. Y., Gutierrez, A., Perrigoue, J., Thapa, R. J., Tu, Z., Jeffers, J. R., Rhodes, M., Anderson, S., Oravecz, T., et al. (2012). Inactivation of ribosomal protein L22 promotes transformation by induction of the stemness factor, Lin28B. Blood 120, 3764–73.

Reinhart, B. J., Slack, F. J., Basson, M., Pasquinelli, A. E., Bettinger, J. C., Rougvie, A. E., Horvitz, H. R., and Ruvkun, G. (2000). The 21-nucleotide let-7 RNA regulates developmental timing in Caenorhabditis elegans. Nature 403, 901–6.

Reinhart, B.J., Slack, F.J., Basson, M., Pasquinelli, A.E., Bettinger, J.C., Rougvie, A.E., Horvitz, H.R., and Ruvkun, G. (2000). The 21-nucleotide let-7 RNA regulates developmental timing in Caenorhabditis elegans. Nature 403, 901-906.

Renault, V. M., Rafalski, V. A., Morgan, A. A., Salih, D. A. M., Brett, J. O., Webb, A. E., Villeda, S. A., Thekkat, P. U., Guillerey, C., Denko, N. C., et al. (2009). FoxO3 Regulates Neural Stem Cell Homeostasis. Cell Stem Cell 5, 527-539.

Rera, M., Bahadorani, S., Cho, J., Koehler, C. L., Ulgherait, M., Hur, J. H., Ansari, W. S., Lo, T., Jr., Jones, D. L. and Walker, D. W. (2011). Modulation of Longevity and Tissue Homeostasis by the Drosophila PGC-1 Homolog. Cell Metabolism 14, 623-634.

Rodini, C. O., Suzuki, D. E., Saba-Silva, N., Cappellano, A., de Souza, J. E. S., Cavalheiro, S., Toledo, S. R. C., and Okamoto, O. K. (2012). Expression analysis of stem cell-related genes reveal OCT4 as a predictor of poor clinical outcome in medulloblastoma. J. Neurooncol. 106, 71–9.

Rosen, J. M., and Jordan, C. T. (2009). The increasing complexity of the cancer stem cell paradigm. Science 324, 1670–3.

Rossi, D. J., Jamieson, C. H. M. and Weissman, I. L. (2008). Stems cells and the pathways to aging and cancer. Cell 132, 681-696.

Roush, S., and Slack, F. J. (2008). The let-7 family of microRNAs. Trends Cell Biol. 18, 505–16.

Rudolph, K. L., Chang, S., Lee, H. W., Blasco, M., Gottlieb, G. J., Greider, C., and DePinho, R. A. (1999). Longevity, stress response, and cancer in aging telomerase-deficient mice. Cell 96, 701–12.

Rybak, A., Fuchs, H., Smirnova, L., Brandt, C., Pohl, E.E., Nitsch, R., and Wulczyn, F.G. (2008). A feedback loop comprising lin-28 and let-7 controls pre-let-7 maturation during neural stem-cell commitment. Nat Cell Biol 10, 987-993.

Sacco, A., Mourkioti, F., Tran, R., Choi, J., Llewellyn, M., Kraft, P., Shkreli, M., Delp, S., Pomerantz, J. H., Artandi, S. E., et al. (2010). Short telomeres and stem cell exhaustion model Duchenne muscular dystrophy in mdx/mTR mice. Cell 143, 1059–71.

Sahin, E. and DePinho, R. A. (2010). Linking functional decline of telomeres, mitochondria and stem cells during ageing. Nature 464, 520-528.

Sampson, V. B., Rong, N. H., Han, J., Yang, Q., Aris, V., Soteropoulos, P., Petrelli, N. J., Dunn, S. P., and Krueger, L. J. (2007). MicroRNA let-7a down-regulates MYC and reverts MYC-induced growth in Burkitt lymphoma cells. Cancer Res. 67, 9762–70.

Sanchez Alvarado, A., and Tsonis, P. A. (2006). Bridging the regeneration gap: genetic insights from diverse animal models. Nat. Rev. Genet. 7, 873–84.

Sasaki, M., Knobbe, C. B., Munger, J. C., Lind, E. F., Brenner, D., Bruestle, A., Harris, I. S., Holmes, R., Wakeham, A., Haight, J., et al. (2012). IDH1(R132H) mutation increases murine haematopoietic progenitors and alters epigenetics. Nature 488, 656-9.

Saxena, R., Hivert, M.F., Langenberg, C., Tanaka, T., Pankow, J.S., Vollenweider, P., Lyssenko, V., Bouatia-Naji, N., Dupuis, J., Jackson, A.U., et al. Genetic variation in GIPR influences the glucose and insulin responses to an oral glucose challenge. Nat Genet 42, 142-148.

Schaetzlein, S., Lucas-Hahn, A., Lemme, E., Kues, W. A., Dorsch, M., Manns, M. P., Niemann, H., and Rudolph, K. L. (2004). Telomere length is reset during early mammalian embryogenesis. Proc Natl Acad Sci USA. 101, 8034–8.

Schieke, S. M., Ma, M., Cao, L., McCoy, J. P., Jr., Liu, C., Hensel, N. F., Barrett, A. J., Boehm, M. and Finkel, T. (2008). Mitochondrial metabolism modulates differentiation and teratoma formation capacity in mouse embryonic stem cells. Journal of Biological Chemistry 283, 28506-28512.

Schreml, S., Szeimies, R. M., Prantl, L., Karrer, S., Landthaler, M., and Babilas, P. (2010). Oxygen in acute and chronic wound healing. Br. J. Dermatol. 163, 257–68.

Schulz, C., Paus, M., Frey, K., Schmid, R., Kohl, Z., Mennerich, D., Winkler, J., and Gillardon, F. (2011). Leucine-rich repeat kinase 2 modulates retinoic acid-induced neuronal differentiation of murine embryonic stem cells. PloS One 6, e20820.

Schwanhausser, B., Gossen, M., Dittmar, G., and Selbach, M. (2009). Global analysis of cellular protein translation by pulsed SILAC. Proteomics 9, 205-209.

Schwer, B. et al. Aging Cell 8, 604 (2009)

Segre, A.V., Groop, L., Mootha, V.K., Daly, M.J., and Altshuler, D. Common inherited variation in mitochondrial genes is not enriched for associations with type 2 diabetes or related glycemic traits. PLoS Genet 6.

Selbach, M., Schwanhausser, B., Thierfelder, N., Fang, Z., Khanin, R., and Rajewsky, N. (2008). Widespread changes in protein synthesis induced by microRNAs. Nature 455, 58-63.

Shah, M. V, Namigai, E. K. O., and Suzuki, Y. (2011). The role of canonical Wnt signaling in leg regeneration and metamorphosis in the red flour beetle Tribolium castaneum. Mech. Dev. 128, 342–58.

Shah, O.J., Wang, Z., and Hunter, T. (2004). Inappropriate activation of the TSC/Rheb/mTOR/S6K cassette induces IRS1/2 depletion, insulin resistance, and cell survival deficiencies. Curr Biol 14, 1650-1656.

Sharpless, N. E., and DePinho, R. A. (2007). How stem cells age and why this makes us grow old. Nat. Rev. Mol. Cell Biol. 8, 703–13.

Shim, J., Mukherjee, T. and Banerjee, U. (2012). Direct sensing of systemic and nutritional signals by haematopoietic progenitors in Drosophila. Nature Cell Biology 14, 394-400.

Shinoda, G., Shyh-Chang, N., de Soysa, T. Y., Zhu, H., Seligson, M. T., Shah, S. P., Abo-Sido, N., Yabuuchi, A., Hagan, J. P., Gregory, R. I., Asara, J. M., Cantley, L. C., Moss, E. G., and Daley, G. Q. (2013). Fetal deficiency of Lin28 programs life-long aberrations in growth and glucose metabolism. Stem Cells. doi: 10.1002/stem.1423. [Epub ahead of print]

Shinoda, G., de Soysa, T. Y., Seligson, M. T., Yabuuchi, A., Fujiwara, Y., Yi Huang, P., Hagan, J. P., Gregory, R. I., Moss, E.G., and Daley, G. Q. (2013). Lin28a Regulates Germ Cell Pool Size and Fertility. Stem Cells, Epub ahead of print.

Shyh-Chang, N., Zheng, Y., Locasale, J. W. and Cantley, L. C. (2011). Human pluripotent stem cells decouple respiration from energy production. EMBO Journal 30, 4851-4852.

Shyh-Chang, N., Locasale, J. W., Lyssiotis, C. A., Zheng, Y., Teo, R. Y., Ratanasirintrawoot, S., Zhang, J., Onder, T., Unternaehrer, J. J., Zhu, H., Asara, J. M.,

Daley, G. Q., and Cantley, L. C. (2013a). Influence of threonine metabolism on S-adenosylmethionine and histone methylation. Science 339, 222-226.

Shyh-Chang, N. and Daley, G. Q. (2013b). Lin28: Primal regulator of growth and metabolism in stem cells. Cell Stem Cell 12, 395-406.

Shyh-Chang, N., Daley, G. Q., and Cantley, L. C. (2013c). Stem cell metabolism during tissue development and aging. Development 12, 2535-47

Shyh-Chang, N., Zhu, H., de Soysa, T. Y., Shinoda, G., Seligson, M. T., Tsanov, K. T., Nguyen L., Asara, J. M., Cantley, L. C., and Daley, G. Q. (2013d). Lin28 enhances tissue repair by reprogramming cellular metabolism. Cell (*in press*)

Simsek, T., Kocabas, F., Zheng, J., DeBerardinis, R. J., Mahmoud, A. I., Olson, E. N., Schneider, J. W., Zhang, C. C. and Sadek, H. A. (2010). The Distinct Metabolic Profile of Hematopoietic Stem Cells Reflects Their Location in a Hypoxic Niche. Cell Stem Cell 7, 380-390.

Small, E.M., and Olson, E.N. Pervasive roles of microRNAs in cardiovascular biology. Nature 469, 336-342.

Smith-Bolton, R. K., Worley, M. I., Kanda, H., and Hariharan, I. K. (2009). Article Regenerative Growth in Drosophila Imaginal Discs Is Regulated by Wingless and Myc. Dev. Cell 16, 797–809.

Sokol, N. S., Xu, P., Jan, Y. N., and Ambros, Victor (2008). Drosophila let-7 microRNA is required for remodeling of the neuromusculature during metamorphosis. Genes Dev 22, 1591–6.

Soranzo, N., Sanna, S., Wheeler, E., Gieger, C., Radke, D., Dupuis, J., Bouatia-Naji, N., Langenberg, C., Prokopenko, I., Stolerman, E., et al. Common variants at 10 genomic loci influence hemoglobin A(C) levels via glycemic and nonglycemic pathways. Diabetes 59, 3229-3239.

Sousa-Nunes, R., Yee, L. L. and Gould, A. P. (2011). Fat cells reactivate quiescent neuroblasts via TOR and glial insulin relays in Drosophila. Nature 471, 508-12.

Spindle, A. I. and Pedersen, R. A. (1973). Hatching, attachment, and outgrowth of mouse blastocysts in-vitro – fixed nitrogen requirements. Journal of Experimental Zoology 186, 305-318.

Stadtfeld, M., Apostolou, E., Ferrari, F., Choi, J., Walsh, R. M., Chen, T., Ooi, S. S. K., Kim, S. Y., Bestor, T. H., Shioda, T., et al. (2012). Ascorbic acid prevents loss of Dlk1-Dio3 imprinting and facilitates generation of all-iPS cell mice from terminally differentiated B cells. Nature Genetics 44, 398-405.

Suda, T., Takubo, K. and Semenza, G. L. (2011). Metabolic Regulation of Hematopoietic Stem Cells in the Hypoxic Niche. Cell Stem Cell 9, 298-310.

Suh, N., Baehner, L., Moltzahn, F., Melton, C., Shenoy, A., Chen, J., and Blelloch, R. (2010). MicroRNA function is globally suppressed in mouse oocytes and early embryos. Curr. Biol. 20, 271–7.

Sulem, P. et al. (2009). Genome-wide association study identifies sequence variants on 6q21 associated with age at menarche. Nat. Genet. 41, 734–8.

Sulston, J. E., and Horvitz, H. R. (1981). Abnormal cell lineages in mutants of the nematode Caenorhabditis elegans. Dev. Biol. 55, 41–55.

Tahiliani, M. et al. Science 324, 930 (2009)

Takahashi, K. and Yamanaka, S. (2006). Induction of pluripotent stem cells from mouse embryonic and adult fibroblast cultures by defined factors. Cell 126, 663-676.

Takubo, K., Nagamatsu, G., Kobayashi, C. I., Nakamura-Ishizu, A., Kobayashi, H., Ikeda, E., Goda, N., Rahimi, Y., Johnson, R. S., Soga, T., et al. (2013). Regulation of glycolysis by pdk functions as a metabolic checkpoint for cell cycle quiescence in hematopoietic stem cells. Cell Stem Cell 12, 49-61.

Tanaka, E. M., and Reddien, P. W. (2011). The cellular basis for animal regeneration. Dev. Cell 21, 172–85.

Tang, F., Barbacioru, C., Bao, S., Lee, C., Nordman, E., Wang, Xiaohui, Lao, K., and Surani, M. A. (2010). Tracing the derivation of embryonic stem cells from the inner cell mass by single-cell RNA-Seq analysis. Cell Stem Cell 6, 468–78.

Thomson, J. M., Newman, M., Parker, J. S., Morin-Kensicki, E. M., Wright, T., and Hammond, S. M. (2006). Extensive post-transcriptional regulation of microRNAs and its implications for cancer. Genes Dev. 20, 2202–7.

Thornton, J. E., Chang, H. M., Piskounova, E., and Gregory, R. I. (2012). Lin28-mediated control of let-7 microRNA expression by alternative TUTases Zcchc11 (TUT4) and Zcchc6 (TUT7). RNA 18, 1875–85.

Tohyama, S., Hattori, F., Sano, M., Hishiki, T., Nagahata, Y., Matsuura, T., Hashimoto, H., Suzuki, T., Yamashita, H., Satoh, Y., et al. (2013). Distinct metabolic flow enables large-scale purification of mouse and human pluripotent stem cell-derived cardiomyocytes. Cell Stem Cell 12, 127-137.

Tomás-Loba, A. et al. (2008). Telomerase reverse transcriptase delays aging in cancer-resistant mice. Cell 135, 609–22.

Tormos, K. V., Anso, E., Hamanaka, R. B., Eisenhart, J., Joseph, J., Kalyanaraman, B. and Chandel, N. S. (2011). Mitochondrial Complex III ROS Regulate Adipocyte Differentiation. Cell Metabolism 14, 537-544.

Tothova, Z. et al. (2007). FoxOs are critical mediators of hematopoietic stem cell resistance to physiologic oxidative stress. Cell 128, 325–39.

Tothova, Z., Kollipara, R., Huntly, B. J., Lee, B. H., Castrillon, D. H., Cullen, D. E., McDowell, E. P., Lazo-Kallanian, S., Williams, I. R., Sears, C., et al. (2007). FoxOs are critical mediators of hematopoietic stem cell resistance to physiologic oxidative stress. Cell 128, 325-339.

Tremblay, F., Brule, S., Hee Um, S., Li, Y., Masuda, K., Roden, M., Sun, X.J., Krebs, M., Polakiewicz, R.D., Thomas, G., et al. (2007). Identification of IRS-1 Ser-1101 as a target of S6K1 in nutrient- and obesity-induced insulin resistance. Proc Natl Acad Sci U S A 104, 14056-14061.

Tu, S., and Johnson, S. L. (2011). Fate restriction in the growing and regenerating zebrafish fin. Dev. Cell 20, 725–32.

Tyner, S. D., Venkatachalam, S., Choi, J., Jones, S., Ghebranious, N., Igelmann, H., Lu, X., Soron, G., Cooper, B., Brayton, C., et al. (2002). p53 mutant mice that display early ageing-associated phenotypes. Nature 415, 45–53.

Ueishi, S., Shimizu, H. and Inoue, Y. H. (2009). Male Germline Stem Cell Division and Spermatocyte Growth Require Insulin Signaling in Drosophila. Cell Structure and Function 34, 61-69.

Um, S.H., Frigerio, F., Watanabe, M., Picard, F., Joaquin, M., Sticker, M., Fumagalli, S., Allegrini, P.R., Kozma, S.C., Auwerx, J., et al. (2004). Absence of S6K1 protects against age- and diet-induced obesity while enhancing insulin sensitivity. Nature 431, 200-205.

Vadla, B., Kemper, K., Alaimo, J., Heine, C., and Moss, E. G. (2012). lin-28 controls the succession of cell fate choices via two distinct activities. PLoS Genet. 8, e1002588

Valancius, V. & Smithies, O. Mol. Cell Biol. 11, 1402(1991)

Van Blerkom, J. (2009). Mitochondria in early mammalian development. Seminars in Cell & Developmental Biology 20, 354-364.

Van Wynsberghe, P. M., Kai, Z. S., Massirer, K. B., Burton, V. H., Yeo, G. W., and Pasquinelli, A. E. (2011). LIN-28 co-transcriptionally binds primary let-7 to regulate miRNA maturation in Caenorhabditis elegans. Nat. Struct. Mol. Bio. 18, 302–308.

Vander Heiden, M. G., Cantley, L. C. and Thompson, C. B. (2009). Understanding the Warburg effect: the metabolic requirements of cell proliferation. Science 324, 1029-1033.

Varum, S., Rodrigues, A. S., Moura, M. B., Momcilovic, O., Easley, C. A., Ramalho-Santos, J., Van Houten, B. and Schatten, G. (2011). Energy Metabolism in Human Pluripotent Stem Cells and Their Differentiated Counterparts. PloS One 6.

Vishwakarma, P. (1962). The pH and bicarbonate ion content of the oviduct and uterine fluids. Fertility and Sterility 13, 481-5.

Viswanathan, S. R., Daley, G. Q. and Gregory, R. I. (2008). Selective blockade of MicroRNA processing by Lin28. Science 320, 97-100.

Viswanathan, S.R., Powers, J.T., Einhorn, W., Hoshida, Y., Ng, T.L., Toffanin, S., O'Sullivan, M., Lu, J., Phillips, L.A., Lockhart, V.L., et al. (2009). Lin28 promotes transformation and is associated with advanced human malignancies. Nat Genet 41, 843-848.

Viswanathan, S.R., and Daley, G.Q. (2010). Lin28: A microRNA regulator with a macro role. Cell 140, 445-449.

Vogt, E. J., Meglicki, M., Hartung, K. I., Borsuk, E., and Behr, R. (2012). Importance of the pluripotency factor LIN28 in the mammalian nucleolus during early embryonic development. Development 139, 4514–4523.

Voight, B.F., Scott, L.J., Steinthorsdottir, V., Morris, A.P., Dina, C., Welch, R.P., Zeggini, E., Huth, C., Aulchenko, Y.S., Thorleifsson, G., et al. Twelve type 2 diabetes susceptibility loci identified through large-scale association analysis. Nat Genet 42, 579-589.

Wagner, D. E., Wang, I. E., and Reddien, P. W. (2011). Clonogenic neoblasts are pluripotent adult stem cells that underlie planarian regeneration. Science 332, 811–6.

Wakabayashi, N., Itoh, K., Wakabayashi, J., Motohashi, H., Noda, S., Takahashi, S., Imakado, S., Kotsuji, T., Otsuka, F., Roop, D. R., et al. (2003). Keap1-null mutation leads to postnatal lethality due to constitutive Nrf2 activation. Nature Genetics 35, 238-245.

Wales, R. G. (1974). The levels of NAD and NADH in mouse embryos during the preimplantation stages of development. Proceedings of the Australian Biochemical Society 7, 28.

Wang X. et al. (2003). The origin and liver repopulating capacity of murine oval cells. Proc. Natl. Acad. Sc. USA 100, 11881–8.

Wang, M. C., O'Rourke, E. J. and Ruvkun, G. (2008). Fat Metabolism Links Germline Stem Cells and Longevity in C. elegans. Science 322, 957-960.

Wang, J., Alexander, P., Wu, L., Hammer, R., Cleaver, O. and McKnight, S. L. (2009). Dependence of Mouse Embryonic Stem Cells on Threonine Catabolism. Science 325, 435-439.

Wang, Y.C., Chen, Y.L., Yuan, R.H., Pan, H.W., Yang, W.C., Hsu, H.C., and Jeng, Y.M. (2010). Lin-28B expression promotes transformation and invasion in human hepatocellular carcinoma. Carcinogenesis 31, 1516-1522.

Wang, T., Chen, K., Zeng, X., Yang, J., Wu, Y., Shi, X., Qin, B., Zeng, L., Esteban, M. A., Pan, G., et al. (2011a). The Histone Demethylases Jhdm1a/1b Enhance Somatic Cell Reprogramming in a Vitamin-C-Dependent Manner. Cell Stem Cell 9, 575-587.

Wang, W., Yang, J., Liu, H., Lu, D., Chen, X., Zenonos, Z., Campos, L. S., Rad, R., Guo, G., Zhang, S., et al. (2011b). Rapid and efficient reprogramming of somatic cells to induced pluripotent stem cells by retinoic acid receptor gamma and liver receptor homolog 1. Proc Natl Acad Sci USA. 108, 18283-8.

Wellen, K. E., Hatzivassiliou, G., Sachdeva, U. M., Bui, T. V., Cross, J. R. and Thompson, C. B. (2009). ATP-Citrate Lyase Links Cellular Metabolism to Histone Acetylation. Science 324, 1076-1080.

Werner, J. C. and Sicard, R. E. (1987). Lactate metabolism of isolated, perfused fetal, and newborn pig hearts. Pediatric Research 22, 552-6.

West, J.D., Flockhart, J.H., Peters, J. and Ball, S.T. (1990) Death of mouse embryos that lack a functional gene for glucose phosphate isomerase. Genetical Research 56, 223-36.

West, J. A., Viswanathan, S. R., Yabuuchi, A., Cunniff, K., Takeuchi, A., Park, I. H., Sero, J. E., Zhu, H., Perez-Atayde, A., Frazier, A. L., et al. (2009). A role for Lin28 in primordial germ-cell development and germ-cell malignancy. Nature 460, 909–13.

Widén, E. et al. (2010). Distinct variants at LIN28B influence growth in height from birth to adulthood. Am. J. Hum. Genet. 86, 773–82.

Wilbert, M. L., Huelga, S. C., Kapeli, K., Stark, T. J., Liang, T. Y., Chen, S. X., Yan, B. Y., Nathanson, J. L., Hutt, K. R., Lovci, M. T., et al. (2012). LIN28 binds messenger RNAs at GGAGA motifs and regulates splicing factor abundance. Mol. Cell 48, 195-206.

Wilson, J. E. (2003). Isozymes of mammalian hexokinase: structure, subcellular localization and metabolic function. Journal of Experimental Biology 206, 2049-2057.

Wu, M. et al. (2007). Multiparameter metabolic analysis reveals a close link between attenuated mitochondrial bioenergetic function and enhanced glycolysis dependency in human tumor cells. Am. J. Physiol. Cell Physiol. 292, C125–36.

Wulczyn, F. G., Smirnova, L., Rybak, A., Brandt, C., Kwidzinski, E., Ninnemann, O., Strehle, M., Seiler, A., Schumacher, S., and Nitsch, R. (2007). Post-transcriptional regulation of the let-7 microRNA during neural cell specification. FASEB J. 21, 415–26.

Xu, B., and Huang, Y. (2009a). Histone H2a mRNA interacts with Lin28 and contains a Lin28-dependent posttranscriptional regulatory element. Nucleic Acids Res 37, 4256-4263.

Xu, B., Zhang, K., and Huang, Y. (2009b). Lin28 modulates cell growth and associates with a subset of cell cycle regulator mRNAs in mouse embryonic stem cells. RNA 15, 357-361.

Xue, D., Peng, Y., Wang, F., Allan, R. W., and Cao, D. (2011). RNA-binding protein LIN28 is a sensitive marker of ovarian primitive germ cell tumours. Histopathology 59, 452-9.

Yanes, O., Clark, J., Wong, D. M., Patti, G. J., Sanchez-Ruiz, A., Benton, H. P., Trauger, S. A., Desponts, C., Ding, S. and Siuzdak, G. (2010). Metabolic oxidation regulates embryonic stem cell differentiation. Nature Chemical Biology 6, 411-417.

Yang, D., and Moss, E. G. (2003). Temporally regulated expression of Lin-28 in diverse tissues of the developing mouse. Gene Expr. Patterns 3, 719–726.

Yi, R., Qin, Y., Macara, I. G., and Cullen, B. R. (2003). Exportin-5 mediates the nuclear export of pre-microRNAs and short hairpin RNAs. Genes Dev. 17, 3011–3016.

Yilmaz, O. H., Valdez, R., Theisen, B. K., Guo, W., Ferguson, D. O., Wu, H., and Morrison, S. J. (2006). Pten dependence distinguishes haematopoietic stem cells from leukaemia-initiating cells. Nature 441, 475–82.

Yilmaz, O. H., Katajisto, P., Lamming, D. W., Gueltekin, Y., Bauer-Rowe, K. E., Sengupta, S., Birsoy, K., Dursun, A., Yilmaz, V. O., Selig, M., et al. (2012). mTORC1 in the Paneth cell niche couples intestinal stem-cell function to calorie intake. Nature 486, 490-5.

Yokoyama, S., Hashimoto, M., Shimizu, H., Ueno-Kudoh, H., Uchibe, K., Kimura, I., and Asahara, H. (2008). Dynamic gene expression of Lin-28 during embryonic development in mouse and chicken. Gene Expr. Patterns 8, 155–60.

Yoshida, Y., Takahashi, K., Okita, K., Ichisaka, T. and Yamanaka, S. (2009). Hypoxia Enhances the Generation of Induced Pluripotent Stem Cells. Cell Stem Cell 5, 237-241.

Young, H. E., Bailey, C. F., and Dalley, B. K. (1983). Gross morphological analysis of limb regeneration in postmetamorphic adult Ambystoma. Anat. Rec. 206, 295–306.

Yu, F., Yao, H., Zhu, P., Zhang, X., Pan, Q., Gong, C., Huang, Y., Hu, X., Su, F., Lieberman, J., et al. (2007). Let-7 regulates self renewal and tumorigenicity of breast cancer cells. Cell 131, 1109–23.

Yu, J., Vodyanik, M. A., Smuga-Otto, K., Antosiewicz-Bourget, J., Frane, J. L., Tian, S., Nie, J., Jonsdottir, G. A., Ruotti, V., Stewart, R., et al. (2007). Induced pluripotent stem cell lines derived from human somatic cells. Science 318, 1917-1920.

Yu, W.-M., Liu, X., Shen, J., Jovanovic, O., Pohl, E. E., Gerson, S. L., Finkel, T., Broxmeyer, H. E. and Qu, C.-K. (2013). Metabolic Regulation by the Mitochondrial

Phosphatase PTPMT1 Is Required for Hematopoietic Stem Cell Differentiation. Cell Stem Cell 12, 62-74.

Yuan, X., Ishibashi, S., Hatakeyama, S., Saito, M., Nakayama, J., Nikaido, R., Haruyama, T., Watanabe, Y., Iwata, H., Iida, M., et al. (1999). Presence of telomeric G-strand tails in the telomerase catalytic subunit TERT knockout mice. Genes Cells 4, 563–72.

Yuan, J., Nguyen, C. K., Liu, X., Kanellopoulou, C., and Muljo, S. A. (2012). Lin28b reprograms adult bone marrow hematopoietic progenitors to mediate fetal lymphopoiesis. Science 335, 1195-200.

Yun, J., Rago, C., Cheong, I., Pagliarini, R., Angenendt, P., Rajagopalan, H., Schmidt, K., Willson, J.K., Markowitz, S., Zhou, S., et al. (2009). Glucose deprivation contributes to the development of KRAS pathway mutations in tumor cells. Science 325, 1555-1559.

Zee, B. M. et al. (2010). In Vivo Residue-specific Histone Methylation Dynamics. J Biol Chem. 285, 3341–3350.

Zhang, J. W. et al. (2006). PTEN maintains haematopoietic stem cells and acts in lineage choice and leukaemia prevention. Nature 441, 518–22.

Zhang, J., Guan, Z., Murphy, A. N., Wiley, S. E., Perkins, G. A., Worby, C. A., Engel, J. L., Heacock, P., Nguyen, O. K., et al. (2011a). Mitochondrial phosphatase PTPMT1 is essential for cardiolipin biosynthesis. Cell Metabolism 8, 690-700.

Zhang, J., Khvorostov, I., Hong, J. S., Oktay, Y., Vergnes, L., Nuebel, E., Wahjudi, P. N., Setoguchi, K., Wang, G., Do, A., et al. (2011b). UCP2 regulates energy metabolism and differentiation potential of human pluripotent stem cells. EMBO Journal 30, 4860-4873.

Zhang, L., Stokes, N., Polak, L., and Fuchs, E. (2011c). Specific microRNAs are preferentially expressed by skin stem cells to balance self-renewal and early lineage commitment. Cell Stem Cell 8, 294–308.

Zhang, W. C., Shyh-Chang, N., Yang, H., Rai, A., Umashankar, S., Ma, S., Soh, B. S., Sun, L. L., Tai, B. C., Nga, M. E., et al. (2012a). Glycine decarboxylase activity drives non-small cell lung cancer tumor-initiating cells and tumorigenesis. Cell 148, 259-72.

Zhang, D. et al. Genes Dev. 26, 461 (2012b)

Zhao, X.D. et al. Cell Stem Cell 1, 286 (2007)

Zheng, K., Wu, X., Kaestner, K. H. and Wang, P. J. (2009). The pluripotency factor LIN28 marks undifferentiated spermatogonia in mouse. BMC Developmental Biology 9.

Zhu, H., Shah, S., Shyh-Chang, N., Shinoda, G., Einhorn, W. S., Viswanathan, S. R., Takeuchi, A., Grasemann, C., Rinn, J. L., Lopez, M. F., et al. (2010a). Lin28a transgenic mice manifest size and puberty phenotypes identified in human genetic association studies. Nat. Genet. 42, 626-30.

Zhu, S., Li, W., Zhou, H., Wei, W., Ambasudhan, R., Lin, T., Kim, J., Zhang, K. and Ding, S. (2010b). Reprogramming of Human Primary Somatic Cells by OCT4 and Chemical Compounds. Cell Stem Cell 7, 651-655.

Zhu, H., Shyh-Chang, N., Segre, A. V., Shinoda, G., Shah, S. P., Einhorn, W. S., Takeuchi, A., Engreitz, J. M., Hagan, J. P., Kharas, M. G., et al. (2011). The Lin28/let-7 axis regulates glucose metabolism. Cell 147, 81-94.

## Appendix

## Supplemental Materials

### Figure S2.1

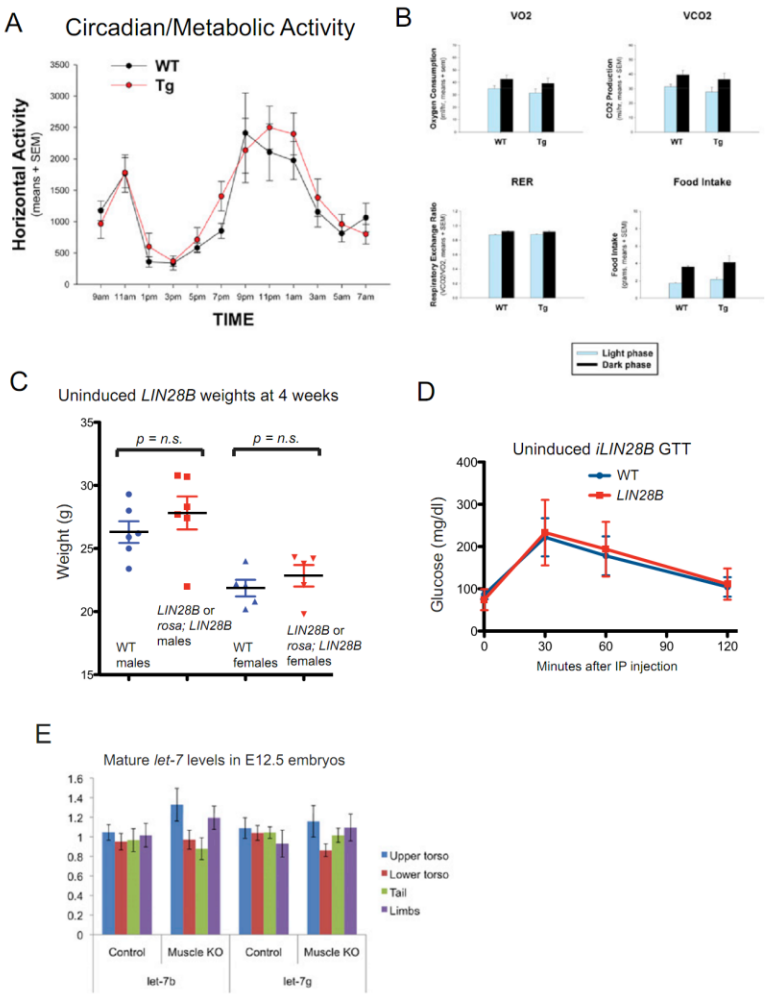


***Figure S2.1. Further characterization of Lin28a/b gain and loss of function mice.*** Over 96 hours, there were no horizontal activity (A), O2/CO2 exchange, or food/water intake (B) differences between wild-type and *Lin28a* Tg mice. (C) Weight and (D) GTT of uninduced wild-type and *LIN28B* Tg containing mice. (E) Mature *let-7* miRNA expression in E12.5 wild-type and *Lin28a* muscle-specific knockout embryos.

**Figure S2.2**

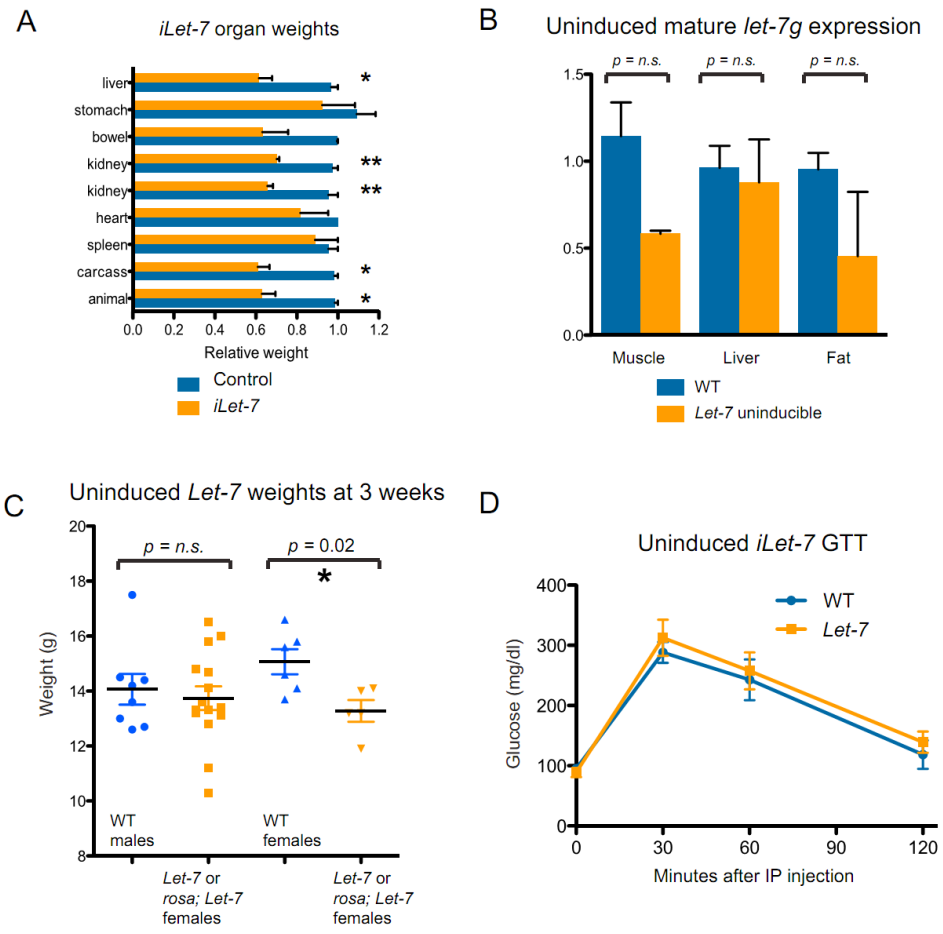


***Figure S2.2. Further characterization of iLet-7 transgenic mice.*** (A) Relative organ weights of *iLet-7* mice induced for 8 weeks. (B) Mature *let-7g* expression in tissues of uninduced *iLet-7* or *Let-7* Tg carrying mice. (C) Weight and (D) GTT of uninduced wild-type and *iLet-7* Tg containing mice.

## Figure S2.3

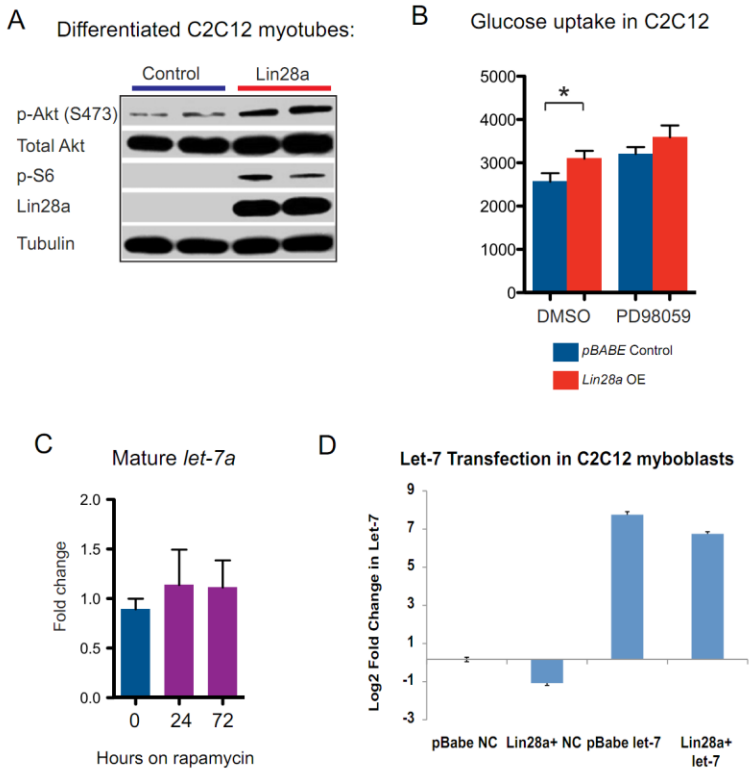


***Figure S2.3. Lin28a increases PI3K-mTOR signaling in differentiated myotubes, the MAPK/Erk inhibitor does not abrogate Lin28a-induced glucose uptake, and rapamycin does not alter let-7 levels in myoblasts.*** (A) Western blot showing Akt and S6 phosphorylation in C2C12 cells differentiated into myotubes for 3 days, expressing either *Lin28a* or the pBabe empty vector. (B) Glucose uptake in 3-day-differentiated C2C12 myotubes after 24 hr treatment with 10 μM of the MAPK/Erk inhibitor PD98059, or DMSO. (C) Effect of rapamycin on mature *let-7a* levels in C2C12 myoblasts. (D) Mature *let-7* miRNA expression in C2C12 myoblasts. NC = negative control.

**Figure S2.4**

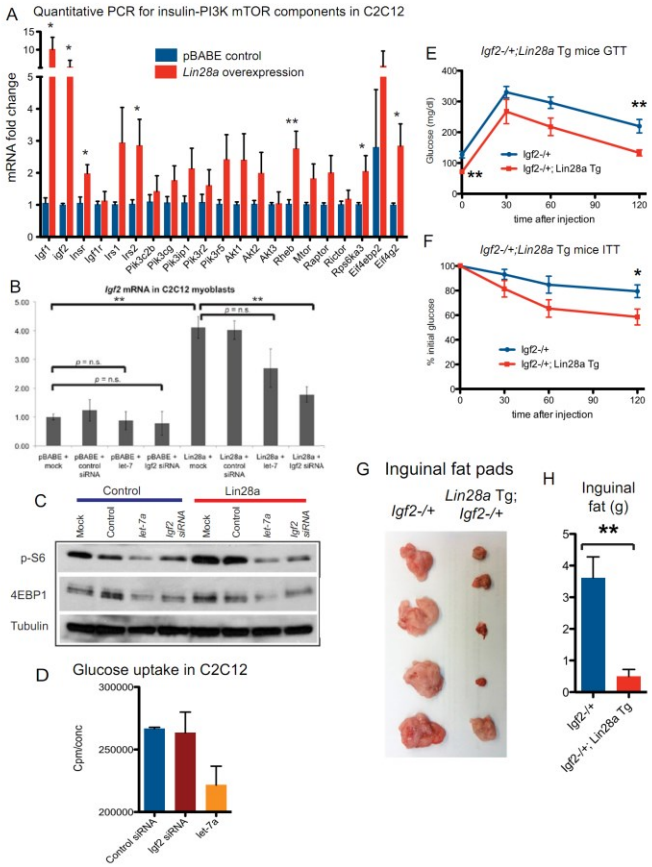


***Figure S2.4. Lin28a promotes insulin-PI3K-mTOR pathway genes and Igf2 is dispensable for Lin28a's functions in vitro and in vivo.*** (A) Quantitative PCR for components of the insulin-PI3K-mTOR signaling pathway in C2C12 myoblasts, normalized to *Gapdh*, after *Lin28a* overexpression. (B) *Igf2* mRNA expression in C2C12 myoblasts. (C) S6 and 4EBP1 phosphorylation in C2C12 myoblasts after overexpression of *let-7a* and knockdown of *Igf2*. (D) Glucose uptake in 3-day-differentiated C2C12 myotubes after siRNA knockdown of *Igf2* and overexpression of *let-7a* duplex. (E) GTT and (F) ITT of *Igf2*-/+; *Lin28a* Tg vs. *Igf2*-/+ mice. Since *Igf2* is imprinted and silenced on the maternal allele, all of the heterozygous offspring (labeled *Igf2-/+*) of a homozygous null father are functionally *Igf2* null. (G) Inguinal fat pads dissected from 1-year-old *Igf2-/+; Lin28a Tg* and *Igf2-/+* mice. (H) Weight in grams of these fat pads.

**Figure S2.5**

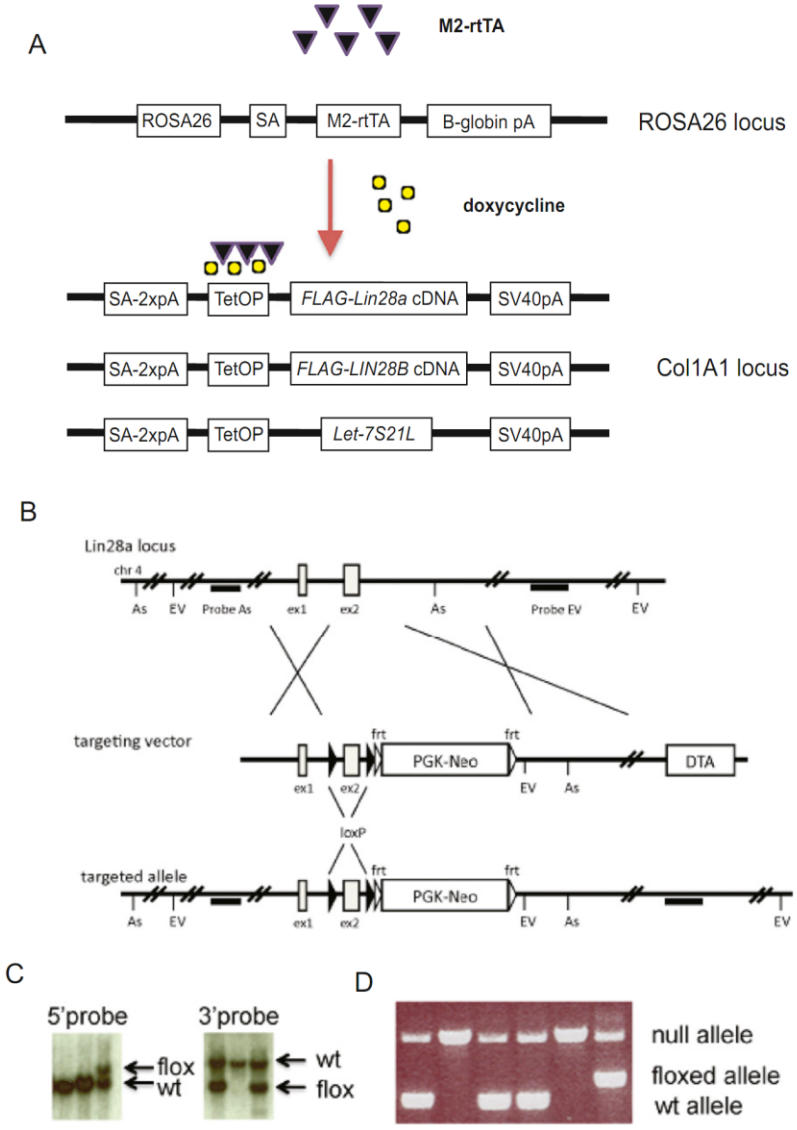


***Figure S2.5. Constructs used to make inducible transgenic and conditional knockout mice.*** (A) Tetracycline inducible mouse constructs for *iLin28a, iLIN28B, and iLet-7* mice. (B) Design of conditional *Lin28a* knockout mice. Upper: Genomic map of the *Lin28a* locus shows exons, restriction sites. Middle: *Lin28a* conditional targeting construct. Exon 2 is flanked by loxP sites. PGK-Neo cassette is flanked by a frt site. Lower: Targeted allele following a homologous recombination. As=Asp718, EV=EcoRV. (C) Southern blot showing ESC clones with the floxed allele. (D) PCR genotyping showing wild-type (wt), floxed and deleted (null) alleles.

**Figure S3.1**

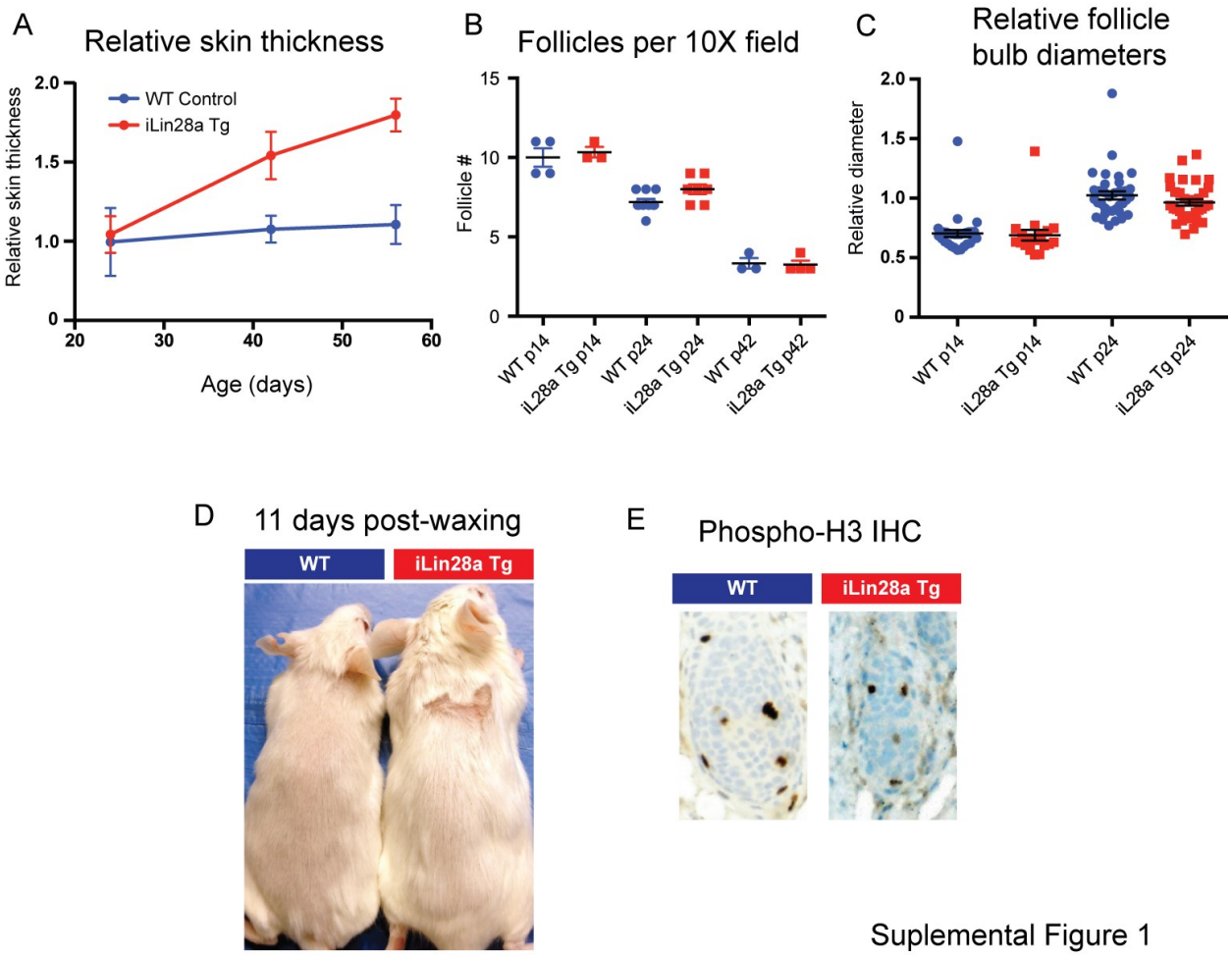


***Figure S3.1: Lin28a reactivation promotes hair regrowth.*** (**A**) Relative skin thickness of WT vs. iLin28a Tg mice over time. Measurements included the epidermis and dermis. (**B**) Number of hair follicles per 10x magnification field. (**C**) Relative follicle bulb diameters were measured. (**D**) WT and iLin28a Tg mice underwent wax depilation at age p44 and images were taken 11 days later. (**E**) Phospho-histone H3 immunohistochemistry staining performed on p24 WT and iLin28a Tg mice, which were both in anagen.

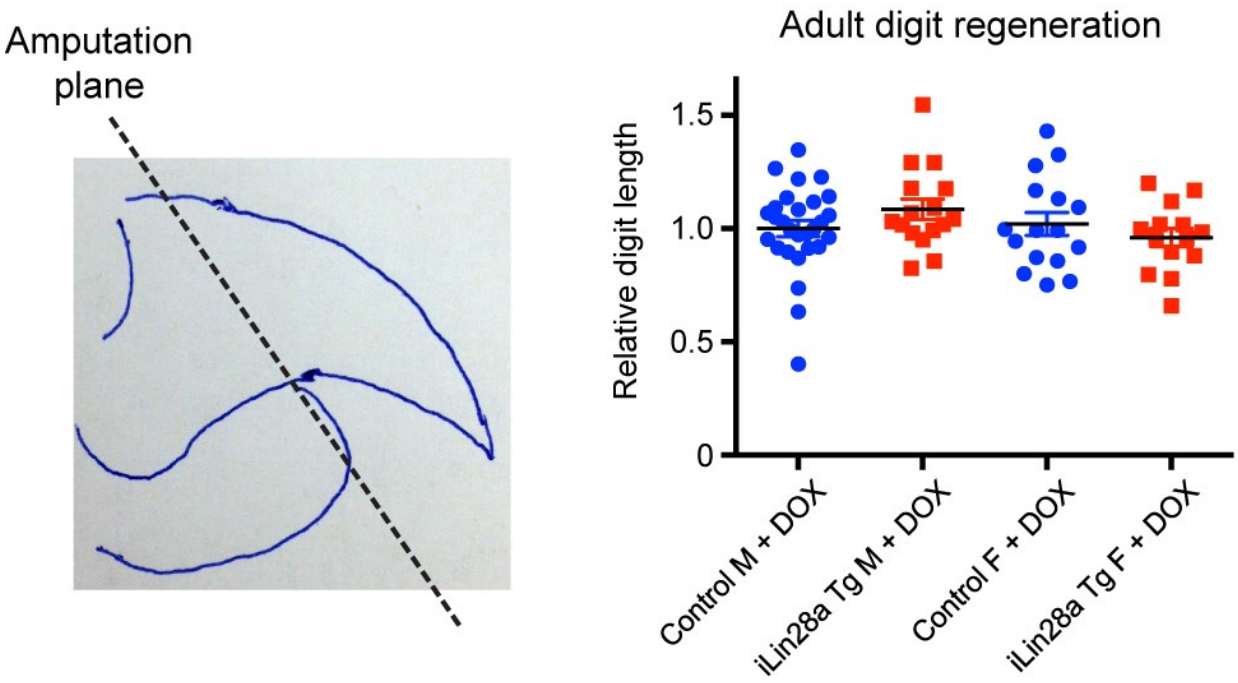


***Figure S3.2: Local Lin28a overexpression does not promote adult digit regeneration after distal amputation.***

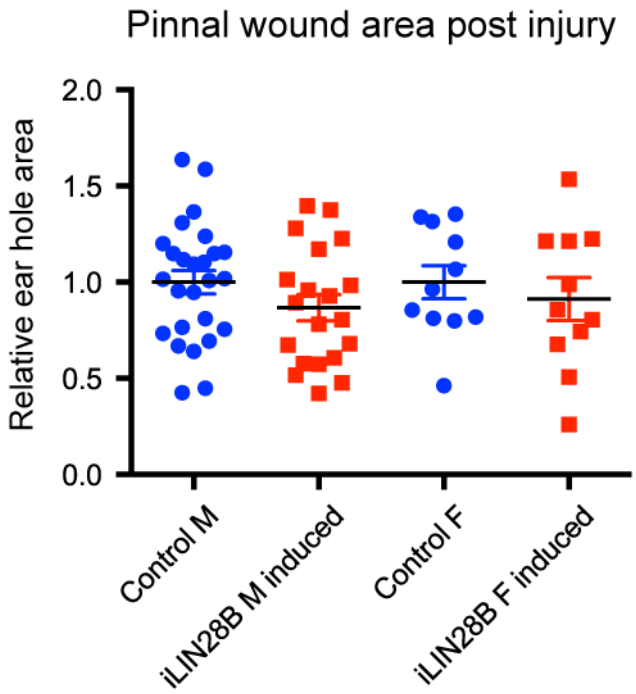


***Figure S3.3: Topical LIN28B overexpression does not promote pinnal tissue repair.***

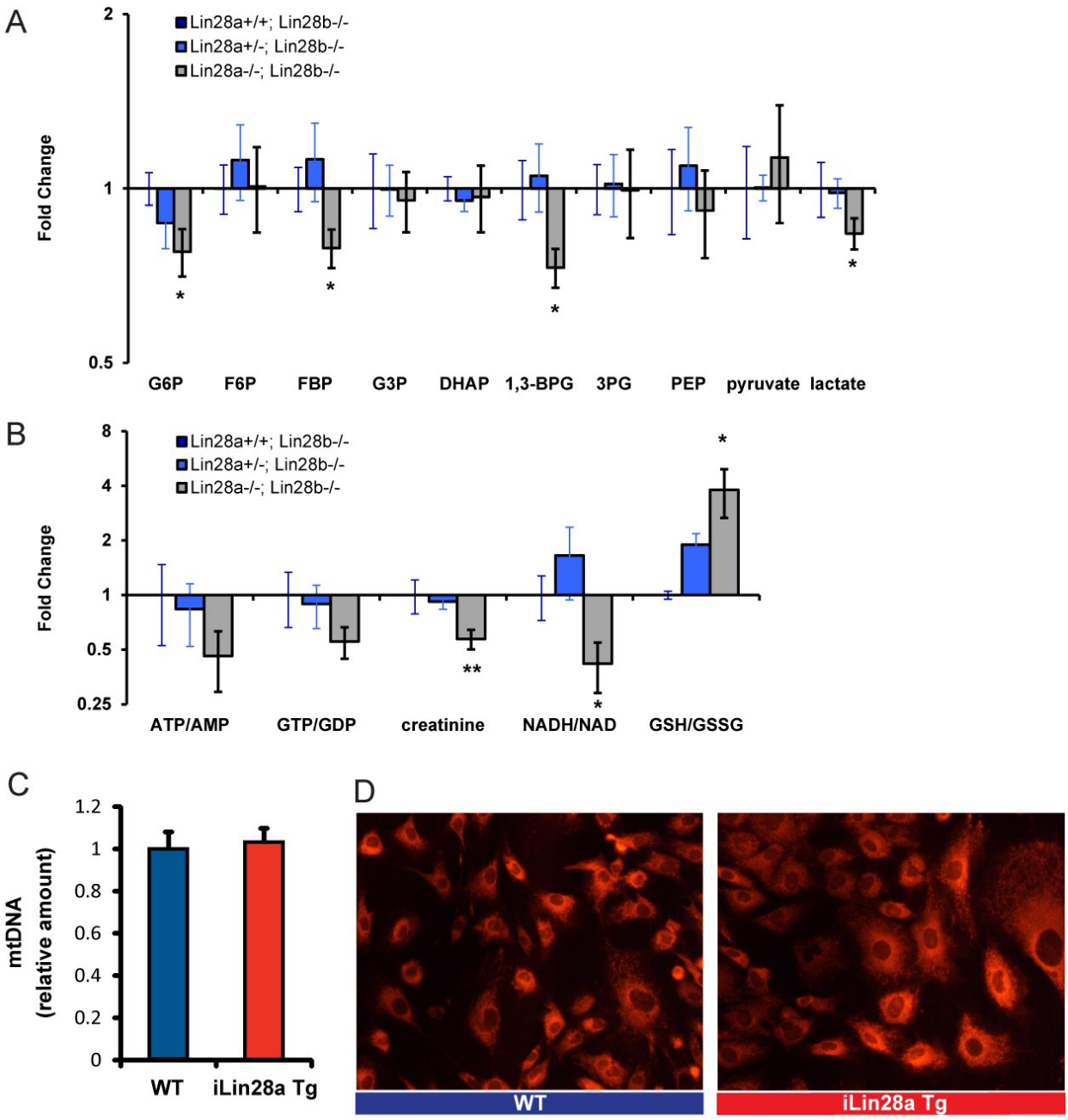


***Figure S3.4: Lin28a alters the bioenergetic state during tissue repair*. (A)** LC-MS/MS selected reaction monitoring (SRM) analysis of abundance in glycolysis intermediates in *Lin28a*$^{+/+}$*;Lin28b*$^{-/-}$ (n=7), *Lin28a*$^{+/-}$*; Lin28b*$^{-/-}$ (n=8) and *Lin28a*$^{-/-}$*; Lin28b*$^{-/-}$ (n=5) embryos at E10.5 post-coitum. * P<0.1 (**B**) SRM analysis of several metabolic indicators in *Lin28a*$^{+/+}$*;Lin28b*$^{-/-}$ (n=7), *Lin28a*$^{+/-}$*; Lin28b*$^{-/-}$ (n=8) and *Lin28a*$^{-/-}$*;Lin28b*$^{-/-}$

***Figur*e *S3.4 (continued)*** (n=5) embryos at E10.5 post-coitum. * P<0.1, ** P<0.01 (**C**) Mitochondrial DNA (mtDNA) content analyzed by means of qRT-PCR. Relative amounts were normalized to WT MEFs. (**D**) Mitochondrial distribution in WT and iLin28a Tg MEFs, as visualized by MitoTracker Red CMXRos staining.

***Figure S3.5: Lin28a enhances mitochondrial oxidation enzymes to promote tissue repair.*** **(A)** Schematic of glucose catabolism through glycolysis, the Krebs cycle and oxidative phosphorylation, and the drug inhibitors that modulate this pathway. 2DG, 2-deoxy-D-glucose. 3BP, 3-bromopyruvate. ROS, reactive oxygen species. GSH, glutathione. GSSG, glutathione disulfide. NAC, N-acetyl-cysteine. Anti-A, antimycin-A. Pfkp, phosphofructokinase, platelet type. Pdha1, pyruvate dehydrogenase alpha 1. Idh3b, isocitrate dehydrogenase 3 NAD(+)-specific, mitochondrial, beta subunit. Sdha, succinate dehydrogenase complex subunit A, flavoprotein. Ndufb3/8, NADH dehydrogenase (ubiquinone) 1 beta subcomplex 3/8. (**B**) Western blots showing efficacy of siRNA knockdown of metabolic enzymes in WT and iLin28a Tg MEFs. (**C**) qRT-PCR showing efficacy of siRNA knockdown of metabolic enzymes in WT and iLin28a Tg MEFs. (**D**) $^{13}$C-glucose flux analysis of glycolytic and Krebs cycle intermediates in WT and iLin28a Tg MEFs treated with siRNAs against glycolysis and Krebs cycle enzymes. (**E**) SRM analysis of the ATP/AMP and GSH/GSSG ratios in WT and iLin28a Tg MEFs treated with siRNAs against electron transport chain enzymes. (**F**) Primary MEF proliferation over 5 days with and without antimycin-A treatment.

**Figure S3.5 (continued)**

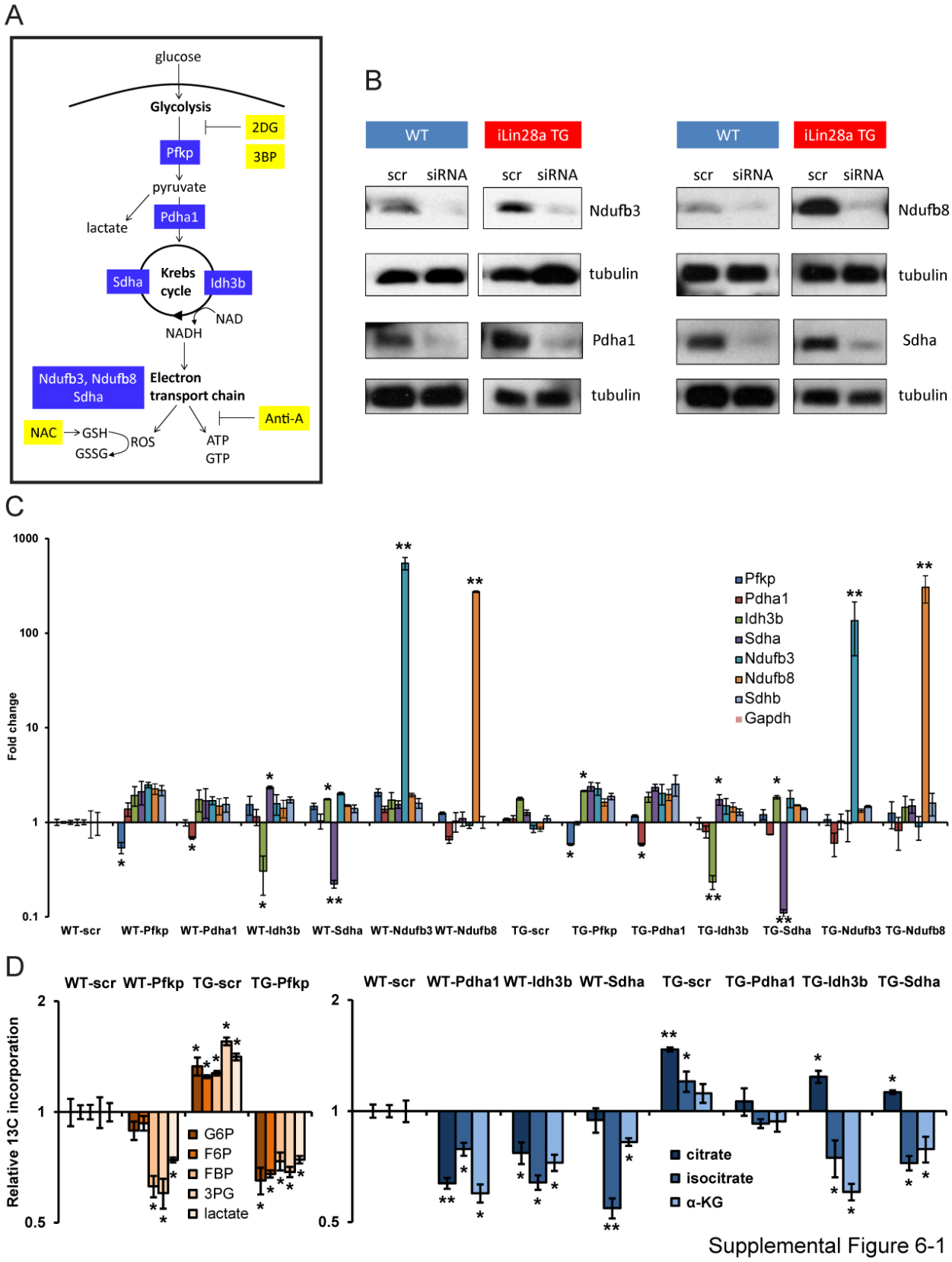


Supplemental Figure 6-1

**Figure S3.5 (continued)**

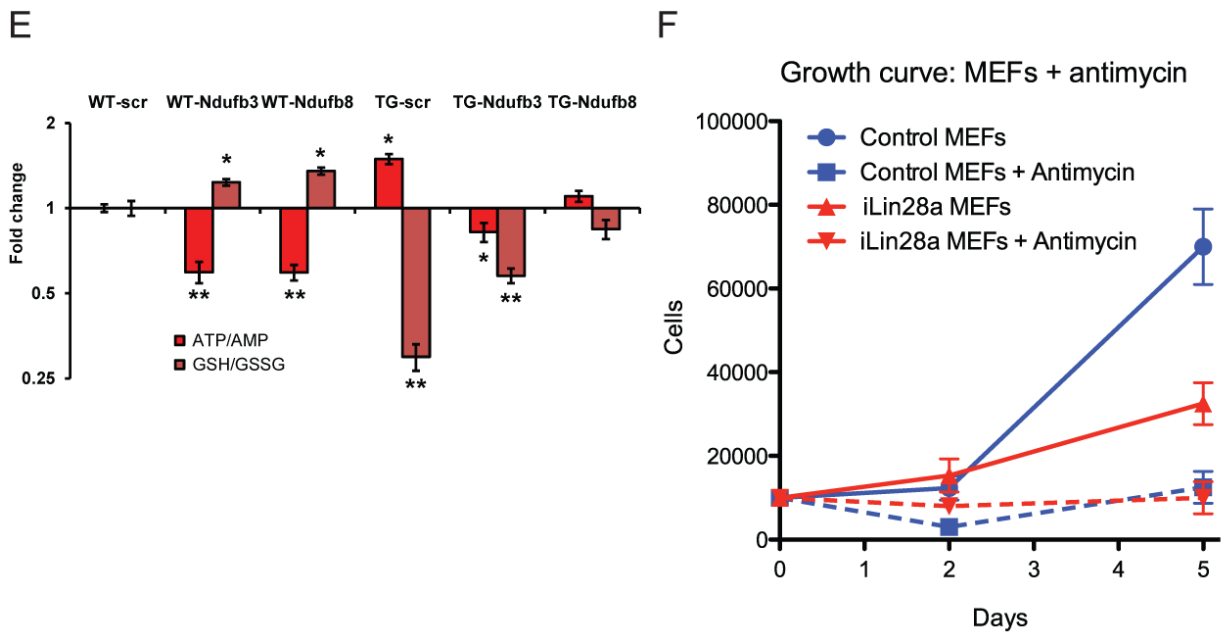

**Figure S3.6**

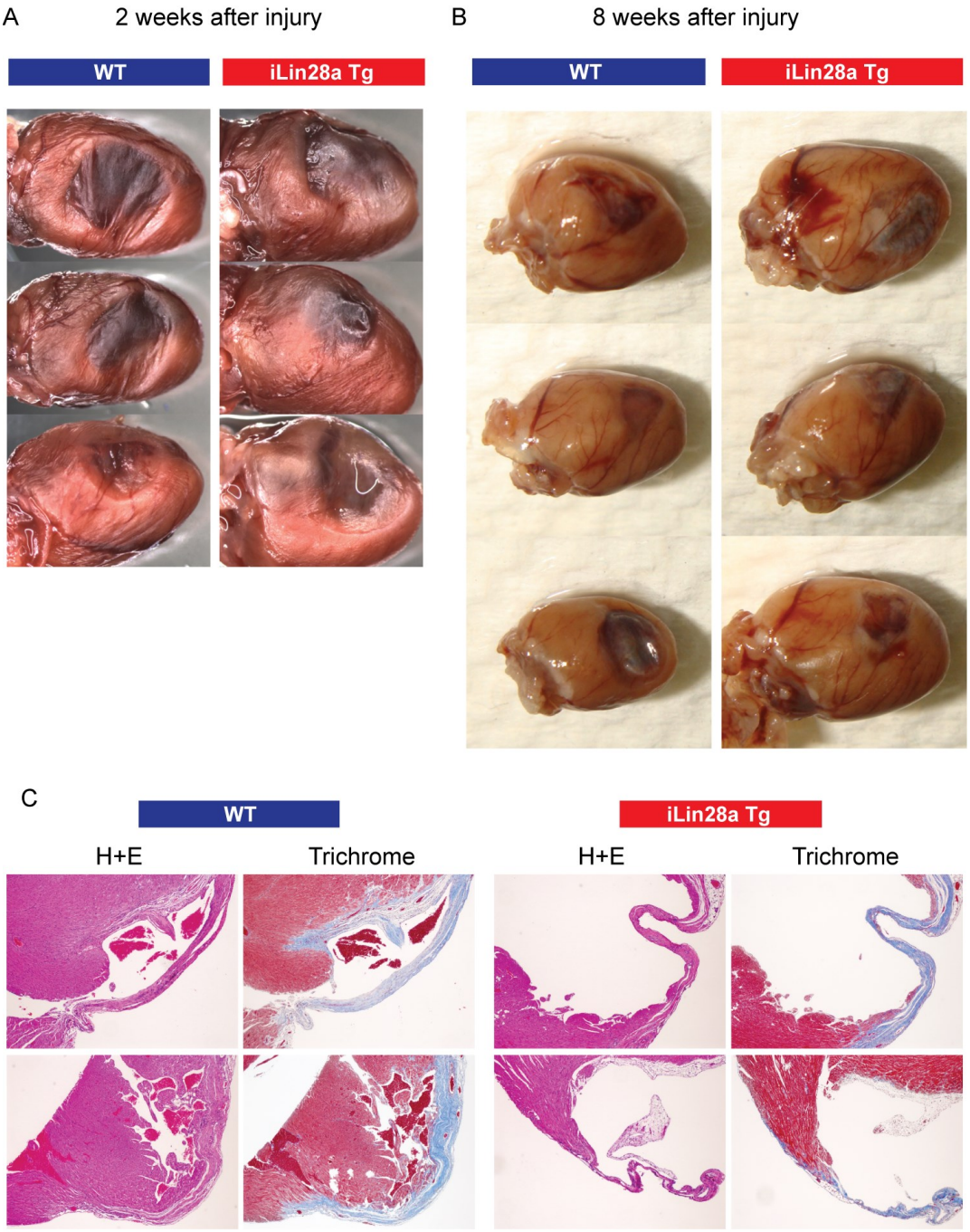


***Figure S3.6: iLin28a Tg mice do not exhibit improved regeneration after cardiac cryoinjury.*** **(A)** Images of the adult heart 2 weeks after cryoinjury with metal probes cooled in liquid $N_2$. (**B**) Injured hearts 8 weeks after cryoinjury. (**C**) H+E and trichrome images of the injured region of the heart at 8 weeks.

**Figure S4.1**

**A**

| 18D dox iPSC: Top 15 | 18D dox iPSC: Bottom 15 |
|---|---|
| 1. glycerophosphocholine | 1. dAMP |
| 2. carnitine | 2. riboflavin |
| 3. cystathionine | 3. cysteine |
| 4. glutathione | 4. folate |
| 5. 4-aminobutyrate | 5. hypoxanthine |
| 6. glutathione disulfide | 6. threonine |
| 7. glucose-1-phosphate | 7. 1,3-diphosphoglycerate |
| 8. a-ketoglutarate | 8. gluconolactone |
| 9. UDP-N-acetyl-glucosamine | 9. uridine |
| 10. dihydroxyacetone phosphate | 10. 3-phosphoserine |
| 11. 3-phosphoglycerate | 11. adenosine |
| 12. phosphoenolpyruvate | 12. 6-phospho-D-gluconate |
| 13. S-adenosyl-methionine | 13. deoxyuridine |
| 14. lactate | 14. cystine |
| 15. isocitrate | 15. methylnicotinamide |

**B**

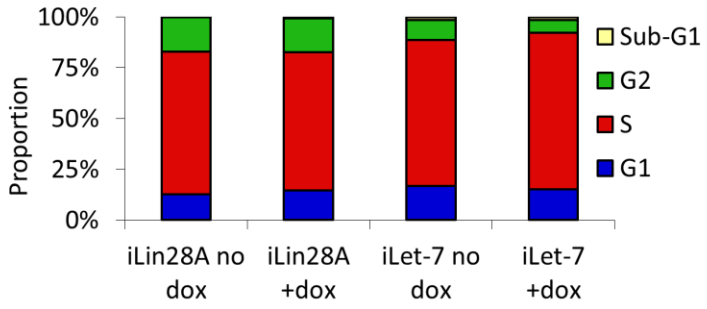


***Figure S4.1: Characterization of iOSKM, iLin28, and iLet-7 cells***

(**A**) Top metabolite changes in iOSKM MEFs after reprogramming for 18 days, and isolated as iPSCs ($P < 0.05$). (**B**) Cell cycle profiles ofiLin28a and iLet-7 mESCs after 2 days of dox induction.

**Figure S4.2**

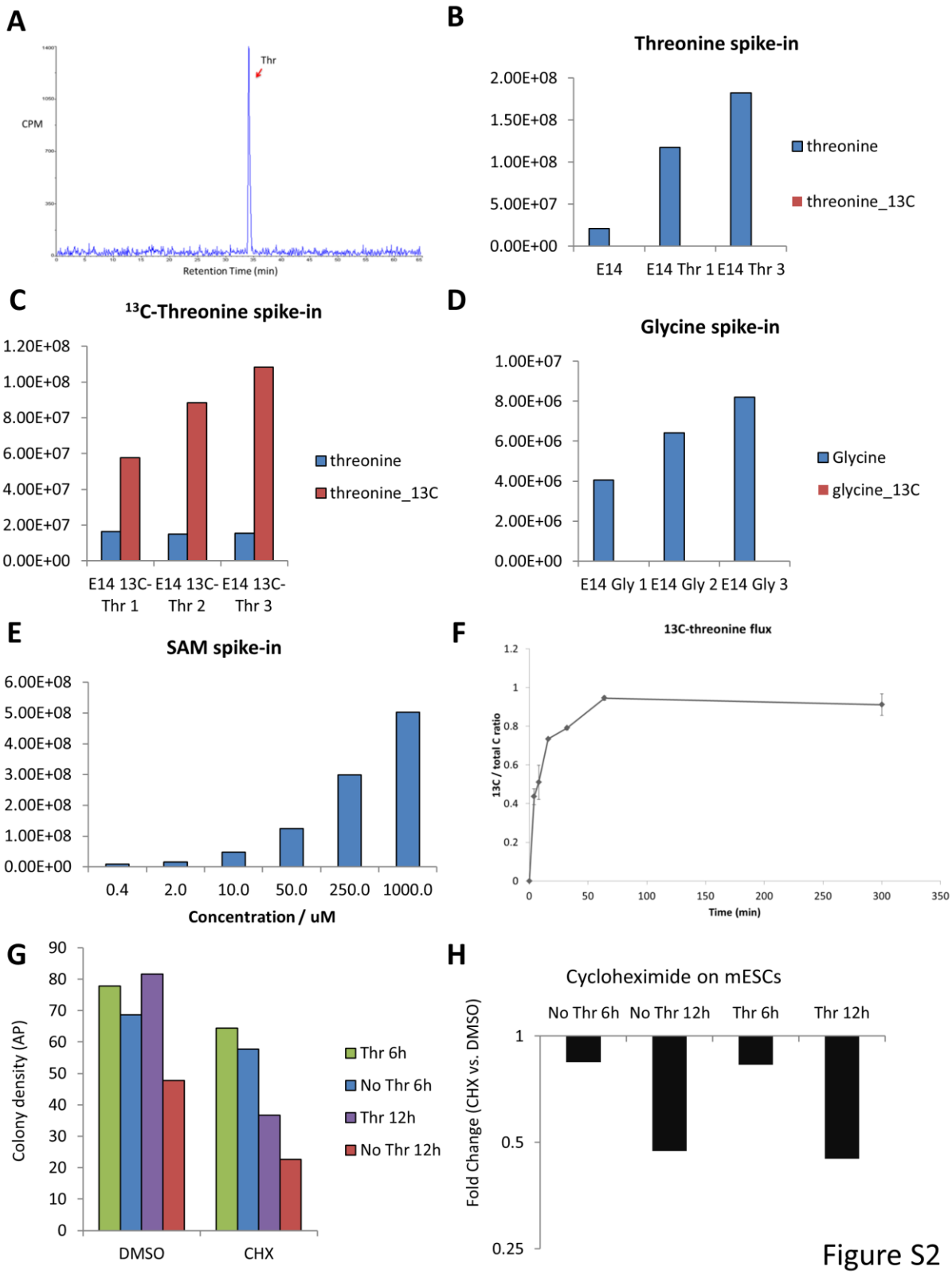


Figure S2

**Figure S4.2 (continued)**

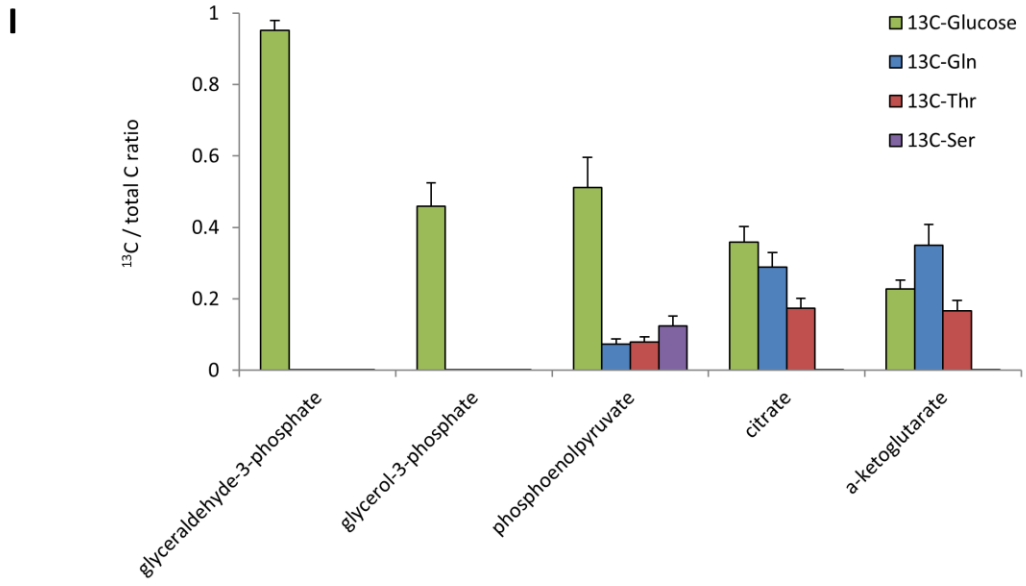


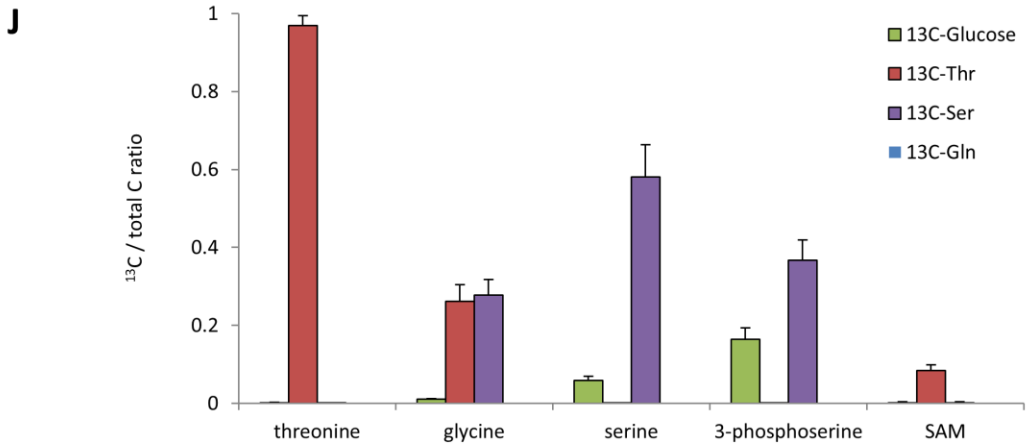


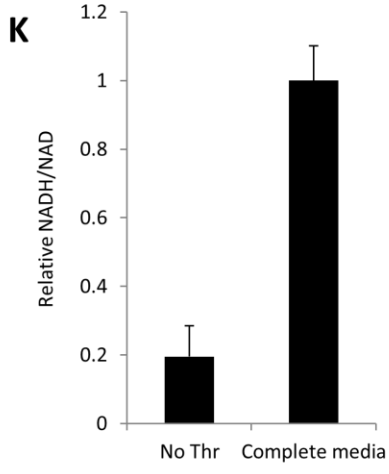


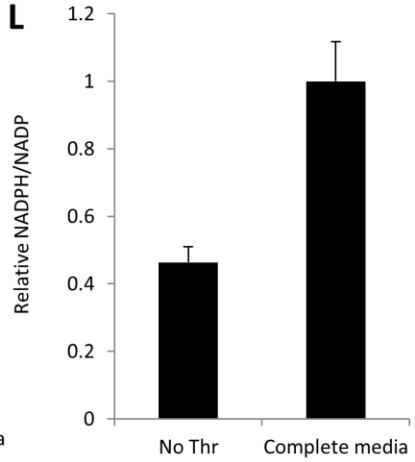


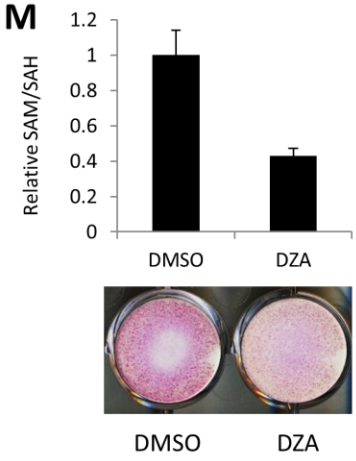

***Figure S4.2 (continued): $^{13}$C-metabolomics of mESCs.*** (**A**) HPLC analysis of radioactive $^{14}$C-labeled amino acids derived from [U-$^{14}$C]Thr in MEFs, after 24h incubation. Thr, threonine. Gly, glycine. Ser, serine. Glu, glutamate. (**B**) Quantitation of spike-ins of 0.1mM and 0.3 mM threonine into mESC samples. (**C**) Quantitation of spike-ins of 0.1 – 0.3 mM [U-$^{13}$C]Thr into mESC samples. (**D**) Quantitation of spike-ins of 0.5 – 1.5 mM glycine into mESC samples. (**E**) Quantitation of spike-ins of 0.4 – 1000 uM S-adenosyl-methionine into mESC samples. (**F**) Time-course of intracellular $^{13}$C-Thr flux in mESCs, measured by LC/MS/MS (n=3). (**G**) Effects of cycloheximide (CHX) and DMSO vehicle on mESC colony density, as measured by alkaline phosphatase staining (AP), under normal (Thr) or Thr-restricted (No Thr) conditions. (**H**) Effect of cycloheximide on mESC growth is independent of Thr restriction. (**I**) $^{13}$C-labeled metabolites in glucose metabolism derived from [U-$^{13}$C]-glucose, [U-$^{13}$C]Thr, [U-$^{13}$C]Ser or [U-$^{13}$C]Gln, after 48h incubation of mESCs (n=3). The fraction of $^{13}$C incorporation ($^{13}$C / total C ratio) is plotted across several metabolites. The +2 citrate and +2 α-ketoglutarate isotopomers are shown for glucose- and Thr-labeling via acetyl-CoA, while the +4 citrate and +5 α-ketoglutarate isotopomers are shown for Gln-labeling via anaplerosis. (**J**) $^{13}$C-labeled metabolites in Thr/Met metabolism derived from [U-$^{13}$C]-glucose, [U-$^{13}$C]Thr, [U-$^{13}$C]Ser or [U-$^{13}$C]Gln, after 48h incubation of mESCs (n=3). The fraction of $^{13}$C incorporation ($^{13}$C / total C ratio) is plotted across several metabolites. The +2 glycine isotopomer, +3 serine and phosphoserine isotopomers, and the +1 SAM isotopomer, are shown for all experiments. (**K**) Colorimetric enzyme-based assay for the total NADH/NAD ratio in mESCs after Thr restriction (0X) for 6h, then re-fed for 6h with 0X Thr or 1X Thr. (**L**) Colorimetric enzyme-based assay for the total

***Figure S4.2 (continued)*** NADPH/NADP ratio in mESCs after Thr restriction (0X) for 6h, then re-fed for 6h with 0X Thr or 1X Thr. (**M**) SRM analysis of the SAM/SAH ratio in mESCs after 24h treatment with 20μM DZA. Corresponding samples were stained for alkaline phosphatase.

**Figure S4.3**

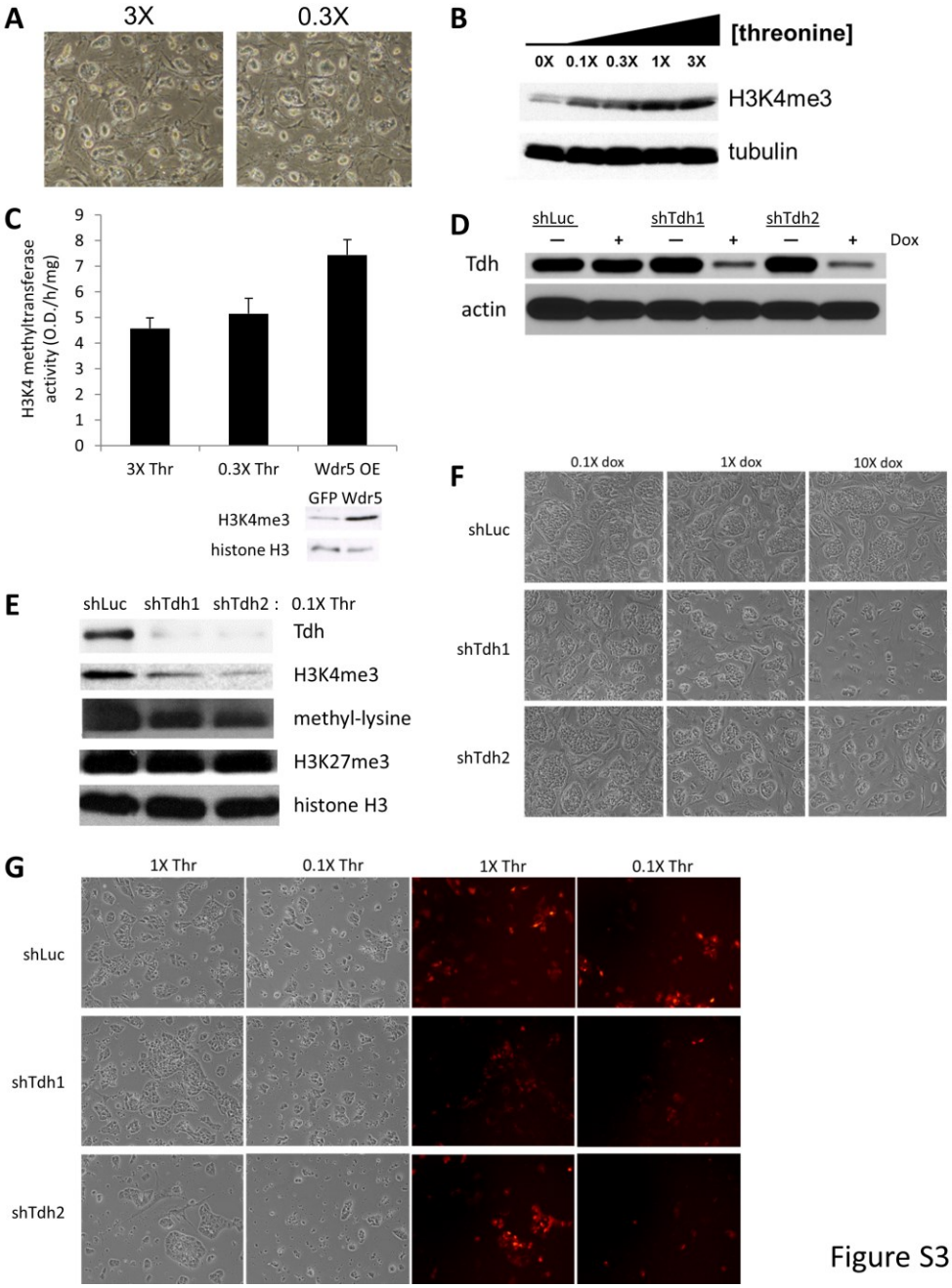


***Figure S4.3 (continued): Thr restriction and Tdh knockdown of mESCs.*** (**A**) Size and morphology of mESC colonies when exposed to 3X and 0.3X Thr concentrations in the media for 48h. (**B**) Immunoblot analysis of mESCs for H3K4me3, after Thr restriction (0X) for 6h, then re-fed for 6h with varying Thr concentrations in the media.

Total tubulin is used as a loading control. (**C**) Colorimetric enzyme-based assay for the total H3K4 methyltransferase activity in nuclear lysates of mESCs after exposure to 3X and 0.3X Thr. The mESCs overexpressing Wdr5, an H3K4 methyltransferase component, were used as a positive control. (**D**) Immunoblot of Tdh in mESCs after dox-induced shRNA knockdown of Tdh with 2 different hairpins (shTdh), relative to a control shRNA against luciferase (shLuc). (**E**) Size and morphology of mESC colonies with inducible shTdh, when exposed to increasing concentrations of dox in 1X Thr media for 48h. Images were taken at 4X magnification. (**F**) Epifluorescence images of mESC colonies with dox-induced shTdh, when exposed to 1X or 0.1X Thr media for 24h. Images were taken at 4X magnification. (**G**) Immunoblot of mESCs grown in 0.1X Thr media for Tdh, H3K4me3, H3K27me3, and pan-methyl-lysine levels, after dox-induced shRNA knockdown of Tdh with 2 different hairpins (shTdh), relative to a control shRNA against luciferase (shLuc).

**Figure S4.4**

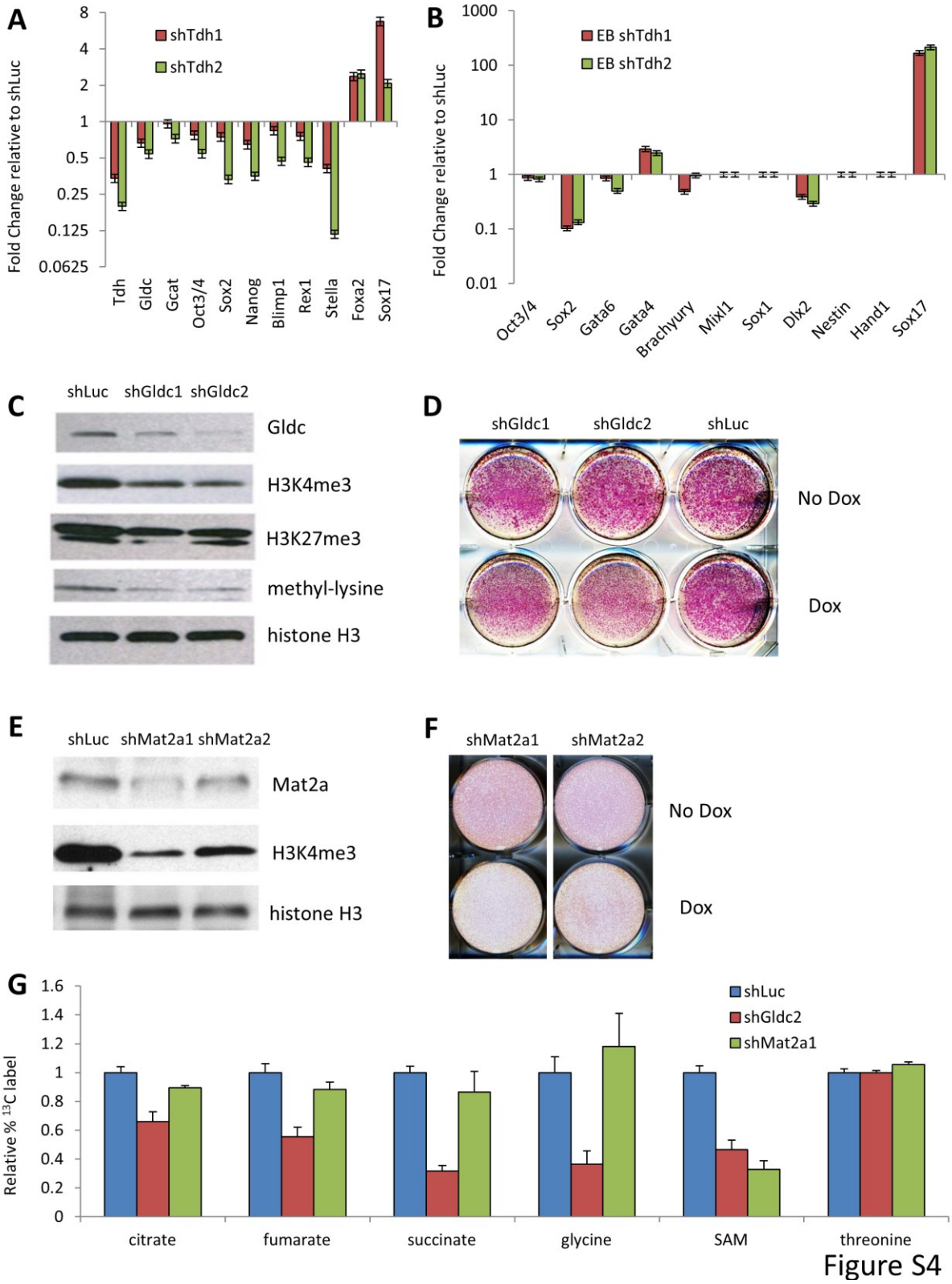


Figure S4

**Figure S4.4 (continued)**

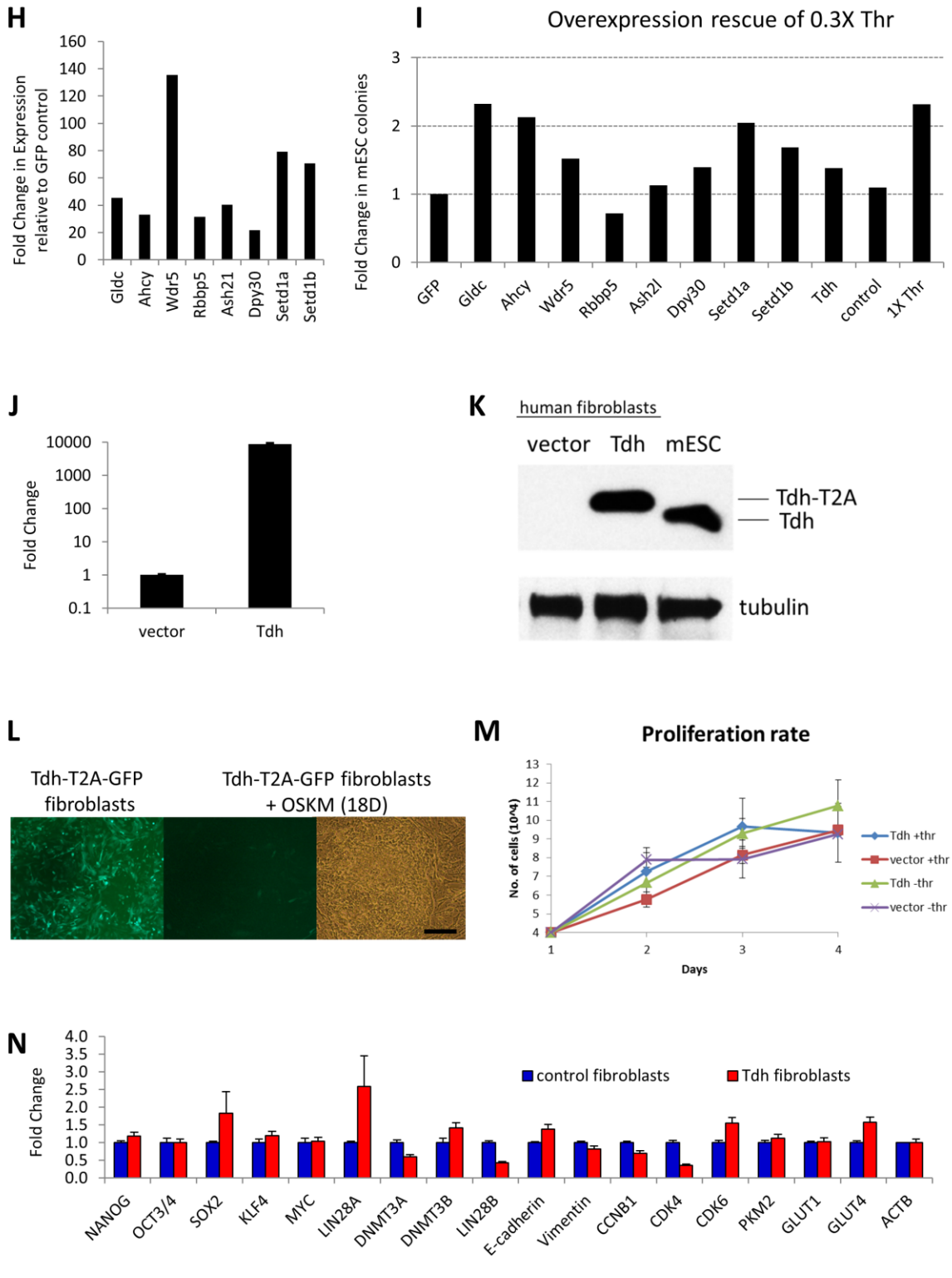

***Figure S4.4 (continued): Tdh knockdown in mESCs and Tdh overexpression in human fibroblasts.*** (**A**) Quantitative RT-PCR for threonine-glycine metabolism enzymes and pluripotency markers in mESCs with dox-induced shTdh, relative to shLuc, in 0.3X Thr media (n=3). (**B**) Quantitative RT-PCR for pluripotency and differentiation markers in 3-day old embryoid bodies (EB) differentiated from mESCs with dox-induced shTdh, relative to shLuc (n=3). (**C**) Immunoblot of Gldc, H3K4me3, H3K27me3, and pan-methyl-lysine in mESCs after dox-induced shRNA knockdown of Gldc with 2 different hairpins (shGldc), relative to a control shRNA against luciferase (shLuc). (**D**) Growth of mESCs with dox-induced shGldc, relative to shLuc, as visualized with alkaline phosphatase staining. (**E**) Immunoblot of Mat2a and H3K4me3 in mESCs after dox-induced shRNA knockdown of Mat2a with 2 different hairpins (shMat2a), relative to a control shRNA against luciferase (shLuc). (**F**) Growth of mESCs with dox-induced shMat2a, relative to shLuc, as visualized with alkaline phosphatase staining. (**G**) $^{13}$C-labeled metabolites derived from [U-$^{13}$C]Thr, after 48h incubation of mESCs (n=3). The relative fraction of $^{13}$C incorporation ($^{13}$C / total C ratio) is plotted. (**H**) Quantitative RT-PCR (Fold change) of mRNA for each respective gene after overexpression in feeder-free mESCs by transfection, relative to overexpression of the GFP control (n=2). (**I**) Threonine restriction and rescue by gene overexpression in mESCs. After overexpression of each gene by transfection, feeder-free mESCs were deprived of Thr in the media for 12h, then supplemented for 36h with 0.3X Thr. Alkaline phosphatase-positive colonies were quantified and normalized to the GFP control (n=2). mESCs supplemented with 0.3X and 1X Thr without transfections, served as negative and positive controls respectively. (**J**) Quantitative RT-PCR for Tdh expression in

***Figure S4.4 (continued)*** human fibroblasts expressing mouse Tdh, relative to control human fibroblasts, prior to iPSC reprogramming (n=3). (**K**) Immunoblot for Tdh expression in human fibroblasts expressing mouse Tdh with the cleaved T2A tag (Tdh-T2A), relative to control human fibroblasts and mESCs with endogenous Tdh. (**L**) Epifluorescence images of human fibroblasts expressing mouse Tdh-T2A-GFP, and a representative human iPSC colony reprogrammed from these fibroblasts for 18 days with *Oct4, Sox2, Klf4, Myc* lentivirus. Images were taken at 10X magnification. (**M**) Proliferation kinetics of human fibroblasts expressing mouse Tdh-T2A-GFP relative to empty vector, with or without Thr in the media (n=3). (**N**) Quantitative RT-PCR profiling of human fibroblasts expressing mouse Tdh, relative to empty vector, prior to iPSC reprogramming (n=3).

All error bars represent the s.e.m. from three independent measurements.